Order Number 9006998

Dynamics and structures of linear and supercoiled DNAs

Song, Lu, Ph.D.

University of Washington, 1989

U·M·I
300 N. Zeeb Rd.
Ann Arbor, MI 48106

Dynamics and Structures of Linear and Supercoiled DNAs

by

Lu Song

A dissertation submitted in partial fulfillment

of the requirements for the degree of

Doctor of Philosophy

University of Washington

1989

Approved by J Michael Schurr
(Chairperson of Supervisory Committee)

Program Authorized
to Offer Degree Chemistry

Date July 28 1989

University of Washington

Abstract

A Study of Dynamics and Structures of Linear and Supercoiled DNAs

by Lu Song

Chairperson of the Supervisory Committee: **Professor J. Michael Schurr**

Department of Chemistry

A normal mode theory is developed for the Brownian dynamics of weakly bending rods with preaveraged hydrodynamic interactions. An expression is given for the mean squared angular displacement $< \Delta_{xm}(t)^2 >$ of the m^{th} bond-vector around the instantaneous x-axis (perpendicular to the end-to-end vector z). The normal mode theory is compared with Brownian dynamics simulations for the same model by examining $3 < \Delta_{xm}(t)^2 >$ for the central bond vector of rods comprising 10 and 30 subunits with various persistence lengths.

Rapidly relaxing components in the decay of the transient electric dichroism of DNA restriction fragments reported by Diekmann et al. (Diekmann et al., 1982) and Pörschke (Pörschke et al., 1987) are analyzed using the new normal mode theory for weakly bending rods and assigned to bending. The longest

bending relaxation times for fragments with 95 to 250 base-pairs coincide with theoretical curve calculated for a dynamic bending rigidity corresponding to a dynamic persistence length $P_d = 2100$ Å.

Autocorrelation functions of the light field scattered by weakly bending rods with various persistence lengthes are simulated using the normal mode analysis. $D_{app}(K)$ could be extracted from these autocorrelation functions and could be used to fit DLS (Dynamic Light Scattering) experimental data.

Samples of pUC8 dimer (5434 base-pairs) with different superhelix densities are prepared by the action of Topoisomerase I in the presence of various amounts of ethidium. The translational diffusion coefficient (D_0) and the plateau diffusion coefficient (D_{plat}) characterizing internal motions over short distances (225 Å) are determined by dynamic light scattering. The torsion constant (α) between base-pairs is determined by time-resolved fluorescence polarization anisotropy. Circular dichroism spectra are also measured for each sample. These data are consistent with the hypothesis that supercoiling induces two successive allosteric transitions to alternate global secondary structures.

Interactions of supercoiled and linear DNAs with EcoRI endonucleose, and dye molecules have been studied with DLS experiments. Results of these experiments have been useful in understanding the mechanisms of these reactions.

Doctoral Dissertation

In presenting this dissertation in partial fulfillments for the doctoral degree at the University of Washington, I agree that the library shall make its copies freely available for inspection. I further agree that extensive copying of this dissertation is allowable only for scholarly purposes, consistent with "fair use" as prescribed in the U.S. Copyright Law. Requests for copying or reproduction of this dissertation may be referred to University Microfilms, 300 North Zeeb Road, Ann Arbor, Michigan 48106, to whom the author has granted "the right to reproduce and sell (a) copies of the manuscript in microform and/or (b) printed copies of the manuscript made from microform."

Signature Lu Song

Date July 28 1989

TABLE OF CONTENTS

List of Tables

List of Figures

Acknowledgements

I would like to thank Professor **J. Michael Schurr** for his guidance, encouragement and support throughout my graduate studies. I appreciate: the help from **Dr. Steve Benight** for showing me how to isolate DNA in my early time of graduate study, and some helpful discussions with **Dr. Bryant Fujimoto.**

to my parents

Yong-wu Song and Gui-zheng Wang

Chapter 1

Introduction

Double-strand DNA is a semiflexible molecule. In solution, large DNA molecules approximate random coils, whereas smaller molecules behave as rods. (Barkley et al., 1979) The dynamics and structures of both linear and supercoiled DNAs have been studied extensively by many workers. Part of my work concerns the development of a normal mode theory for the bending dynamics of weakly bending rods. I have also performed considerable experimental work in an effort to examine changes in secondary and tertiary structures of circular DNAs as a function of superhelix density. Experiments that contribute to an understanding of DNA-dye interactions, DNA-protein interactions, and effects of pH on the structure of linear DNA have also been completed.

1.1 Bending Rigidity of DNA

The wormlike chain model has very often been adopted as a useful approximation for the equilibrium and nonequilibrium behavior of stiff chain macromolecules such as DNA (Sharp et al., 1968; Yamakawa et al., 1973). In this model, the chain is considered to consist of N+1 repeating elements connected by N bond vectors with a very small degree of bending between each pair of adjacent bond vectors. The persistence length of a wormlike chain is the average projection of an infinitely long chain along the direction of its first bond vector. The persistence length is proportional to the bending rigidity (Bloomfield et al., 1974). The consensus persistence length for native DNA in 0.1 M NaCl is obtained from experiments that are sensitive to the equilibrium root mean square(rms) curvature of DNA, and is found to be $P = 450 - 500$ Å. (Song et al., 1989)

Analytical theories of (Gaussian) or Rouse-Zimm models have been successful

in interpreting long-time (low frequency) experiments on high molecular weight polymers. These models are, however, inadequate when the short-time or high-frequency behavior is of interest (Allison, 1986). Transient electric dichroism, transient photo dichroism, fluorescence depolarization, depolarized dynamic light scattering and polarized dynamic light scattering at large scattering vector are several experimental methods that probe rapid internal motions of polymers (Song, et al., 1989). Brownian dynamics simulation methods have been used to simulate fluorescence depolarization from a discrete wormlike chain model of DNA in which the emission dipole is in a parallel configuration (Allison, 1986). Considerable CPU time is required for the simulation and data fitting, and direct insights regarding the internal motions are limited. For example, the relaxation times of each bending mode could not be obtained explicitly. Therefore, a normal mode theory for weakly bending rods was developed in my work, and the validity of this theory was confirmed by comparing the polarization anisotropy results with those from Brownian dynamics simulations. In Chapter 2, the normal mode theory for weakly bending rods is described. The dynamic bending persistence length P_d is obtained by analyzing the rapidly relaxing component of off-field transient electric dichroism data (Diekmann et al., 1982; Pörschke et al., 1987) using the normal mode theory. Numerical results from that analysis are presented and the possibility that the dynamic bending rigidity of DNA differs significantly from the static bending rigidity are discussed in Chapter 3. The autocorrelation function of the light field scattered by weakly bending rods is calculated by using the normal mode theory as described in Chapter 4.

1.2 Structures of DNA, Interactions of DNA with Protein, and with Dye

A DNA molecule is usually thought of as two linear strands interwined to form a double helix with a linear axis. In many cases, however, DNA has the form of a ring consisting of two strands wound in a double helix. Because of the double-helical structure of DNA, a duplex DNA ring can be viewed as two topologically linked single-strand rings. The order of linkage is described by a quantity L termed the linking number. If the molecule is laid flat on a plane, the linking number is equal to the number of helical twists or the number of times each strand revolves around the helical axis of the molecule. A closed circular molecule of DNA is usually underwound compared with a linear DNA of the same length. This unwinding substantially strains the molecule; as a result the axis of the double helix itself twists into a helix. In this form the DNA is said to be supercoiled (Wang, 1982). Sequence-specific changes in local secondary structure of DNA that are induced by changing the superhelix densities of the DNA have been reported (Wells, 1988; Lilley, 1986). Evidence for allosteric transitions in global secondary structure that are induced by superhelical stress has been found in my work. These phenomena are described in Chapter 5 for pUC8 dimer DNA and in Chapter 6 for pBR322 DNA.

The interactions of proteins with DNA are intereating and popular topics in the field of molecular biology. Various kinds of exeriments to study the interactions between EcoRI and DNA have been performed. Dynamic light scattering affords a useful method to study the interacting system withoud disturbing the reaction. Therefore, the interactions between EcoRI with both linear and supercoiled DNA have been studied by dynamic light scattering. The results of such experiments are presented in Chapter 7.

The effects of photochemistry of DNA-dye complexs are briefly discussed In

Chapter 8.

1.3 Dynamic Light Scattering

Light will be scattered by a molecule in solution, if the molecule has a polarizability different from its surroundings. In this case, the oscillating dipole moment induced by the electric field of the incident light beam will radiate in all directions. The intensity of the scattered light will be related to the direction of polarization of the incident light, scattering angle, and solution parameters. Light scattering is a result of local fluctuations in the polarizability or dielectric constant of the medium. In solution, molecules are constantly translating, rotating, and deforming so that the instantaneous dielectric constant of a given subregion (which depends on the position, orientation, and deformed state of the molecules) will fluctuate and thus give rise to light scattering. Because of such motions the positions of the scattering elements are constantly changing, and the total scattered electric field at the detector fluctuates in time. Implicit in these fluctuations is important structural and dynamical information about the molecules (Berne et al., 1976).

Correlation functions provide a concise method for expressing the degree to which two dynamical properties are correlated over a period of time. The traditional two point autocorrelation function has been very useful in dynamic light scattering experiment, specifically to obtain relaxation times of the fluctuating systems. In Chapter 9, the theory of three point correlation function for Gaussian random variables is described as a part of an effort to extract more dynamical information about the stochastic system.

1.4 Experimentation

The Scattering vector $\mathbf{k}$ is defined as $\mathbf{k} = \mathbf{k}_i - \mathbf{k}_f$, where $\mathbf{k}_i$ is the incident propagation vector, and $\mathbf{k}_f$ is the propagation vector in the direction of the detector. The magnitude of $\mathbf{k}$ is given by (Berne et al., 1976)

$$k^2 = (\frac{4\pi n}{\lambda_i})^2 \ \sin^2 \frac{\theta}{2} \tag{1.1}$$

In order to access a k^2 range from $0-20\times10^{10}cm^{-2}$, two different light scattering instruments are used. One is equipped with a Spectra-physics 261 He-Ne laser with $\lambda = 632.8$ nm. Its detection angles are uaually set in a range from 20 to 120 degree: The other is equipped with a Spectra-physics 2025 Ar^+ laser. The line selected is $\lambda = 351.1$ nm. The detection angles are usually changed from 30 to 140 degree.

The old rail which supported the UV laser scattering system was replaced by a NRC(Newport Research Corporation) table. The table top is attached to the air mounts so that the system is isolated from floor vibrations. The two stands that support the laser head and the stand that supports the optical rail were designed by me and manufactured by the machine shop in the chemistry department. An index matching and temperature controlling cell was also designed by me and manufactured by machine shop in the chemistry department. However, the installation and tesiting of that apparatus is being carried out by Ug-Sung Kim.

The schematic diagram of the dynamic light scattering (DLS) experiment is shown in Figure 1.1. The light source is either a He-Ne (Spectra-physics Model 261) or an Ar ion (Spectra-physics Model 2025) laser. The procedures of operation, of cleaning, of alignment, of standard calibration, and the basic principles of each component of the optical and electrical experiments are covered

in Dr. J. Wilcoxon's Ph. D. thesis (Wilcoxon, 1983).

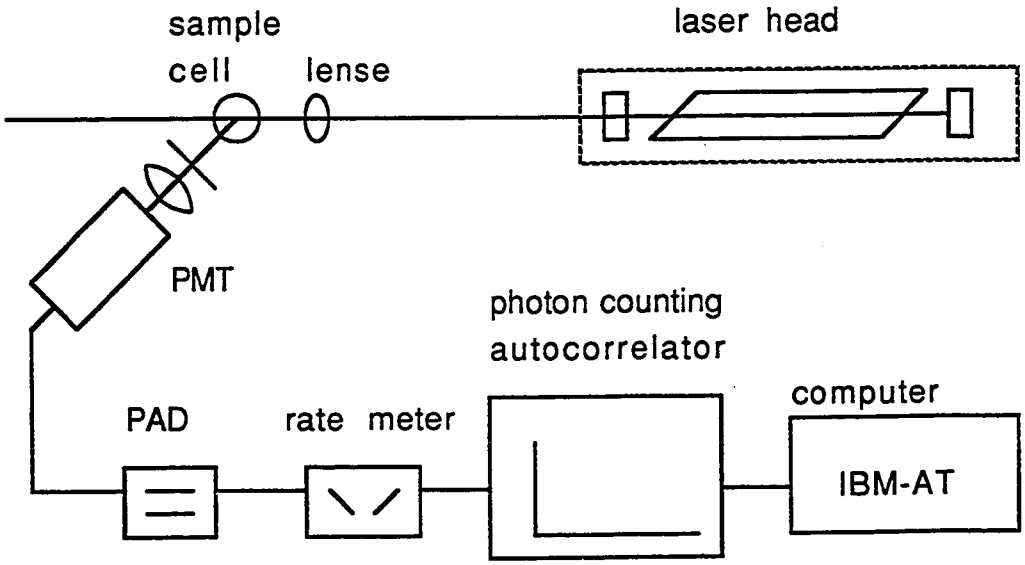

Figure 1.1 DLS apparatus. Laser: He-Ne or Ar ion CW laser. PMT: photomultiplier tube connected to high voltage power supply with 1866 Volts output voltage. PAD: pulse amplifier-discriminator.

The intensity autocorrelation function fitted with three parameter function

$$A(t) = A \ \exp(-t/\tau) + B \tag{1.2}$$

The channel delay and length of the record are adjusted so that the total time fitted is close to 8τ. The relaxation time τ is obtained, the apparent diffusion coefficient is then calculated from

$$D_{app} = \frac{1}{2\tau K^2} \tag{1.3}$$

The old PDP-12 computer was replaced by an IBM-AT. The Program LSFEX.FOR (see Appendix B) was created to operate the interface between the autocorrelator and the IBM-AT, to control the data transfer, to least-squares fit the experimental data to Eq.(1.2), to save the data, to derive the relaxation time, and to calculate the apparent diffusion coefficient. The results from the AT computer were compared with those from the PDP-12 for same experimantal data. All results were identical. The statistical errors were the same or smaller. The time required for data fitting is much shorter on the AT.

Chapter 2

Normal Mode Theory for the Brownian Dynamics of a Weakly Bending Rod. Comparision with Brownian Dynamics Simulations.

2.1 Introduction

Theoretical analysis of the Brownian dynamics of inextensible flexible filaments and their manifestations in various experiments has proved to be a vexing problem. For strongly bending filaments, the chief difficulty arises from the constraints on lengths of the individual bond vectors (Soda, 1973; Yamakawa, 1984), which give rise to a fluctuating tension along the chain. Various strategies have been advanced for either avoiding or dealing with these non-linear constraints in linear but approximate ways (Soda, 1973; Yamakawa, 1984: Barkley et al., 1979; Fujime et al., 1985; Fujime et al., 1984; Berg, 1979; Soda, 1985: Aragon et al., 1985). However, the quantitative consequences of these uncontrolled approximations are largely unknown. Even for weakly bending filaments, where the bond length constraints pose essentially no problem, and significant tension is not developed, there has been no rigorous analytical treatment. The development of analytical theory in this area has been inhibited somewhat by the belief, or fear, that different normal coordinates of the dynamical operator in the presence of pre-averaged hydrodynamic interactions would be coupled by the potential energy, and no longer pairwise "orthogonal" under equilibrium averaging. Such a circumstance would enormously complicate the analysis. Barkley and Zimm (Barkley et al., 1979) avoided precisely this complication by using (approximate) normal coordinates of their force, or potential energy, operator in the place of the normal coordinates of the dynamical operator containing the hydrodynamic interactions. Luckily, this concern is unfounded, and the normal coordinates of the dynamical operator, even in the presence of pre-averaged hydrodynamic interactions, remain pairwise orthogonal, or uncorrelated, under equilibrium averaging, as shown subsequently.

Techniques for simulating the Brownian dynamics of flexure (Allision et al., 1984; Allision, 1986), and also the simultaneous torsion and flexure (Allision et al., 1989), of discrete filaments were recently developed, partly to compensate for the absence of reliable analytical theory. Despite the successes of that approach, there remain several valid reasons for developing an analytical normal mode theory, even when its domain of validity is limited to weakly bending rods, as is the case here. First, the normal mode theory provides significant insights into the structure of the problem that are not available from the simulations. Second, the computational requirements for the normal mode theory are far less than for the Brownian dynamics simulations, except possibly for extremely short evolution times. Moreover, the computational effort required for the normal mode theory is independent of the time (or times) examined. Thus, the normal mode theory constitutes a much more economical approach for treating longer filaments out to arbitrarily long times. Third, the normal mode theory is much better suited for extensive data fitting. The major time-consuming step depends only upon the number of subunits, and is independent of the bending rigidity, subunit spacing, and subunit friction factor. Hence, adjustment of these latter parameters can be performed without repeating the time consuming part of the calculation on each least-squares iteration. Fourth, the analytical theory yields directly the amplitude and relaxation time of each bending normal mode, specifically of the longest (slowest) normal mode, which has been directly observed in electric dichroism experiments (Diekmann et al., 1982; Pörschke, 1987). Such data are analyzed in the following companion paper. Fifth, a comparison of the results of both simulations and analytical theory for filaments of different lengths provides new information regarding the possible effects of the fluctuating tension along the chain, as will be seen.

The present normal mode theory for the flexure dynamics of weakly bending filaments improves on the Barkley-Zimm theory (Barkley et al., 1979) (as applied to finite filaments) in the three main respects. (1) The hydrodynamic interactions are appropriate for the finite length. (2) The Langevin equations of motion are solved exactly (numerically). (3) The mean-squared amplitudes of the dynamical normal coordinates are evaluated exactly. The present theory is closely related to previous work from this laboratory in two regards. First, many of the theoretical techniques used here were originally developed in the treatment of the Rouse-Zimm model by Lin and Schurr (Lin et al., 1978), and applied in the treatment of the twisting dynamics by Allison and Schurr (Allision et al., 1979). Second, it was shown earlier how the emission or absorption anisotropy of a chromophore attached to a subunit of the filament could be expressed simply in terms of the mean squared angular displacements, $< \Delta_z(t)^2 >$ and $< \Delta_x(t)^2 >$, of that subunit around its instantaneous symmetry (z) and transverse (x) axes, respectively (Schurr, 1984). The previously developed theory for the twisting dynamics yields $< \Delta_z(t)^2 >$, while the present theory yields $< \Delta_x(t)^2 >$, and thereby completes the analytical theory of the optical anisotropy for weakly bending filaments.

The present normal mode theory also provides a basis for constructing an analytical theory for dynamic light scattering from weakly bending rods, which will be described in a forthcoming communication.

2.2 Theory

2.2.1 The Weakly Bending Rod Model

The rod is assumed to consist of $N+1$ identical spherical beads whose centers are connected by N bond vectors ($\mathbf{h}_i$) of fixed length h as shown in Figure 2.1. Between each pair of successive bond vectors is a Hookean bending spring that acts to straighten the chain. An instantaneous coordinate system, called the rod frame, is defined in the molecule as follows. The z-axis of the rod is taken parallel to the instantaneous end-to-end vector and is chosen to pass through the center of mass. The x and y axes are initially taken to be any two orthogonal axes in a plane perpendicular to z. Of course, the x and y axes will change as the z-axis rotates. It is helpful to imagine that the rod is encased in a long box with a square-cross section, such that the z-axis intersects the center of every square cross section and the x and y axes intersect the centers of the respective rectangular side faces. The rod flexes inside the box, while the box itself undergoes uniform end-over-end rotations simultaneously with the z-axis of the rod. Throughout this work it is assumed that no twisting torques are exerted on the rod, or on the box. Thus the box undergoes no net twisting motions, but merely reorients its long axis. That is, the Euler rotation that orients the frame of the box in any initial frame is $\Phi = (\alpha\beta - \alpha)$, which implies zero net twist. The changes in the x and y axes of the rod as its z-axis rotates are now the same as those of the box, which can be used to define the instantaneous axis system. The projections of the rod onto the xz and yz planes of this instantaneous coordinate frame change in time only as a consequence of rod flexure. Provided the rod bends only weakly, all flexural motion is essentially transverse to the rod-axis and significant tension is not developed. Hence restoring forces arise only from the bending springs. Each bead (labelled j, $j = 1, \ldots N+1$) is assumed to reside at a fixed z-coordinate (z_j) and to undergo motions in the rod frame only along y and x, but not along z. Of course, motion of the center of mass of the rod may

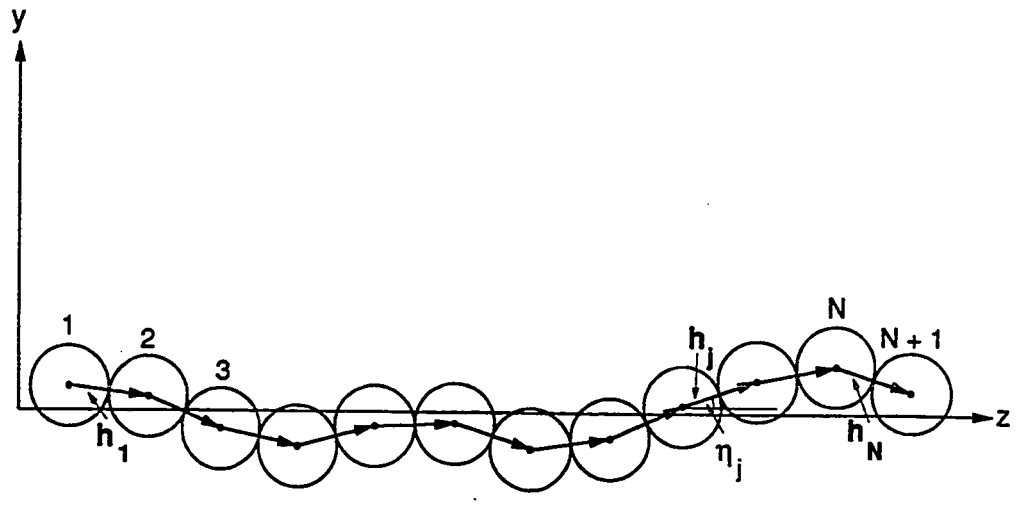

Figure 2.1. Weakly bending rod model. The rod consists of N+1 beads connected by N virtual bond vectors ($\mathbf{h}_i$) of fixed length h. The $z-axis$ of the rod is taken parallel to the instantaneous end-to-end vector and is chosen to pass through the center of mass. η_i is the angle between the projection of the bond-vector $\mathbf{h}_i$ in the yz plane and the $z-axis$. The bond vectors $\mathbf{h}_i$ and $\mathbf{h}_i+1$ are connected by Hooken bending springs that act to straighten the chain.

transport all beads, and the center of drag, uniformly in any direction including z.

2.2.2 The Potential Energy and Direct Forces on the Beads

The bending potential energy is

$$U = \frac{\kappa_h}{2} \sum_{i=1}^{N-1} \beta_{i,i+1}^2 \quad , \tag{2.1}$$

where κ_h is the bending torque constant and $\beta_{i,i+1}$ is the (polar) bending angle between the bond vectors $\mathbf{h}_i$ and $\mathbf{h}_{i+1}$. It was shown previously that. for weakly bending filaments. Eq. (2.1) can be cast in the form (Wu et al., 1987)

$$U = \frac{\kappa_h}{2} \sum_{i=1}^{N-1} \left[(\eta_{i+1} - \eta_i)^2 + (\xi_{i+1} - \xi_i)^2 \right] \quad . \tag{2.2}$$

where

$$\eta_i = \frac{y_{i+1} - y_i}{h} \quad , \tag{2.3}$$

is the angle between the projection of the bond-vector $\mathbf{h}_i$ in the yz plane and the z-axis, and $\xi = (x_{i+1} - x_i)/h$ is the angle between the projection of the bond-vector $\mathbf{h}_i$ in the xz plane and the z-axis. As the dynamical motions of the beads i the yz and xz planes are uncoupled and fundamentally identical for weakly bending filaments, we need only treat the motions of the beads in the yz plane in detail. The part of the potential energy that governs motion in the yz plane was previously shown (Wu et al., 1987)ref17 to be equivalent to that employed by Barkley and Zimm (Barkley et al., 1979). That part of the potential energy can also be written in the matrix form

$$U = \frac{\kappa_h}{2} \boldsymbol{\eta}^T \boldsymbol{A} \boldsymbol{\eta} \tag{2.4}$$

where $\boldsymbol{A}$ is an $N \times N$ Rouse-Zimm interaction matrix.

$$\boldsymbol{A} = \begin{vmatrix} 1 & -1 & 0 & \dots & & 0 \\ -1 & 2 & -1 & 0 & \dots & 0 \\ 0 & -1 & 2 & -1 & \dots & 0 \\ & & & & & \vdots \\ & & & & & 0 \\ 0 & \dots & 0 & -1 & 2 & -1 \\ 0 & \dots & 0 & 0 & -1 & 1 \end{vmatrix} \tag{2.5}$$

and $\boldsymbol{\eta}$ is the $N \times 1$ column vector

$$\boldsymbol{\eta} = \begin{pmatrix} \eta_1 \\ \eta_2 \\ \vdots \\ \eta_N \end{pmatrix} \tag{2.6}$$

Eq. (2.3) can be written in matrix form as

$$\boldsymbol{\eta} = (1/h)\, \boldsymbol{\delta}\, \mathbf{y} \tag{2.7}$$

where $\mathbf{y}$ is a $(N+1) \times 1$ column vector

$$\mathbf{y} = \begin{pmatrix} y_1 \\ y_2 \\ \vdots \\ \\ \\ \\ y_{N+1} \end{pmatrix} \tag{2.8}$$

and $\boldsymbol{\delta}$ is the $N \times (N+1)$ rectangular matrix

$$\boldsymbol{\delta} = \begin{vmatrix} -1 & 1 & 0 & 0 & \dots & & & 0 \\ 0 & -1 & 1 & 0 & \dots & & & 0 \\ 0 & 0 & -1 & 1 & \dots & & & 0 \\ & & & & & & & \\ 0 & \dots & & & 0 & -1 & 1 & 0 \\ 0 & \dots & & & 0 & 0 & -1 & 1 \end{vmatrix} \tag{2.9}$$

Eq. (2.4) can now be expressed as

$$\begin{aligned} \mathcal{U} &= \frac{\kappa_h}{2h^2}\, \mathbf{y}^T \boldsymbol{\delta}^T \boldsymbol{A}\, \boldsymbol{\delta}\, \mathbf{y} \\ &= \frac{\kappa_h}{2h^2}\, \mathbf{y}^T \boldsymbol{D}\, \mathbf{y} \end{aligned} \tag{2.10}$$

where $\boldsymbol{D} = \boldsymbol{\delta}^T \boldsymbol{A}\, \boldsymbol{\delta}$. Carrying out the indicated matrix multiplications yields the $(N+1) \times (N+1)$ matrix

$$\boldsymbol{D} = \begin{vmatrix} 1 & -2 & 1 & 0 & 0 & 0 & 0 & \dots & 0 \\ -2 & 5 & -4 & 1 & 0 & 0 & 0 & \dots & 0 \\ 1 & -4 & 6 & -4 & 1 & 0 & 0 & \dots & 0 \\ 0 & 1 & -4 & 6 & -4 & 1 & 0 & \dots & 0 \\ & & & & & & & & \\ & & & & & & & & \\ 0 & \dots & 0 & 1 & -4 & 6 & -4 & 1 & 0 \\ & & 0 & 0 & 0 & 1 & -4 & 5 & -2 \\ 0 & \dots & 0 & 0 & 0 & 0 & 1 & -2 & 1 \end{vmatrix} \tag{2.11}$$

$\boldsymbol{A}$ is symmetric and so is $\boldsymbol{D}$, since $\boldsymbol{D}^T = (\delta^T \boldsymbol{A}\, \delta)^T = \delta^T \boldsymbol{A}^T \delta = \delta^T \boldsymbol{A}\, \delta = \boldsymbol{D}$.

The force in the y-direction acting on the j^{th} bead is

$$\begin{aligned} F_{yj} = -\frac{\partial \mathcal{U}}{\partial y_j} &= \frac{\kappa_h}{2h^2} \frac{\partial}{\partial y_j} \left(\sum_\ell \sum_m y_\ell D_{\ell m} y_m \right) \\ &= -\frac{\kappa_h}{h^2} \sum_\ell D_{j\ell}\, y_\ell \end{aligned} \tag{2.12a}$$

Eqs. (2.12a) can be written in matrix form as

$$\mathbf{F}_y = -\frac{\kappa_h}{h^2} \boldsymbol{D}\, \mathbf{y} \quad . \tag{2.12b}$$

which shows that $\boldsymbol{D}$ is both the potential energy and force constant matrix for bead displacements in the y-direction. For weakly bending rods, the forces used here are identical to those employed in the Brownian dynamics simulations of discrete wormlike coils by Allison and coworkers (Allision et al., 1984; Allision et al., 1986; Allision et al., 1989), and to the bending forces for a discrete bead model used by Harris and Hearst, who also introduced tensile forces (Harris et al., 1966). An independent expression similar to Eq. (2.12) holds also for the forces on the beads in the x-direction. However, in this model there are no direct forces on the beads in the z-direction, as that motion is taken to be just the uniform rigid body motion of all beads in unison.

2.2.3 The Equation of Motion

The Langevin equation for motion of the beads in the y-direction is

$$m\ddot{\mathbf{y}} + \gamma(\dot{\mathbf{y}} - \mathbf{v}) + (\kappa_h/h^2)\boldsymbol{D}\, \mathbf{y} = \mathbf{E}_y(t) \tag{2.13}$$

where $\mathbf{v} = (v_1, v_2, \ldots v_{N+1})^T$ is the $(N+1) \times 1$ column vector of fluid velocities in the y-direction at the positions of the respective beads, $\mathbf{E}_y(t) =$

$(E_{y1}(t), E_{y2}(t) \ldots . E_{y,N+1}(t))^T$ is the $(N+1) \times 1$ column vector of fluctuating Brownian forces in the y-direction on the respective beads, m is the bead mass, and $\gamma = (1/k_B T) \int_0^\infty d\tau < E_{yj}(0) E_{yj}(\tau) >$ is the friction factor for a single bead. The time-average $< E_{yj}(t) >= 0$ for all beads. Also $\mathbf{E}_y(t)$ is not correlated with the bead positions or velocities at any earlier time, that is $< y_j(t') E_{y\ell}(t) >= 0 =< \dot{y}_j(t') E_{y\ell}(t) >$ for $t' < t$. The autocorrelations of $E_{yj}(t)$ die out very quickly, so that on the time scales of interest $< E_{yj}(0) E_{yj}(t) >= 2 k_B T \gamma \Delta(t)$, where $\Delta(t)$ is a rapidly decaying function with unit area that can be practically approximated by a delta function $\Delta(t)$. The friction drag term is a simplification of a more general memory term expression (Forster, 1975; Berne, 1976), and applies when the autocorrelation function of the fluctuating force on a bead relaxes very rapidly compared to motions of the beads themselves. From this point of view, the friction drag actually arises from the reaction of the fluid to the bead motion at (very slightly) earlier times. The fluid velocity v_j similarly represents the response of the fluid to forces exerted on the fluid by all of the other beads ($i \neq j$) at very slightly earlier times. We employ the usual relation

$$\mathbf{v} = \boldsymbol{T}_{yy} \mathbf{F} y / \gamma \tag{2.14}$$

where $\boldsymbol{T}_{yy}$ is the $(N+1) \times (N+1)$ matrix of $(T_{yy})_{\ell m}$ hydrodynamic interaction tensor elements, and $\mathbf{F}_y$ is an $N \times 1$ column vector of the y-forces that are effective in generating hydrodynamic interactions. Here we assume that hydrodynamic interactions arise exclusively from the direct interactions between particles, so that

$$\mathbf{F}_y = -(\kappa_h / h^2) \boldsymbol{D}\ \mathbf{y} \tag{2.15}$$

This choice for $\mathbf{F}_y$ corresponds to that employed in the treatment of the

Rouse-Zimm model by Lin and Schurr (Lin et al., 1978). Inserting Eqs. (2.14) and (2.15) in Eq. (2.1) yields the final form of the Langevin equation

$$m\ddot{\mathbf{y}} + \gamma\dot{\mathbf{y}} + (\kappa_h/h^2)\boldsymbol{H}\boldsymbol{D}\,\mathbf{y} = \mathbf{E}_y(t) \tag{2.16}$$

wherein $\boldsymbol{H} = \mathbf{1} + \boldsymbol{T}_{yy}$ is the $(N+1) \times (N+1)$ hydrodynamic interaction matrix, and $\mathbf{1}$ is the $(N+1) \times (N+1)$ unit matrix.

In his treatment of a related model, Soda (Soda, 1985) employed a somewhat different procedure, which is equivalent to using Eq. (2.14) with $\mathbf{F}_y = (\mathbf{E}_y(t) - m\ddot{\mathbf{y}} - (\kappa_h/h^2)\boldsymbol{D}\,\mathbf{y})$, to obtain a somewhat different final form for the Langevin equation. Although this ambiguity is not yet conclusively resolved, we prefer the approach adopted here for two reasons. (1) The fluid y-velocity v_j at time t, like the friction drag, must arise from forces exerted by the beads on the fluid at (very slightly) earlier times. However, $\mathbf{E}_y(t)$ and much of $m\ddot{\mathbf{y}}(t)$ are rapidly fluctuating forces at the present time that are essentially uncorrelated with their corresponding values at slightly earlier times. Such present time forces should not give rise to hydrodynamic flows at the present time. In contrast, $\mathbf{F}_y = (\kappa_h/h^2)\boldsymbol{D}\,\mathbf{y}$ changes only slowly and is highly correlated with itself at slightly earlier times. Indeed, its present value is a very good approximation to its value at very slightly earlier times, and that is the sense in which Eq. (2.15) is valid. (2) In generalized Langevin theory, the equation of motion connects the rates of change of the slow variables to the rapidly fluctuating forces. In that spirit, the fluid velocity $\mathbf{v}$ in Eq. (2.13) should represent only the slow component of the fluid velocity, as given by Eqs. (2.14) and (2.15). In contrast, the choice of Soda appears to introduce rapidly fluctuating components into $\mathbf{v}$ via $\mathbf{E}_y(t)$ and $m\ddot{\mathbf{y}}$. In any event, either Eq. (2.16) or the corresponding expression obtained by Soda's method yield identical solutions for the overdamped bending

normal coordinates when the inertial terms are ignored, and the translational and rotational diffusion coefficients for the uniform modes are identical, despite their different appearance, as noted below.

Eq. (2.16) with $\ddot{\mathbf{x}}$, $\dot{\mathbf{x}}$, and $\mathbf{x}$ in place of $\ddot{\mathbf{y}}$, $\dot{\mathbf{y}}$, and $\mathbf{y}$ holds for bead motions in the x-direction. For the uniform rigid body motion of all beads in the instantaneous z-direction, the Langevin equation of motion is

$$M\ddot{z} + \Gamma_z \dot{z} = E_z(t) \quad , \tag{2.17}$$

where $\ddot{z}$ and $\dot{z}$ pertain to any bead or to the center of mass, $M = (N+1)m$ is the total mass, $E_z(t)$ is the fluctuating Brownian force in the z-direction on the whole molecule, and Γ_z is the friction factor for rigid-body translation of the whole molecule in the z-direction, which is evaluated below.

2.2.4 Hydrodynamic Interactions

We adopt the hydrodynamic interaction tensor of Rotne and Prager (Rotne, 1969) and Yamakawa (Yamakawa, 1970) (for $\ell \neq m$),

$$\boldsymbol{T}_{\ell m} = \frac{3a}{4R_{\ell m}} \left\{ \mathbf{1} + \hat{\mathbf{R}}_{\ell m}\hat{\mathbf{R}}_{\ell m} + \frac{2a^2}{R_{\ell m}^2}\left(\frac{\mathbf{1}}{3} - \hat{\mathbf{R}}_{\ell m}\hat{\mathbf{R}}_{\ell m}\right) \right\} \tag{2.18a}$$

to obtain

$$(T_{yy})_{\ell m} = \hat{\mathbf{y}} \cdot \boldsymbol{T}_{\ell m} \cdot \hat{\mathbf{y}} = \frac{3}{4}\frac{a}{R_{\ell m}} \left\{ 1 + \frac{2}{3}\frac{a^2}{R_{\ell m}^2} \right\} \tag{2.18b}$$

$$(T_{xx})_{\ell m} = \hat{\mathbf{x}} \cdot \boldsymbol{T}_{\ell m} \cdot \hat{\mathbf{x}} = \frac{3}{4}\frac{a}{R_{\ell m}} \left\{ 1 + \frac{2}{3}\frac{a^2}{R_{\ell m}^2} \right\} \tag{2.18c}$$

$$(T_{zz})_{\ell m} = \hat{\mathbf{z}} \cdot \boldsymbol{T}_{\ell m} \cdot \hat{\mathbf{z}} = \frac{3}{4}\frac{a}{R_{\ell m}} \left\{ 2 - \frac{4}{3}\frac{a^2}{R_{\ell m}^2} \right\} \tag{2.18d}$$

where $\mathbf{R}_{\ell m}$ is the center-to-center vector from the ℓ^{th} to the m^{th} bead, $\mathbf{1}$ is the unit tensor, a is the hydrodynamic radius of a bead, and the carets denote unit vectors. Eqs. (2.18b-d) are obtained under the assumption that $\mathbf{R}_{\ell m}$ is on the average parallel to $\hat{z}$, hence perpendicular to $\hat{y}$. We have employed two procedures to estimate the appropriate value of $R_{\ell m}$. The first is to assume that the weakly bending rod is effectively straight so that $R_{\ell m} = |\ell - m|h$. The second is to replace $R_{\ell m}$ by the square-root of the mean-squared distance between the ℓ^{th} and m^{th} beads using the formula for a wormlike coil (Bloomfield et al., 1974)

$$\begin{aligned} R_{\ell m} &\cong < R_{\ell m}^2 >^{1/2} \\ &\cong \{2P\,[\,|\ell - m|h - P + P\exp(-|\ell - m|h/P)]\}^{1/2} \end{aligned} \tag{2.19}$$

These two procedures yield almost identical numerical results for the relaxation times of the bending normal modes and for the mean-squared angular displacement $< \Delta x_m(t)^2 >$ of the m^{th} bond vector around an instantaneous axis perpendicular to y and z as a function of time. Hence, we employ the simpler relation $R_{\ell m} = |\ell - m|h$ in the sequel. In addition, we set $a = h/2$, precisely half the bead separation. Finally, then, the elements of the hydrodynamic interaction matrix for the y-motion in Eq. (2.16) are given by

$$H_{\ell m} = \delta_{\ell m} + (1 - \delta_{\ell m})\frac{3}{8|\ell - m|}\left\{1 + \frac{1}{6|\ell - m|^2}\right\} \quad . \tag{2.20}$$

Of course, the hydrodynamic interaction tensor for the corresponding x-motion is identical.

2.2.5 The Friction Factor for Rigid Body Translation in the z-Direction

The relation between a constant z-velocity $\dot{z} = \dot{z}_0$ of all of the beads and

the constant external forces on the beads required to maintain such a constant velocity is given by

$$\mathbf{F}_z = \gamma(\dot{\mathbf{z}}_0 - \mathbf{w}) \quad , \tag{2.21}$$

where $\mathbf{F}_z$ is the $(N+1) \times 1$ column vector of z-forces on the respective beads, $\mathbf{z}_0$ is the $(N+1) \times 1$ column vector containing $\dot{z}_0$ at every position, and $\mathbf{w} = (w_1, w_2 \ldots w_{N+1})^T$ is the $(N+1) \times 1$ column vector of fluid velocities in the z-direction at the respective beads. The equation analogous to Eq. (2.14) for the z-direction is $\mathbf{w} = \boldsymbol{T}_{zz}\mathbf{F}_z/\gamma$. This is inserted in Eq. (2.21), which is rearranged to yield

$$\mathbf{F}_z = \gamma(\mathbf{1} + \boldsymbol{T}_{zz})^{-1}\dot{\mathbf{z}}_0 \tag{2.22}$$

Summing the external forces on all beads gives the total z-force on the rod,

$$F_z^{\text{tot}} = \sum_{\ell} F_{z\ell} = \dot{z}_0\gamma \sum_{\ell=1}^{N+1}\sum_{m=1}^{N+1} \left((\mathbf{1} + \boldsymbol{T}_{zz})^{-1}\right)_{\ell m} \tag{2.23}$$

Comparison of Eq. (2.23) with the defining relation for Γ_z, (namely $F_z^{\text{tot}} = \Gamma_z \dot{z}_0$) yields

$$\Gamma_z = \gamma \sum_{\ell=1}^{N+1}\sum_{m=1}^{N+1} \left((\mathbf{1} + \boldsymbol{T}_{zz})^{-1}\right)_{\ell m} \tag{2.24}$$

which is the well-known result of the Kirkwood algorithm for rigid body motion.

2.2.6 Normal Modes of the y-Motion

After introducing the normal coordinate transformation

$$\mathbf{y} = \boldsymbol{Q}\,\boldsymbol{\rho} \tag{2.25}$$

into Eq. (2.16) and multiplying by $\boldsymbol{Q}^{-1}$ on the left, there results

$$m\ddot{\boldsymbol{\rho}} + \gamma\dot{\boldsymbol{\rho}} + \frac{\kappa_h}{h^2}\,\boldsymbol{Q}^{-1}\boldsymbol{H}\boldsymbol{D}\,\boldsymbol{Q}\,\boldsymbol{\rho} = \mathbf{G}(t) \quad , \tag{2.26}$$

where $\mathbf{G}(t) = \boldsymbol{Q}^{-1}\mathbf{E}_y(t)$. $\boldsymbol{Q}$ is chosen so that $\boldsymbol{HD}$ is diagonalized by the similarity transformation, that is $(\boldsymbol{Q}^{-1}\boldsymbol{HDQ})_{\ell m} = \Lambda_\ell \delta_{\ell m}$. The force matrix $\boldsymbol{D}$, and hence also $\boldsymbol{HD}$, has two eigenvectors with zero eigenvalue. The sum of elements in every row of $\boldsymbol{D}$ vanishes, hence any uniform vector with the same element in every position is an eigenvector of $\boldsymbol{D}$ with zero eigenvalue. This right eigenvector of $\boldsymbol{D}$, hence also of $\boldsymbol{HD}$, corresponds to uniform translation of all beads in the y-direction. It is readily verified that any vector with its j^{th} element proportional to $j - (N+2)/2$ is also an eigenvector of $\boldsymbol{D}$ with zero eigenvalue. This eigenvector of $\boldsymbol{D}$, hence also of $\boldsymbol{HD}$, is a shear motion that for small amplitudes corresponds to uniform rotation of the rod around its center of mass. The inertial terms are neglected for those normal coordinates with non-vanishing eigenvalue, but must be retained for those with vanishing eigenvalue. The Langevin equations for the normal coordinates are now written as

$$m\frac{d\dot{\rho}_1}{dt} + \gamma\dot{\rho}_1 = G_1(t) \tag{2.27a}$$

$$m\frac{d\dot{\rho}_2}{dt} + \gamma\dot{\rho}_2 = G_2(t) \tag{2.27b}$$

$$\gamma\dot{\rho}_\ell + \frac{\kappa_h}{h^2}\Lambda_\ell\rho_\ell = G_\ell(t);\ \ell = 3,4,\ldots N+1 \tag{2.27c}$$

For completeness, we note that $\boldsymbol{HD}$ is not generally symmetric, even though $\boldsymbol{H}$ and $\boldsymbol{D}$ are separately symmetric. Consequently, the right eigenvectors $(\mathbf{v}_\ell)$ of $\boldsymbol{HD}$, which are the columns of $\boldsymbol{Q}$, are not identical to the left eigenvectors $(\mathbf{u}_m{}^T)$, which are the rows of $\boldsymbol{Q}^{-1}$. Hence, $\boldsymbol{Q}^{-1} \neq \boldsymbol{Q}^T$. In general, the right eigenvectors $\mathbf{v}_\ell$ are not orthogonal to each other, and the same holds for the left eigenvectors $\mathbf{u}_\ell{}^T$. However, the right eigenvectors $\mathbf{v}_\ell$ are orthogonal to the left eigenvectors $\mathbf{u}_m{}^T$ belonging to different eigenvalues. This is seen by noting that

$$\mathbf{u}_m{}^T \cdot (\boldsymbol{HD}\mathbf{v}_\ell) = \Lambda_\ell \mathbf{u}_m{}^T \cdot \mathbf{v}_\ell = (\mathbf{u}_m{}^T\boldsymbol{HD}) \cdot \mathbf{v}_\ell = \Lambda_m \mathbf{u}_m{}^T \cdot \mathbf{v}_\ell \tag{2.28}$$

This implies that $\mathbf{u}_m{}^T \cdot \mathbf{v}_\ell = 0$ whenever $\Lambda_\ell \neq \Lambda_m$. In order for $\mathbf{v}_\ell$ and $\mathbf{u}_m{}^T$ to be, respectively, the columns of $\boldsymbol{Q}$ and rows of $\boldsymbol{Q}^{-1}$, it is also required that $\mathbf{u}_m^T \cdot \mathbf{v}_m^T = 1.0$.

Because $\boldsymbol{H}$ and $\boldsymbol{D}$ are symmetric, they are simultaneously diagonalized by the congruent transformations

$$\left(\boldsymbol{Q}^T \boldsymbol{D} \boldsymbol{Q}\right)_{pq} = \mu_p \, \delta_{pq} \tag{2.29}$$

$$\left(\boldsymbol{Q}^{-1} \boldsymbol{H} \boldsymbol{Q}^{-1T}\right)_{pq} = \nu_q \, \delta_{pq} \tag{2.30}$$

Eq. (2.29) is established by multiplying the right eigenvector relation $\boldsymbol{H}\boldsymbol{D}\mathbf{v}_q = \Lambda_q \mathbf{v}_q$ by $\boldsymbol{D}$ on the left to obtain $\boldsymbol{D}\boldsymbol{H}(\boldsymbol{D}\mathbf{v}_q) = \Lambda_q(\boldsymbol{D}\mathbf{v}_q)$. This last relation is recognized as the transpose of a left eigenvector relation, hence $\boldsymbol{D}\mathbf{v}_q = \mu_q \mathbf{u}_q$, where μ_q is a proportionality constant and $(\mathbf{u}_q)_\ell = u^T_{q\ell}$. Now making use of the fact that $Q_{m\ell} = v_{m\ell}$ (i.e. m^{th} element of $\mathbf{v}_\ell$), $(Q^T)_{\ell m} = v_{m\ell}$, and $(\boldsymbol{D}\mathbf{v}_q)_\ell = \sum_{(m)} D_{\ell m} v_{mq} = \mu_q \, u^T_{q\ell}$, we obtain

$$\begin{aligned}(\boldsymbol{Q}^T \boldsymbol{D} \boldsymbol{Q})_{pq} &= \sum_\ell \sum_m Q^T_{p\ell} D_{\ell m} Q_{mq} = \sum_\ell \sum_m v_{\ell p} D_{\ell m} v_{mq} \\ &= \sum_\ell v_{\ell p} \mu_q u^T_{q\ell} = \mu_q (\mathbf{u}_q{}^T \cdot \mathbf{v}_p) \\ &= \delta_{pq} \, \mu_q \quad ,\end{aligned} \tag{2.31}$$

which is identical to Eq. (2.29). The value of μ_q depends upon the normalization of the columns of Q. Eq. (2.30) is derived in a similar fashion by multiplying the left eigenvector relation by $\boldsymbol{H}$ on the right, etc.. We note also that

$$\begin{aligned}(\boldsymbol{Q}^{-1} \boldsymbol{H} \boldsymbol{D} \boldsymbol{Q})_{\ell m} = \Lambda_\ell \delta_{\ell m} &= (\boldsymbol{Q}^{-1} \boldsymbol{H} \boldsymbol{Q}^{-1T} \boldsymbol{Q}^T \boldsymbol{D} \boldsymbol{Q})_{\ell m} \\ &= \mu_\ell \nu_\ell \delta_{\ell m}\end{aligned} \tag{2.32}$$

Hence, $\mu_\ell \nu_\ell = \Lambda_\ell$. Analogous relations to Eqs. (2.28)-(2.32) were derived for the $\boldsymbol{H}\boldsymbol{A}$ matrix by Zimm (Zimm, 1956). Their validity depends only upon the symmetric nature of the product matrices that compose the dynamical matrix,

and the existence of distinct eigenvalues, except for the zero eigenvalues. For the latter, an orthogonal set of eigenvectors can be found. Indeed, the uniform translation and rotation eigenvectors discussed above are already orthogonal.

Eq. (2.29) is responsible for uncoupling the normal coordinates of the dynamical $\boldsymbol{HD}$ operator under equilibrium averaging. Inserting the normal coordinate transformation Eq. (2.25) into Eq. (2.10) for the potential energy, and making use of Eq. (2.29) gives

$$u = \frac{\kappa_h}{h^2} \sum_{\ell} \mu_\ell \rho_\ell^2 \quad . \tag{2.33}$$

Eq. (2.33) shows that the potential energy is exactly quadratic in the amplitudes ρ_ℓ of the normal coordinates of the $\boldsymbol{HD}$ matrix, so the different normal modes of $\boldsymbol{HD}$ are not coupled by the potential energy! It is expected generally that whenever pre-averaged hydrodynamic interactions are employed, they do not result in a circumstance where the normal coordinates of the dynamical operator are coupled by the potential energy. It is an advantage of treating the discrete bead model that this important point emerges so clearly.

2.2.7 Properties of the Bending Normal Modes ($\ell \geq 3$)

If the ℓ^{th} normal coordinate has the value $\rho_\ell(0)$ at $t = 0$, then the ensemble average (over all trajectories of the fluctuating force) of its subsequent extension is obtained directly from Eq. (2.27c),

$$< \rho_\ell(t) >= \rho_\ell(0) \exp(-t/\tau_\ell) \tag{2.34}$$

where

$$\tau_\ell = \gamma h^2/\kappa_h \Lambda_\ell = \gamma h^3/k_B T \; P\Lambda_\ell \tag{2.35}$$

is the Langevin relaxation time, k_BT is thermal energy, and $P = h\kappa_h/k_BT$ is the persistence length. The Langevin equation (27c) can also be multiplied on both sides by $\rho_\ell(0)$, ensemble averaged, and solved to yield the autocorrelation function

$$< \rho_\ell(0)\rho_\ell(t) >=< \rho_\ell(0)^2 > \exp(-t/\tau_\ell) \quad . \tag{2.36}$$

The mean-squared fluctuation about the relaxing mean-extension can also be obtained from Eq. (2.27c) (Schurr, 1976) as

$$\langle|\rho_\ell(t) - < \rho_\ell(t) > |^2\rangle =< \rho_\ell(0)^2 > (1 - \exp(-2t/\tau_\ell)) \quad . \tag{2.37}$$

Equations (2.34) and (2.36) require only properties of the fluctuating force already stated. Eq. (2.37) requires the additional assumption that all coefficients in the Fourier time-series of the fluctuating force have a vanishing ensemble average, a finite ensemble averaged square, and are not correlated with each other in ensemble averages (Schurr, 1976).

If it is further assumed that the fluctuating force is a Gaussian random variable, which may in fact be implied by the conditions for validity of Eq. (2.37), then the linearity of the Langevin equation insures that $\rho_\ell(t)$ is also a Gaussian random variable. In this case, the joint probability distribution is given by the usual product of the equilibrium initial and conditional probability distributions (Lin et al., 1978; Schurr. 1976: Uhlenbeck et al., 1930; Wang et al., 1945),

$$P(\rho_\ell(0))P(\rho_\ell(t)|\rho_\ell(0))d\rho_\ell(0)d\rho_\ell(t) = \exp\{-\rho_\ell(0)^2/2d_\ell^2\}\times$$

$$\frac{\exp\{-[\rho_\ell(t) - \rho_\ell(0)\exp(-t/\tau_\ell)]^2/2d_\ell^2(1 - \exp(-2t/\tau_\ell))\}}{2\pi d_\ell^2(1 - \exp(-2t/\tau_\ell))^{1/2}} \times d\rho_\ell(0)d\rho_\ell(t) \tag{2.38}$$

where $d_\ell^2 =< \rho_\ell(0)^2 >$ is the mean-squared extension of the ℓ^{th} normal mode.

Since an equation like (2.32) holds for each normal mode ($\ell \geq 3$), one may infer that the amplitudes of these normal modes are statistically independent at any time, including $t = \infty$ (equilibrium). This conclusion is consistent with that of the preceding section.

2.2.8 The $\ell = 1$ Normal Mode: Uniform Translation in the y-Direction

Eq. (2.27a) for the $\ell = 1$ mode is multiplied by $\dot{\rho}_1(0)$, ensemble averaged, and solved for the resulting autocorrelation function to obtain

$$< \dot{\rho}_1(0)\dot{\rho}_1(t) >=< \dot{\rho}_1(0)^2 > \exp(-\gamma t/m) \quad . \tag{2.39}$$

This is employed to obtain the diffusion coefficient D_1 along the $\ell = 1$ normal coordinate,

$$D_1 = \int_0^\infty < \dot{\rho}(0)\dot{\rho}_1(t) > dt = (m/\gamma) < \dot{\rho}_1(0)^2 > \quad . \tag{2.40}$$

The quantity $< \dot{\rho}_1(0)^2 >$ can be evaluated by expanding $\dot{\rho}_1(0)$ in terms of the $\dot{y}_j(0)$,

$$< \dot{\rho}_1(0)^2 >= \sum_{p=1}^{N+1} \sum_{q=1}^{N+1} (Q^{-1})_{1p}(Q^{-1})_{1q} < \dot{y}_p(0)\dot{y}_q(0) > \quad . \tag{2.41}$$

In this treatment, it is necessary to take account of the correlations between the bead velocities induced by the formally instantaneous hydrodynamic flow,

$$< \dot{y}_p(0)\dot{y}_q(0) >= \frac{k_B T}{m}(\delta_{pq} + \gamma T_{pq}) = \frac{k_B T}{m} H_{pq} \quad . \tag{2.42}$$

The γT_{pq} term represents the fluid velocity at the p^{th} bead due to the motion of the q^{th} bead (or vice versa). This is superimposed on the velocity of the p^{th}

bead and provides the only correlation between the motion of the p^{th} bead and that of the q^{th} bead. Combining Eqs. (2.41) and (2.42) yields

$$D_1 = (k_B T/\gamma) \sum_{p=1}^{N+1} \sum_{q=1}^{N+1} (Q^{-1})_{1p} H_{pq} (Q^{-1})_{1q} \ . \tag{2.43}$$

It is inferred directly from the Langevin equation (2.27a) that the probability distributions for $\dot{\rho}_1(t)$ and for $\rho_1(t) - \rho_1(0)$ must be gaussian. Eq. (2.40) implies that $< (\rho_1(t) - \rho_1(0))^2 > \ = 2D_1 t$. The $\ell = 1$ mode is evidently statistically independent of the other modes. The mean-squared displacement of any given bead in the rod, when only the uniform $\ell = 1$ mode is active, is given by

$$\begin{aligned} < (y_j(t) - y_j(0))^2 >_1 &= Q_{j1}^2 < (\rho_1(t) - \rho_1(0))^2 > \\ &= Q_{j1}^2 2D_1 t \end{aligned} \tag{2.44}$$

where the Einstein relation $< (\rho_1(t) - \rho_1(0))^2 >= 2D_1 t$ has been employed to obtain the second line. The normalization of the first column of $\boldsymbol{Q}$ is chosen so that

$$Q_{j1} = (N+1)^{-1/2}, \ \ j = 1, 2, \ldots N+1 \ , \tag{2.45}$$

hence $\sum_{j=1}^{N+1} Q_{j1}^2 = 1.0$. From Eqs. (2.44) and (2.45) we infer that the diffusion coefficient of the rod in the body-fixed y-direction is

$$D_{yy} = Q_{j1}^2 D_1 = \frac{1}{N+1} \frac{k_B T}{\gamma} \sum_{p=1}^{N+1} \sum_{q=1}^{N+1} (Q^{-1})_{1p} H_{pq} (Q^{-1})_{1q} \ . \tag{2.46}$$

An alternate approach to determining D_{yy} is to determine the friction factor Γ_y for uniform translation of the rod in the y-direction. The constant forces on the beads required to maintain a constant y-velocity of all the beads ($\dot{y}_0$) is given by

$$\mathbf{F}_y = \gamma(\dot{\mathbf{y}}_0 - \mathbf{v}) \ , \tag{2.47}$$

which is analogous to Eq. (2.21). Substitution of Eq. (2.14) into Eq. (2.47) and rearranging yields

$$\mathbf{F}_y = \gamma \boldsymbol{H}^{-1} \dot{\mathbf{y}}_0 \quad . \tag{2.48}$$

which is analogous to Eq. (2.22). The total force F_y^{tot} is obtained by summing the forces on the individual beads, as in Eq. (2.23). Use of the defining relation, $F_y^{\text{tot}} = \Gamma_y \dot{y}_0$, then yields

$$\Gamma_y = \gamma \sum_{\ell=1}^{N+1} \sum_{m=1}^{N+1} (\boldsymbol{H}^{-1})_{\ell m} \quad , \tag{2.49}$$

which is the expected result from the Kirkwood algorithm. Finally, the Stokes-Einstein relation gives

$$D_\perp = D_{yy} = k_B T / \Gamma_y \tag{2.50}$$

From symmetry considerations, $D_{xx} = D_{yy}$.

Despite their very different appearance, the diffusion coefficients in Eqs. (2.46) and (2.49-2.50) are identical. This can be seen by first writing Eq. (2.46) as

$$D_\perp = D_{yy} = \frac{k_B T}{(N+1)\gamma} (\boldsymbol{Q}^{-1} \boldsymbol{H} \boldsymbol{Q}^{-1T})_{11} \tag{2.51}$$

and Eq. (2.50) as

$$D_\perp = D_{yy} = \frac{k_B T}{(N+1)\gamma} \frac{1}{\left(\frac{1}{N+1}\right) \sum_{\ell=1}^{N+1} \sum_{m=1}^{N+1} (\boldsymbol{H}^{-1})_{\ell m}} \tag{2.52}$$

Now, begin with the identity $\boldsymbol{Q}^{-1} \boldsymbol{H} \boldsymbol{Q}^{-1T} \boldsymbol{Q}^T \boldsymbol{H}^{-1} \boldsymbol{Q} = \mathbf{1}$ in the form

$$\sum_{\ell=1}^{N+1} (\boldsymbol{Q}^{-1} \boldsymbol{H} \boldsymbol{Q}^{-1T})_{1\ell} (\boldsymbol{Q}^T \boldsymbol{H}^{-1} \boldsymbol{Q})_{\ell 1} = 1.0 \tag{2.53}$$

From Eq. (2.30), it is clear that only the $\ell = 1$ term in the sum is non-vanishing. Hence,

$$(\boldsymbol{Q}^{-1}\boldsymbol{H}\boldsymbol{Q}^{-1T})_{11} = \frac{1}{(\boldsymbol{Q}^{T}\boldsymbol{H}^{-1}\boldsymbol{Q}_{11})}$$
$$= \frac{1}{\left(\frac{1}{N+1}\right)\sum_{\ell=1}^{N+1}\sum_{m=1}^{N+1}(\boldsymbol{H}^{-1})_{\ell m}} \qquad (2.54)$$

In the final line use has been made of Eq. (2.45). Substitution of Eq. (2.54) into (2.51) yields (2.52), which completes the proof.

We have confirmed that numerical values obtained from Eqs. (46) and (49-50) are identical within limits set by computer round-off errors. In practice, we employ Eqs. (49-50), because that calculation is both simpler and less expensive. In general, it is simpler to invert $\boldsymbol{H}$ than $\boldsymbol{Q}$.

2.2.9 The $\ell = 2$ Normal Mode: Uniform Rotation Around the Instantaneous x-Axis

Eq. (2.27b) for $\dot{\rho}_2$ is developed precisely like Eq. (2.27a) for $\dot{\rho}_1$ and leads to expressions directly analogous to Eqs. (2.39)-(2.42) with the index 1 replaced by 2. In place of Eq. (2.43), we obtain

$$D_2 = \int_0^\infty < \dot{\rho}_2(0)\dot{\rho}_2(t) > dt = (k_B T/\gamma)(\boldsymbol{Q}^{-1}\boldsymbol{H}\boldsymbol{Q}^{-1T})_{22} \qquad (2.55)$$

for diffusion along the $\ell = 2$ normal coordinate. The elements of the eigenvector of the $\ell = 2$ normal coordinate are

$$Q_{n2} = b(n - (N+2)/2)\ , \quad n = 1, 2, \ldots N+1 \qquad (2.56)$$

where b is an arbitrary "normalization" constant. As noted above, this corresponds to a shearing motion. not a simple rotation. and can be indefinitely

large, due to the absence of constraints on the total rod length. The length constraints actually turn the shear into a rotation. The corresponding rotational diffusion coefficient is obtained as follows. If only the ρ_2 mode is active, the angular velocity of the rod z-axis around the instantaneous x-axis is

$$\omega_y = \frac{\dot{y}_{N+1}}{Nh/2} = \frac{Q_{N+1,2}\dot{\rho}_2}{Nh/2} = \frac{b}{h}\dot{\rho}_2 \tag{2.57}$$

Then, $< \omega_y(0)\omega_y(t) >= (b^2/h^2) < \dot{\rho}_2(0)\dot{\rho}_2(t) >$, and the rotational diffusion coefficient for the rod z-axis around the instantaneous x-axis is

$$\begin{aligned} D_R = \int_0^\infty < \omega_y(0)\omega_y(t) > dt &= (b^2/h^2)\int_0^\infty < \dot{\rho}_2(0)\dot{\rho}_2(t) > dt \\ &= (b^2/h^2)\frac{k_B T}{\gamma}(\boldsymbol{Q}^{-1}\boldsymbol{H}\boldsymbol{Q}^{-1T})_{22} \, . \end{aligned} \tag{2.58}$$

It is inferred directly from the Langevin equation (2.27b) that the probability distribution for $\dot{\rho}_2(t)$ must be gaussian. From Eq. (2.57) it follows that the probability distribution for $\omega_y(t)$, hence also for the angular displacement $\theta_y(t) - \theta_y(0)$ of the rod z-axis around its instantaneous x-axis, is similarly gaussian. Eq. (2.58) implies that

$$< (\theta_y(t) - \theta_y(0))^2 >= 2D_R t \, . \tag{2.59}$$

The $\ell = 2$ mode is evidently statistically independent of the other modes.

An alternate expression for D_R is derived from Eq. (2.48), when the elements of $\dot{\mathbf{y}}_0$ are replaced by $\dot{\mathbf{y}}_{0m} = \omega h(m - (N+2)/2)$, corresponding to uniform rotation with angular velocity ω_y. The total external torque T_y^{tot} required to maintain constant angular velocity is obtained by summing the torques due to the external forces on the individual beads,

$$\begin{aligned} T_y^{\text{tot}} &= \sum_{\ell=1}^{N+1} h\left[\ell - \frac{(N+2)}{2}\right] F_\ell \\ &= h^2\gamma \sum_{\ell=1}^{N+1}\sum_{m=1}^{N+1}\left[\ell - \frac{(N+2)}{2}\right](H^{-1})_{\ell m}\left[m - \frac{(N+2)}{2}\right] \end{aligned} \tag{2.60}$$

The rotational friction factor (Γ_R) is defined by $T_y^{\rm tot} = \Gamma_R \omega_y$. Use of the Stokes-Einstein relation, $D_R = K_B T/\Gamma_R$, finally yields

$$D_R = \frac{k_B T}{\gamma h^2} \frac{1}{\sum_{\ell=1}^{N+1}\sum_{m=1}^{N+1}[\ell - \frac{(N+2)}{2}](H^{-1})_{\ell m}[m - \frac{(N+2)}{2}]} \tag{2.61}$$

which is the expected result of the Kirkwood algorithm.

Eq. (2.61) can be derived from Eq. (2.58) by starting with the identity

$$\boldsymbol{Q}^{-1}\boldsymbol{H}\boldsymbol{Q}^{-1T}\boldsymbol{Q}^{T}\boldsymbol{H}^{-1}\boldsymbol{Q} = \mathbf{1}$$

in the form

$$\sum_{\ell=1}^{N+1} (\boldsymbol{Q}^{-1}\boldsymbol{H}\boldsymbol{Q}^{-1T})_{2\ell}(\boldsymbol{Q}^{T}\boldsymbol{H}^{-1}\boldsymbol{Q})_{\ell 2} = 1.0 \tag{2.62}$$

In view of Eq. (2.30), only the $\ell = 2$ term is non-vanishing. After dividing both sides by $(Q^T H^{-1} Q)_{22}$, and making use of Eq. (2.56), there results

$$(\boldsymbol{Q}^{-1}\boldsymbol{H}\boldsymbol{Q}^{-1T})_{22} = \frac{1}{b^2 \sum_{\ell=1}^{N+1}\sum_{m=1}^{N+1}[\ell - \frac{(N+2)}{2}](H^{-1})_{\ell m}[m - \frac{(N+2)}{2}]} \tag{2.63}$$

Insertion of Eq. (2.63) into Eq. (2.58) now yields Eq. (2.61), in which the normalization factors have cancelled out. We have confirmed that Eqs. (2.58) and (2.61) yield identical numerical values within limits set by computer round-off errors. In practice, we employ Eq. (2.60), again because it is easier to invert $\boldsymbol{H}$ than $\boldsymbol{Q}$.

2.2.10 Mean Squared Angular Displacement of A Bond Vector

The rotational dynamics of the rod is manifested in the mean squared angular displacements of its various bond vectors as a function of time. The $\ell = 1$ normal

mode does not contribute to rotation of any of the bond vectors. The net angular displacement of the m^{th} bond vector around the instantaneous x-axis in time t is

$$\Delta_{xm}(t) \equiv \theta_y(t) - \theta_y(0) + \eta_m(t) - \eta_m(0) \tag{2.64}$$

where $\theta_y(t) - \theta_y(0)$ is the contribution due to uniform rotation ($\ell = 2$ normal mode) and $\eta_m(t) - \eta_m(0)$ is the contribution due to the $\ell \geq 3$ bending normal modes. Now, making use of Eqs. (2.3) and (2.25) this can be written as

$$\Delta_{xm}(t) \equiv \theta_y(t) - \theta_y(0) + \frac{1}{h}\sum_{\ell=3}^{N+1}(Q_{m+1,\ell} - Q_{m\ell})(\rho_\ell(t) - \rho_\ell(0)) \tag{2.65}$$

After utilizing Eqs. (2.36), (2.59) and the statistical independence of the normal modes, there results

$$< \Delta_{xm}(t)^2 >= 2D_R t + (2/h^2)\sum_{\ell=3}^{N+1}(Q_{m+1,\ell} - Q_{m\ell})^2 < \rho_\ell(0)^2 > (1 - e^{-t/\tau_\ell}) \tag{2.66}$$

Eq. (2.66) is one of the main results of this work.

If the bond vector $\mathbf{h}_m$ coincides with the transition dipole of a fluorophore, then its fluorescence polarization anisotropy is readily obtained from previous results (Schurr, 1984; Schurr et al., 1989),

$$r(t) = (2/5)\exp(-6 < \Delta_{xm}(t)^2 > /2) \tag{2.67}$$

The calculation of $< \Delta_{xm}(t)^2 >$ is described in the following sections.

2.3 Numerical Computation

2.3.1 Numerical Computation of the Eigenvalues and Eigenvectors of $\boldsymbol{HD}$.

The eigenvalue problem

$$\boldsymbol{HD}\,\mathbf{v}_\ell = \Lambda_\ell \mathbf{v}_\ell \tag{2.68}$$

is solved by an algorithm similar to that employed by Lin and Schurr (Lin, et al., 1978).

First the eigenvalues λ_ℓ and eigenvectors $\mathbf{c}_\ell$ of the real symmetric matrix $\boldsymbol{D}$ are computed using the subroutine DEVCSF from the IMSL library.

$$\boldsymbol{D}\,\mathbf{c}_\ell = \lambda_\ell \mathbf{c}_\ell \tag{2.69}$$

As noted above, the first two eigenvalues vanish ($\lambda_1 = 0 = \lambda_2$), and their eigenvectors correspond to uniform translation and shear (or rotation). Both sides of Eq. (2.69) are printed out for each λ_ℓ and $\mathbf{c}_\ell$ in order to check the diagonalization subroutine DEVCSF. The initially unnormalized eigenvectors $\mathbf{c}'_\ell$ are normalized by the factors

$$N_\ell = \left(\sum_{m=1}^{N+1} {c'_{m\ell}}^2 \right)^{-1/2} , \tag{2.70}$$

where $c'_{m\ell}$ is the m^{th} element of $\mathbf{c}'_\ell$. The normalized eigenvectors of $\boldsymbol{D}$, namely $\mathbf{c}_\ell = N_\ell \mathbf{c}'_\ell$, are now orthonormal, hence the matrix $\boldsymbol{C}$ of elements $c_{m\ell}$ is unitary, so $\boldsymbol{C}^{-1} = \boldsymbol{C}^T$. The property $\boldsymbol{C}^T\boldsymbol{C} = \mathbf{1}$ is also checked by the program, which displays the product matrix $\boldsymbol{C}^T\boldsymbol{C}$ for operator inspection.

The matrix $\boldsymbol{D}^{1/2}$ is constructed according to the relation

$$\boldsymbol{D}^{1/2} = \boldsymbol{C}\boldsymbol{\lambda}^{1/2}\boldsymbol{C}^{-1} , \tag{2.71}$$

where $(\lambda^{1/2})_{\ell m} = \delta_{\ell m}(\lambda_\ell)^{1/2}$ is the diagonal matrix with square roots of the eigenvalues down the diagonal. It is readily verified that $\boldsymbol{D}^{1/2}\boldsymbol{D}^{1/2} = \boldsymbol{D}$, and that $\boldsymbol{D}^{1/2}$ is symmetric.

Multiplying Eq. (2.68) on the left by $\boldsymbol{D}^{1/2}$ gives

$$\boldsymbol{D}^{1/2}\boldsymbol{H}\boldsymbol{D}^{1/2}(\boldsymbol{D}^{1/2}\mathbf{v}_\ell) = \Lambda_\ell(\boldsymbol{D}^{1/2}\mathbf{v}_\ell) \tag{2.72}$$

The matrix $\boldsymbol{D}^{1/2}\boldsymbol{H}\boldsymbol{D}^{1/2}$ is obviously symmetric. Eq. (2.72) shows that the symmetric matrix $\boldsymbol{D}^{1/2}\boldsymbol{H}\boldsymbol{D}^{1/2}$ has the same eigenvalues as the non-symmetric matrix $\boldsymbol{H}\boldsymbol{D}$. The eigenvalue problem has now been reduced to one of the form

$$\boldsymbol{D}^{1/2}\boldsymbol{H}\boldsymbol{D}^{1/2}\mathbf{b}_\ell = \Lambda_\ell\mathbf{b}_\ell \ , \tag{2.73}$$

where the elements $b_{m\ell}$ of $\mathbf{b}_\ell$ are related to those $v_{m\ell}$, or $Q_{m\ell}$, of $\mathbf{v}_\ell$ by the relation

$$b_{m\ell} = (\boldsymbol{D}^{1/2}\mathbf{v}_\ell)m = (\boldsymbol{D}^{1/2}\boldsymbol{Q})_{m\ell} \tag{2.74}$$

Because $\boldsymbol{D}^{1/2}\boldsymbol{H}\boldsymbol{D}^{1/2}$ is symmetric, its eigenvectors are orthogonal. However, it is apparent from Eq. (2.74) that the $\mathbf{b}_\ell$ and $\mathbf{v}_\ell$ (or columns of $\boldsymbol{Q}$) cannot, in general, both be simultaneously normalized. We have already chosen to normalize the $\ell = 1$ column of $\boldsymbol{Q}$ in Eq. (2.45), and now also choose to normalize the $\ell = 2$ column of $\boldsymbol{Q}$, which was left arbitrary in Eq. (2.56). However, for the bending modes $\ell = 3, 4, \ldots N+1$, we choose to retain the normalization of the $\mathbf{b}_\ell$, and let the $\mathbf{v}_\ell$ (or columns of $\boldsymbol{Q}$) remain unnormalized. That is, ${\mathbf{b}_k}^T \cdot \mathbf{b}_\ell = \delta_{k\ell}$. This greatly simplifies the subsequent evaluation of $< \rho_\ell(0)^2 >$, because μ_ℓ in Eqs. (2.29), (2.31), (2.32) and (2.33) takes the value 1.0, as shown in the following section.

The eigenvalues Λ_ℓ and eigenvectors $\mathbf{b}_\ell$ of $\boldsymbol{D}^{1/2}\boldsymbol{H}\boldsymbol{D}^{1/2}$ are determined using the DEVCSF subroutine mentioned above. The initially unnormalized eigenvectors $\mathbf{b}'_\ell$ are multiplied by the factor

$$M_\ell = \left(\sum_{m=1}^{N+1} {b'_{m\ell}}^2\right)^{-1/2} \ , \tag{2.75}$$

where $b'_{m\ell}$ is the m^{th} element of $\mathbf{b}'_\ell$. Thus, for $\ell \geq 3$, the vectors $\mathbf{b}_\ell = M_\ell \mathbf{b}'_\ell$ are normalized. The $Q_{n\ell}$ are obtained by the following procedure. Multiply Eq. (2.74) by $(C^{-1})_{km}$ on the left and sum on m to obtain

$$\sum_{m=1}^{N+1} (C^{-1})_{km} b_{m\ell} = \sum_{n=1}^{N+1} \lambda_k^{1/2} (C^{-1})_{kn} Q_{n\ell} \ , \tag{2.76}$$

where use has been made of Eq. (2.71). Because $\lambda_1 = 0 = \lambda_2$, Eq. (2.76) is meaningful only for $k \geq 3$, and will be understood to be valid only when $k \geq 3$. In that case, Eq. (2.76) is multiplied by $(\lambda_k)^{-1/2}$ (which is not singular for $k \geq 3$) and C_{jk} and summed on k from $k = 3$ to $N+1$. This gives

$$\begin{aligned}\sum_{k=3}^{N+1} \sum_{m=1}^{N+1} (\lambda_k)^{-1/2} C_{jk} (C^{-1})_{km} b_{m\ell} &= \sum_{k=3}^{N+1} \sum_{n=1}^{N+1} C_{jk} (C^{-1})_{kn} Q_{n\ell} \\ &= \sum_{k=1}^{N+1} \sum_{n=1}^{N+1} C_{jk} (C^{-1})_{kn} Q_{n\ell} \\ &\quad - \sum_{n=1}^{N+1} (C_{j1} (C^{-1})_{1n} + C_{j2} (C^{-1})_{2n}) Q_{n\ell}\end{aligned} \tag{2.77}$$

Now, Eq. (2.77) is multiplied on both sides by $(\boldsymbol{HD})_{pj}$ and summed on j from 1 to $N+1$. The right-hand side becomes

$$\begin{aligned} rhs &= \sum_{j=1}^{N+1} (\boldsymbol{HD})_{pj} Q_{j\ell} \\ &\quad - \sum_{j=1}^{N+1} \sum_{n=1}^{N+1} (\boldsymbol{HD})_{pj} (C_{j1} (c^{-1})_{1n} + C_{j2} (c^{-1})_{2n}) Q_{n\ell} \\ &= \Lambda_\ell Q_{p\ell} \end{aligned} \tag{2.78}$$

where use has been made of the relation $(\boldsymbol{HDQ})_{p\ell} = \Lambda_\ell Q_{p\ell}$ in the first term, and of the relations $(\boldsymbol{HDC})_{p1} = 0 = (\boldsymbol{HDC})_{p2}$ (because $\mathbf{c}_1$ and $\mathbf{c}_2$ are eigenvectors with zero eigenvalue) in the second term. Dividing both sides of Eq. (2.78) by

Λ_ℓ yields

$$Q_{p\ell} = \frac{rhs}{\Lambda_\ell} = \frac{lhs}{\Lambda_\ell} = \Lambda_\ell^{-1} \sum_{k=3}^{N+1} \sum_{j=1}^{N+1} \sum_{m=1}^{N+1} (\boldsymbol{HD})_{pj} C_{jk} (C^{-1})_{km} (\lambda_k)^{-1/2} b_{m\ell} \tag{2.79}$$

for $\ell \geq 3$. The symbol lhs refers to the left hand side of Eq. (2.77) after multiplication by $(\boldsymbol{HD})_{pj}$, summation on j, and division by Λ_ℓ. Eq. (2.79) gives $Q_{p\ell}$ for $\ell \geq 3$ in terms of known quantities. Eq. (2.45) gives Q_{p1}. We also choose $C_{p2} = Q_{p2}$ to be a normalized column vector, so that

$$Q_{p2} = \frac{[p - \left(\frac{N+2}{2}\right)]}{(N(N+1)(N+2)/12)^{1/2}} \tag{2.80}$$

Eqs. (2.45), (2.79) and (2.80) suffice to determine $\boldsymbol{Q}$. Each Λ_ℓ and its associated right eigenvector $v_{m\ell} = Q_{m\ell}$ are checked by multiplying $\mathbf{v}_\ell$ by $\boldsymbol{HD}$ and comparing the result with $\Lambda_\ell \mathbf{v}_\ell$. Eq. (2.68) is fully satisfied for all $\ell = 1, 2, \ldots N+1$.

The bending relaxation times for the $\ell \geq 3$ normal modes are given in terms of Λ_ℓ by Eq. (2.35).

2.3.2 Evaluation of $< \boldsymbol{\rho_\ell(0)^2} >$

Eqs. (2.10) and (2.25) can be combined to yield the total potential energy in the form

$$\begin{aligned} \mathcal{U} &= \frac{\kappa_h}{2h^2} \boldsymbol{\rho}^T \boldsymbol{Q}^T \boldsymbol{D}\, \boldsymbol{Q}\, \boldsymbol{\rho} \\ &= \frac{\kappa_h}{2h^2} \sum_{k=1}^{N+1} \sum_{\ell=1}^{N+1} \rho_k \rho_\ell (\boldsymbol{Q}^T \boldsymbol{D}\, \boldsymbol{Q})_{k\ell} \end{aligned} \tag{2.81}$$

All terms with $k = 1, 2$ or $\ell = 1, 2$ can be omitted from the sum, since the first two columns of Q and rows of Q^T are eigenvectors of $\boldsymbol{D}$ with zero eigenvalue.

For $k, \ell \geq 3$, the matrix product can be written as

$$(\boldsymbol{Q}^T \boldsymbol{D} \boldsymbol{Q})_{k\ell} = (\boldsymbol{Q}^T \boldsymbol{D}^{1/2} \boldsymbol{D}^{1/2} Q)_{k\ell} = ((\boldsymbol{D}^{1/2} \boldsymbol{Q})^T \boldsymbol{D}^{1/2} \boldsymbol{Q})_{k\ell} = \mathbf{b}_k^T \cdot \mathbf{b}_\ell = \delta_{k\ell} \tag{2.82}$$

where use has been made of Eq. (2.74) and the orthonormality of the $\mathbf{b}_k$ for $k \geq 3$. Making use of Eq. (2.82) in (2.81) yields

$$\mathcal{U} = \frac{\kappa_h}{2h^2} \sum_{k=3}^{N+1} \rho_k^2 \tag{2.83}$$

Comparison with Eq. (2.33) shows that our choice of normalization is equivalent to setting $\mu_\ell = 1.0$ for $\ell \geq 3$. For any choice of normalization, $\mu_1 = 0 = \mu_2$. The equilibrium probability distribution for the normal modes is given by

$$P(\rho_3, \rho_4, \cdots \rho_{N+1}) \propto \exp\left(-\frac{\kappa_h}{k_B T h^2} \sum_{k=3}^{N+1} \rho_k^2\right) \tag{2.84}$$

This is evidently a product of gaussians with mean squared displacement

$$d_\ell^2 = < \rho_\ell^2 > = \frac{k_B T h^2}{\kappa_h} = h^3/P, \quad \ell \geq 3 \tag{2.85}$$

Hence, $< \rho_\ell(0)^2 > = h^3/P = < \rho_\ell(t)^2 >$.

2.3.3 Numerical Evaluation of the Diffusion Coefficients for Uniform Motion

The translational diffusion coefficient for motion along the body-fixed z-axis follows from Eq. (2.24)

$$D_{\|} = D_{zz} = \frac{k_B T}{\gamma \sum_{\ell=1}^{N+1} \sum_{m=1}^{N+1} ((\mathbf{1} + \boldsymbol{T}_{zz})^{-1})_{\ell m}} \tag{2.86}$$

where $(T_{zz})_{\ell m}$ is given by Eq. (2.18d), and the friction factor of a single bead is assumed to obey stokes' Law, $\gamma = 6\pi\eta a$, where a is the bead radius and η

the solvent viscosity. The translational diffusion coefficient $D_{\perp}$ for motion along the body-fixed y-axis is given by Eq. (2.52), where $\boldsymbol{H}$ is given by Eq. (2.20). Similarly, the diffusion coefficient for uniform rotation around the x-axis is given by Eq. (2.61). Inversion of the $(N+1) \times (N+1)$ matrices $(\mathbf{1} + \boldsymbol{T}_{zz})$ in Eq. (2.86), and $\boldsymbol{H}$ in Eqs. (2.52) and (2.61) are accomplished using the subroutine DLINRG from the IMSL library. In each case, the inversion is verified by taking the matrix product $(\mathbf{1} + \boldsymbol{T}_{zz})^{-1}(\mathbf{1} + \boldsymbol{T}_{zz}) = \mathbf{1}$ or $\boldsymbol{H}^{-1}\boldsymbol{H} = \mathbf{1}$.

Particular values of the parameters employed for all these calculations are $a = 15.9$ Å, and $h = 2a = 31.8$ Å. $T = 293$ K and $\eta = 0.01$ poise. For $N+1 = 10$ subunits, we obtain $D_{\parallel} = 4.7792 \times 10^{-7}$ cm^2/s, $D_{\perp} = 3.4467 \times 10^{-7}$ cm^2/s, $D_R = 2.4820 \times 10^5$ s^{-1}. These values may be compared with those predicted for a 318 Å long cylinder with a radius of 12.5 Å, characteristic of DNA, by the theory of Tirado and Garcia de la Torre (Schurr et al., 1989; Tirado et al., 1979), namely $D_{\parallel} = 4.89 \times 10^{-7}$ cm^2/s, $D_{\perp} = 3.44 \times 10^{-7}$ cm^2/s, $D_R = 2.34 \times 10^5$ S^{-1}. The translational diffusion coefficients of the present chain of beads with radius $a = 15.9$ Å agree very well with those predicted for the cylinder with a 12.5 Å radius, and the rotational diffusion coefficients are also rather close. This good agreement is the criterion for optimal choice of the bead radius.

2.3.4 Numerical Results and Comparison with Brownian Dynamics Simulations.

After numerical values of D_R, $Q_{m\ell}$, $\tau_\ell = \gamma h^3/k_B T\ P\Lambda_\ell$, and $< \rho_\ell(0)^2 >= h^3/P$ have been determined by methods described in the preceding three sections, $< \Delta x_m(t)^2 >$ is readily calculated from Eq. (2.66).

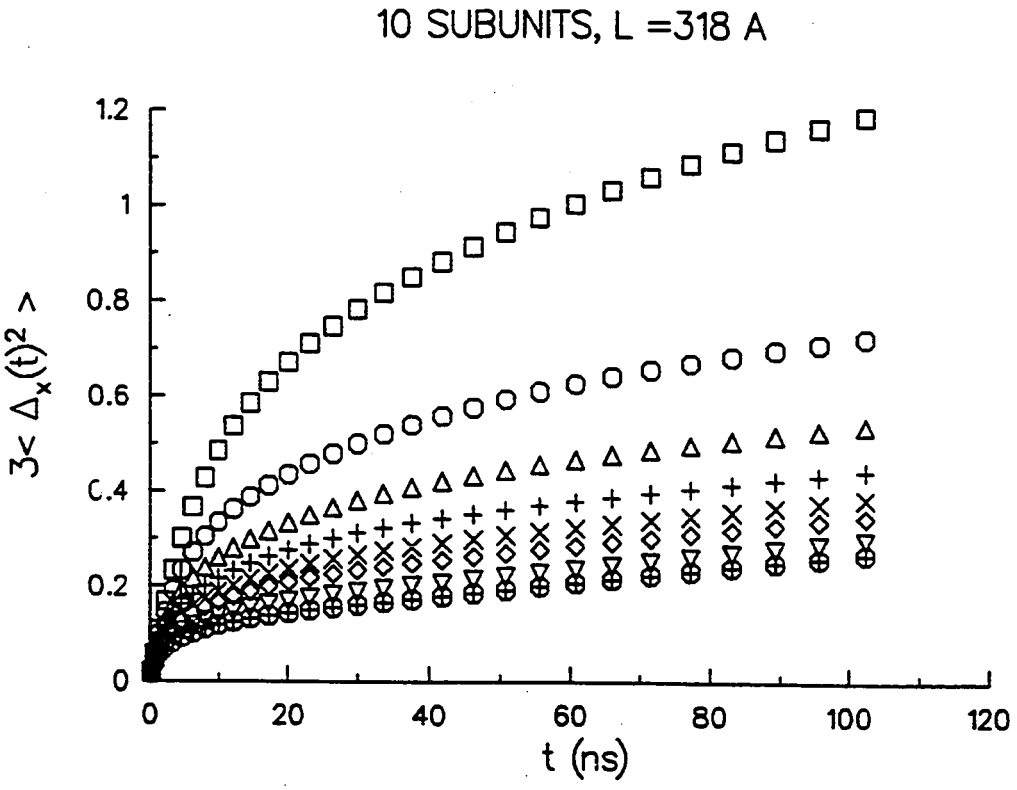

Figure 2.2. Three times the mean squared angular displacement around the $x-axis$ $< \Delta x_m(t)^2 >$ *vs.* t for the central bond vector of a 10-subunit rod with various persistence lengths. $3< \Delta x_m(t)^2 >$ are calculated from Eq. (66). Parameters employed are $L = 318$ Å, $h = 2a = 31.8$ Å. $T = 293K$, and $\eta = 0.01$ poise. (□): $P = 100$ Å, (○): $P = 200$ Å, (△): $P = 300$ Å, (+): $P = 400$ Å, (×): $P = 500$ Å, (◇): $P = 600$ Å, (▽): $P = 800$ Å, (⊕): $P = 1000$ Å.

Brownian dynamics simulations of discrete wormlike coils with preaveraged hydrodynamic interactions are carried out using the same procedures that were described previously (Allision et al., 1984; Allision, 1986). These simulations yield the fluctuating unit vector $\mathbf{u}_m(t) = \mathbf{h}_m(t)/h$ along the m^{th} bond vector in the laboratory frame. From that, the fluorescence polarization anisotropy is calculated using the relation (Schurr, 1984; Schurr et al., 1989)

$$r(t) = (2/5) < P_2(\mathbf{u}_m(t) \cdot \mathbf{u}_m(0)) > \tag{2.87}$$

Eqs. (2.67) and (2.87) are combined to give

$$3 < \Delta_{xm}(t)^2 >= -ln < P_2(\mathbf{u}_m(t) \cdot \mathbf{u}_m(0)) > \tag{2.88}$$

In order to examine the domain of validity of the normal mode theory, values of $3 < \Delta_{xm}(t)^2 >$ calculated for the central bond vector from Eq. (2.66) are compared with those obtained from the simulations via Eq. (2.88). The same parameters, $a = 15.9$ Å, $h = 2a = 31.8$ Å, temperature $T = 293$ K, and solvent viscosity $\eta = 0.01$ are employed in the simulations as in the normal mode theory. Both types of calculation are performed for different values of the persistence length P and numbers of subunits $N + 1$.

(1) Chains with $N + 1 = 10$ Subunits ($L = 318$ Å)

Values of $3 < \Delta_x(t)^2 >$ for the central bond vector ($m = 5$) of a 10-subunit chain are calculated from Eq. (2.66) for various persistence lengths and plotted vs. time in Figure 2.2. At any given time, $< \Delta_x(t)^2 >$ increases with decreasing persistence length, as expected.

Results from normal mode theory (Eq. (2.66)) are compared with those from Brownian dynamics simulations (Eq. (2.88)) for $P = 1000$ Å in Figure 2.3, for $P = 600$ Å in Figure 2.4, for $P = 400$ Å in Figure 2.5, and for $P = 100$ Å in Figure

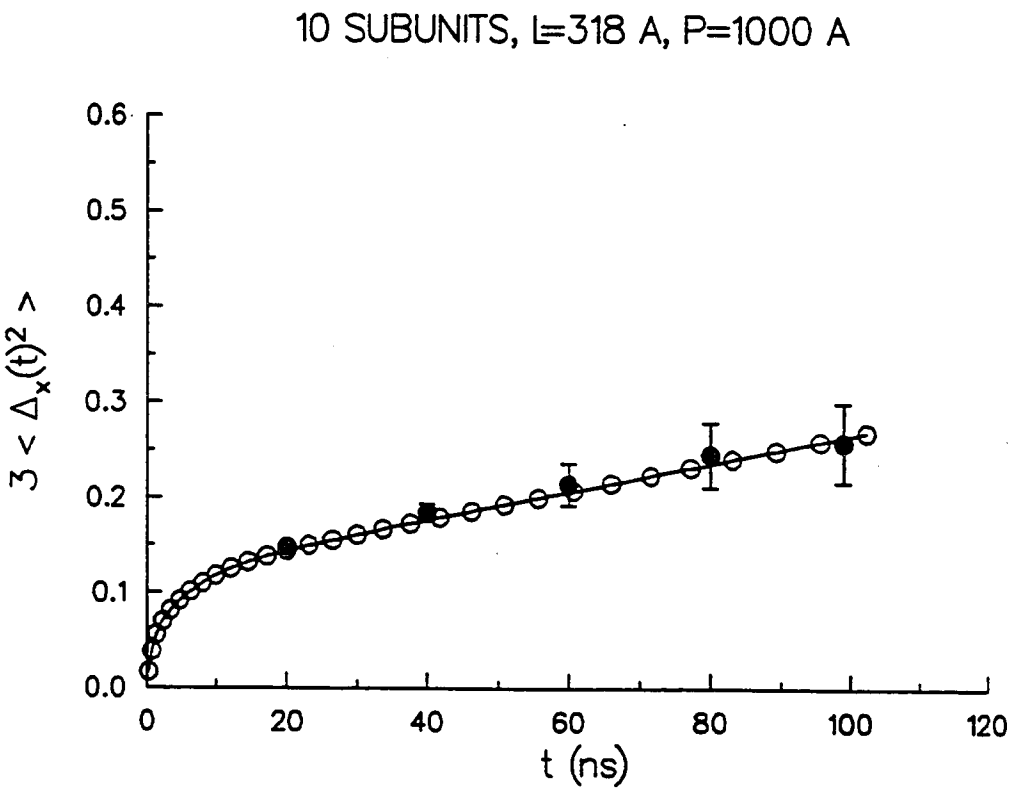

Figure 2.3. Comparision of the normal mode theory with Brownian dynamics simulations for the central bond vector of a 10-subunit rod with $P = 1000$ Å, $L = 318$ Å $(L/P = 0.318)$. $3< \Delta x_m(t)^2 > vs$ t. Solid circles (•) denote results of Brownian dynamics simulations obtained via Eq. (88). Open circles (○) denote results of normal mode theory calculated from Eq. (66). Parameters employed for both methods are $h = 2a = 31.8$ Å, $T = 293K$, and $\eta = 0.01$ poise.

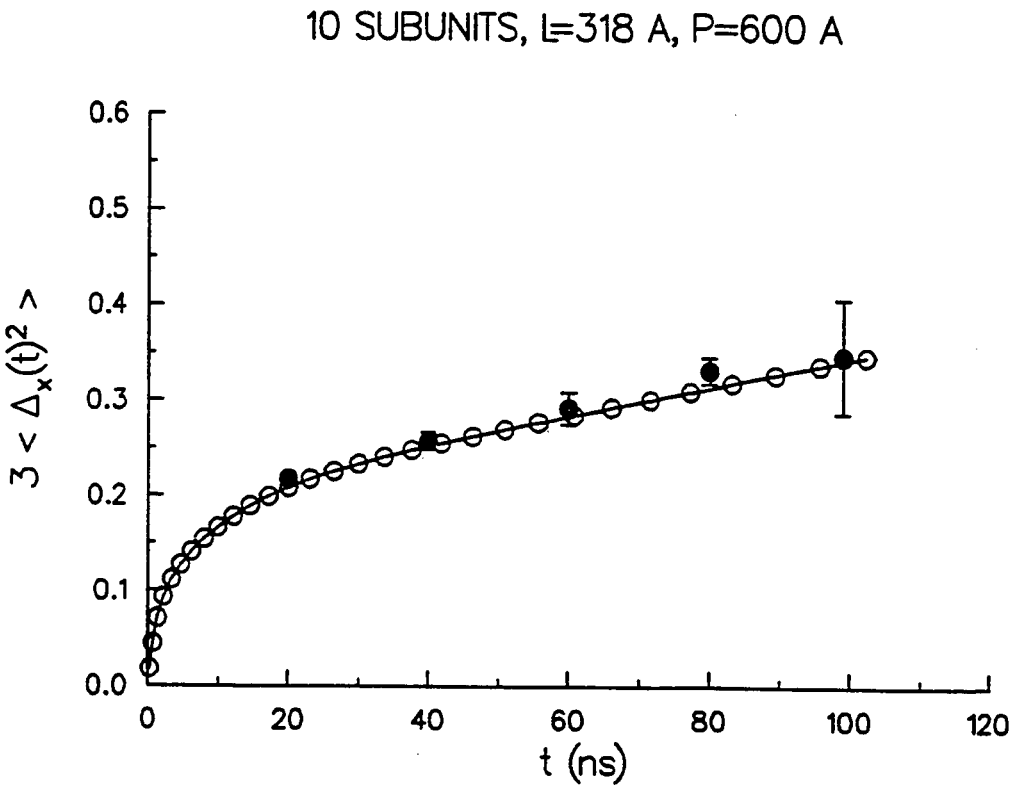

Figure 2.4. Comparision of normal mode theory with Brownian dynamics simulations for the central bond vector of a 10-subunit rod with $P = 600$ Å. $L = 318$ Å $(L/P = 0.53)$. $3 < \Delta x_m(t)^2 > vs \triangleright t$. Solid circles (•) denote results of Brownian dynamics simulations obtained via Eq. (88). Open circles (○) denote results of normal mode theory calculated from Eq. (66). Parameters employed for both methods are $h = 2a = 31.8$ Å, $T = 293K$, and $\eta = 0.01$ poise.

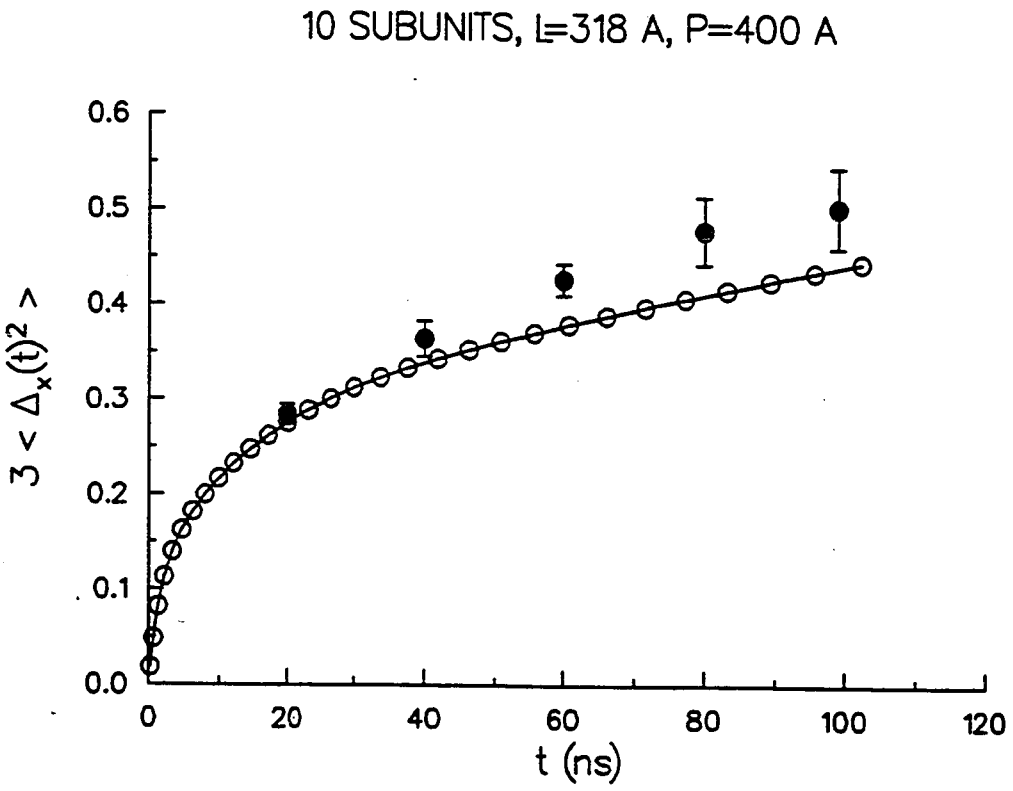

Figure 2.5. Comparision of normal mode theory with Brownian dynamics simulations for the central bond vector of a 10-subunit rod with $P = 400$ Å, $L = 318$ Å $(L/P = 0.795)$. $3< \Delta x_m(t)^2 >$ *vs.* t. Solid circles (•) denote results of Brownian dynamics simulations obtained via Eq. (88). Open circles (○) denote results of normal mode theory calculated from Eq. (66). Parameters employed for both methods are $h = 2a = 31.8$ Å, $T = 293K$, and $\eta = 0.01$ poise.

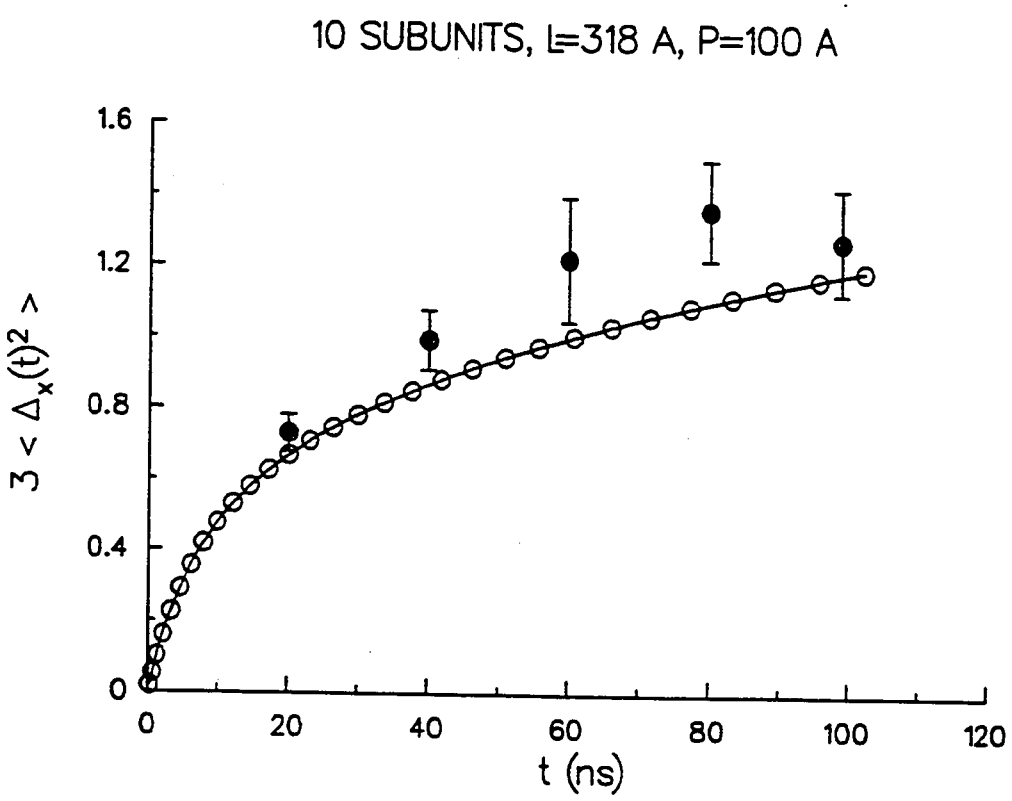

Figure 2.6. Comparision of normal mode theory with Brownian dynamics simulations for the central bond vector of a 10-subunit rod with $P = 100$ $\AA$, $L = 318$ $\AA$ ($L/P = 3.18$). $3< \Delta x_m(t)^2 >$ $vs\blacktriangleright$ t. Solid circles ($\bullet$) denote results of Brownian dynamics simulations obtained via Eq. (88). Open circles ($\bigcirc$) denote results of normal mode theory calculated from Eq. (66). Parameters employed for both methods are $h = 2a = 31.8$ $\AA$, $T = 293K$, and $\eta = 0.01$ poise.

2.6. For $P = 1000$ Å $(L/P = 0.32)$ and $P = 600$ Å $(L/P = 0.53)$, the agreement is excellent, well within the statistical errors of the simulations, over the range from 0 to 100 ns for which simulation data are available. For these stiffer chains, the bending modes have decayed away by 50 ns, leaving just the uniform rotational motion, which produces the constant slope $(d < \Delta_x(t)^2 > /dt)$ that is plainly apparent in Figures 2.3 and 2.4. Thus, for $L/P \leq 0.53$, the normal mode theory should continue to match the simulations at arbitrarily long times. For $P = 400$ Å $(L/P = 0.80)$, agreement is good for $t \lesssim 40$ ns, in the sense that the normal mode value of $< \Delta_x(t)^2 >$ lies only 6.5% below the simulation value at $t = 40$ ns. However, the agreement is significantly worse at longer times, as is evident from Figure 2.5. For $P = 100$ Å $(L/P = 3.18)$, agreement is fairly good for $t \lesssim 20$ ns, but a substantial discrepancy emerges at longer times, as is evident from Figure 2.6. In this case, the normal mode value of $< \Delta_x(t)^2 >$ lies below the simulated value by 16.4% at $t = 60$ ns.

We conclude that the normal mode theory works very well for sufficiently weakly bending rods $(L/P \leq 0.53)$ up to arbitrarily long times. However, as P decreases and the amplitude of bending increases, the domain of validity of the normal mode theory is restricted to ever smaller times. Thus, in the time zone where angular displacements are not yet large, violations of the weak bending approximation are evidently not so serious, and the normal mode theory continues to work rather well, even for $L/P = 3.18$.

(2) Chains with $N + 1 = 30$ Subunits $(L = 954$ Å$)$

Values of $3 < \Delta_x(t)^2 >$ for the central bond vector $(m = 15)$ of a 30-subunit chain are calculated from Eq. (2.66) for various persistence lengths and plotted vs. t in Figures 2.7 and 2.8. Corresponding values for $3 < \Delta_x(t)^2 >$ obtained

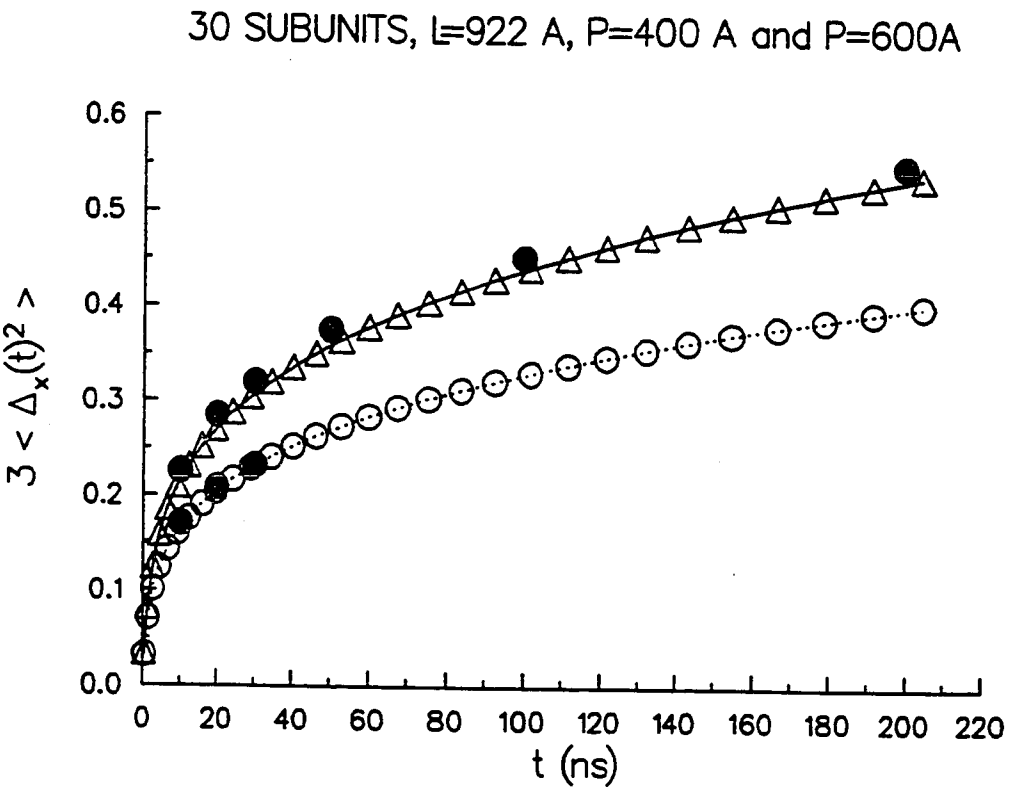

Figure 2.7. Comparision of normal mode theory with Brownian dynamics simulations for the central bond vector of a 30-subunit rod with $L = 922$ Å. $3< \Delta x_m(t)^2 >$ vs▷ t. Solid circles (•) denote results of Brownian dynamics simulations obtained via Eq. (88) for $P = 400$ Å and $P = 600$ Å. Results of normal mode theory calculated from Eq. (66) are denoted by open circles (○) for $P = 600$ Å ($L/P = 1.54$) and by triangles (△) for $P = 400$ Å ($L/P = 2.31$). Parameters employed for both methods are $h = 2a = 31.8$ Å, $T = 293K$, and $\eta = 0.01$ poise.

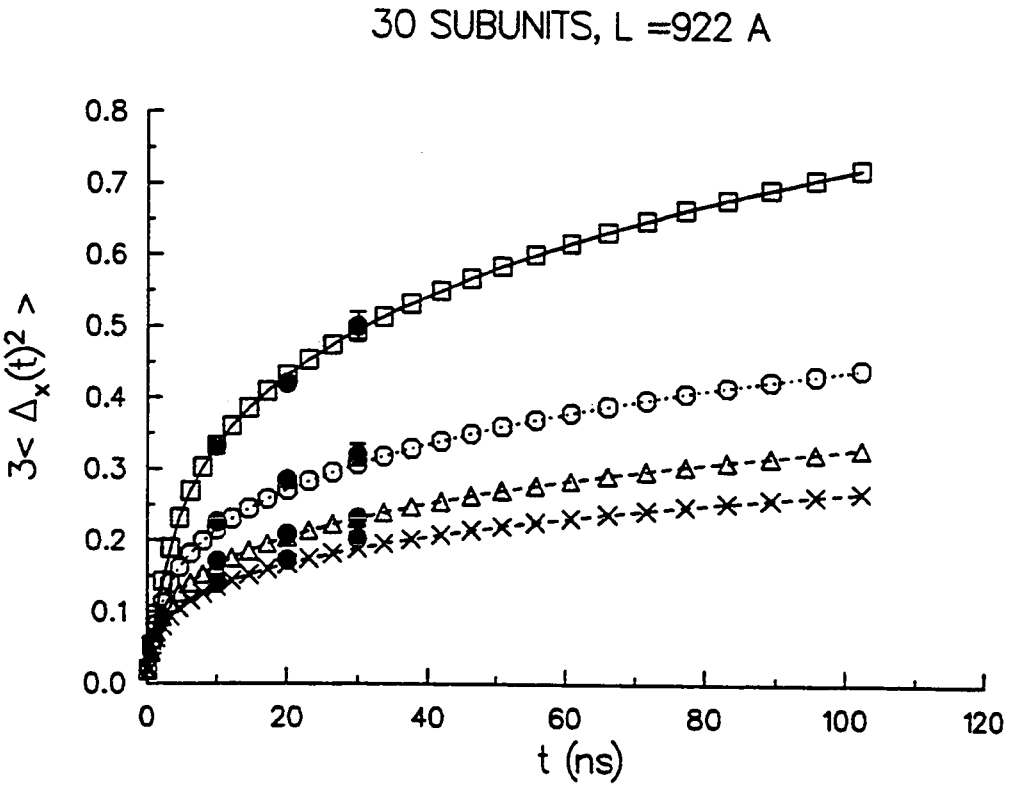

Figure 2.8. Comparision of normal mode theory with Brownian dynamics simulations for the central bond vector of a 30-subunit rod with $L = 922$ Å. $3< \Delta x_m(t)^2 >$ *vs.* t. Solid circles (•) denote results of Brownian dynamics simulations obtained via Eq. (88) for $P = 200$ Å, $P = 400$ Å, $P = 600$ Å, $P = 800$ Å. Results of normal mode theory calculated from Eq. (66) are denoted by squares (□) for $P = 200$ Å, circles (○) for $P = 400$ Å, triangles (△) for $P = 600$ Å and crosses (×) for $P = 800$ Å. Parameters employed for both methods are $h = 2a = 31.8$ Å, $T = 293K$, and $\eta = 0.01$ poise.

from Brownian dynamics simulations are co-plotted in these same figures. For $P = 400$ Å $(L/P = 2.39)$, the value of $< \Delta_x(t)^2 >$ from normal mode theory is 2.5% higher than that from the simulation at $t = 100$ ns, and is 1.9% higher at $t = 200$ ns, as shown in Figure 2.7. In comparison with results for 10-subunit chains, the normal mode theory works better for 30-subunit chains at comparable, or even longer, times. Comparison between the normal mode theory and the simulations for several different values of P is shown in Figure 2.8. Over the limited time-range of the simulations (0-30 ns), agreement is excellent even for P as small as 200 Å $(L/P = 4.77)$.

Several conclusions can be drawn from these comparisons of the normal mode theory with the Brownian dynamics simulations for 10- and 30-subunit chains. First, for weakly bending rods $(L \leq 0.53)$, the normal mode theory works very well at all times t. Second, for more strongly bending rods, the normal mode theory works appreciably better for (1) stiffer rather than more flexible rods of a given length, (2) shorter times for which the more rapidly relaxing normal modes dominate the relaxation, and (3) longer rather than shorter rods at the same time. Evidently, failure of the weak bending approximation is most serious for normal modes of low index (e.g. $k = 3$), and less serious for normal modes of higher index, even when the relaxation times and normal mode wavelengths are comparable.

Some of these observations can be partially rationalized as follows. As the rod bends, the beads do not actually move in straight lines perpendicular to the end-to-end vector as assumed in the normal mode theory, but travel in arcs. A given angular deflection of the rod in general requires a larger amplitude of rectilinear motion than arc motion. By constraining the bead motion to

be rectilinear, the present normal mode theory effectively underestimates the angular deflections of the rod in a given time, and this underestimation is relatively more severe for more flexible rods and longer times, where deflections are larger, as is evident in Figure 2.5 and 2.6. However, for the longer rods, the simulation no longer predicts larger angular displacements than the normal mode theory at the same, or even longer times. The origins of this effect are not yet understood, but are probably related to the effects of fluctuating tension along the chain, which is omitted from the normal mode theory, but is present in the realistic simulations. The effect of the fluctuating tension to retard the relaxation apparently increases rapidly with increasing chain length in this range of L/P values.

The Brownian simulations require much more computer time than the normal mode theory. For example, the simulation of $< \Delta x(t)^2 >$ up to $t = 100$ ns for the 10-subunit chain with $P = 400$ Å required 17 minutes of central processor unit (cpu) time on an Amdahl mainframe. In contrast, for the 10-subunit chain, evaluation of $< \Delta x(t)^2 >$ for all values of P and t in Figures 2.2-2.6 required 20 seconds of cpu time on a Micro-VAX-II. The quantity $\boldsymbol{D}$ depends only on $N+1$, while $\boldsymbol{H}$, Λ_ℓ, and $\boldsymbol{Q}_{n\ell}$ depend in general only on $N+1$, h, and a, but not upon P, γ, or t. In fact, when $h = 2a$, and Eq. (2.20) is employed, as done here, then $\boldsymbol{H}$, Λ_ℓ and $Q_{m\ell}$ also depend only on $N+1$, independent of h and a. Once the Λ_ℓ and $Q_{m\ell}$ are determined for a given value of $N+1$, Eq. (2.66) can be evaluated for many different values of γ, P, $h = 2a$, and t in almost negligible additional computer time. Thus, the normal mode theory can be used in a practical way to fit extensive experimental data involving $< \Delta x(t)^2 >$, such as fluorescence or absorbance polarization anisotropy data, to Eq. (2.66) by adjusting P. The more computationally intensive determination of Λ_ℓ and $Q_{m\ell}$ needs to be done

only once at the outset, but not on each least-squares iteration.

A particular advantage of the normal mode theory is that it provides a simple determination of the longest bending relaxation time. This is employed in the following companion paper to estimate the dynamic persistence length, or dynamic bending rigidity of DNA.

An analytical theory of dynamic light scattering from weakly bending rods that is based on the present normal mode theory will appear in a subsequent publication.

2.3.5 Program QQ9.FOR

Program QQ9.FOR (see Appendix C) was created to do the numerical computations. Subroutine DEVCSF in IMSL library was called to calculate eigenvalues and eigenvectors of a real symmetric matrix. Subroutine DLINRG in IMSL library was called to calculate the inverse of a matrix. The relaxtion times for each normal mode and the mean square angular displacement are calculated. Program QQ9.FOR also outputs the eigenvalues and eigenvectors of **HD** matrix so that they can also be used in the calculation of diffusion coefficient of a weakly bending rod in Program CORLAT.FOR (see Appendix D).

Chapter 3
Dynamic Bending Rigidity of DNA

3.1 Introduction

Thermally excited bending of DNA produces an equilibrium root-mean -squared (rms) curvature at each base-pair, which in turn gives rise to a finite equilibrium persistence length. Over the past two decades, the equilibrium persistence lengths (P) of different DNAs have been measured in order to determine their bending rigidities ($\kappa = k_B T\ P$) and the dependence of those rigidities on various factors, such as salt concentration and temperature (Bloomfield, et al., 1974; Schurr, et al., 1986). The simple relation, $\kappa = k_B T\ P$, is predicated on the assumption that the unstrained DNA is straight (Bloomfield, et al., 1974), in which case permanent bends make no contribution to the apparent flexibility. The possible enhancement of apparent flexibility, or reduction in apparent P, by permanent bends is discussed subsequently. Equilibrium persistence lengths have been measured by a wide variety of methods that are sensitive to the equilibrium rms curvature, including static light scattering (Yamakawa, et al., 1974; Mandel, et al., 1980; Borochov, et al., 1981; Kam, et al., 1981; Borochov, et al., 1984; Thomas, et al, 1983) magnetic birefringence (Maret, et al., 1983), flow dichroism (Rizzo, V., et al., 1981; Baase, et al., 1984) and birefringence (Cairney, et al., 1982), transient electric dichroism (Diekmann, et al., 1982; Pörschke, et al. 1987) and birefringence (Hagerman, 1981; Elias, et al., 1981), sedimentation (Kovacic, et al. 1976; Yamakawa, et al., 1973), intrinsic viscosity (Yamakawa, et al., 1974; Odijk, 1979), analysis of relative rates of circularization of small DNAs of different length (Shimada, et al., 1984), analysis of the distribution of topoisomers formed by ligating small DNAs of different length (Shimada, et al., 1985), electron microscopy

(Griffith, 1988; Théveny, et al., 1988), and light microscopy of fluorescent stained DNAs (Yanagida, et al., 1983; Smith, et al., 1989). Possible problems with the interpretation of some of these data, and contradictory results regarding the magnitude of the salt-dependence of P over the range 0.01 M to 1.0 M are briefly reviewed elsewhere (Schurr, 1986). Despite the problems, there is now a consensus that P lies in the range 450-500 Å for native DNAs in 0.1 M NaCl (Schurr. 1986). Somewhat larger values (600-650 Å) are obtained from analyses of sedimentation coefficients, intrinsic viscosities, and circularization rates or topoisomer distributions of small DNAs, but these may be overestimates due to the neglect of electrostatic repulsions, or excluded volume interactions, in the theories employed (Kovacic, et al., 1976; Yamakawa. et al., 1973; Yamakawa. et al., 1974; Shimada, et al., 1984; Shimada, et al., 1985). Similar remarks apply to the still higher estimates ($P = 700 - 800$ Å) obtained from light microscopy of rather large DNAs (Yanagida, et al., 1983; Smith. et al., 1989). For DNAs in 2 mM Na^+, several groups report (Maret, et al., 1983) $P \cong$580-750 Å, although values as high as 800 Å are also reported.

It must be emphasized that the measurements and values cited above pertain to equilibrium or static bending of DNA, specifically to equilibrium populations of variously bent DNAs. None of these measurements is dynamic in the sense that it monitors the flexing of DNA per se as a function of time. One may well ask whether the dynamic bending rigidity that governs the temporal bending process on time-scales of a microsecond or less, is the same as the static value that governs the equilibrium, or static, persistence length. The dynamic bending rigidity can in principle be obtained from transient photodichroism experiments (Hogan. et al., 1989; Allison. et al., 1989) and from rapid initial transients in the off-field decay of the electric dichroism (Diekmannn, et al., 1982; Pörschke, et al.,

1987). The necessary Brownian dynamics simulation techniques (Allison, et al., 1989) and analytical theory (Song, et al., 1989) required to treat such experiments were just recently developed. Other dynamical experiments, such as polarized and depolarized dynamic light scattering and transient electric birefringence may also eventually yield the dynamic bending rigidity, but the necessary theory is still under development.

There are previous indications that the dynamic bending rigidity may substantially exceed the consensus static value. It was noted that the Barkley-Zimm (BZ) bending theory (Barkley, et al., 1979) with a persistence length $P = 500$ Å substantially overestimates the mean-squared angular displacements of 600 bp DNAs (Hogan, et al., 1989) at times longer than 200 ns, where bending dominates the rotational relaxation (Allison, et al., 1984). The possibility that this discrepancy arises from a failure of the BZ bending theory was considered, but subsequent simulations by Allison and coworkers (Allison, et al., 1984; Allison, et al., 1986) showed that the BZ theory works surprisingly well for short DNAs. One must now give considerable weight to the alternate possibility that the BZ bending theory is not greatly in error, but instead the dynamic bending rigidity (κ_d) is much larger than the static value inferred from the equilibrium persistence length. Indeed, recent Brownian dynamics simulations of the transient photodichroism of a 209 bp restriction fragment in 10 mM Tris show that a dynamic persistence length ($P_d = \kappa_d / k_B T$) $P_d = 1250$ Å best fits the experimental data. This value is somewhat uncertain due to the anomalously low initial anisotropy of the experimental data, more specifically to our present lack of detailed knowledge regarding that. This problem is reviewed briefly elsewhere (Schurr, et al., 1989). Nevertheless, it is rather unlikely that the dynamic bending rigidity of this DNA is not at least twice as great as the

consensus value of 500 Å.

In this work we use a normal mode theory for weakly bending rods that is developed in the companion paper(Song, et al., 1989) to analyze fast initial transients in the off-field decay of the electric dichroism (Diekmann, et al., 1982; Pörschke, et al., 1987). The close agreement of that theory in its domain of validity with Brownian dynamics simulations inspires considerable confidence in the results of the present analysis.

3.2 Experimental Background

In the experiments to be analyzed, DNA restriction fragments containing 95 to 250 bp are first partially aligned during square electric field pulses of up to 60 kV/cm. The important signal for present purposes is the decay of the dichroism after the field is switched off. The dichroism $A(t)$ is calculated from the time-resolved absorbances $A_{\parallel}(t)$ and $A_{\perp}(t)$ for 260 nm light with polarizations parallel and perpendicular, respectively, to the direction of the electric field according to $A(t) = A_{\parallel}(t) - A_{\perp}(t)$. The original data were analyzed using a double-exponential decay for the theoretical anisotropy (Diekmannn, et al., 1982; Pörschke, et al., 1987),

$$A(t) = A_1 e^{-6D_R t} + A_2 e^{-t/\tau} \tag{3.1}$$

where D_R is the rotational diffusion coefficient for the uniform end-over-end tumbling mode, and τ is tentatively assigned to a bending mode. In weak electric fields the uniform mode is observed to dominate the decay ($A_1/A_2 \gg 1.0$) and to relax much more slowly than the bending mode ($6D_R \ll 1/\tau$). The relative amplitude of the fast component (A_2/A_1) rises with increasing field strength to

a plateau value that varies from 0.4 for 95 bp to 1.4 for 250 bp.

3.3 Theory

The $N+1$ base-pairs in each DNA are labelled with an index j ($j = 1.2,\ldots N+1$). Each base-pair is regarded as a rigid subunit with a body-fixed coordinate system (x,y,z) such that the z-axis lies along the local symmetry axis of the molecule. The laboratory coordinate frame (x_L, y_L, z_L) is chosen so that z_L lies along the electric field. We use the azimuthally, or cylindrically, averaged cross sections $a_{\parallel}$ and $a_{\perp}$ for absorption of a photon with polarizations parallel and perpendicular, respectively to the z-axis of the base-pair considered. We focus first on the contribution to the dichroism from all base-pairs in the sample with the same index j. The instantaneous orientation of the z-axis of the j^{th} subunit in a particular molecule in the laboratory frame is $\Omega(t) = (\theta(t), \phi(t))$, where $\theta(t)$ is the polar angle with respect to the laboratory z-axis, and $\phi(t)$ is the usual azimuthal angle. The cross section for absorption of a photon polarized parallel to z_L is

$$\begin{aligned} a_{z_L}(t) &= a_{\perp} + (a_{\parallel} - a_{\perp})\cos^2\theta(t) = a_0 + \delta(\cos^2\theta(t) - 1/3) \\ &= a_0 + (2\delta/3)(4\pi/5)^{1/2} Y_{20}(\Omega(t)) \end{aligned} \tag{3.2}$$

where $a_0 = (\alpha_{\parallel} + 2\alpha_{\perp})/3$ is the isotropic (spherically averaged) cross section, $\delta = a_{\parallel} - a_{\perp}$ is the anisotropy of the cross section, and $Y_{20}(\Omega(t))$ is a spherical harmonic. Similarly, the cross section for absorption of a photon polarized

parallel to x_L is

$$\begin{aligned} a_{x_L}(t) &= a_\perp + (a_\parallel - a_\perp)\sin^2\theta(t)\cos^2\phi(t) \\ &= a_0 + \delta(\sin^2\theta(t)\cos^2\phi(t) - 1/3) \\ &= a_0 + (\delta/3)\Big\{ -(4\pi/5)^{1/2} Y_{20}(\Omega(t)) \\ &\quad + 3(2\pi/15)^{1/2}\left[Y_{22}(\Omega(t)) + Y_{2-2}(\Omega(t))\right]\Big\} \end{aligned} \tag{3.3}$$

At the moment the electric field is switched off (i.e. at $t = 0$) the solid angular distribution of z-axes of the j^{th} subunits of all DNAs in the laboratory frame is cylindrically symmetric about z_L and given by

$$P_j(\Omega(0)) = \sum_\ell b_{j\ell} Y_{\ell 0}(\Omega(0)) \quad , \tag{3.4}$$

wherein only $m = 0$ spherical harmonics (proportional to Legendre polynomials) appear due to the cylindrical symmetry. The coefficients $b_{j\ell}$ in general vary with index (ℓ), position (j) of the base-pair in the DNA, and the DNA flexibility, and in any case depend on the strength and duration of the orienting electric field pulse. For present purposes, it is not necessary to know how $b_{j\ell}$ varies with ℓ, j, bending rigidity, and electric field pulse parameters. The average difference in cross sections for absorption of photons polarized parallel to z_L and x_L by the j^{th} base-pairs at time t is

$$< A_j(t) > \equiv \int d\Omega(t) \int d\Omega(0)(\alpha_{z_L}(t) - \alpha_{x_L}(t)) g(\Omega(t)|\Omega(0)) P_j(\Omega_0) \tag{3.5}$$

where

$$g(\Omega(t)|\Omega(0)) = \sum_\ell c_\ell(t) \sum_m Y_{\ell m}(\Omega(t)) Y^*_{\ell m}(\Omega(0)) \tag{3.6}$$

is the conditional probability that a subunit with orientation $\Omega(0)$ at time $t = 0$ has rotated to $\Omega(t)$ at time t, and $c_\ell(t) = 4\pi < Y_{\ell 0}(\Omega(0) Y_{\ell 0}(\Omega(t)) >$ is an average property of the equilibrium isotropic solution (Schurr, et al., 1989; Allison, et al.,

1979; Schurr, 1984). After substituting Eqs. (2), (3), (4) and (6) into Eq. (5) and performing the integrals there results

$$< A_j(t) >= \delta(4\pi/5)^{1/2} b_{j2} 4\pi < Y_{20}(\Omega(0)) Y_{20}(\Omega(t)) > ; \qquad (3.7)$$

Eq. (7) applies for arbitrary reorientation mechanisms. We now assume that DNA exhibits mean local cylindrical symmetry. The quantity $4\pi <$ $Y_{20}(\Omega(0))Y_{20}(\Omega(t)) >$ is just 5/2 times the fluorescence (or absorbance) polarization anisotropy following an infinitely short exciting (or photobleaching) pulse of polarized light for the case when the transition dipole lies along the local symmetry axis. The previously derived result, Eq. (48) of reference (Schurr, 1984), can be taken over directly to obtain

$$< A_j(t) >= \delta(4\pi/5)^{1/2} b_{j2} \exp[-6 < \Delta_{xj}(t)^2 > /2] , \qquad (3.8)$$

where $< \Delta_{xj}(t)^2 >$ is the mean-squared angular displacement of the j^{th} base-pair around its instantaneous x-axis in time t.

We now assume that the actual filament can be replaced by a chain of contiguous spherical subunits with radii a=15.9 Å and with linearly scaled absorbance cross sections and anisotropies $\Delta = (2(15.9)/3.4)\ \delta = 9.35\ \delta$. Eq. (7) with Δ in place of δ applies for this discrete bead filament. We further assume that $< \Delta_{xj}(t)^2 >$ can be approximated by the mean-squared angular displacement of the bond vector from the center of the j^{th} subunit to the center of the $(j+1)^{th}$ subunit. For a sufficiently long filament, this should be a satisfactory approximation. For a short filament there are $N+1$ subunits, but only N bond vectors, so the final sum over bond vectors must be multiplied by the ratio $(N+1)/N$ to obtain the total absorbance anisotropy. For weakly bending DNAs we can now employ Eq. (66) of the preceding paper(Song et al., 1989) in the

form

$$< \Delta_{xj}(t)^2 >= 2D_R t + 2(h/P_d) \sum_{\ell=3}^{N+1} (Q_{j+1,\ell} - Q_{j\ell})^2 (1 - e^{-t/\tau_\ell}) \qquad (3.9)$$

where h is the rise per base-pair, τ_ℓ is relaxation time of the bending normal mode with index ℓ and the $Q_{j\ell}$ are matrix elements of the similarity transformation that diagonalizes the dynamical operator. Protocols for determining the eigenvalues Λ_ℓ and eigenvectors (columns of $\boldsymbol{Q}$) of the dynamical operator, and the relaxation times τ_ℓ are described in the preceding paper (Song, et al., 1989). Eq. (85) of that same paper is also incorporated into Eq. (9).

The normal mode theory in the preceding paper applies rigorously to weakly bending rods, for which the terms in Eq. (9) containing the sums are small compared to 1.0. In that case, one can expand the exponential factor

$$exp\left\{ + \frac{6h}{P_d} \sum_{\ell \geq 3}^{N+1} (Q_{j+1,l} - Q_{j,l})^2 e^{-t/\tau_l} \right\} \cong 1 + \frac{6h}{P_d} \sum_{\ell \geq 3}^{N+1} (Q_{j+1,l} - Q_{j,l})^2 e^{-t/\tau_l} \quad (3.10)$$

Combining Eqs. (8)-(10), substituting $\Delta = 9.35\ \delta$, and summing on j (with inclusion of (N+1)/N) yields the total anisotropy

$$A(t) = \frac{(N+1)}{N} \Delta (4\pi/5)^{1/2} \left\{ a_1\ e^{-6D_R t} + \sum_j b_{j2} E_j \frac{6h}{P_d} \times \right.$$
$$\left. \sum_{\ell \geq 3} (Q_{j+1,l} - Q_{j,l})^2\ \ e^{-(6D_R + 1/\tau_\ell)t} \right\} \qquad (3.11)$$

where

$$a_1 = \sum_j b_{j2} E_j \qquad (3.12)$$

and

$$E_j = e^{-\frac{6h}{P_d} \sum_{m \geq 3} (Q_{j+1,m} - Q_{j,m})^2} \qquad (3.13)$$

The longest bending mode ($\ell = 3$) contributes about half the total mean squared angular displacement due to bending, and its relaxation time exceeds

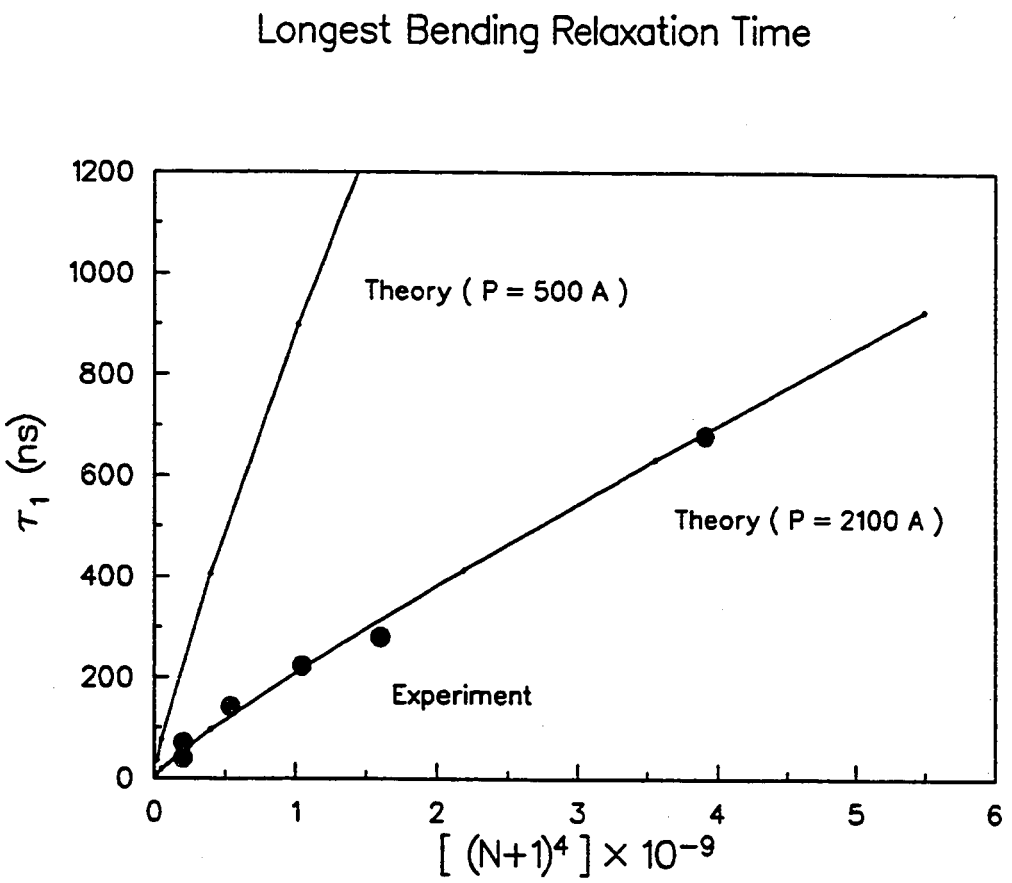

Figure 3.1. Relaxation time τ of the longest bending normal mode vs. $(N+1)^4$, where N+1 is the number of base-pairs in each restriction fragment. Filled circles (•) represent data reported by Diekmann et al. (Diekmannn, et al., 1982) and Pörschke et al. (Pörschke, et al., 1987) Solid lines are " curves " calculated for a dynamic persistence length P_d = 500 Å and P_d = 2100 Å, as indicated. Details of the model are described in the text.

that of the next longest mode ($\ell = 4$) by nearly an order of magnitude. Thus, the relaxation due to bending will be dominated by the $\ell = 3$ mode during the last half of the bending relaxation. when $t > \tau_4$. For such times it is permissible to omit all $l \geq 4$ terms in the final summation of Eq. (11), in which case A(t) takes the form of Eq.(1) with

$$A_1 = ((N+1)/N)\Delta(4\pi/5)^{1/2}a_1 \tag{3.14}$$

$$A_2 = ((N+1)/N)\Delta(4\pi/5)^{1/2}a_2 \tag{3.15}$$

$$a_2 = \sum_j b_{j2}E_j\frac{6h}{P_d}(Q_{j+1,3} - Q_{j3})^2 \tag{3.16}$$

$$1/\tau = 6D_R + 1/\tau_3 \tag{3.17}$$

Typically, $1/\tau$ exceeds $6D_R$ by more than a factor of 10 (Diekmann, et al., 1982). Hence, the error incurred by setting

$$\tau_3 = \tau \tag{3.18}$$

is less than 10%, which is less than the experimental uncertainty in τ ($\pm$15%). According to Eq.(18), the fast component resolved in the off-field relaxation of the electric dichroism is essentially that of the longest bending mode.

3.4 Analysis of the Data

3.4.1 Relaxation Times

The relaxation times of the fast components reported by Diekmann et al. (Diekmannn, et al., 1982) and Pörschke et al. (Pörschke, et al., 1987) are plotted vs. $(N+1)^4$ in Figure 1. The near proportionality between these relaxation times

and $(N+1)^4$ is a characteristic signature for long-wavelength bending normal modes. The longest bending relaxation times are calculated for DNAs of different length from Eq.(35) of the preceding companion paper using $P_d = 500$ Å in one case, and using $P_d = 2100$ Å in the other. The other parameters of the filament, namely subunit radius $a = 15.9$ Å and subunit spacing $h = 31.8$ Å, are the same as employed in the preceding paper. In the present calculations we use T=294 K and $\eta = 0.0098$ poise, corresponding to the experimental conditions. The theoretical points are connected to yield the solid "curves" in Figure 1. Clearly, the experimental relaxation times are much too short in comparision with the curve calculated for $P_d = 500$ Å, but are in excellent agreement with that calculated for $P_d = 2100$ Å. We infer that the dynamic persistence length of this DNA during the first several hundred nanoseconds after the electric field is switched off is approximately $P_d = 2100$ Å. This is about four times greater than the static persistence length, P=500 Å, which is inferred from analysis of D_R values derived from the slow components in the relaxation of these same DNAs (Diekmannn, et al., 1982; Pörschke, et al., 1987). This is also about three times greater than the consensus values of P for DNAs in 2mM Na^+ (580-750 Å). The implied dynamic bending rigidity is $\kappa_d = k_B T P_d = 8.5 \times 10^{-19}$ dyne cm^2.

3.4.2 Relative Amplitudes

The relative amplitude, $A_2/A_1 = a_2/a_1$, of the fast and slow components could in principle be estimated from Eqs. (12)-(16), if b_{j2} were known. Unfortunately, we have no satisfactory theory for b_{j2} as a function of the orienting electric field and dynamic persistence length. However, the analysis can be carried forward in certain limits.

In the limit of large P_d and weak electric fields, the subunits orient nearly together as a rod, so the b_{j2} are virtually identical for all subunits, independent of j, and can be factored outside the j-sum in a_1 and a_2, and cancel out of the relative amplitude. In this case, the relative amplitude becomes approximately

$$A_2/A_1 = \left[\sum_j E_j(6h/P_d)(Q_{j+1,3} - Q_{j,3})^2\right] \Big/ \sum_k E_k \qquad (3.19)$$

For a 20 subunit filament, we calculate $A_2/A_1 = 0.16$ when $P_d = 2100$ Å, and $A_2/A_1 = 0.48$ when $P_d = 500$ Å. The length of this "theoretical" DNA filament is 636 Å. The observed relative amplitude of the fast component of a DNA with comparable length (199 bp, 660 Å) following a weak electric field pulse is so small as to be statistically insignificant (Diekmannn, et al., 1982). It is not clear precisely what numerical value of A_2/A_1 corresponds to the dividing line between statistical significance and insignificance, as judged by the signal-to-noise ratio for 2-exponential fits of the relaxation curves (Diekmannn, et al., 1982). However, a relative amplitude of 0.60 is reported for this same fragment following a strong electric field pulse, and a relative amplitude as small as 0.25 is reported for a 95 bp fragment also following a strong electric field pulse (Diekmannn, et al., 1982). For shorter DNAs (43 to 84 bp) any amplitude of rapidly relaxing component following strong electric field pulses is evidently not statistically significant (Diekmannn, et al., 1982). From this information, we conclude that the dividing line between statistical significance and insignificance certainly lies below $A_2/A_1 = 0.25$, and is plausibly around 0.2. Clearly, the theoretical value $A_2/A_1 = 0.6$ calculated for $P_d = 500$ Å is much too large. However, the value $A_2/A_1 = 0.15$ for $P_d = 2100$ Å may agree with the observations in the sense that it would be statistically insignificant in the experiments reported. Thus, the observed relative amplitude of the fast relaxation following a weak electric

field pulse is not consistent with $P_d = 500$ Å, but is plausibly consistent with $P_d = 2100$ Å.

A striking feature of the fast component of the relaxation is that its amplitude rises from a statistically insignificant value up to a significant plateau value as the strength of the orienting field is increased over a characteristic range (10 to 30 kV/cm for the 194 bp fragment), and increases only slowly with further increases in field strength. The authors suggest that that this increase in amplitude results from straightening of the aligned filaments by the pulse (Diekmannn, et al., 1982). In this limit of straight aligned filaments, it is again expected that b_{j2} is independent of j, so Eq.(19) applies, and the previous estimates of A_2/A_1 are again obtained. The observed relative amplitude of the fast component following a strong electric field pulse, namely $A_2/A_1 = 0.60$, is much larger than that calculated for $P_d = 2100$ Å, and agrees much better with the value calculated for $P_d = 500$ Å. However, this latter value of P_d must be eschewed, because it fails to yield the correct relaxation times. The question now arises as to why the observed relative amplitude of the fast component following a strong electric field pulse is so large, if P_d actually is 2100 Å. We suggest that this enhancement of the relative amplitude of the fast component by strong electric field pulses results primarily from bending, rather than straightening, of some of the filaments. That is, when the orienting pulse is switched on, a sufficiently long DNA that is initially oriented perpendicular to the field and slightly bent, may bend further into an extreme horseshoe or hairpin shape with the two fold symmetry axis directed along the field. Such species, which have enormously enhanced amplitudes of their $\ell = 3$ bending modes, may well be kinetically trapped, unable to reach the energetically more stable straight aligned state during the relative brief, but strong pulse. That is, when a sufficiently strong electric field pulse is suddenly

applied, those molecules with more or less equatorial orientations may be rapidly driven to an alternate U-configuration that does not correspond to the global straight aligned minimum, but which is separated from that global minimum by a barrier that is too high to traverse in the time of duration of the pulse. We suggest that DNAs trapped in a highly bent U-configuration are responsible for the large enhancement of the amplitude of the fast component in the off-field relaxation. At present, the theory is inadequate to yield a more quantitative statement.

3.5 Discussion

The results in Figure 1 leave little doubt that the dynamic persistence length, P_d = 2100 Å, of the relaxing DNAs following a strong electric field pulse is about three times higher than consensus values of the static persistence length (P=580-750 Å) at the same ionic strength. We note that the dynamic persistence length, P_d = 1250 Å, inferred from transient photodichroism studies on a 209 bp restriction fragment (Allison, et al., 1984) is 2.5 times larger than the consensus static value, $P \cong 500$ Å, at its corresponding ionic strength. This suggests that the large value of P_d obtained by the present analysis is not merely an artifact associated with the electic field pulse.

If P_d actually is 2100 Å, then the ratio of contour length to dynamic persistence length for the longest DNA (250 bp) is $L/P_d = 0.40$. Such a ratio lies well within the domain of validity of the normal mode theory (Song, et al., 1989).

The important question now is how to reconcile the large value of the dynamic persistence length (P_d = 2100 Å) inferred from the relaxation time of the fast

component with the much smaller static persistence length (P=500 Å) inferred from the slow component via the rotational diffusion coefficient. Three possible explanations are suggested below.

(1) Suppose that the potential energy for DNA bending is not a smooth quadratic function of the angular displacement between bond vectors of adjacent base-pairs, but instead is dimpled or scalloped, so that it exhibits several thermally accessible discrete minima separated by barriers. Suppose also that these barriers are sufficiently high that they are not significantly traversed in times of 100 μsec, or more, even in the presence of strong electric fields, but nevertheless are sufficiently low that equilibration between dimples is readily achieved on somewhat longer time-scales. The static equilibrium persistence length, P=500 Å, results from averaging the equilibrium population over all of the dimples. However, over the comparatively short duration of the transient electric dichroism experiment, including both on-field and off-field times, each pair of adjacent bond vectors is effectively trapped in a single dimple or scallop on its potential curve, which exhibits a much larger effective bending constant, corresponding to $P_d = 2100$ Å. In this way, the bending rigidity of DNA becomes time-dependent, so that it actually exhibits a larger value in experiments that monitor flexure on very short time-scales ($t \leq 10^{-4}$ s) than in experiments that monitor equilibrium rms curvature. In this interpretation, the fast component in the off-field relaxation monitors the short-time bending rigidity characteristic of individual dimples, whereas the rotational diffusion coefficient characterizes the rms curvature of the equilibrium population averaged over all the dimples.

(2) Suppose that the DNA exhibits sequence-dependent permanent bends between adjacent base-pairs. This would provide an identical static contribution

to the curvature for all DNAs of a given kind. That would in turn cause a permanent decrease in the end-to-end distance, and a corresponding increase in D_R. Thus, permanent bending would contribute to the apparent flexibility in equilibrium measurements that probe the end-to-end distance, and cause the apparent P to lie below the dynamic value $P_d = 2100$ Å expected from the actual bending rigidity. Under this interpretation, most of the equilibrium curvature would have to arise from permanent bends rather than from thermally excited bending.

(3) Suppose that the bending potential is highly anharmonic and that the effective force constant for bending rises rapidly with increasing bending angle between base-pairs. If the statistically significant amplitude of bending actually comes primary from highly bent fragments, as already proposed, then the bulk of the relaxing amplitude of those DNAs would be characterized by a much larger bending rigidity than what is characteristic of weakly bent DNAs near the equilibrium configuration. One consequence of this hypothesis is that the effective force constant for bending would decrease during the relaxation, thus yielding a spectrum of relaxation times for the fast "component".

We note that the three possible explanations just presented are not mutually exclusive, so all three may be operating to some degree. Sufficient information to completely rule out any of these possibilities is not yet available.

An argument weighing against possibility (3) is that three or more statistically significant exponential decays could not be detected even for rather large relative amplitudes ($A_2/A_1 = 1.4$) of the fast component. This suggests that the bending constant does not decrease greatly as the system relaxes, because the resulting spectrum of the relaxation times for the fast "component" should

then appear as a multi-exponential decay in the data fitting. Also, from analysis of the relative rates of circularization and of topoisomer distributions of DNAs in this size range Shimada, et al., 1984; Shimada, et al., 1985), there is no indication of any large increase in bending rigidity associated with bending into circles.

Possibility (2) must prevail, at least qualitatively, if DNA actually exhibits sufficient sequence-dependent permanent bending from one base-pair to the next. However, several lines of experimental evidence now appear to contradict the hypothesis that DNA exhibits substantial permanent curvature. Solid-state NMR studies of oriented DNA fibers deuterated at the 8-position of the purine rings indicate that the C-D bond vectors lie within ± 8 degrees of perpendicular to the fiber axis (Brandes, et al., 1988). Allowance for imperfect orientation of the DNA helices with respect to the fiber-axis implies an even smaller angular deviation of the CD bonds from perpendicular to the helix-axis. Scanning tunnelling microscope images of DNAs also show little or no perceptible bending in either the A or B form (Lee, et al., 1989). Significant curvature evidently does not occur under the relatively anhydrous conditions of these experiments. Solution structures of dodecamer duplexes containing the putatively bent sequences of Wu et al (Marini, et al., 1982; Wu, et al., 1984). and Hagerman (Hegerman, 1985) have been investigated by 2-D NMR methods (A. Kintinar and B. R. Reid, personal communication; D. R. Davis, D. H. Hare, and B. R. Reid, personal communication). At the present stage of refinement, it appears that the minor groove narrows considerably in the oligoA tracts, and that base-tilt varies considerably along helix, but the helices themselves appear to be quite straight. Recent results of Stellwagen (Stellwagen, 1988, and personal communication) raise doubts regarding the original interpretation of the anomalously low gel electrophoretic mobilities of such sequences, namely

that they are due to permanent bends (Marini, et al., 1982; Wu, et al., 1984; Hagerman, et al., 1985; Diekmann, et al., 1985). Sequences that exhibit such anomalous mobilities in polyacrylamide gels do not exhibit anomalous mobilities either in 10% agarose gels or in polyacrylamide gels incorporating 1% acrylic acid monomers to impart some negative charge to the network (Diekmann, et al., 1985). Preferential adsorption of specific DNA sequences onto the polyacrylamide strands now appears to be an equally plausible explanation for the anomalous mobilities. Perhaps, the narrowed minor groove of the oligoA tracts (Nelson, et al., 1987) provides a comparatively strong binding site for polyacrylamide. A series of such sequences phased to place the binding sites on the same side of the DNA would cause maximum binding and minimum mobility. Phasing the sequences so that they occur alternately on opposite sides of the DNA would require the polyacrylamide strand to wrap half-way around the DNA between sites in order to maintain contact, thereby reducing the binding affinity and the magnitude of the mobility anomaly, as observed. The point here is that sequence-dependent permanent bends in DNA are by no means conclusively established yet. Hence, possibility (2) dose not necessarily prevail, and may even be precluded in the absence of permanent bends.

For reasons cited above we favor possibility (1), but the other possibilities are by no means excluded at this time.

Clearly, additional work is required to better define the dynamic bending rigidity and persistence length and understand its origins. The theory to do that is now in place.

Chapter 4
Calculation of Dynamic Structure Factor of Weakly Bending Rods

4.1 Theory

4.1.1 Coordinate Frames

The weakly bending rod model is that described previously (Song et al., 1989). Briefly, the rod is assumed to consist of $N+1$ identical spherical beads whose centers are connected by N bond vectors ($\mathbf{h}_i$) of fixed length h. Between each pair of successive bond vectors is a Hookean bending spring that acts to straighten the chain. We introduce three coordinate systems: (1) the laboratory frame (double-primed coordinates) x'', y'', z''; (2) the rod frame (unprimed coordinate) x, y, z with the origin at the center-of-mass and z parallel to the instantaneous end-to-end vector: and (3) the rotated frame x', y', z' whose origin coincides with that of the laboratory frame, but whose axes are parallel to those (x, y, z) of the rod frame. The x and y axes of the rod frame are initially taken to be any two orthogonal axes in a plane perpendicular to z. Of course, the x and y axes will change as the z axis rotates. We imagine that the rod is encased in a long box with a square cross section, such that the z-axis intersects the center of every square cross section and the x- and y-axes intersect the centers of the respective rectangular side faces. This box undergoes uniform end-over-end rotations simultaneously with the z-axis of the rod, which flexes inside the box. It is assumed that no twisting torques are exerted on the rod, or on the box. Thus, the box undergoes no net twisting motions, but merely reorients its long axis. That is, the Euler rotation that orients the current frame of the box in any previous frame if $\Phi = (\alpha\beta - \alpha)$, which implies zero net twist. The changes in the x and y axes of the rod as its z-axis rotates are now the same as those of the box, which can be used to define the instantaneous rod frame. The projections of the rod onto the xz and yz planes of this instantaneous rod

frame depart from zero and change in time only as a consequence of rod flexture, but not as a consequence of uniform translation or rotation of the rod. These latter uniform motions are manifested only in the laboratory frame (x'', y'', z'') and the rotated frame (x', y', z').

4.1.2 Dynamical and Equilibrium Properties of Weakly Bending Rods

For a weakly bending rod, the potential energy, forces, and dynamical motions can be resolved into components in the xz and yz planes (Song et al., 1989; Wu et al., 1987). The potential energy associated with displacements of the beads in the y-direction is

$$U = (\kappa_h/2h^2)\mathbf{y}^T \boldsymbol{D}\mathbf{y} \quad , \tag{4.1}$$

where κ_h is the bending torque constant, $\mathbf{y} = (y_1, y_2, \ldots, y_{N+1})$, $\mathbf{y}$ is the $(N+1) \times 1$ column vector of y-coordinates of all the beads, and $\boldsymbol{D}$ is the $(N+1)\times(N+1)$ symmetric potential energy/force matrix given previously (Song et al., 1989). The Langevin equation for motion of the beads in the y-direction is (Song et al., 1989)

$$m\ddot{\mathbf{y}} + \gamma\dot{\mathbf{y}} + (\kappa_h/h^2)\boldsymbol{H}\boldsymbol{D}\mathbf{y} = \mathbf{E}_y(t) \quad , \tag{4.2}$$

wherein m is the bead mass, γ is the bead friction factor, $\boldsymbol{H}$ is the $(N+1)\times(N+1)$ symmetric hydrodynamic interaction matrix given previously, and $\mathbf{E}_y(t)$ is the $(N+1)\times 1$ column vector of fluctuating Brownian forces, which are assumed to be uncorrelated with either bead positions or velocities at earlier times. The $\mathbf{E}_y(t)$ are also assumed to be Gaussian random variables with autocorrelation functions

$< E_{yj}(0)E_{yj}(t) >= 2k_BT\gamma\delta(t)$. The amplitudes of bending are assumed to be sufficiently small that significant tension along the chain is not developed.

Upon introducing the normal coordinate transformation

$$\mathbf{y} = \boldsymbol{Q}\boldsymbol{\rho} \ , \tag{4.3}$$

such that $(\boldsymbol{Q}^{-1}\boldsymbol{H}\boldsymbol{D}\boldsymbol{Q})_{qp} = \Lambda_q\delta_{qp}$ is diagonal, one obtains uncoupled Langevin equations for the normal coordinates

$$m\frac{d\dot{\rho}_1}{dt} + \gamma\dot{\rho}_1 = G_1(t) \tag{4.4}$$

$$m\frac{d\dot{\rho}_2}{dt} + \gamma\dot{\rho}_2 = G_2(t) \tag{4.5}$$

$$\gamma\dot{\rho}_q + (\kappa_h/h^2)\Lambda_q\rho_q = G_q(t): \quad q = 3,4,\ldots N+1 \tag{4.6}$$

The $G_q(t) = (\boldsymbol{Q}^{-1}\mathbf{E}_y(t))_q$ are still Gaussian random variables with delta-function auto-correlation functions that are uncorrelated with either bead positions or velocities at earlier times. The $q \geq 3$ normal modes are assumed to be overdamped, so their inertial terms are neglected.

The $q = 1$ normal mode corresponds to uniform translation of the beads in the y-direction. It follows that the difference $y'_c(t) - y'_c(0)$ is a Gaussian random variable with zero mean, but mean squared displacement

$$< (y'_c(t) - y'_c(0))^2 >= 2D_{\perp}t \ , \tag{4.7}$$

where the transverse diffusion coefficient $D_{\perp} = D_{yy}$ is given by previously derived expressions(Song et al., 1989).

The $q = 2$ normal mode corresponds to a uniform shear motion in the y-direction, which for very small (strictly infinitesimal) amplitudes corresponds to uniform rotation of the rod around the x-axis. This motion is transformed to a proper rotational motion to obtain the probability distribution and diffusion

coefficient for uniform rotation around the x-axis. The angular displacement $\Delta x(t)$ around the x-axis in the period from 0 to t is also a Gaussian random variable with zero mean, but mean squared displacement

$$< \Delta x(t)^2 >= 2D_R t \ , \tag{4.8}$$

where the rotational diffusion coefficient D_R is given by previously derived expressions (Song et al., 1989).

The normal coordinates for the $q \geq 3$ bending normal modes are also Gaussian random variables with zero mean, but with autocorrelation functions

$$< \rho_q(0)\rho_p(t) >= \delta_{pq} < \rho_q(0)^2 > \exp(-t/\tau_q) \tag{4.9}$$

wherein $\tau_q = \gamma h^2/\kappa_h \Lambda_q = \gamma h^3/P k_B T \Lambda_q$, and $P = \kappa_h h/k_B T$ is the dynamic persistence length. The mean squared amplitude d_q^2 of the q^{th} bending mode generally depends on the choice of "normalization" for the transformation $\boldsymbol{Q}$. For the particular choice adopted here and in the previous work (Song et al., 1989)

$$d_q^2 =< \rho_q(0)^2 >= K_B T h^2/\kappa_h = h^3/P \tag{4.10}$$

The conditional probability density $P(\rho_q(t)|\rho_q(0))$ is given previously and in Eq. (4.47). It is also true that the amplitudes of any two bending normal modes at the same or different times are statistically independent (Song et al., 1989). An algorithm for calculating the eigenvalues Λ_q of the $\boldsymbol{HD}$ matrix and the transformation matrix elements $Q_{\ell q}$ is described in our previous work.

Identical arguments and equations apply for motions in the x-direction (in the xz plane. and identical results follow (Song et al., 1989).

The rod is assumed to undergo uniform rigid body translation in the z-direction. Hence. the difference $z_c'(t) - z_c'(0)$ is a Gaussian random variable with zero mean. but with mean squared displacement

$$< (z_c'(t) - z_c'(0))^2 >= 2D_{\parallel} t \tag{4.11}$$

where the $D_{||} = D_{zz}$ is given by a previously derived expression.

Finally, we note that all of these normal modes of motion at the same or different times are statistically independent.

4.1.3 Motion of the Beads for Small Times in the Laboratory Frame

In treating dynamic light scattering from scattering elements undergoing correlated Brownian motions, it is common to derive the diffusion coefficient obtained from the initial slope, or first cumulant of the dynamic structure factor. Indeed, this was the approach adopted for thin rigid rods (Wilcoxon et al., 1983) and rigid double and single-spirals (Wu et al., 1989). Although we have also obtained the rigorous initial slope of the dynamic structure factor for the present model, as described subsequently, we find that it cannot be used to adequately fit the data, because many of the bending normal modes relax completely on a time-scale much shorter than the experimental time resolution, which is set by the channel delay. Thus, not all of the bending normal modes that contribute to the initial slope of the dynamic structure factor are actively decaying in the experimentally resolved time-range. Thus, we need to consider the time evolution of the dynamic structure factor over initial times at least comparable to the channel delay. An additional consideration is that very long rigid rods exhibit non-exponential decay of their dynamic structure factors at large scattering vector, quite apart from any contribution of bending modes. By extending the theory to small, but finite times, it should be possible to obtain a better approximation to the experimentally observed initial slope, even for rigid

rods.

The Euler rotation $\Phi = (\alpha\beta\gamma)$ around body-fixed axes carries a coordinate system from coincidence with the lab frame (x'', y'', z'') to coincidence with the rotated frame x', y', z', whose axes are parallel to x, y, z. In the laboratory frame, the coordinates of the ℓ^{th} bead are given by

$$\begin{pmatrix} x''_\ell \\ y''_\ell \\ z''_\ell \end{pmatrix} = \begin{pmatrix} x''_c \\ y''_c \\ z''_c \end{pmatrix} + \mathbf{R}^{-1} \begin{pmatrix} x_\ell \\ y_\ell \\ z_\ell \end{pmatrix} \tag{4.12}$$

where x''_c, y''_c, z''_c are the coordinates of the center of mass in the laboratory frame and R is a rotation matrix that transforms a vector in the lab frame to a vector in the rotated frame. $\mathbf{R}^{-1}$ can be expressed in terms of α, β and γ as (Schutle, 1984):

$$\mathbf{R}^{-1} = \begin{pmatrix} \cos\alpha\cos\beta\cos\gamma - \sin\alpha\sin\gamma & -\cos\alpha\cos\beta\sin\gamma - \sin\alpha\cos\gamma & \cos\alpha\sin\beta \\ \sin\alpha\cos\beta\cos\gamma + \cos\alpha\sin\gamma & -\sin\alpha\cos\beta\sin\gamma + \cos\alpha\cos\gamma & \sin\alpha\sin\beta \\ -\sin\beta\cos\gamma & \sin\beta\sin\gamma & \cos\beta \end{pmatrix} \tag{4.13}$$

The z''-coordinate of the ℓ^{th} bead in the laboratory frame is easily obtained from the transformation above,

$$z''_\ell = z''_c - x_\ell \sin\beta\cos\gamma + y_\ell \sin\beta\sin\gamma + z_\ell\cos\beta \tag{4.14}$$

Although $z_\ell = h(\ell - (N+2)/2)$ is a constant α, β, γ, z_c, x_ℓ and y_ℓ are generally time-dependent, and in time dt undergo the respective changes $d\alpha$, $d\beta$, $d\gamma$, dz_c, dx_ℓ, dy_ℓ. The corresponding change in z''_ℓ is

$$\begin{aligned} dz''_\ell =& dz''_c - dx_\ell \sin\beta\cos\gamma + dy_\ell \sin\beta\sin\gamma \\ &+ d\beta[-x_\ell\cos\beta\cos\gamma + y_\ell\cos\beta\sin\gamma - z_\ell\sin\beta] \\ &+ d\gamma[x_\ell\sin\beta\sin\gamma + y_\ell\sin\beta\cos\gamma] \end{aligned} \tag{4.15}$$

the change dz_c'' in the lab frame can be expressed in terms of corresponding changes dx_c', dy_c', dz_c' of the center of mass coordinates in the rotated frame by the above transformation

$$dz_c'' = -dx_c' \sin\beta\cos\gamma + dy_c' \sin\beta\sin\gamma + dz_c' \cos\beta \tag{4.16}$$

In addition, $d\beta$ and $d\gamma$ can be expressed in terms of the corresponding rotations δ_x and δ_y of the rod frame around its body-fixed x and y axes by the canonical relations (Schutle, 1984; Edmonds, 1974)

$$d\beta = \sin\gamma\delta_x + \cos\gamma\delta_y \tag{4.17}$$

$$d\gamma = \cos\gamma\frac{\cos\beta}{\sin\beta}\delta_x - \sin\gamma\frac{\cos\beta}{\sin\beta}\delta_y \tag{4.18}$$

Eqs. (4.6) and (4.7) are valid only for very small (strictly infinitesimal) angular displacements. This restriction applies also to the subsequent development. Inserting Eqs. (4.16)-(4.18) into Eq. (4.15) and combining terms yields finally

$$\begin{aligned} dz_\ell'' = &- dx_c' \sin\beta\cos\gamma + dy_c' \sin\beta\sin\gamma + dz_c' \cos\beta \\ &- dx_\ell \sin\beta\cos\gamma + dy_\ell \sin\beta\sin\gamma \\ &- \delta_y x_\ell \cos\beta + \delta_x y_\ell \cos\beta \\ &- [\delta_x \sin\beta\sin\gamma + \delta_y \sin\beta\cos\gamma] h[\ell - (N+2)/2] \end{aligned} \tag{4.19}$$

The values x_ℓ, Y_ℓ, β, γ are taken to apply at $t = 0$. Then, for very small but finite times, $t = \Delta t$, the differentials dz_ℓ'', dx_c', dy_c', dz_c', δ_y, δ_x, dx_ℓ, dy_ℓ in Eq. (4.19) can be replaced by the corresponding small but finite displacements, $\Delta z_\ell''(t)$, $\Delta x_c'(t)$, $\Delta y_c'(t)$, $\Delta z_c'(t)$, $\Delta x_\ell(t)$, $\Delta y_\ell(t)$, $\Delta_x(t)$, $\Delta_y(t)$ during that time.

For very small times, $z_\ell''(t) = z_\ell(0) + \Delta z_\ell(t)$, where $z_\ell(0)$ is given by Eq. (4.14) with all quantities on the right-hand side evaluated at $t = 0$. An equation similar to Eq. (4.14) applies also for $z_m(0)$. From the preceding considerations,

we obtain for very small times the result

$$\begin{aligned} z''_\ell(t) - z''_m(0) = &- \Delta x'_c(t)\sin\beta\cos\gamma + \Delta y'_c(t)\sin\beta\sin\gamma + \Delta z'_c(t)\cos\beta \\ &- (x_\ell(t) - x_m(0))\sin\beta\cos\gamma + (y_\ell(t) - y_m(0))\sin\beta\sin\gamma \\ &- h(\ell - (N+2)/2)[\Delta_x(t)\sin\beta\sin\gamma + \Delta_y(t)\sin\beta\cos\gamma] \\ &+ [h(\ell - m) - \Delta_y(t)x_\ell(0) + \Delta_x(t)y_\ell(0)]\cos\beta \end{aligned} \tag{4.20}$$

wherein $x_\ell(t) = \Delta x_\ell(t) + x_\ell(0)$, $y_\ell(t) = \Delta y_\ell(t) + y_\ell(0)$. In Eq. (4.20), the $x_\ell(t)$, $y_\ell(t)$, $x_m(0)$, $y_m(0)$ contain contributions only from the $q \geq 3$ bending normal modes, since uniform translation and rotation do not alter the coordinates of any beads in the rod frame. Uniform translation only moves the rod frame in the laboratory and rotated frames, and uniform rotation only moves the rod frame in the laboratory frame. The angles on the right-hand side of eq. (4.20) apply at $t = 0$.

4.1.4 The Dynamic Structure Factor

When the laboratory z''-axis is taken parallel to the scattering vector $\mathbf{K}$, the dynamic structure factor for a single rod is given by

$$S(K,t) = \frac{1}{N+1}\sum_{\ell=1}^{N+1}\sum_{m=1}^{N+1}\langle\exp[iK(z''_\ell(t) - z''_m(0))]\rangle \tag{4.21}$$

The expression for $z''_\ell(t) - z''_m(0)$ from Eq. (4.20) is now inserted in Eq. (4.21) and the indicated averages performed. We first average over the statistically independent uniform translations, $\Delta x'_c(t)$, $\Delta y'_c(t)$, $\Delta z'_c(t)$, the bending normal modes $\rho_q(t)$ and $\varsigma_q(t)$ $(q = 3, 4, \ldots N+1)$ in the y and x directions, respectively, and the uniform rotations $\Delta_x(t)$ and $\Delta_y(t)$ around the x and y axes, respectively, leaving the average over the initial angles β and γ (which drops out) till

later. The general result, which is quite complicated, is derived in Section 4.2, and presented in Eqs. (4.59-4.66). The complication arises from the terms $[-\Delta y(t)x_\ell(0) + \Delta x(t)y_\ell(0)]\cos\beta$ in the last line of Eq. (4.20). These terms are bilinear in both bending displacement and uniform rotation and couple those motions. However, these terms represent the z-component of the motion that is induced by uniform rotation with the ℓ^{th} and m^{th} beads are off-axis. Such motion should be negligible compared to the x- and y-components of the motion induced by rotation, which are represented by the $h(\ell-(N+2)/2)\Delta x(t)\sin\beta\sin\gamma$ and corresponding $\Delta y(t)$ terms, as well as to the x- and y-components induced by bending, which are represented by the $(x_\ell(t) - x_m(0))\sin\beta\cos\gamma$ and $(y_\ell(t) - y_m(0))\sin\beta\sin\gamma$ terms. Indeed, an argument is presented in Section 4.2 that all terms arising from the bilinear terms contribute negligibly to the observable decay for any K^2 in the domain of validity of the present theory namely times sufficiently short that the angular displacement of the rod-axis, $(2D_R t)^{1/2}$, is very small compared to 1.0. The simplified result obtained when the bilinear terms in Eq. (4.20) are neglected is

$$
\begin{aligned}
S(K,t) = \frac{1}{N+1}\sum_{\ell=1}^{N+1}\sum_{m=1}^{N+1}\Bigg\langle & \cos[Kh|\ell - m|\cos\beta]\times \\
& \exp[-K^2(\sin^2\beta D_\perp + \cos^2\beta D_{||})t] \\
& \exp[-K^2h^2(\ell - (N+2)/2)^2\sin^2\beta D_R t] \\
& \exp\Big[-(1/2)K^2\sin^2\beta\sum_{q=3}^{N+1} d_q^2\Big(Q_{\ell q}^2 + Q_{mq}^2 - 2Q_{\ell q}Q_{mq}e^{-t/\tau_q}\Big)\Big]\Bigg\rangle
\end{aligned}
\tag{4.22}
$$

The first three factors in Eq. (4.22) apply for a completely rigid rod ($P = \infty$), whereas the last factor contains the effects of bending. The static structure factor

follows immediately,

$$S(K,0) = \frac{1}{N+1} \sum_{\ell=1}^{N+1} \sum_{m=1}^{N+1} \Big\langle \cos[Kh|\ell - m|\cos\beta] \times \exp\Big[-(1/2)K^2 \sin^2\beta \sum_{q=3}^{N+1} d_q^2 \Big(Q_{\ell q}^2 + Q_{mq}^2 - 2Q_{\ell q} Q_{mq} \Big) \Big] \Big\rangle \tag{4.23}$$

The remaining average in Eqs. (4.22) and (4.23) over the angle β and the sums over ℓ and m are performed numerically. Summing over m and ℓ first, leaving the integration over $d(\cos\beta)$ till last, is most efficient, because the integrand is much smoother in that case.

4.1.5 Time-Dependent Apparent Diffusion Coefficient

Dynamic light scattering experiments measure the normalized dynamic structure factor $S(K,t)/S(K,0)$. The time-dependent apparent diffusion coefficient is defined in terms of the instantaneous slope of the normalized dynamic structure factor by

$$\begin{aligned} D_{app} &= -K^2 (\partial S(K,t)/\partial t)/S(K,t) \\ &= -K^2 (\partial (S(K,t)/S(K,0))/\partial t)/(S(K,t)/S(K,0)) \end{aligned} \tag{4.24}$$

We simulate data by computing $(S(K,t)/S(K,0))$ at selected times within the experimentally resolved time-range and fitting the resulting curves in the same way as the experimental data. For weakly bending rods at large K^2, it is especially important not to fit simulated data for times less then one experimental delay. The bending normal modes can in some cases produce substantial relaxation of the normalized dynamic structure factor during that first unresolved channel delay period, and that contribution to D_{app} is simply not resolved experimentally.

4.1.6 The Initial Slope Value of D_{app}

A derivation of the exact initial slope diffusion coefficient at $t = 0$ is presented in Section 4.3 and leads to the following expression:

$$D_{app} = \frac{1}{(N+1)S(K,0)} \sum_{\ell=1}^{N+1} \sum_{m=1}^{N+1} \{D_{\parallel} < \cos^2 \beta F_{\ell m} > + D_{\perp} < \sin^2 \beta F_{\ell m} > + D_R h^2 (\ell - (N+2)/2)(m - (N+2)/2) < \sin^2 \beta F_{\ell m} > + \sum_{p \geq 3}^{N+1} (d_p^2/\tau_p) Q_{\ell p} Q_{mp} < \sin^2 \beta F_{\ell m} > \tag{4.25}$$

where $F_{\ell m}$ is given by Eq. (4.82).

Curiously, this result (Eq. (4.25) differs slightly from that obtained from Eq. (4.24) by directly differentiating Eq. (4.22) and setting $t = 0$. In that case the factor $(\ell - (N+2)/2)(m - (N+2)/2)$ in the D_R term is replaced by $(\ell - (N+2)/2)^2$. We presently believe that Eq. (4.25) is the exact initial slope value of D_{app}. By inference, Eq. (4.22) does not yield the completely correct initial slope at $t = 0$. This circumstance probably arises because the initial ($t = 0$) and final times are not treated completely symmetrically in the derivation of Eq. (4.22). However, we have been unable to completely resolve this problem. Eq. (4.25) applies rigorously only for times so small that $S(K,t)$ does not deviate significantly from 1.0, whereas Eq. (4.22) should apply for longer times that encompass substantial relaxation of $S(K,t)$, provided that the rms angular displacement due to uniform rotation remains very small compared to 1.0 radian. We believe that, for finite times, Eq. (4.22) is a much better approximation to the truth than Eq. (4.25). In fact, the difference between the initial slope of Eq. (4.22) and Eq. (4.25) vanishes not only in the limit $K \to 0$, but also in the limit $K(N+1)h = KL \gg 1.0$, where $L = (N+1)h$ is the contour length of the rod. The critical term in question in Eq. (4.25) can be rewritten to

yield

$$D_R h^2 \sum_{\ell=1}^{N+1} \sum_{m=1}^{N+1} (\ell - (N+2)/2)(m - (N+2)/2) f(|\ell - m|) =$$
$$D_R h^2 \sum_{\ell=1}^{N+1} \sum_{m=1}^{N+1} [(\ell - (N+2)/2)^2 - (\ell - (N+2)/2)(\ell - m)] f(|\ell - m|) \tag{4.26}$$

where $F(|\ell - m|) =< \sin^2 \beta F_{\ell m} >$. As noted in Section 4.2, the $\cos(Kh(\ell - m)\cos\beta)$ factor in $F_{\ell m}$ acts to cancel the contributions of terms with ℓ very different from m (i.e. with $Kh|\ell - m| \gtrsim 1.0$). In that case, the second term on the right hand side of Eq. (4.25) typically makes a negligible contribution compared to the first. and the latter is precisely the critical term in the initial slope of Eq. (4.22). Thus, we expect the practical difference between Eq. (4.25) and the initial D_{app} from Eq. (4.22) to be very slight.

Eq. (4.25) can be transformed exactly to yield

$$D_{app} = \frac{1}{(N+1)S(K,0)}$$
$$\sum_{\ell=1}^{N+1} \sum_{m=1}^{N+1} \left\{ D_{\parallel} < \cos^2 \beta F_{\ell m} > + \frac{k_B T}{\gamma} H_{\ell m} < \sin^2 \beta F_{\ell m} > \right\} \tag{4.27}$$

Eq. (4.27) yields D_{app} directly in terms of $D_{\parallel}$, hydrodynamic interaction matrix elements $H_{\ell m}$, and equilibrium averages. Eq. (4.27) illuminates a serious problem with these exact initial slope diffusion coefficients, namely that they do not yield the correct expression in the limit of infinitely rigid rods (i.e. $P = k_h h / k_B T \rightarrow \infty$). The correct expression, originally derived by Wilcoxon and Schurr (Wilcoxon, 1983) is precisely the first three terms in Eq. (4.25). Specifically, the sum over bending normal modes is absent. The difficulty is as follows. The coefficient of $< \sin^2 \beta F_{\ell m} >$ in Eq. (4.25), namely $[D_{\perp} + D_R h^2 (\ell - (N+2)/2)(m - (N+2)/2) + \sum_{p \geq 3} (d_p^2 / \tau_p) Q_{\ell p} Q_{mp}]$ must approach the expression $[D_{\perp} + D_R h^2 (\ell - (N+2)/2)(m - (N+2)/2)]$ as $\kappa_h \rightarrow \infty$.

However, Eq. (4.27) reveals that the former coefficient is actually a constant, $(k_BT/\gamma)H_{\ell m}$, which is independent of κ_h. Thus, Eqs. (4.25) and (4.27) cannot reduce to the correct expression for a rigid rod. This difficulty stems from a fundamental inconsistency in the theory. The bending normal modes are all assumed to be overdamped, yet as the rod becomes extremely rigid, all of its relaxation times shorten until the normal modes actually become underdamped. In such a case, it is no longer reasonable to neglect inertial or memory terms in the equation of motion. In any case, such rapid underdamped motions do not respect the Brownian separation of time scales for relaxation of velocities on one hand and coordinates on the other, on which Eqs. (4.25) and (4.27) are based. Our belief is that underdamped bending modes contribute mainly just to the phonon spectrum of the rod, but not to significant relaxation of $S(K,t)$.

It is important to note that Eq. (4.22) is more or less immune to the preceeding difficulty, because it applies for finite times $t > 0$. As $\kappa_h \to \infty$, the $\tau_q \to 0$, so relaxation of the final factor in Eq. (4.22) is complete for any finite time, $t > 0$. also, as $\kappa_h \to \infty$, then $d_q^2 \to 0$, so the entire last factor can be replaced by 1.0 at any finite time $t > 0$. After subsequent differentiation, the remaining factors yield a D_{app} at $t \to 0$ that is close to the result expected for rigid rods, as noted above. In other words, one must first take the limit $\kappa_h \to \infty$ for $t > 0$ in a sensible way, then evaluate D_{app} for $t > 0$, and finally take the limit $t \to 0$ in order to obtain a valid initial slope value of D_{app} for a rigid rod. In deriving Eqs. (4.25) and (4.27) the $t \to 0$ limit, which presumes the Brownian separation of time-scales, is taken before the $\kappa_h \to \infty$ limit, and is therefore invalid.

4.1.7 A Peculiarity of the Present Model

It should be emphasized that the present model of a weakly bending rod is not completely equivalent to an inextensible discrete wormlike coil, even though its rotational dynamics are virtually the same (Song et al.,1989). Because the z-length of the present model remains constant as it bends, its contour length and also its radius of gyration must increase somewhat upon bending. Its mean squared radius of gyration is calculated according to

$$< R^2 >= \frac{1}{N+1} \sum_{\ell=1}^{N+1} < x_\ell^2 > + < y_\ell^2 > + z_\ell^2 \qquad (4.28)$$

where $z_\ell^2 = h^2(\ell-(N+2)/2)^2$ is a constant, and the mean-squared displacements due to bending are calculated according to $< y_\ell^2 >= \sum_{q\geq 3} d_q^2 Q_{\ell q}^2 =< x_\ell^2 >$. In the convention adopted here, $d_q^2 = h^3/P$, but the $Q_{\ell q}$ are independent of the bending rigidity or dynamic persistence length P. Hence $< R^2 >$ for the present model increases monotonically with decreasing P, or decreasing bending rigidity. However, for a wormlike coil with constant contour length, $< R^2 >$ is given by a different formula, and is found to decrease monotonically with decreasing P. Thus, at small K, where $S(K,0) \cong (N+1)(1 - K^2 < R^2 > /3)$, the slope of $S(K,0)$ vs. K^2 for the present model varies with P in the opposite direction to that for the wormlike coil.

Certainly, the interbead spacing h that appears in Eqs. (4.22) and (4.23) can always be reduced to yield the same $< R^2 >$ value and limiting slope of $S(K,0)$ vs. K^2 as the wormlike coil with the same P. However, h must not be similarly contracted in the equations of motion, hydrodynamic interaction tensors, bending relaxation times, or expressions for the diffusion coefficients. We have elected here not to scale the h-values in Eqs. (4.22) and (4.23), because we seek primarily D_{app} from the decay rate of the normalized dynamic structure factor, $S(K,t)/S(K,0)$. We assume that the peculiar effect of bending of

the present model on $S(K,0)$ will largely cancel out of this ratio, and not be manifested in D_{app}.

4.2 Averaging $\exp[iK(z''_\ell(t) - z''_m(0))]$ Over Certain Variables

The objective here is to average $\exp[iK(z''_\ell(t) - z''_m(0))]$ over the displacements of the center of mass in the rotated frame $\Delta x'_c(t)$, $\Delta y'_c(t)$, $\Delta z'_c(t)$, over the bending normal coordinates $\rho_\ell(t)$ and $\varsigma_\ell(t)$ in the yz and xz planes, respectively, and over the uniform mode rotations $\Delta_y(t)$ and $\Delta_x(t)$ around the y and x axes, respectively. By using Eq. (4.19), the objective is transformed to

$$<< \exp[iK(z''_\ell(t) - z''_m(0))] >>=<< F_1F_2F_3\dots F_{10} >> , \tag{4.29}$$

where

$$F_1 = \exp[iKh|\ell - m|\cos\beta] \tag{4.30}$$

$$F_2 = \exp[-iK\sin\beta\cos\gamma\Delta x'_c(t)] \tag{4.31}$$

$$F_3 = \exp[iK\sin\beta\sin\gamma\Delta y'_c(t)] \tag{4.32}$$

$$F_4 = \exp[iK\cos\beta\Delta z'_c(t)] \tag{4.33}$$

$$F_5 = \exp[-iK\sin\beta\cos\gamma(x_\ell(t) - x_m(0))] \tag{4.34}$$

$$F_6 = \exp[-iK\cos\beta\Delta_y(t)x_\ell(0)] \tag{4.35}$$

$$F_7 = \exp[-iKh(\ell - (N+2)/2)\sin\beta\cos\gamma\Delta_y(t)] \tag{4.36}$$

$$F_8 = \exp[iK\sin\beta\sin\gamma(y_\ell(t) - y_m(0))] \tag{4.37}$$

$$F_9 = \exp[iK\cos\beta\Delta_x(t)y_\ell(0)] \tag{4.38}$$

$$F_{10} = \exp[-iKh(\ell - (N+2)/2)\sin\beta\sin\gamma\Delta_x(t)] \tag{4.39}$$

The inner angular brackets in Eq. (4.29) denote an average over the quantities mentioned above, while the outer angular brackets denote the remaining average of β and γ (which drops out in any case), which is performed subsequently by numerical means, as described in the text.

Factors F_j that contain statistically independent variables can be averaged separately. Using $w = \Delta x_c'(t) = x_c'(t) - x_c'(0)$, the gaussian distribution for $\Delta x_c(t)'$, and $\sigma_w^2 = < (x_c'(t) - x_c'(0))^2 > = 2D_\perp t$ (c.f. Eq. (4.8)), we obtain

$$< F_2 >= \int_{-\infty}^{\infty} dw \frac{\exp[-w^2/2\sigma_w^2] \exp[-iK \sin\beta \cos\gamma\ w]}{\sqrt{2\pi\sigma_w^2}} \tag{4.40}$$

$$= \exp[-K^2 \sin^2\beta \cos^2\gamma\ D_\perp t]$$

Similarly, we obtain

$$< F_3 >= \exp[-K^2 \sin^2\beta \sin^2\gamma\ D_\perp t] \tag{4.41}$$

and

$$< F_4 >= \exp[-K^2 \cos^2\beta\ D_\parallel t] \tag{4.42}$$

Because F_6 contains both $x_\ell(0)$ and $\Delta_y(t)$, it must be averaged together with F_5, which contains $x_\ell(t) - x_m(0)$, and F_7, which contains $\Delta_y(t)$. Likewise F_9 must be averaged together with R_8 and F_{10}. We treat $F_8F_9F_{10}$ explicitly. The $y_\ell(t)$ are expanded in terms of the bending normal coordinates, i.e. $y_\ell(t) = \sum_{q=3}^{N+1} Q_{\ell q}\rho_q(t)$, after which $< G_y >\equiv < F_8F_9F_{10} >$ can be written as the product of factors

$$< G_y >=< F_8F_9F_{10} >= \left\langle \left(\prod_{q=3}^{N+1} T_q \right) \exp[iKh(\ell - (N+2)/2) \sin\beta \cos\gamma \Delta_y(t) \right\rangle \tag{4.43}$$

wherein

$$T_q = \exp[i(a_w\rho_q(t) + b_q\rho_q(0))] \ . \tag{4.44}$$

$$a_q = K \sin\beta \sin\gamma Q_{\ell q} \ , \tag{4.45}$$

$$b_q = -K \sin\beta \sin\gamma Q_{mq} + K \cos\beta Q_{\ell q} \Delta_x(t) \tag{4.46}$$

Each factor T_q can be averaged separately over its $\rho_q(t)$ and $\rho_q(0)$ using the product of initial and conditional probability distributions

$$\begin{aligned} P(\rho(0))P(\rho(t)|\rho(0)) =&(2\pi d_q^2)^{-1/2}\exp[-\rho(0)^2/wd_q^2] \\ &(2\pi d_q^2(1-e^{-2t/\tau_q}))^{-1/2} \\ &\exp[-(\rho(t)-\rho(0)e^{-t/\tau_q})^2/2d_q^2(1-e^{-2t/\tau_q})] \end{aligned} \tag{4.47}$$

where d_q^2 is the equilibrium mean squared amplitude and τ_q is the relaxation time of the q^{th} normal mode. There results

$$< T_q >= \exp[-(1/2)d_q^2(a_q^2+b_q^2+2a_qb_qe^{-t/\tau_q})] \tag{4.48}$$

After inserting Eqs. (4.45) and (4.46) into Eq. (4.48), which in turn is inserted into Eq. (4.43), one obtains

$$\begin{aligned} < G_y >=\Big\langle &\exp\Big[-(1/2)K^2\sin^2\beta\sin^2\gamma\sum_{q\geq 3}d_q^2(Q_{\ell q}^2+Q_{mq}^2-2Q_{\ell q}Q_{mq}e^{-t/\tau_q})\Big]\times \\ &\exp\Big[-(1/2)K^2\cos^2\beta\sum_{q\geq 3}d_q^2Q_{\ell q}^2\Delta_x(t)^2\Big]\times \\ &\exp\Big[-iKh(\ell-(N+2)/2)\sin\beta\cos\gamma\Delta_x(t)\Big]\Big\rangle \end{aligned} \tag{4.49}$$

The average over the gaussian distribution of $v=\Delta_x(t)$ is performed according to

$$\begin{aligned} < G_y >=&G_0\int_{-\infty}^{\infty}dv(2\pi\sigma_v^2)^{-1/2}\exp[-v^2/2\sigma_v^2]\times \\ &\exp[-c^2v^2+a^2v-ibv] \end{aligned} \tag{4.50}$$

wherein

$$G_0=\exp\Big[-(1/2)K^2\sin^2\beta\sin^2\gamma\sum_{q\geq 3}d_q^2(Q_{\ell q}^2+Q_{mq}^2-2Q_{\ell q}Q_{mq}e^{-t/\tau_q})\Big] \tag{4.51}$$

$$c^2=(1/2)K^2\cos^2\beta\sum_{q\geq 3}d_q^2Q_{\ell q}^2 \tag{4.52}$$

$$a^2=K^2\cos\beta\sin\beta\sin\gamma\sum_{q\geq 3}d_q^2(Q_{\ell q}Q_{mq}-Q_{\ell q}^2e^{-t/\tau_q}) \tag{4.53}$$

$$b=Kh(\ell-(N+2)/2)\sin\beta\sin\gamma \tag{4.54}$$

and

$$\sigma_v^2 = 2D_R t \tag{4.55}$$

Eq. (4.55) follows from Eq. (4.8). After rewriting Eq. (4.50), the integral is readily performed,

$$\begin{aligned} < G_y > &= G_0(2\pi\sigma_v^2 f^2)^{-1/2} \exp[-ibe/f] \exp[a^4\sigma_v^2/2(1+2c^2\sigma_v^2)] \times \\ &\int_{-\infty}^{\infty} d(fv-e) \exp[-(fv-e)^2/2] \exp[-i(b/f)(fv-e)] \\ &= (G_0/\sigma_v f) \exp[-ibe/f] \exp[-b^2/2f^2] \times \exp[a^4/2f^2] \end{aligned} \tag{4.56}$$

wherein

$$f = ((1/\sigma_v^2) + 2c^2)^{1/2} = \left[(1/2D_R t) = K^2 \cos^2\beta \sum_{q\geq 3} d_q^2 Q_{\ell q}^2\right]^{1/2} \tag{4.57}$$

and

$$e = a^2/f \ . \tag{4.58}$$

The same expression holds for $< G_x >=< F_5 F_6 F_7 >$, except that $\sin\gamma$ is everywhere replaced by $\cos\gamma$. Finally, making use of all these results,

$$\begin{aligned} << \exp[iK(z_\ell''(t) - z_m''(0))] >> &=< F_1 < F_2 >< F_3 >< F_4 >< G_x >< G_y >> \\ &=< H_1 H_2 H_3 H_4 H_5 H_6 H_7 > \end{aligned} \tag{4.59}$$

where

$$H_1 = F_1 = \exp[iKh(\ell - m)\cos\beta] \tag{4.60}$$

$$\begin{aligned} H_2 &= (\exp[-ibe/f])_{G_y} (\exp[-ibe/f])_{G_x} \\ &= \exp\left[\frac{-iK^3 h(\ell - (N+2)/2)\sin^2\beta\cos\beta \sum_{q\geq 3} d_q^2 (Q_{\ell q} Q_{mq} - Q_{\ell q}^2 e^{-t/\tau_q}) 2D_R t}{1 + K^2\cos^2\beta \sum_{q\geq 3} d_q^2 Q_{\ell q}^2 2D_R t}\right] \end{aligned} \tag{4.61}$$

$$H_3 =< F_2 >< F_3 < F_4 >= \exp[-K^2 \sin^2\beta \ D_\perp t + K^2\cos^2\beta \ D_\parallel t] \tag{4.62}$$

$$H_4 = (\exp[-b^2/2f^2])_{G_y}(\exp[-b^2/2f^2])_{G_x}$$

$$= \exp\left[\frac{-K^2h^2(\ell-(N+2)/2)^2\sin^2\beta 2D_R t}{1+K^2\cos^2\beta\sum_{q\geq 3} d_q^2 Q_{\ell q}^2 2D_R t}\right] \tag{4.63}$$

$$H_5 = (G_0)_{G_y}(G_0)_{G_x}$$

$$= \exp\left[-(1/2)K^2\sin^2\beta\sum_{q\geq 3} d_q^2(Q_{\ell q}^2 + Q_{mq}^2 - 2Q_{\ell q}Q_{mq}e^{-t/\tau_q})\right] \tag{4.64}$$

$$H_6 = (\exp[-a^4/2f^2])_{G_y}(\exp[-a^4/2f^2])_{G_x}$$

$$= \exp\left[\frac{K^4\cos^2\beta\sin^2\beta\left(\sum_{q\geq 3} d_q^2(Q_{\ell q}Q_{mq} - Q_{\ell q}^2 e^{-t/\tau_q})\right)^2 2D_R t}{1+K^2\cos^2\beta\sum_{q\geq 3} d_q^2 Q_{\ell q}^2 2D_R t}\right] \tag{4.65}$$

$$H_7 = (1/\sigma v f)_{G_y}(1/\sigma v f)_{G_x}$$

$$= 1/\left(1+K^2\cos^2\beta\sum_{q\geq 3} d_q^2 Q_{\ell q}^2 2D_R t\right) \tag{4.66}$$

The subscript G_y or G_x denotes the corresponding quantity obtained for G_y in Eq. (4.56), or for G_x in Eq. (4.56) with $\sin\gamma$ replaced by $\cos\gamma$. Both H_1 and H_2 contain odd functions of $\cos\beta$ in the exponent, hence only their real cosine parts survive the subsequent averaging over $d(\cos\beta)$.

The domain of validity of Eq. (4.59) is restricted to times sufficiently small that $(2D_R t)^{1/2} \ll 1.0$. Substantial simplification can be achieved by neglecting the factors F_6 and F_9 in Eq. (4.29). These factors represent the z-component of the motion that is induced by uniform rotation when the ℓ^{th} and n^{th} beads are off-axis. Such motion should be negligible compared to the x- and y-components of the motion induced by rotation F_7 and F_{10}) and the x- and y-components induced by bending (F_5 and F_8). When F_6 is omitted, the averages over F_5 and F_7 can be performed separately. Likewise, when F_9

is omitted, the averages over F_8 and F_{10} can be performed separately. The final result in this case is Eq. (4.59), but with the omission of H_2, H_6, and H_7 and the omission of $K^2\cos^2\beta\sum_{q\geq 3} d_q^2 Q_{\ell q}^2 2D_R t$ in the denominator of the exponent in H_4. It can be seen that these omitted terms do not contribute significantly to the observable part of the decay, as follows. First, we note that $\sum_{q\geq 3} d_q^2 Q_{\ell q} Q_{mq} =< x_\ell(0)x_m(0) >$. Recall that the rod bends only weakly. Thus, when K is sufficiently large to resolve the deformations, that is when $(K^2 < x_\ell(0)^2 >)^{1/2} \gtrsim 1.0$, then $Kh(N+1) \gg 1.0$. In that case, the H_1 term dictates that the dominant contribution comes form terms with $|\ell - m| \ll N$. Now, when $|\ell - m| \ll N$, the relaxing term in the exponent of H_5, namely $-2 < x_\ell(0)x_m(0) >$ is approximately the same size as $-2 < x_\ell(0)^2 >$, and is comparable to the q-sums in H_2 and H_6, which correspond to $< x_\ell(0)x_m(0) > - < x_\ell(t)x_\ell(0) >$, and to the q-sums in the denominators of the exponents in H_2, H_6 and H_4 and to the q-sum in H_7, which correspond to $< x_\ell(0)^2 >$. However, those q-sums in H_2, H_4, H_6, and H_7 are all multiplied by $2D_R t$, which is a second order small quantity in the domain of validity of the present theory! Thus, the relaxing part of the exponent in H_5, namely $K^2(-)2 < x_\ell(0)x_m(0) >$, substantially exceeds the corresponding products, namely $K^2 \cdot (q-\text{sum}) \cdot 2D_R t$ in H_2, H_4, H_6 and H_7. Moreover, for weakly bending rods, the bending normal modes typically relax in a short time compared to $(2D_R)^{-1}$. Thus, with increasing K^2, it will generally be found that the dynamic structure factor is almost completely relaxed by the H_5 term before K^2 is so large that H_2, H_6, H_7 or the denominator in H_4 differ significantly from 1.0. Thus, in the domian of validity of the present model, it is permissible to neglect those terms.

4.2.1 The Initial Slope Diffusion Coefficient

An expression for the exact initial slope diffusion coefficient si derived in Section 4.3 and presented in Eq. (4.83). Curiously, the D_R term in this expression differs slightly from that obtained by substituting Eq. (4.22) into Eq. (4.24) and taking the limit $t \rightarrow 0$. This problem is discussed at some length in Section 4.2 following Eq. (4.83). Practically, the difference is expected to be negligible. In any case. Eq. (4.83) does not strictly apply at times so large that $S(K,t)$ differs significantly from $S(K,0)$, whereas Eq. (4.22) should apply for much longer times encompassing substantial relaxation of $S(K,t)$, provided that the root-mean-square angular displacement due to uniform rotation is very small compared to 1.0 radian.

4.3 The Initial Slope Diffusion Coefficient

The apparent diffusion coefficient obtained from the initial slope of the dynamic structure factor is obtained as follows. We begin with the relation,

$$D_{app} = \lim_{t \rightarrow \tau_B} \frac{-1}{K^2 S(K,t)} \frac{\partial S(K,t)}{\partial t}$$
$$= \frac{1}{(N+1)S(K.0)} \sum_{\ell=1}^{N+1} \sum_{m=1}^{N+1} \int_0^{\tau_B} dt \left\langle \dot{z}''_\ell(0) \dot{z}''_m(t) e^{iK(z''_\ell(0) - z''_m(t))} \right\rangle \tag{4.67}$$

wherein τ_B is chosen sufficiently large that the velocity correlation integrals have all converged, but sufficiently short that $\beta(\tau_B) \cong \beta(0)$, $\gamma(\tau_B) \cong \gamma(0)$, $Kx_m(\tau_B) = Kx_m(0)$, and $S(K,\tau_B) = S(K,0)$. Dividing Eq. (4.19) by dt

yields

$$\begin{aligned}\dot{z}''_\ell(t) = &-\dot{x}'_c(t)\sin\beta\cos\gamma + \dot{y}'_c(t)\sin\beta\sin\gamma + \dot{z}'_c(t)\cos\beta \\ &- \dot{x}_\ell(t)\sin\beta\cos\gamma + \dot{y}_\ell(t)\sin\beta\sin\gamma \\ &- [\omega_y(t)\sin\beta\cos\gamma + \omega_x(t)\sin\beta\sin\gamma]h(\ell - (N+2)/2)\ ,\end{aligned} \tag{4.68}$$

wherein $\omega_y(t) = \delta y/dt$ and $\omega_x(t) = \delta x/dt$. In Eq. (4.26) the bilinear terms have been neglected. The $x_\ell(t)$, $y_\ell(t)$ again represent displacements from the center of mass due to bending and can be expressed in terms of the normal modes $\rho_q(t)$ and $\varsigma_q(t)$ $(q = 3, 4, \ldots N+1)$ in the x- and y-directions, respectively. From Eq. (4.20) with $t = 0$, and one obtains

$$\begin{aligned}\dot{z}''_\ell(0) - \dot{z}''_m(0) =&h(\ell - m)\cos\beta - (x_\ell(0) - x_m(0))\sin\beta\cos\gamma + \\ &(y_\ell(0) - y_m(0))\sin\beta\sin\gamma\end{aligned} \tag{4.69}$$

where the angles β, γ apply at $t = 0$.

We now assume that the center-of-mass velocities $\dot{x}'_c$, $\dot{y}'_c$, $\dot{z}'_c$ and angular velocities ω_x, ω_y are uncorrelated with each other, with the normal coordinate velocity manifested in $\dot{x}_\ell$, $\dot{y}_\ell$, and with the values of the various coordinates at $t = 0$. Under these assumptions the velocities can be averaged separately from the coordinates. We define the following translational and rotational diffusion coefficients.

$$D_\perp = \int_0^{\tau_B} dt < \dot{x}'_c(0)\dot{x}'_c(t) >= \int_0^{\tau_B} dt < \dot{y}'_c(0)\dot{y}'_c(t) > \tag{4.70}$$

$$D_\parallel = \int_0^{\tau_B} dt < \dot{z}'_c(0)\dot{z}'_c(t) > \tag{4.71}$$

$$D_R = \int_0^{\tau_B} dt < \omega_x(0)\omega_x(t) >= \int_0^{\tau} dt < \omega_y(0)\omega_y(t) > \tag{4.72}$$

Making use of these results, Eq. (4.67) becomes

$$D_{app} = \frac{1}{(N+1)S(K,0)} \sum_{\ell=1}^{N+1} \sum_{m=1}^{N+1} \Big\{ D_{\|} < \cos^2 \beta F_{mn} > + D_{\perp} < \sin^2 \beta F_{mn} > + D_R h^2 [\ell - (N+2)/2][m - (N+2)/2] < \sin^2 \beta F_{mn} > + \int_0^{\tau} dt < \dot{x}_\ell(0) \dot{x}_m(t) \sin^2 \beta \sin^2 \gamma F_{\ell m} > + \int_0^{\tau} dt < \dot{y}_\ell(0) \dot{y}_m(t) \sin^2 \beta \cos^2 \gamma F_{\ell m} > \Big\} \tag{4.73}$$

wherein

$$F_{\ell m} = \Big\langle \exp[iKh(\ell - m)\cos\beta] \exp[-iK(x_\ell(0) - x_m(0)) \sin\beta\cos\gamma] \times \exp[iK(y_\ell(0) - y_m(0)) \sin\beta\cos\gamma] \Big\rangle \tag{4.74}$$

The angles β, γ in Eqs. (4.73) and (4.74) apply at $t = 0$.

Each of the last two terms in Eq. (4.73) can be written as follows. Define

$$\dot{S}_x(t) = \frac{-K^2}{N+1} \sum_{\ell=1}^{N+1} \sum_{m=1}^{N+1} \int_0^t dt' \Big\langle \dot{x}_\ell(0) \dot{x}_m(t') > \sin^2 \beta \sin^2 \gamma Y_{\ell m} \exp[-iK(x_\ell(0) - x_m(t')) \sin\beta\cos\gamma] \Big\rangle \tag{4.75}$$

where

$$Y_{\ell m} = \exp[iKh(\ell - m)\cos\beta] \exp[iK(y_\ell(0) - y_m(0)) \sin\beta\sin\gamma] \tag{4.76}$$

At the Brownian time $t = \tau_B$, $\dot{S}_x(t)$ is just the second-to-last term in Eq. (4.73) multiplied by $-K^2 S(K,0)$. The integral in Eq. (4.75) can be removed by differentiating to obtain $\ddot{S}_x(\tau)$. Subsequent integration of dt from 0 to t yields

$$\dot{S}_x(t) = \frac{iK}{N+1} \sum_{\ell=1}^{N+1} \sum_{m=1}^{N+1} \Big\langle \dot{x}_\ell \sin\beta\cos\gamma Y_{\ell m} \exp[-iK(x_\ell(0) - x_m(t')) \sin\beta\cos\gamma] \Big\rangle \tag{4.77}$$

After shifting the origin from 0 to $-t$, $\dot{S}_x(-t)$ can be multiplied by dt and integrated agin from 0 to t to obtain

$$S_x(-t) = \frac{1}{(N+1)} \sum_{\ell=1}^{N+1} \sum_{m=1}^{N+1} \Big\langle Y_{\ell m} \exp[-iK(x_\ell(-t) - x_m(0)) \sin\beta\cos\gamma] \Big\rangle \tag{4.78}$$

$S_x(t)$ is recognized as an autocorrelation function (of $(N+1)^{-1/2}\sum_{\ell=1}^{N+1}\exp[-iKx_\ell(t)]$), hence $S_x(-t) = S_x(t)$. Eq. (4.78) can be evaluated by expanding the $x_\ell(t) = \sum_{q=3}^{N+1} Q_{\ell q}\varsigma_q(t)$, and using the probability distributions for $\varsigma_q(0)$, $\varsigma_q(t)$ analogous to Eq. (4.47) for $\rho(0)$, $\rho(t)$. The result is

$$S_x(t) = \frac{1}{(N+1)}\sum_{\ell=1}^{N+1}\sum_{m=1}^{N+1}\Big\langle \exp\big[-(1/2)K^2\sin^2\beta\cos^2\gamma \\ \Big(\sum_{q=3}^{N+1} d_q^2(Q_{\ell q}^2 + Q_{mq}^2 - 2Q_{\ell q}Q_{mq}e^{-t/\tau_q})\Big]\Big\rangle \tag{4.79}$$

Now taking one more derivative at time $\tau \ll \tau_q$ yields

$$\dot{S}_x(\tau) = \frac{-K^2}{(N+1)}\sum_{\ell=1}^{N+1}\sum_{m=1}^{N+1}\sum_{p=3}^{N+1}(d_p^2/\tau_p)Q_{\ell p}Q_{mp}\Big\langle \sin^2\beta\cos^2\gamma \times \\ Y_{\ell m}\exp\big[-(1/2)K^2\sin^2\beta\cos^2\gamma\sum_{q=3}^{N+1} d_q^2(Q_{\ell q}^2 + Q_{mq}^2 - 2Q_{\ell q}Q_{mq})\big]\Big\rangle \tag{4.80}$$

$Y_{\ell m}$ can be averaged over the bending normal modes by expanding $y_\ell(0) = \sum_{q=3}^{N+1} Q_{\ell q}\rho_q(0)$ and again utilizing the probability distribution in (4.47). The result is

$$Y_{\ell m} = \exp[iKh(\ell-m)\cos\beta]\exp\big[-(1/2)K^2\sin^2\beta\cos^2\gamma \\ \sum_{q=3}^{N+1} d_q^2(Q_{\ell q}^2 + Q_{mq}^2 - 2Q_{\ell q}Q_{mq})\big] \tag{4.81}$$

Eq. (4.81) is inserted in (4.80), which is then divided by $-K^2S(K,0)$ and substituted for the second-to-last term in (4.73). A similarly derived term is employed to replace the last term in (4.73). Averages over the bending normal modes in F_{mn} in the first two terms in Eq. (4.73) are performed in a similar fashion to obtain

$$F_{\ell m} = \cos(Kh(\ell-m)\cos\beta)\exp\big[-(1/2)\sin^2\beta(\sum_{q=3}^{N+1} d_q^2(Q_{\ell q}^2+Q_{mq}^2-2Q_{\ell q}Q_{mq})\big] \tag{4.82}$$

Making use of all these results yields Eq. (4.25) in the text.

Eq. (4.25) can be transformed to a somewhat different expression as follows. F rom Eqs. (4.29-4.33) of reference (Song et al., 1989), one has for $q \geq 3$:

$$d_q^2 = \frac{k_B T h^2}{\kappa_h \mu_q} , \tag{4.83}$$

where

$$\mu_q = (\boldsymbol{Q}^T \boldsymbol{D} \boldsymbol{Q})_{qp} = \delta_{qp} \mu_q , \tag{4.84}$$

and also

$$1/\tau_1 = \frac{\kappa_h}{\gamma h^2} \Lambda_q = \frac{\kappa_h}{\gamma h^2} (Q^{-1} H Q^{-1T} Q^T D Q)_{qq} = \frac{\kappa_h}{\gamma h^2} \mu_q \nu_q \tag{4.85}$$

where

$$\nu_q = (Q^{-1} H Q^{-1T})_{qp} = \delta_{qp} \nu_q \tag{4.86}$$

Thus, for $q \geq 3$, one can write

$$Q_{\ell q} Q_{mq} d_q^2 / \tau_q = Q_{\ell q} Q_q \nu_q \tag{4.87}$$

From Eqs. (45) and (46) of reference (Song et al., 1989) one can write

$$D_\perp = \frac{k_B T}{\gamma} Q_{\ell 1} Q_{m1} \nu_1 \tag{4.88}$$

Likewise, from Eqs. (56) and (58) of reference (Song et al., 1989) one can write

$$H^2 (\ell - (N+2)/2)(m - (N+2)/2) D_R = \frac{k_B T}{\gamma} Q_{\ell 2} Q_{m2} \nu_2 \tag{4.89}$$

Now, note that

$$\sum_{q=1}^{N+1} Q_{\ell q} Q_{mq} \nu_q = \sum_{q=1}^{N+1} Q_{\ell q} (Q^{-1} H Q^{-1T})_{qq} Q_{qm}^T = H_{\ell m} \tag{4.90}$$

After substituting Eqs. (4.21-4.23) into (4.25) and making use of (4.90) there results Eq. (4.27) in the text.

4.4 Computation Program

The dynamic structure factor S(k,t) of a weakly bending rod consisted of $N+1$ beads which are connected by N bond vectors is defined as:

$$S(k,t) = \frac{1}{N+1} \sum_l \sum_m < \mathbf{e}^{i\mathbf{k}\cdot[\mathbf{r}_l(t) - \mathbf{r}m(0)]} > \tag{4.91}$$

Consider small times such that $\beta(t) = \beta(0) = \beta$, so that β can be regarded as fixed, but consider rotation as well as translation mode of y displacements,

$$\begin{aligned} \mathbf{k}\cdot[\mathbf{r}_l(t) - \mathbf{r}_m(0)] =& k cos\beta [z_l(t) - z_m(0)] \\ &+ k sin\beta [y_l(t) - y_m(0)] \\ =& k[\hat{z}_c(t) + h(l - (\frac{N+2}{2})) \\ &- \hat{z}_c(0) - h(m - (\frac{N+2}{2}))] cos\beta \\ &+ k(\hat{y}_l(t) - \hat{y}_m(0)) sin\beta \end{aligned} \tag{4.92}$$

where $\hat{z}_c, \hat{y}$ denote values in the $t = 0$ frame of the rod.

$$\begin{aligned} S(k,t) =& \frac{1}{N+1} \sum_l \sum_m < \mathbf{e}^{ikh|l-m|cos\beta} \\ & \mathbf{e}^{ikcos\beta[\hat{z}_c(t) - \hat{z}_c(0)]} \ \mathbf{e}^{iksin\beta[\hat{y}_l(t) - \hat{y}_m(0)]} > \end{aligned} \tag{4.93}$$

The probability distribution of $\hat{z}_c(t) - \hat{z}_c(0)$ is gaussian

$$P(\hat{z}_c(t) - \hat{z}_c(0)) = \frac{\mathbf{e}^{-\frac{(\hat{z}_c(t) - \hat{z}_c(0))^2}{2 \cdot 2 D_{\|} t}}}{\sqrt{2\pi 2Dt}} \tag{4.94}$$

Likewise,

$$P(\hat{y}_l(t) - \hat{y}_m(0)) = \frac{\mathbf{e}^{-\frac{(\hat{y}_l(t)-\hat{y}_m(0))^2}{2\sigma_{lm}(t)^2}}}{\sqrt{2\pi\sigma_{lm}(t)^2}} \tag{4.95}$$

which is also gaussian. Where

$$\sigma_{lm}(t)^2 \equiv < (\hat{y}_l(t) - \hat{y}_m(0))^2 > \tag{4.96}$$

Averaging over theses distributions yields:

$$\begin{aligned} S(k,t) =& \frac{1}{N+1}\sum_l\sum_m (cos(kh(|l-m|cos\beta)\cdot \\ & \cdot \mathbf{e}^{-k^2cos^2\beta D_{\|}t}\cdot \mathbf{e}^{-k^2sin^2\beta\frac{\sigma_{lm}(t)^2}{2}} > \end{aligned} \tag{4.97}$$

$$\begin{aligned} \sigma_{lm}(t)^2 \equiv& < (\hat{y}_l(t) - \hat{y}_m(0))^2 > \\ =& < [\sum_{q=1}^{N+1} Q_{lq}\rho_q(t) - Q_{mq}\rho_q(0)]\cdot \\ & [\sum_{p=1}^{N+1} Q_{lp}\rho_p(t) - Q_{mp}\rho_p(0)] > \end{aligned} \tag{4.98}$$

We can (and should) specify that $\rho_1(0) = \rho_2(0) = 0$, so there is no uniform $\hat{y}$ displacement or rotation at t=0. Likewise, we should set $\hat{z}_c = 0$. (which has no consequence in retrospect). In any case,

$$\begin{aligned} < \rho_q(t)\rho_p(0) > &= \delta_{pq} < \rho_q(t)\rho_q(0) > \\ < \rho_q(t)\rho_p(t) > &= \delta_{pq} < \rho_q^2 > \end{aligned} \tag{4.99}$$

are valid for all modes.

$$\begin{aligned} \sigma_{lm}(t)^2 =& Q_{l1}^2 < \rho_1(t)^2 > + Q_{l2}^2 < \rho_2(t)^2 > \\ & + \sum_{q\geq 3} (Q_{lq}^2 + Qmq^2) < \rho_q^2 > - 2Q_{lq}Q_{mq} < \rho_q(t)\rho_q(0) > \end{aligned} \tag{4.100}$$

For $q \geq 3$,

$$\begin{aligned} < \rho_q(t)\rho_q(0) > &= < \rho_q^2 > \mathbf{e}^{-t/\tau_q} \\ < \rho_q^2 > &= \frac{k_B T}{\kappa_h} h^2 \\ < \rho_1(t)^2 > &= 2(N+1) D_\perp t \\ < \rho_2(t)^2 > &= 2\frac{h^2}{b^2} D_R t \end{aligned} \tag{4.101}$$

Finally,

$$\begin{aligned} \sigma_{lm}(t)^2 =& 2D_\perp t + 2[l - \frac{(N+1)}{2}]^2 h^2 D_R t + \\ & \frac{k_B T h^2}{\kappa_h} \sum_{q \geq 3} (Q_{lq}^2 + Q_{mq}^2 - 2Q_{lq}Q_{mq} e^{-t/\tau_l}) \end{aligned} \tag{4.102}$$

The dynamic structure factor $S(k,t)$ is

$$\begin{aligned} S(k,t) =& \frac{1}{N+1} \sum_l \sum_m < cos(kh|l-m|cos\beta) e^{-k^2(cos^2\beta)D_\parallel t} \cdot \\ & \mathbf{e}^{-k^2(sin^2\beta)D_\perp t} \mathbf{e}^{-k^2 h^2 (sin^2\beta)[l - \frac{(N+1)}{2}]^2 D_R t} \\ & \mathbf{e}^{-k^2(sin^2\beta)\frac{k_B T h^2}{2\kappa_h} \sum_{q \geq 3} (Q_{lq}^2 + Q_{mq}^2 - 2Q_{lq}Q_{mq}\, e^{-t/\tau_q})} > \end{aligned} \tag{4.103}$$

and the static structure factor $S(k,0)$ is

$$\begin{aligned} S(k,0) =& \frac{1}{N+1} \sum_l \sum_m < cos(kh|l-m|cos\beta) \cdot \\ & \mathbf{e}^{-k^2(sin^2\beta)\frac{kTh^2}{2\kappa_h} \sum_{q \geq 3} (Q_{lq}^2 + Q_{mq}^2 - 2Q_{lq}Q_{mq})} > \end{aligned} \tag{4.104}$$

The field correlation function can be constructed by $\frac{S(k,t)}{S(k,0)}$ at different time scale. The correlation function can be fitted to $A\mathbf{e}^{-k^2 Dt}$ to determine $D_{app}(K)$.

Program CORLAT.FOR was developed to calculate the field correlation function (Appendix D). In order to fit the experimental $D_{app}(K)$ vs. K^2 curve of M13 virus from Wilcoxon's work (Wilcoxon, 1983), the correlation function for a weakly bending rod at $K^2 = 20.005 \times 10^{10} cm^{-2}$ with persistence lengths of 20000Å, or 100000Åare calculated and shown in figure 4.1. A least square fitting program is under developing now to fit the correlation function to determine the diffusion coefficient.

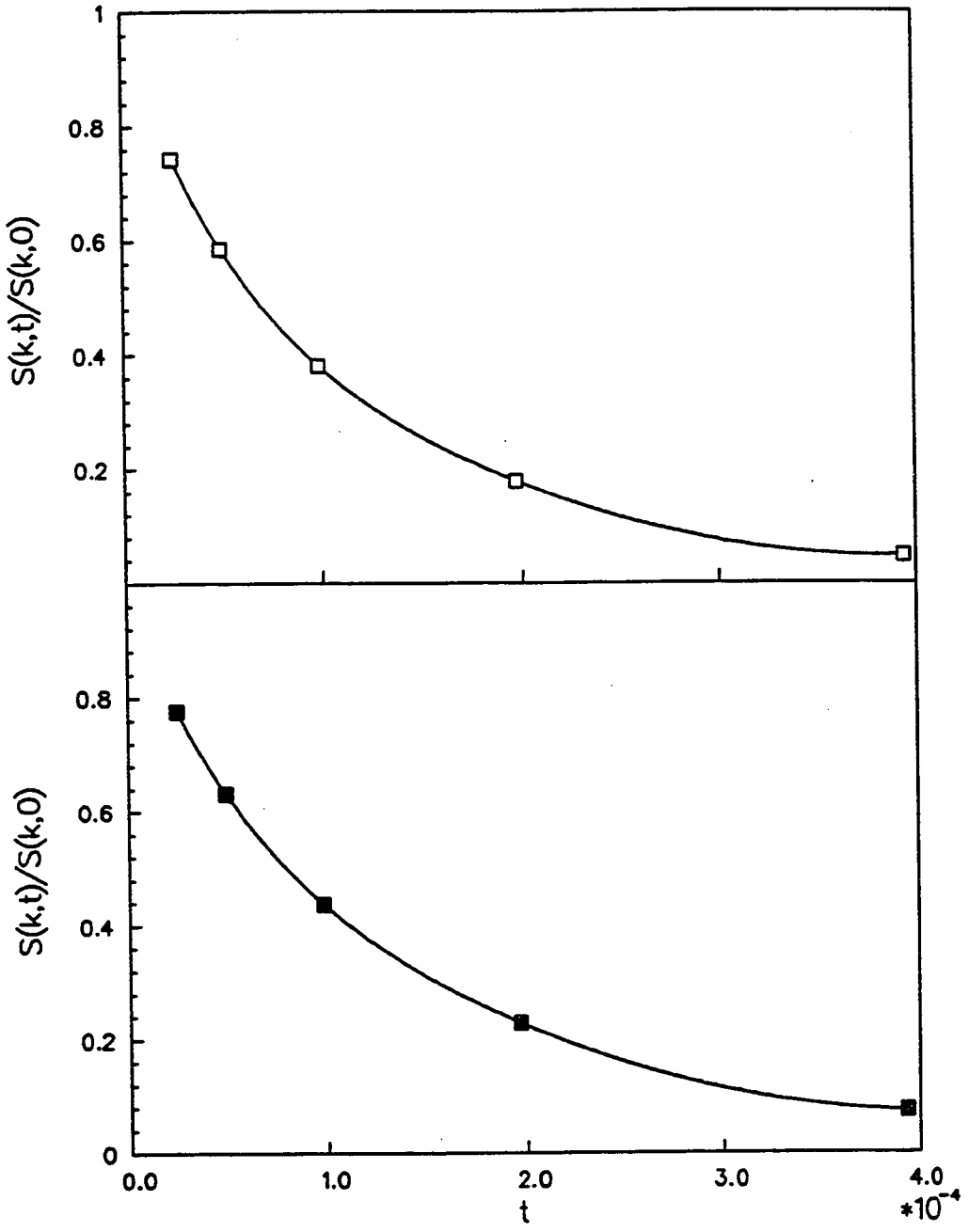

Figure 4.1. Field correlation function at $K^2 = 20.005 \times 10^{10} cm^{-2}$ calculated from the program CORLAT.FOR for a weakly bending rod, number of beads is $N + 1 = 97$, bead radius $a = 47.0\text{Å}$, bead seperation $h = 94.0\text{Å}$, length $L = 9000.0\text{Å}$. Upper: persistence length $P = 20000\text{Å}$. Lower: $P = 100000\text{Å}$.

Chapter 5
Evidence for Allosteric Transitions in Secondary Structure Induced by Superhelical Stress

5.1 Introduction

5.1.1 Background

Supercoiling a cloased circular DNA molecule results in structural deformation, which can be of two kinds: secondary and tertiary structure change. Considerable interest presently attaches to the secondary and tertiary structures of supercoiled DNAs, to the energetics of supercoiling, and to the interactions of supercoiled DNAs with intercalating dyes and proteins that modify the intrinsic twist. Much effort has been devoted to the detection of sequence-specific radical alterations of secondary structure induced by superhelical stress, such as stretches of Z-helix at $(G\text{-}C)_n$ (Klysik et al., 1981; Peck et al., 1982, Singleton et al., 1982; Nordheim and Rich, 1983a; Thomae et al., 1983; Giaever et al., 1988) and $(C\text{-}A)_n$ sequences (Haniford and Pulleyblank, 1983; Nordheim and Rich, 1983b), cruciforms at inverted repeats (Gellert et al., 1979; Lilley, 1980; Panayotatos and Wells, 1981, Mizuuchi et al., 1982; Gellert et al., 1983; Courey and Wang, 1983; Lyamichev, et al., 1983; Panyutin, et al., 1984; Lilley and Hallam, 1984; Greaves et al., 1985; Haniford and Pulleyblank, 1985; Sullivan and Lilley, 1986; McClellan and Lilley, 1987; Murchie and Lilley, 1987) anisomorphic DNA at oligopurine·oligopyrimidine sequences (Pulleyblank et al., 1985; Wohlraub et al., 1987), and an underwound structure at (A-T)-rich sequences (Greaves et al., 1985; Kowalski et al., 1988). Investigation of the global secondary structure, which prevails apart from rare radical alterations at specific sequences, has been much less extensive. One of the main techniques for detecting radical structural variants, namely differential reactivity of such sequences toward various reagents, is ill-suited to the study of global secondary structure. In contrast, the twisting and bending rigidities of the DNA and its circular dichroism provide rather

direct indications of differences in global secondary structure (Shibata et al., 1984; Schurr et al., 1988). The effective torsion constant between base-pairs is obtained directly from time-resolved fluorescence polarization anisotropy (FPA) of intercalated ethidium, and is also manifested in the apparent diffusion coefficient at large scattering vector (D_{plat}) in dynamic light scattering (DLS). The bending rigidity is manifested in the translational diffusion coefficient of the center-of-mass (D_0), which is obtained from DLS in the limit of small scattering vector (Schurr and Schmitz, 1986).

Early studies of the sedimentation coefficient as a function of negative superhelix density in the absence of intercalator (Uphold et al., 1971; Wang, 1974) indicated a rather peculiar variation of the friction factor with superhelicity. The sedimentation coefficient initially exhibits only a very slight increase as the superhelix density decreases from 0 then rises steeply to an inflection point, which is near $\sigma = -0.015$ for SV40 and polyoma DNAs, then continues up to a broad maximum which occurs in the range $\sigma = -0.025$ to -0.030, and then decreases gradually as the superhelix density becomes more negative to $\sigma = -0.07$. As the superhelix density continues toward still more negative values, the sedimentation coefficient increases again more or less linearly. Experiments, such as circular dichroism, to assess possible changes in secondary structure that might be associated with, or responsible for, the unusual changes in tertiary structure and friction factor were not undertaken in these early studies.

A primary objective of this work is first to confirm that the friction factor of our supercoiled DNA exhibits a similar variation with superhelix density as observed in the earlier sedimentation studies, and then to provide measurements pertaining to possible changes in secondary structure, especially over the range

$-0.05 \geq \sigma \geq -0.015$, where the friction factor exhibits peculiar behavior.

In the absence of direct structural information regarding the global secondary structure, which prevails everywhere except for radical structures at specific sequences, a set of beliefs or assumptions that constitute the prevailing standard model of supercoiled DNAs has been employed to interpret a wide variety of experimental data, especially regarding the energetics of supercoiling and the interaction of supercoiled DNAs with intercalating dyes.

5.1.2 Standard Model of Superhelical DNAs

The main assumptions of the standard model, which is believed to apply for superhelix densities from zero to native, are as follows.

1. The global secondary structure is simply strained B-helix (normally underwound). By simple strain is meant a circumstance wherein the deformational free energy rises monotonically with the strain coordinate (e.g. twist or bend), without traversing any passes to enter valleys of secondary minima on the strain free-energy surface. That is, deformation does not reach any yield points leading to alternate global secondary structures.

2. Simple strain per se does not alter the twisting and bending rigidities of the global secondary structure, which remain the same as for linear DNA at all superhelix densities from 0 to native ($\sigma = -0.05$). Of course, when radical structures are induced at specific sequences, the twisting and bending rigidities at those sites might be substantially altered. However, only decreases in rigidity at such a specific site can significantly affect our measurements. Induction of a stretch of Z-helix in otherwise B-DNA does not appear to appreciably decrease either the bending or twisting rigidity (Pörschke et al., 1987; Kim et al., 1989; Fujimoto et al., 1989).

3. Upon relaxation (or reduction) of superhelical strain by nicking, by linearization, by intercalating dyes, by single-strand binding protein, or by the action of Topoisomerase I, the global secondary structure converts smoothly and rapidly to unstrained (or less strained) B-helix.

4. Interactions with intercalating dyes are the same in supercoiled DNA as in nicked circular or linear DNA, except for the change in global superhelical strain due to unwinding and extension of the helix upon intercalation. In particular, the intrinsic binding constant is the same. Of course this assumption does not apply to any radical structures induced at specific sequences.

From these assumptions follow numerous predictions. However, a serious experimental contradiction confronts almost every prediction that requires strict validity of one or more of the standard model assumptions. Noting these contradictions of the standard model is the first objective of the present work. We then provide evidence that increasing negative superhelical stress induces what appear to be significant changes in the secondary structure of a substantial fraction of the plasmid. Several hypotheses regarding the nature of these changes are compared with the experimental data. Finally, a hypothesis to account for the observed contradictions of the standard model is formulated, and compared with certain experimental data.

5.2 Contradictions of the Standard Model

5.2.1 Preliminary Considerations

Each supercoiled DNA topoisomer exhibits a particular integral number of

turns of one strand around the other, called the linking number ℓ. In general ℓ is partitioned among twist T and writhe W (of the helix axis), which obey the constraint (Fuller, 1971)

$$\ell = T + W \tag{5.1}$$

A theoretical treatment of the standard model based on the results of analytical theory (Shimada and Yamakawa, 1985) and simulations (Vologodskii et al., 1979; LeBret, 1980; Chen, 1981) for the distribution of writhe in nicked circular DNAs yields an expression for the difference in deformational free-energy between topoisomers of sufficient length (Wu et al., 1988).

$$\Delta A = (E_T/N)(\Delta\ell^2 - \Delta m^2) \tag{5.2}$$

where N is the number of base-pairs, $\Delta\ell = \ell - \ell_0$ is the (normally negative) linking number difference, $\ell_0 = N\delta_0/360 \cong N/10.4$ is the nonintegral equilibrium net twist in the unstrained (nicked) circular molecule containing N base-pairs, and $\delta_0 \cong 34.6^\circ$ is the twist angle between successive base-pairs. A corresponding definition applies to Δm for the other topoisomer. The twist energy parameter E_T is related to microscopic quantities by (Wu et al., 1988)

$$E_T = ((2\pi)^2/2k_BT)(\alpha\kappa_W/(\alpha + \kappa_W)), \tag{5.3}$$

wherein α is the torsion constant between base-pairs, and κ_W is the effective force constant for fluctuations in writhe in a population of nicked circular DNAs with the same N. κ_W is proportional to the bending constant κ_β between base-pairs, but also contains a length-dependent factor that is known from analytical theory for small circles containing up to 8 persistence lengths (Shimada and Yamakawa, 1984a,b, 1985), and via Monte Carlo calculations for longer circles (Le Bret, 1979, 1980; Chen, 1981; Vologodskii, et al., 1979; Levene and Crothers, 1986).

For DNAs of sufficient length, $\kappa_W = \kappa_\beta/((0.095)(2\pi^2))$ (Shimada and Yamakawa, 1985; Schurr et al., 1989).

The twist energy parameter E_T can be measured by either of two general procedures: the ligation method or the dye-binding method. In the former method, an equilibrium population of circular DNAs with a nick in (at least) one strand, is ligated. The nicking-closing enzyme Topoisomerase I is commonly used both to create and ligate the population of nicked circular DNAs. Once ligated, the equilibrium populations of different topoisomers are "frozen". The distribution of topoisomers is determined directly from the band intensities in gel electrophoresis, and analyzed using Eq. (2) to obtain E_T (Pulleyblank et al., 1975; DePew and Wang, 1975: Shore and Baldwin, 1983; Horowitz and Wang, 1983).

The dye binding method is based on the fact that an intercalating dye unwinds the normal B-helix by an angle ϕ, thus decreasing the equilibrium net twist ℓ_0 in a nicked circular molecule (Bauer and Vinograd, 1970; Hsieh and Wang, 1975; Bauer, 1979). Intercalation of a dye into a native closed circular DNA with fixed ℓ initially increases its linking number difference and superhelix density, $\sigma = \Delta\ell/\ell_0$, toward smaller absolute values. The deformational free-energy A (c.f. Eq. (2)) decreases to 0 as $\Delta\ell$ (or σ) approaches 0, and then increases again for positive $\Delta\ell$. This change in deformational free-energy contributes to the effective binding constant of the dye. For a dye, such as ethidium or chloroquine, which obeys the nearest-neighbor exclusion model, the binding isotherm predicted for the standard model is (Wu et al., 1988)

$$\frac{r}{C} = K \exp\left[a(r^* - r)\right](1-2r)^2/(1-r), \tag{5.4}$$

where r is the binding ratio (bound dye/bp). C is the concentration of free

intercalator, K is the intrinsic binding constant, and $r^* = -\Delta\ell(360)/\phi N$ is the binding ratio at which $\sigma = 0$. The exponential coefficient is $a = E_T(\phi/360)^2$. The unwinding angles for ethidium (26°) (Wang, 1974) and chloroquine (17°) (Jones et al., 1980) are known, so E_T can be determined from measurements of a. A similar equation was previously derived from an assumed free-energy expression (Bauer and Vinograd, 1970), but the relation between E_T and the microscopic constants α and κ_β was not addressed. At the dye concentration where $r = r^*$ and $\sigma = 0$, the superhelical strain is completely relaxed, and the binding ratio is predicted to be the same as for the corresponding linear or nicked circular DNA.

E_T values obtained by various workers from the ligation method and from ethidium and chloroquine binding are summarized by Wu et al. (1988).

5.2.2 Predictions and Contradictions of the Standard Model

A number of predictions of the standard model, denoted by **P1**, ..., **P10**, are contrasted below with pertinent observations, denoted by **O1**, ..., **O10**.

(**P1**) The torsion constants of supercoiled and linear forms of the same DNA should be identical, regardless of the superhelix density of the former.

(**O1**) The torsion constant of supercoiled M13mp7 DNA substantially exceeds that of the corresponding linear DNA in 0.01 M NaCl, 2 mM Tris ((5.0 vs. 3.8) $\times 10^{-12}$ dyne-cm) (Shibata et al., 1984).

(**P2**) Mild environmental stresses, such as changing the buffer type from Tris to citrate, or changing [NaCl] from 0.1 to 0.4 M, should <u>not</u> substantially alter the secondary structure and rigidity of supercoiled DNAs, as they do <u>not</u> for linear DNAs.

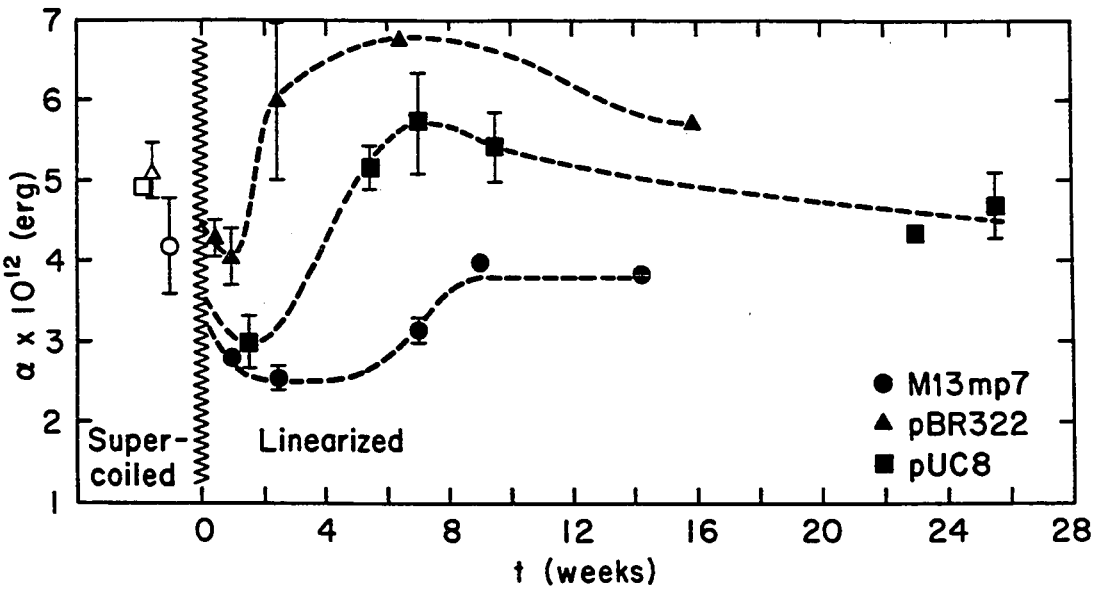

Figure 5.1. Torsion constant α as a function of time after linearization for three supercoiled DNAs. The open and filled symbols are, respectively, the values of α before and after linearization. ○ M13mp7, in 1.5mM citrate, 10mM NaCl, 0.2mM EDTA, pH 7.0. △ pBR322 in 2mM Tris, 10mM NaCl, 2mM EDTA, pH 7.0. □ pUC8 in 10mM Tris, 10mM NaCl, 1mM EDTA, pH 7.0.

(**O2a**) Changing the buffer of supercoiled M13mp7 from Tris to citrate in ~0.01 M ionic strength induces a major transition in torsion constant ((5.0 to 2.7) $\times$ 10^{-12} dyne-cm) and also significant changes in circular dichroism (CD) (Shibata et al., 1984) and D_{plat} (Wilcoxon, J., and Schurr, J.M., unpublished data).

(**O2b**) Changing [NaCl] from 0.1 to 0.4 M induces prominent transitions in D_{plat} ((9.3 to 8.3) $\times 10^{-8}$ cm^2/s) and D_0 ((0.9 to 1.3) $\times 10^{-8}$ cm^2/s) of supercoiled M13mp7 DNA (Wilcoxon, J., and Schurr, J.M., unpublished data), in writhe of supercoiled COP608 DNA (7.8 to 1.0 turns) (Brady et al., 1987), in radius of gyration (Rg) of supercoiled PM2 DNA (73 to 130 nm) (Campbell, 1978), and in E_T of supercoiled lambda DNA (1250 to 530) (Hinton and Bode, 1974; Wu et al., 1988).

(**P3**) Upon linearization, the torsion constant of the equilibrium linear DNA should be manifested immediately.

(**O3**) After linearization, the torsion constants of M13mp7, pBR322, and pUC8 DNAs are sometimes rather low and evolve to a maximum at 6-8 weeks, before settling to their equilibrium values, as shown in Figure 5.1.

(**P4**) When a native supercoiled DNA is run in a gel containing sufficient intercalating dye, the topoisomer (if any) with $\sigma = 0$ should have the same gel electrophoretic (GEL) mobility as the nicked circular DNA. Both DNAs are predicted to have the same binding ratio r.

(**O4**) In the absence of intercalating dye, a topoisomer with $\sigma = 0$ migrates with the same GEL mobility as nicked circles, as predicted. Likewise, when native supercoiled DNA is relaxed by chloroquine, any topoisomer with $\sigma = 0$ migrates at or near the position of the nicked circles, as

predicted. However, when native supercoiled DNA is relaxed by ethidium, proflavine, 9-aminoacridine, or quinacrine, any topoisomer with $\sigma = 0$ migrates significantly faster than the nicked circular DNA, and the difference increases with increasing dye concentration (Keller, 1975; Wu, P.-G., and Schurr, J.M., unpublished data). Moreover, the nearly relaxed topoisomer bands coalesce, which may reflect a loss of writhe.

(P5) Twist energy parameters determined by the ligation method should be identical to those determined by the dye-binding method.

(O5) The consensus E_T values obtained from ethidium and chloroquine binding (500) are only about half, or less, of the consensus values obtained from the ligation method (1000), as noted by Wu et al., (1988). This conclusion extends to dye-binding in 0.1 M NaCl, as well as in concentrated CsCl.

(P6) The local structure, torsional rigidity, and dynamics of supercoiled DNAs that are relaxed to $\sigma = 0$ by intercalated dye should be identical to those of the corresponding linear DNA/dye complexes with the same binding ratio.

(O6) The torsion constants of supercoiled pBR322 DNAs that are relaxed to $\sigma = 0$ by intercalated chloroquine differ significantly from those of the corresponding linear DNA/chloroquine complexes (Wu et al., 1988). Substantially larger differences are observed when supercoiled pBR322 DNA is relaxed by ethidium, after accounting for the effects of excitation transfer (Wu et al., 1989a), or by proflavine, or 9-aminoacridine (Wu et al., 1989b). The discrepancy between relaxed supercoiled and linear DNA/chloroquine complexes is substantially greater in 3 mM Tris than in 0.1 M NaCl (Wu et al., 1989c). Despite these differences in magnitude, the torsion constants all appear uniform.

(**P7**) The flow dichroism of supercoiled DNA/ethidium complexes should vary in the same way with increasing ethidium concentration, whether observed at 260 nm or at 520nm in the absorption band of ethidium, as it does for linear DNA/ethidium complexes.

(**O7**) The flow dichroism of supercoiled ϕX-174, SV40, and pBR322 DNA/ethidium complexes observed at 520 nm varies with ethidium concentration in a very different manner from that observed at 260 nm (Swenberg et al., 1988). The former behaves more like a linear DNA, whereas the latter shows the expected decrease in (negative) dichroism to a minimum and subsequent increase as the DNA is progressively unwound then overwound. This implies that ethidium is either bound to regions of the supercoiled DNA with peculiar properties (e.g. dye tilt) or induces peculiar properties wherever it binds. Nothing of the sort is manifested by the corresponding linear DNAs.

(**P8**) The translational friction factors of completely relaxed superhelical DNA/dye complexes should be nearly independent of the initial superhelix density and nearly the same as that of completely relaxed superhelical DNA without dye.

(**O8**) When superhelical SV40 DNAs with <u>initial</u> superhelix densities $\sigma_0 \leq -0.078$ are relaxed by ethidium to $\sigma = 0$, their friction factors are 10% greater than when the initial superhelix density is less negative $-0.018 \leq \sigma_0$, or when $\sigma = 0$ in the absence of dye (Upholt et al., 1971). This difference can not be attributed to elongation of the DNA by the dye.

(**P9**) Partial relaxation of the superhelix density by any means should not affect the torsion constant.

(**O9**) Partial relaxation of supercoiled pBR322 DNA by saturation binding of eight E. coli single strand binding proteins causes a large decrease in torsion

constant (5.0 to 3.2 $\times 10^{-12}$ dyne-cm) to a low value that is stable for 6 weeks (Langowski, et al., 1985). An isosbestic point in the $D_{app}(K)$ vs. K^2 curves, as well as pertinent theory (Benight et al., 1987; Wu et al., 1989), strongly suggests that ssb binds to pBR322 in a highly cooperative, all-or-none fashion, presumably at a single site. Partial relaxation by intercalated chloroquine and ethidium in 0.1 M NaCl causes a significant decrease in torsion constant (Wu et al., 1988, Schurr et al., 1989; Wu et al., 1989).

(**P10**) When a native supercoiled DNA is partially relaxed by Topoisomerase I, the properties of any given topoisomer should be independent of its time of exposure to the action of Topoisomerase I.

(**O10**) Depending on the time of exposure to Topoisomerase I action, topoisomers with the same linking number (and the same more or less uniform pattern of susceptibility to S1 and P1 nucleases) exhibit significantly different gel mobilities in the presence of ethidium (Negri et al., 1989). This difference in response of putatively identical DNAs to added ethidium is restricted to partially relaxed topoisomers with $-0.02 \lesssim \sigma \lesssim 0$ in the absence of dye. In the presence of sufficient ethidium that topoisomers in this range are positively supercoiled, those exposed for the longer time to Topoisomerase I migrate faster. Such differences vanish when the exposure times of the DNAs to Topoisomerase I action exceed several hours. This implies that there exists a residual difference in presumably metastable secondary structure between these otherwise identical, partially relaxed topoisomers with the same linking number, and that equilibration of the secondary structure in these topoisomers is catalyzed by Topoisomerase I at a much slower rate than the initial relaxation of superhelix density.

Together these observations provide compelling evidence that (1) supercoiled DNAs in various circumstances can exhibit a state with a rather low torsion constant, and (2) release of superhelical strain by linearization, by intercalated dye, by E. coli single-strand binding protein, or by (brief) action of Topoisomerase I does not generally yield a species that is structurally completely equivalent to an equilibrium linear or nicked circular DNA within two or three weeks. Indeed, several of these observations, namely 03, 04, 06, 08, and 010, imply the existence a long-lived metastable state, regardless of the means of relaxation. In the case of dye-relaxed DNAs, the argument is as follows. The same final state can be reached by either of two routes: (1) relaxing the native supercoiled DNA to $\sigma = 0$ by adding intercalating dye until $r = r^*$ or (2) adding intercalating dye to either linear or nicked circular DNA until $r = r^*$, and then ligating those molecules to form covalently closed circles. Circular closure is expected to cause no significant change in binding ratio r, distribution of bound dye, secondary structure, or twisting or bending rigidity, or even gel mobility in the case of nicked circular DNA. Thus, the observation of substantial differences in torsion constant (06) or gel mobility (04) between relaxed supercoiled DNA and, respectively, linear or nicked circular DNA implies that at least one of the two species exhibits a persistent metastable state. Presumably this metastability is exhibited by the more recently relaxed supercoiled DNA.

It is most unlikely that these contradictions of the standard model could arise from one or a few localized radical structures embedded in otherwise global B-helix, for several reasons. (1) To account for these data, the radical structures would have to exhibit, or be adjacent to, a major torsional rigidity weakness, would have to exhibit one or more binding sites with much higher than ($\gtrsim$300x) normal affinity for the dye, and would have to persist for weeks even in the

absence of superhelical strain. However, there is no evidence for any of these required properties. Indeed, competitive dialysis measurements show that the effective binding constant for ethidium at low r values is actually smaller than expected (Wu et al., 1988). Moreover the observed torsional dynamics is that expected for uniform torsional rigidity without any weak spots. (2) D_{plat} samples the local dynamics of the entire filament, not just at the site of the dye, so it should be largely unaffected by one or a few localized rigidity weaknesses. Thus, the observed changes in D_{plat} probably stem from another cause. (3) The CD samples the secondary structure of the entire filament, so it should be largely unaffected by a very small fraction of localized radical structure. Thus, the observed changes in CD most likely arise from another cause. (4) The residual differences between topoisomers with the same linking number that are exposed to Topoisomerase I action for different times are not accompanied by any detectable change in the pattern of susceptibility to S1 or P1 nuclease, which preferentially cut at or near most of the presently identified types of radical structure. (5) In observations O4 to O8, the number of bound dyes is so large (400 for pBR322), that any effect of a few dyes at abnormal sites would be totally overwhelmed. One or a few localized structural anomalies in a completely relaxed supercoiled DNA/dye complex should not significantly alter its electrophoretic mobility, flow dichroism, or translational friction factor. Thus, the observed differences in these properties must be ascribed to other causes. A few localized anomalies probably could not significantly alter the FPA torsion constant without also introducing significant nonuniformity, or variation of α with experimental time-span (Schurr et al., 1988), which is not observed (Wu et al., 1988: Wu et al., 1989a-c). Thus, the discrepant, but uniform, torsion constants probably arise from another cause. Even if the dyes were tightly clustered, subject to

nearest-neighbor exclusion, they would still span a domain of more than 800 bp. Segregation on such a grand scale would imply the existence of extremely large domains of different secondary structure. Thus, we discount the possibility that the aforementioned contradictions of the standard model could be ascribed to one or a few localized radical structures.

The present experiments were undertaken as part of our attempt to elucidate the origins of various contradictions of the standard model.

5.3 Experimental Protocol

5.3.1 Sample Preparation

(1) Isolation of pUC8 dimer

pUC8 dimer (5434 bp) was prepared according to standard plasmid preparation procedures (see Appendix A). The plasmid pUC8 dimer DNA solution was extracted three times with buffered phenol, then three times with diethyl ether. The sample was dialyzed against 2 L of a buffer (LSTE) consisting of 10 mM NaCl, 10 mM Tris, 1 mM EDTA, pH 8.0, for 24 hrs, and then for a second 24 hrs against fresh LSTE buffer. The supercoiled DNA was then isolated by equilibrium banding in CsCl/ethidium bromide. After removal of the supercoiled DNA from the CsCl gradient, it was extracted repeatedly with buffer-washed isopropanol until residual ethidium was no longer visible (about 6x). The sample was then dialyzed for 24 hrs against 2 L of a buffer (HSTE) consisting of 0.5 M NaCl, 10 mM Tris, 1 mM EDTA, pH 8.0, followed by a second 24 hr dialysis against LSTE buffer. This dialysis cycle of alternating high (0.5 M) and low (10 mM) NaCl concentration every 24 hrs was continued for 20

days, until ethidium fluorescence could no longer be detected in a 50 mW beam of 351.1 nm light from an Ar-ion laser. The DNA concentration was determined from its absorbance at 260 nm, assuming $A_{260} = 1.0$ for a 0.05 mg/mL solution. The A_{260}/A_{280} ratio was 2.04. The percent nicked circular DNA was less than about 10%, as judged from relative band intensities in gel electrophoresis. The stock solution was stored at 5°C.

This preparation was shown to consist entirely of covalent dimers by kinetic restriction digests using EcoRI, which cuts pUC8 dimer at two identical positions to yield ultimately just the linear monomer. The linear dimer was the only intermediate species that appeared in agarose gels. which were run at various extents of reaction.

(2) Preparation of Samples with Different Mean Linking Number Difference

A common procedure to prepare topoisomers of supercoiled DNA involves the relaxation of a closed-duplex DNA ring in the presense of an agent that unwinds or winds the helical structure. Most of the intercalator molecules unwind double helices between DNA base pairs. Nicking-closing enzyme Topoisomerase I (Topo I) relaxese supercoiled DNA. By relaxing a covalently closed DNA ring with a DNA Topoisomerase I, in the presence of varying amounts of the intercalator, DNA samples with various median number of superhelical turns can be obtained after the intercalator is removed from the DNA.

a. Intercalator Ethidium Bromide

Ethidium Bromide (EB) binds to DNA by intercalating in between two adjacent base pairs and unwinds the double-helix by about 26°. The bound EB, which is positively charged, can be readily removed by solvent extraction or series

of dialysis. The extraction solvent usually used are some alcoholic solvents like isopropanol, 2-butanol, phenol, et al. The properties of unwinding DNA double helix when it binds to DNA and allowing the DNA double helix to rewind when it is removed from DNA makes EB useful in preparation of DNA topoisomers.

b. Topoisomerase I Reaction

Topoisomerase I (Topo I) is a nicking-closing enzyme. It keeps nicking and closing one strand of the double helices until the supercoiled DNA is relaxed. Complexes of closed circular DNA and EB can also be relaxed by Topo I. After Topo I is removed from the reaction mixture, the linking number of closed circular DNA cannot be further changed. Upon removal of EB from the closed circular DNA, the double helices should rewind to a predictable superhelix density, unless the secondary structure undergoes some change. That is, the number of superhelical turns formed should be determined only by the amount of intercalated EB when Topo I is removed. This number is (26Nr/360), where r is the binding ratio (number of bound EB per DNA bp).

Aliquots of pUC8 dimer sample (about 0.63 mg for each prep) were treated by Topo I in the presence of various amounts of ethidium. The Topo I (from calf-thymus) was purchased from Bethesda Research laboratories, and used in a reaction mixture containing 50 mM Tris-HCl, 50 mM KCl, 10 mM $MgCl_2$, 0.5 mM dithiothreitol (DTT), 0.1 mM EDTA, and 30 μg/mL bovine serum albumin (BSA). In producing the samples with -20, -13, and 0 median superhelical turns, 30 units of Topo I per unit optical density (A_{260}) of DNA were incubated at 37° for more than one hour. In producing the samples with -10, -8, and $+4$ median superhelical turns. 15 units of Topo I per unit optical density of DNA were incubated at 15° for more than 1/2 hour. The relaxation of the initial superhelix

density is confirmed to be complete by running gel of reaction mixture in either case. Upon completion of the reaction, each sample was extracted three times with buffered phenol and three times further with diethylether. Each sample was then dialyzed against HSTE buffer for 24 hrs, then against LSTE buffer for 24 hrs. This dialysis cycle of alternating high and low salt was continued for 5 days. After such treatment with ethidium and Topoisomerase I, $A_{260}/A_{280} = 1.93 - 1.96$. All of the optical measurements were performed on DNAs in the LSTE buffer at 21°C.

The Topo I reaction conditions for six samples are summerized in Table 5.1. τ_2 is the measured linking number difference or number of superhelical turns. r is the binding ratio of EB per DNA bp. $\tau(EB)$ is the calculated number of turns removed by EB by employing equation (5.4) in the calculation. The binding constant K is assumed to be 3×10^5 at 21°C. $\Delta\tau(T)$ is the correction of the superhelical turns due to changing temperature from the Topo I reaction temperature (15°C or 37°C) to the gel temperature (21°C) by assuming $\Delta\sigma/\Delta T$ to be 3.1×10^{-4} degree^{-1} (Bauer, 1978). Temperature T refers to the Topo I reaction temperature. Time t is the duration of the Topo I reaction. τ_1 is the expected number of superhelical turns after temperature correction, $\tau_1 = \tau(EB) + \Delta\tau(T)$. τ_1 is plotted vs. τ_2 in figure 5.2. The -13 and -20 samples which underwent longer Topo I treatment than the other four samples are on the upper line. The two lines are nearly parallel, but their slopes differ from 1.0. This could be due to different counterions and ionic strength between the reaction solution and gel buffer. The higher number of median superhelical turns of samples (-13) and (-20) probably result from the longer exposure to Topo I. Negri et al.(1989) have found that exposure of native supercoiled DNAs to Topo I for different times progressively reduces the amount of a presumably metastable

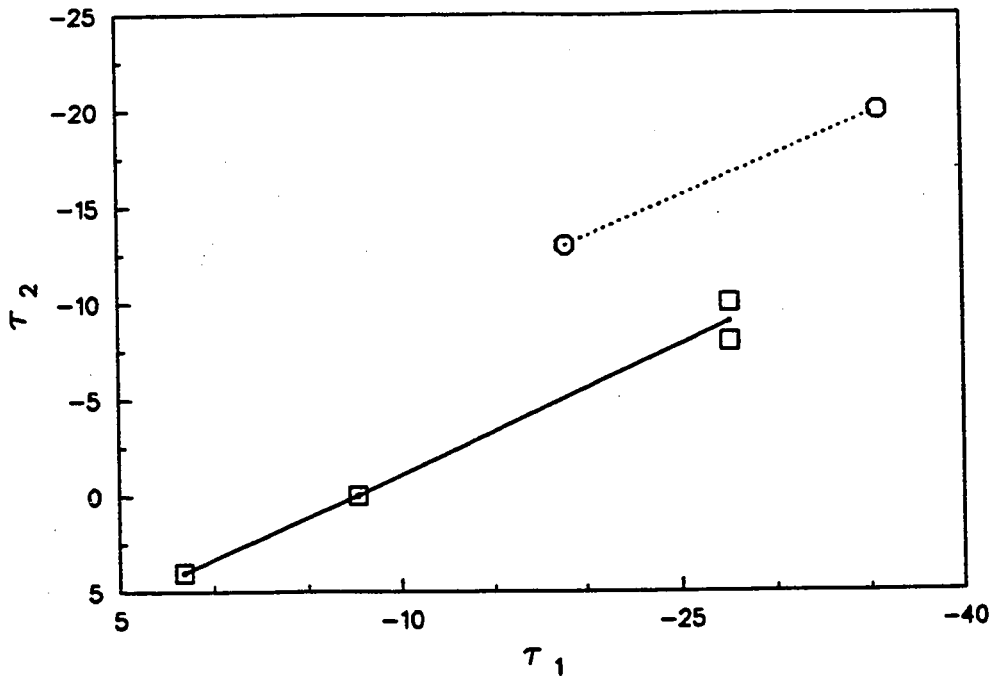

Figure 5.2 The measured median number of superhelical turns τ_2 vs. the expected median number of superhelical turns τ_1 of the topoisomer sample preparation. The two samples on the upper line are $\tau_2 = -20$ and -13, which underwent Topo I treatment for longer than three hours. The lower line connects $\tau_2 = -10, -8, 0$ and $+4$ samples which underwent shorter Topo I treatment.

secondary structure that exhibits a significantly different gel electrophoretic response to ethidium. That is, the ethidium induces a smaller increase in writhe (what the gel senses) in the metastable DNA than in the equilibrium DNA. Our results suggest that removal of ethidium from the metastable DNA, which presumably exists in larger amounts in the DNAs exposed more briefly to Topo I, results in less rewinding than does removal from the completely relaxed DNA. This finding is consistent with that of Negri et al. (1989). It suggests that ethidium may exhibit a significantly lower unwinding angle than 26°when intercalated into the metastable secondary structure.

Table 5.1 Topo I Reaction Conditions

τ_2	+4	0	−8	−10	−13	−20
r	0.000	0.016	0.085	0.085	0.047	0.095
τ(EB)	0.00	−5.72	−29.25	−29.25	−17.02	−33.59
T	15°C	37°C	15°C	15°C	37°C	37°C
$\Delta\tau$(T)	1.62	−1.94	1.62	1.62	−1.94	−1.94
t(hrs)	1.0	1.0	0.5	1.5	3.0	8.0
τ_1	1.62	−7.66	−27.63	−27.63	−18.96	−35.53

About 15 mL of each sample was used in each DLS experiment, 1 mL was used in FPA, 1 mL was used in CD. These samples were maintained separatly in their light scattering cells and in Eppendorf tubes at 21°C for about three months. during which time they were subjected to several measurements. The absence of any detectable nicking at the end of three months. despite the lengthy

storage at room temperature and prolonged exposure to 351.1 nm radiation in DLS, attests to the fact that they are clean and virtually free of ethidium.

5.3.2 Gel Electrophoresis

The gel electrophoresis buffer (TBE) contains 0.089 M Tris-borate, 0.002 M EDTA, PH 8.0. Immediately after the final dialysis into LSTE buffer, each DNA sample was electrophoresed at 21°C in 0.8% (w/v) agarose gels in TBE buffer, and also in a TBE buffer containing 0 to 1.6 μg/mL chloroquine in order to resolve topoisomer bands. These gels were run at 2 V/cm for about 24 hrs at room temperature, then stained for 1 hr in a solution containing 0.5 μg/mL EB. and photographed in the usual way. The gels for all samples were run together after all the experiments were finished. Figure 5.3a shows typical results in the absence of chloroquine, and Figure 5.3b shows the results in 0.4 μg/mL chloroquine.

a. Determination of Median Number of Superhelical Turns

For the less twisted samples, the number of superhelical turns of the median (brightest) topoisomers are determined by counting bands from the nicked circle position in gels without chloroquine. This procedure yields +4, 0, −8, and −10, which are regarded as the approximate median linking number differences of those samples. For the more twisted preparations, the difference in number of bands between the median topoisomer of any given sample and that of a known sample is readily determined from gels containing the appropriate amount of chloroquine. This procedure yields −25 (native), −20, and −13 for the linking number differences of the other samples in Figure 5.3a, and −17 and −14 for two additional samples that were prepared from the original stock solution about four months after the others, all of which are shown in Figure 5.3b. The

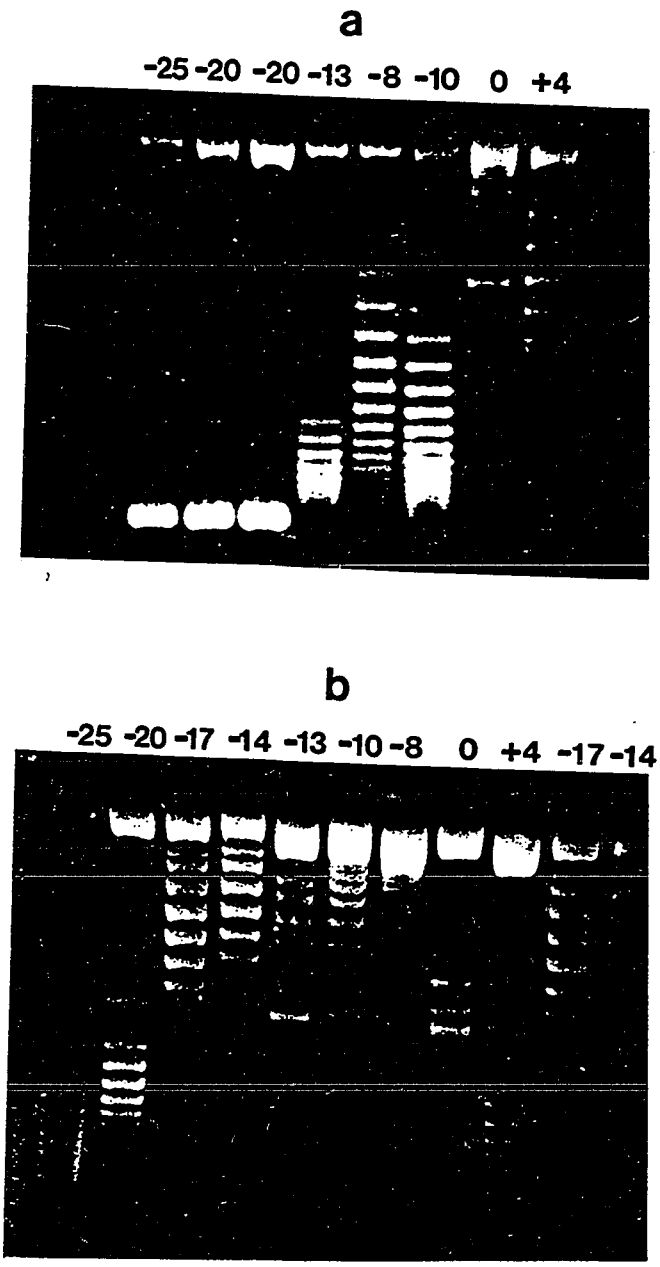

Figure 5.3. Gels of pUC8 dimer samples. The median linking number difference ($\Delta\ell$) is indicated at the top of the pictures. (Gel conditions: 0.8%(w/v) agarose, TBE buffer, pH 8, field strength 2V/cm, 24 hours). (a) without chloroquine. (b) with 0.4 μg/mL chloroquine.

median linking number differences $\Delta\ell$ and calculated superhelix densities σ for the different samples are presented in Table 5.2.

Table 5.2 Median Linking Number Differences and Superhelix Densities for Samples of pUC8 Dimer

$\Delta\ell$	σ
−25	−0.048
−20	−0.038
−17	−0.033
−14	−0.027
−13	−0.025
−10	−0.019
−8	−0.015
0	0.000
+4	+0.008

b. Final Gels

Besides the gels run before and during the measurement period, gels were run for every sample at the conclusion of the optical measurements. No significant nicking or other degradation due to the experiments, or to prolonged storage (up to 4 months) at room temperature could be discerned.

5.3.3 Dynamic Light Scattering

About 15 mL of samples containing 40-50 μg/mL DNA in LSTE buffer were filtered under gravity flow through a cascade of two 0.45 μ Millipore filters into

pre-washed, dust-free scattering cells immediately after removal from the dialysis tube (c.f. sample preparation). DLS measurements are performed essentially as described previously (Thomas et al., 1980; Lin et al., 1981; Wilcoxon and Schurr, 1983). The present UV laser (Spectra-Physics model 2025) delivers 400 mW, or more, in all UV lines. The 351.1 nm line is selected by a prism external to the cavity instead of the spike filter used previously. In this way, incident powers approaching 200 mW are attained for the 351.1 nm line. The original He-Ne laser is employed for scattering measurements at the smallest scattering vectors. The scattering vector is given by $\vec{K} = (4\pi n/\lambda)\cdot\sin(\theta/2)$, where n is the refractive index of the medium, λ the wavelength of light in vacuo, and θ is the scattering angle. The values $n = 1.334$ at $\lambda = 632.8$ nm and $n = 1.348$ at $\lambda = 351.1$ nm are used to calculate K. Our digital photon correlator is the same locally constructed device described briefly in earlier accounts (Thomas and Schurr, 1979; Thomas et al., 1980; Lin et al., 1981). All DLS measurements were performed at 21°C.

The photon correlation functions appear to be reasonably good single exponentials. When collected for normal times (10 to 20 minutes) and UV powers (400 mW) and analyzed using a maximum entropy algorithm, unimodal distributions of decay rates are obtained. However, when the correlation functions are collected for much longer times (1 to 2 hrs) at higher UV powers (600 MW), two separate peaks in the distribution of decay rates could be resolved, as noted by others at lower K^2 (Lewis et al., 1985; Langowski et al., 1986; Langowski, 1987). Normally, the photon correlation functions are simply fitted to a single exponential plus base-line,

$$G^{(2)}(t) = A\ e^{-t/\tau} + B, \tag{5.5}$$

and the apparent diffusion coefficients are calculated according to $D_{app}(K) =$

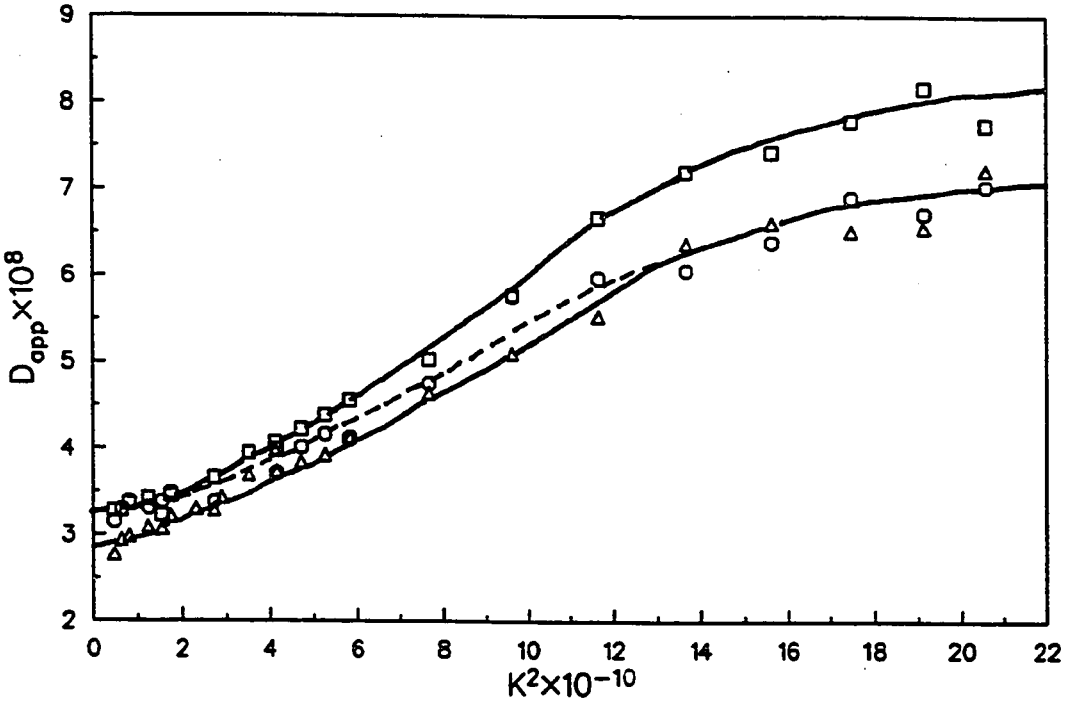

Figure 5.4. $D_{app}(K)$ *vs.* K^2 for pUC8 dimer DNA samples with different median linking number differences ($\Delta\ell$). □: -20 ($\sigma = -0.038$), ○: -13 ($\sigma = -0.025$), △: -8 ($\sigma = -0.015$). D_c and D_{plat} for each sample are obtained from the small K^2 and large K^2 values of the smooth curves hand-drawn through the data points. DNA is present at 40–50 μg/mL in LSTE buffer, pH 8.0, $T = 21°$.

$1/2\tau K^2$. The channel delay is adjusted so that the total time span of the fit is always close to 8 relaxation times. The $D_{app}(K)$ obtained in this way is close to the first-cumulant, or initial slope, value and is undoubtedly the most robust single number that can be extracted from such a correlation function. Values from three or more correlation functions are averaged to obtain the final $D_{app}(K)$. Typical DLS data are shown in Figure 5.4, where smooth curves are simply hand-drawn through the data. The translational diffusion coefficient of the center-of-mass (D_0) at $K^2 = 0$ and the quasi-plateau value (D_{plat}) at $K^2 = 20 \times 10^{10}$ cm^{-2} are obtained from the smoothed curves.

The physical significance of $D_{app}(K)$ for linear DNAs has been discussed previously (Schurr, 1983; Wilcoxon and Schurr, 1983; Schurr and Schmitz, 1986). D_0 gives the friction factor of the entire molecule, which reflects its tertiary structure, whereas D_{plat} characterizes diffusive motions of the scattering elements over a distance of about 225 Å, which is less than half a persistence length, and reflects local twisting and bending rigidities that depend on the secondary structure. For linear DNAs, D_{plat} is empirically found to vary sensitively and in parallel with the torsion constant. For nearly relaxed supercoiled DNAs, the tertiary structure may impose a significant interference effect on D_{plat} (Benight et al., 1987), but that is not large and is evident only in the sample with $\sigma = 0$. That will be described in a forthcoming publication.

5.3.4 Fluorescence Polarization Anisotropy

Time-resolved FPA measurements were performed as reported earlier (Thomas et al., 1980; Thomas and Schurr, 1983; Shibata et al., 1984; Fujimoto et al., 1985; Wu et al., 1987; Wu et al., 1988). Improvements in instrumentation and modifications of the data analysis procedures are described in a recent review

(Schurr et al., 1989). Samples contain 40-50 μg/mL DNA in LSTE buffer at 21°C with 1 ethidium per 300 bp. The sample is excited with $\sim$ 15 ps pulses of polarized 575 nm light, and the parallel ($i_{\parallel}(t)$) and perpendicular ($i_{\perp}(t)$) components of the subsequent emission are detected at 640 nm. The width of the instrument response function $e(t)$ varies between 100 and 50 ps in these studies. All FPA measurements were performed at 20°C.

The emission intensities $i_{\parallel}(t)$ and $i_{\perp}(t)$ are combined to yield the total fluorescence decay, $s(t) = i_{\parallel}(t) + 2i_{\perp}(t)$, or the difference decay, $d(t) = i_{\parallel}(t) - i_{\perp}(t)$, which are convolutions of, respectively, the true sum response function $S(t)$ or true difference response function $D(t) = r(t)S(t)$ with the instrument response function $e(t)$. Adjustable parameters in $S(t)$ and $r(t)$ are determined from $s(t)$, $d(t)$ and $e(t)$ using least-squares convolute and compare algorithms (Schurr et al., 1988). $S(t)$ is modelled by a sum of two exponentials, $S_1(t) = S_1^{\circ} \exp[-t/\tau_1]$ and $S_2(t) = S_2^0 \exp[-t/\tau_2]$, plus a delta-function $A_S\delta(t)$ to account for Raman scattered light. The present samples all exhibit a dominant component, $S_1(t)$, with a (22$\pm$0.5) ns lifetime, corresponding to intercalated dye, and a minor component, $S_2(t)$, with a (1-2) ns lifetime, corresponding to non-intercalated dye. The amplitude ratio S_1°/S_2° varies from 10/1 to 20/1. The true difference function is modelled by

$$D(t) = r_S A_S \delta(t) + r_1(t) S_1(t), \tag{5.6}$$

wherein r_S is the anisotropy of the Raman scattered light (typically about 0.3), and $r_1(t)$ is the anisotropy decay for ethidium intercalated in DNA.

The theoretical anisotropy function for a filament with mean local cylindrical symmetry (Schurr, 1984: Schurr et al., 1988) is used here,

$$r_1(t) = r_0 \sum_{n=0}^{2} I_n C_n(t) F_n(t) \tag{5.7}$$

The adjustable initial anisotropy r_0 accounts for isotropic local angular motions that are too rapid to resolve (Schurr and Fujimoto, 1988). The twisting correlation functions $C_n(t)$ are given by the intermediate zone expression (Barkley and Zimm, 1979; Allison and Schurr, 1979), which also applies for long circular DNAs (Langowski et al., 1985). That is,

$$C_n(t) = \exp[-n^2 k_B T(\pi\alpha\gamma)^{-1/2}\ t^{1/2}], \tag{5.8}$$

where α is the torsion constant between base-pairs and $\gamma = 6.15 \times 10^{-23}$ dyn-cm-s is the recently measured friction factor for rotation around the symmetry axis. (Wu et al., 1987). The tumbling correlation functions are assumed to be $F_n(t) = 1.0$. This assumption yields a lower bound for the best-fit torsion constant. If, instead, the Barkley-Zimm tumbling correlation functions are employed with a persistence length $P = 500$ Å, the value of the best-fit torsion constant is increased by 1.9-fold, but no other conclusions are altered (Shibata et al.., 1985; Schurr et al., 1988). The internal correlation functions are well-known trigometric quantities (Allison and Schurr, 1979; Schurr, 1984; Schurr et al., 1989): $I_0 = ((3/2)\cos^2\epsilon_0 - 1/2)^2$: $I_1 = 3\sin^2\epsilon_0\cos^2\epsilon_0$; and $I_2 = (3/4)\sin^4\epsilon_0$, where $\epsilon_0 = 70.5°$ is the polar angle between the transition dipole and the helix-axis (Hogan et al., 1979; Schurr and Fujimoto, 1988). The adjustable parameters in $r_1(t)$ are the initial anisotropy r_0 and torsion constant α.

Data are collected on four different time-spans, 0-17, 0-35, 0-70, and 0-120 ns, and analyzed to obtain α and r_0. The sample with $\Delta\ell = -20$ ($\sigma = -0.040$) exhibits a large and highly non-uniform α that decreases rapidly with increasing time-span. Only the value obtained on the longest time-span is reported here. For some of the other samples, α declined from a slightly higher value on the 0-17 ns time-span to a constant limiting value on the 0-70 and 0-120 ns time spans.

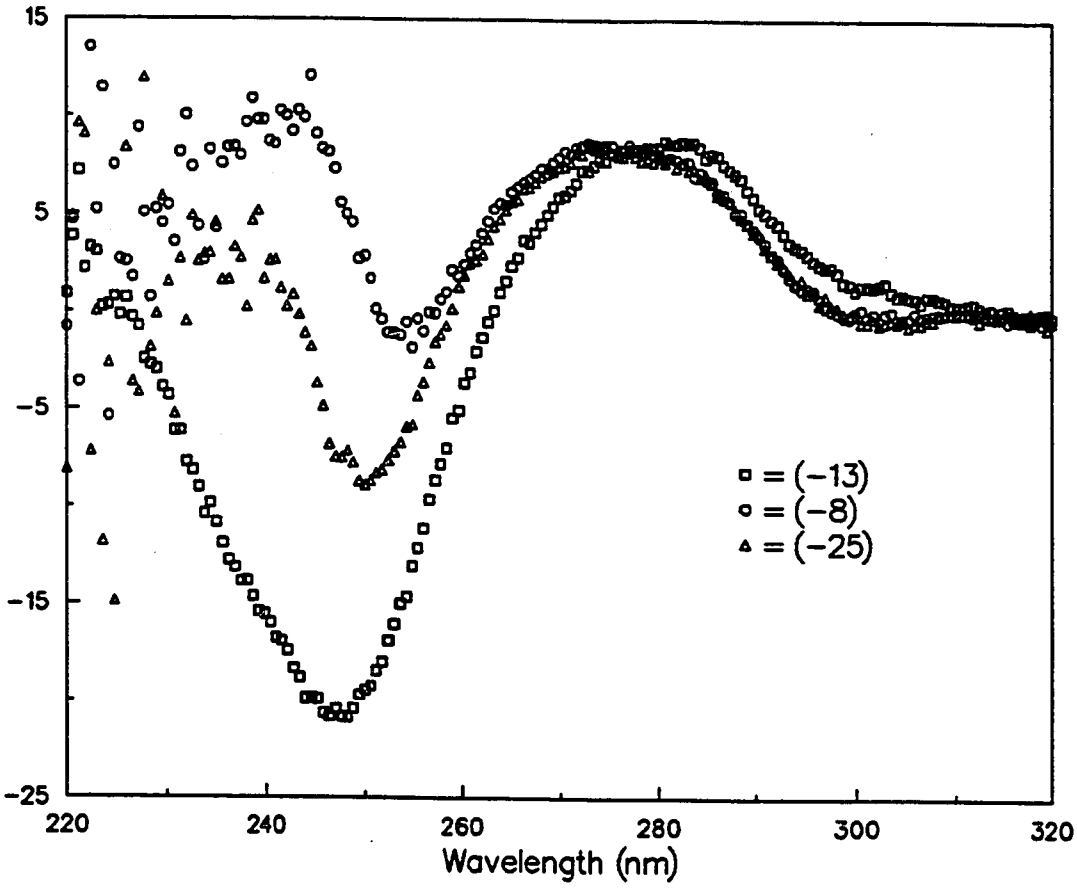

Figure 5.5. CD spectra of pUC8 dimer DNA samples with median linking number differences $\Delta\ell = -8$(top), -13(bottom), and -25(middle), where the relative positions apply at 250 nm. DNA is present at 40–50 μg/mL in LSTE buffer, pH 8.0, $T = 21°$. The $\Delta\ell = -8$ spectrum was measured at 2 weeks after treatment with Topoisomerase I, and underwent substantial changes between 2 weeks and 2 months. The $\Delta\ell = -13$ spectrum was measured 5 days after treatment with Topoisomerase I, and underwent substantial changes between 5 days and 2 months. The $\Delta\ell = -25$ spectrum did not change over time.

To obtain maximum precision, we report here the average torsion constants over only the 0-70 ns and 0-120 ns time spans. Use of averages over all four time spans changes the absolute values of α slightly, increases the standard deviations (which are due to systematic rather than random deviations) considerably, and leaves the ratios of torsion constants for the different samples essentially unchanged.

The distinction between short-wavelength fluctuations in twist (up to several hundred bp) that are measured in the present FPA experiments and the very much slower fluctuations in net twist that are coupled to fluctuations in writhe, is discussed elsewhere (Wu et al., 1988).

5.3.5 Circular Dichroism

CD spectra of the different DNA samples were measured using the Onlines Systems-modified Cary-61 Circular Dichroism spectrometer. The DNA concentration and solution conditions are essentially the same as in DLS experiments, namely 35-50 μg/mL DNA in LSTE buffer at 21$\pm$1°C. The sample was contained in a quartz cuvette with 1 cm light path. CD spectra ($\Delta\epsilon$ vs. λ) for the samples were corrected by subtracting that of the buffer in the same cell, and afterward converted to molar ellipticity units using $[\theta] = 100\Delta\epsilon/c \cdot 1$, where c is the molar concentration of base pairs. CD spectra of three samples (-8, -13 and -25) are shown in Figure 5.5. The long wavelength CD band is essentially unchanged, but the trough at 240 nm varies substantially from one sample to another.

5.4 RESULTS AND DISCUSSION

5.4.1 Basic Experimental Results

Figure 5.6. D_o and D_{plat} for pUC8 dimer *vs.* superhelix density. All samples were prepared from the same stock solution as described in the text. DNA is present at 40–50 μg/mL in LSTE buffer, pH 8.0, $T = 21°$. All samples were measured at 5-7 days after preparation, again at 2-3 weeks, and finally at $1\frac{1}{2}$-2 months. (■) 5-7 days after preparation; (+) 15 days after preparation; (•) 50 days after preparation. Only the $\sigma = -0.015$ sample showed any significant change over time.

Top: D_{plat} *vs.* superhelix density. D_{plat} is the apparent DLS diffusion coefficient at $K^2 = 20 \times 10^{10}\,\mathrm{cm}^{-2}$. The lower values at $\sigma = -0.015$, -0.020, and -0.025 suggest that in this intermediate range, DNA exhibits a different secondary structure with decreased torsional rigidity.

Bottom: Coplot of D_o (on the left hand axis) and $S^0_{20,w}$ (0n the right hand axis) *vs.* superhelix density σ. D_o is the translational diffusion coefficient of the center of mass of pUC8-dimer (This work). $S^0_{20,w}$ (○) is coplotted here for comparision which is the sedimentation coefficient of SV40 DNA (Upholt et. al. in 1971).

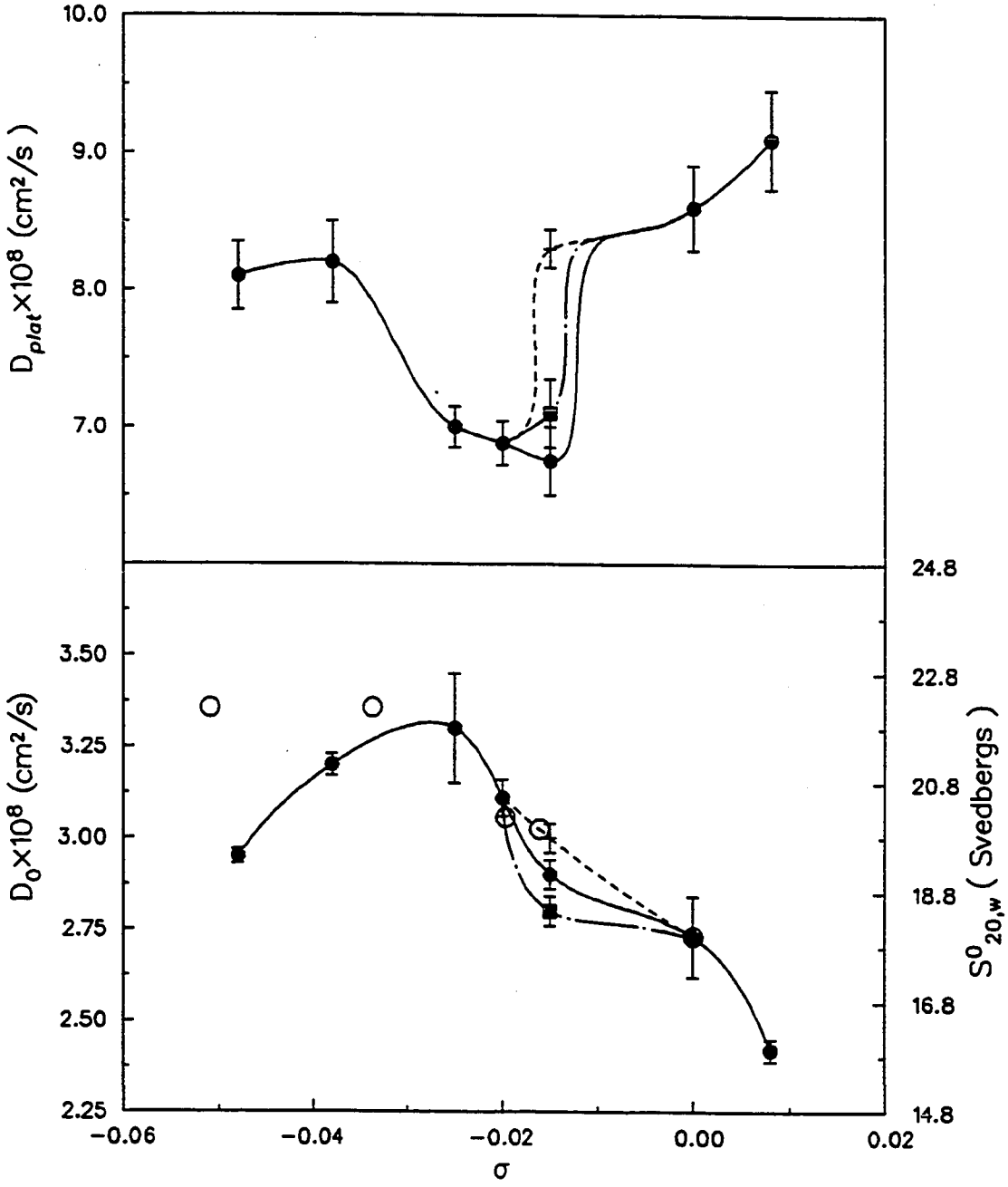
10.0
9.0
8.0
7.0
$D_{plat} \times 10^8$ (cm²/s)
3.50
3.25
3.00
2.75
2.50
2.25
$D_0 \times 10^8$ (cm²/s)
24.8
22.8
20.8
18.8
16.8
14.8
$S^0_{20,w}$ (Svedbergs)
−0.06
−0.04
−0.02
0.00
0.02
σ

a. Changes of D_{plat} and D_0 with DNA Superhelical density σ

D_{plat} and D_0 are plotted vs. superhelix density in Figure 5.6. All samples are measured at 5-7 days, at 15 days, and again at 50 days after treatment with Topoisomerase I. These values did not change significantly with time, except for the $\sigma = -0.015$ ($\Delta\ell = -8$) sample. All three measurements are indicated for that sample, but only the final values are presented for the others. The sedimentation data of Upholt et al. (1971) are coplotted with D_0 for comparison.

The curve of D_0 vs. σ is rather similar to the curve of sedimentation coefficient ($S^0_{20,w}$) vs. σ for SV40 and polyoma DNAs in 2.83 M CsCl (Upholt et al., 1971) after correcting (by a factor of 2.16) their superhelix densities, which were originally estimated using an unwinding angle of 12° for ethidium. It is also qualitatively similar to that for PM2 DNA in 3.0 M CsCl (Wang, 1974). The prominent feature of both the D_0 and $S^0_{20,w}$ data is the abrupt rise, or increase in slope. with increasing $|\sigma|$ at a critical superhelix density, which occurs between -0.015 and -0.020 for the present DNA. This indicates a rather abrupt transition to a more compact tertiary structure. Upon increasing $|\sigma|$ still further, the tertiary structure of pUC8 dimer contracts to a minimum hydrodynamic size near $\sigma = -0.025$, then becomes substantially more extended with further supercoiling up to $\sigma = -0.048$. The parallel variation (with σ) of D_0 for pUC8 dimer and $S^0_{20,w}$ for SV40 and polyoma DNAs (Upholt et al., 1971) from $\sigma = 0$ to -0.030 indicates that these molecules undergo essentially the same changes in structure with increasing superhelical strain up to that point. This argues persuasively that the observed variations in D_0, and in the other properties as well, from $\sigma = 0$ to -0.030 are not simply erratic behavior unique to our pUC8 dimer sample. but are characteristic also of other supercoiled DNAs. Readers

who may be tempted to regard the observed variations in D_0, D_{plat}, α and $[\theta]$ as spurious are encouraged to bear in mind this congruence of the D_0 vs. σ curve for the present sample with the $S^0_{20,w}$ vs. σ curves for other DNAs from $\sigma = 0$ to -0.030. The lack of congruence for $\sigma \leq -0.030$ might be due to the rather different prevailing salt concentrations.

Data taken at 15 days show that D_{plat} undergoes an abrupt substantial decrease between $\sigma = -0.015$ and $\sigma = -0.020$. However, data taken at 50 days imply that this transition then occurs at a somewhat lower superhelix density. A second structural transition between $\sigma = -0.025$ and -0.038 restores D_{plat} from the low value prevailing at intermediate superhelix densities to a more normal value.

b. Changes of $[\theta]$ and α with Superhelical Density σ

The molar ellipticity $[\theta]$ at the minimum of the CD near 240 nm and the torsion constant α are plotted vs. superhelix density in Figures 5.7a and 5.7b, respectively. $[\theta]$ measurements were made either at 5-7 days or at 15 days, and again at 2 months after treatment with Topoisomerase I. α measurements were made at 5 days and at 2 months, and up to 5 months in some cases. Most samples exhibited no significant changes over 2 months, and their 5 day values are displayed. However, between 5 days and 2 months, the sample with $\sigma = -0.025$ exhibited a considerable increase in both $[\theta]$ and α (but not D_{plat}) to values that are still somewhat low. The sample with $\sigma = -0.015$ exhibited a pronounced decrease in $[\theta]$ between 15 days and 2 months. However, in view of the temporal oscillations of D_{plat} and D_0 for that same sample, the difference between its 5 day and 2 month molar ellipticities might well have been much smaller or even negligible. New samples with $\sigma = -0.027$ and -0.033 were prepared from

Figure 5.7. Variation of the molar ellipticity $[\theta]$ (at the minimum near 250 nm) and the torsion constant α of pUC8 dimer with superhelix density. Conditions are the same as in Figure 5, with the exception that the torsion constants were measured at 20°C. (■) 5-7 days after preparation; (+) 15 days after preparation: (□) 50 days after preparation; (•) samples prepared from the same intial stock solution 4 months after the other samples and measured within 5 days.

Top: $[\theta]$ *vs.* superhelix density σ. Only the $\sigma = -0.015$ and -0.025 samples changed significantly over time.

Bottom: α *vs.* superhelix density. Torsion constants are averages for 70 and 120 ns time spans. For the FPA measurements only, ethidium was added to a concentration of 1 dye per 300 base pairs. With the exception of $\sigma = -0.025$, the samples denoted by ■ did not change significantly over a period of 2 months, and it is the final values that are plotted. The final measurement for the $\sigma = -0.025$ sample is denoted by □. The error bars are less than or equal to the size of the symbols in the figure. Complete data for $\sigma = -0.048$ and $\sigma = -0.031$ are given in by Schurr et al. (1988), and demonstrate the ability of FPA measurements to distinguish between samples whose torsion constants differ by only 10%.

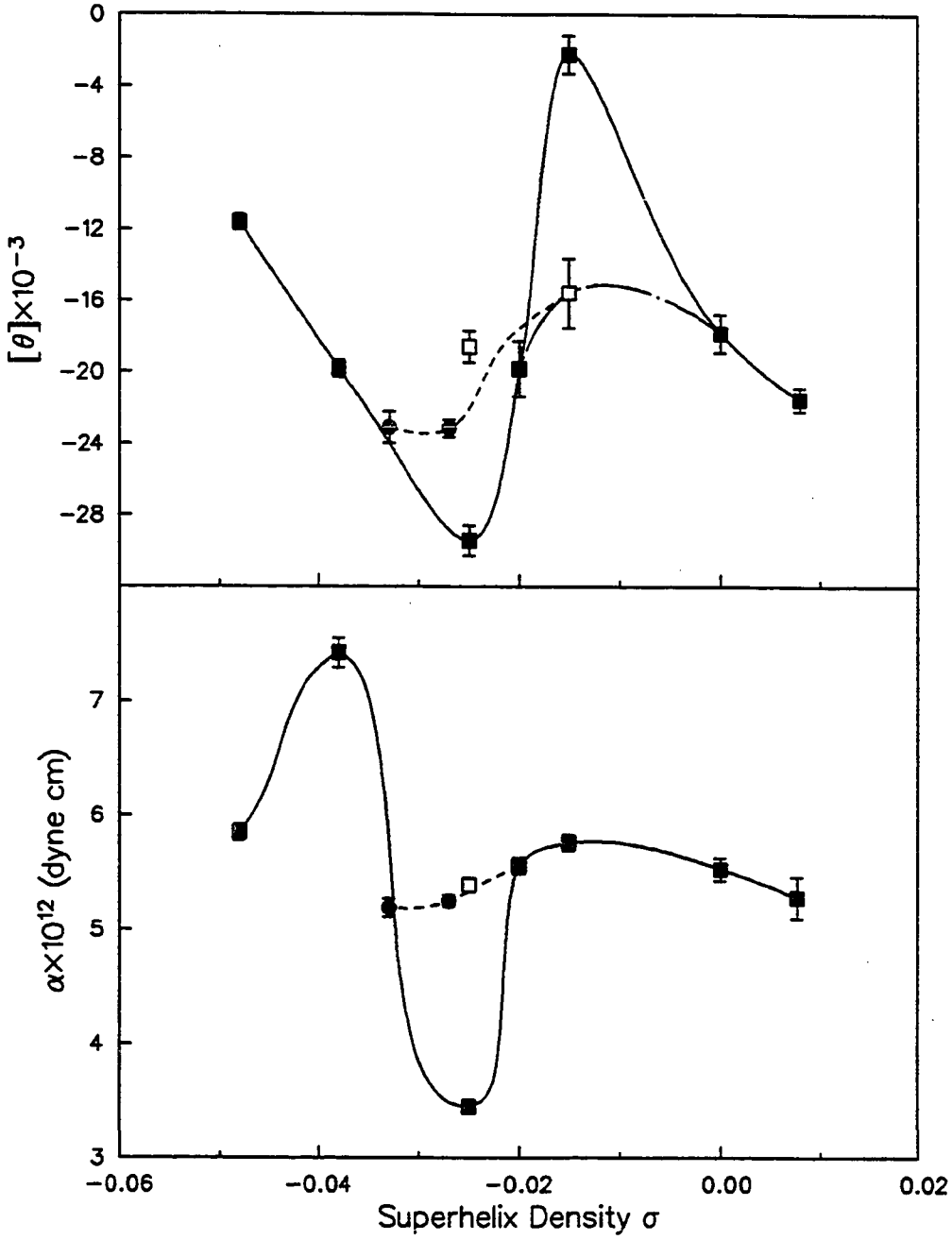
0
-4
-8
-12
-16
-20
-24
-28
[θ]×10⁻³
7
6
5
4
3
α×10¹² (dyne cm)
-0.06
-0.04
-0.02
0.00
0.02
Superhelix Density σ

the original stock solution 3-4 months after the other samples and measured at 5 days after treatment with Topoisomerase I. Sufficient sample for DLS was not available. These newer samples also exhibit low $[\theta]$ and α-values that are comparable to other values in the intermediate range of superhelix densities from $\sigma = -0.025$ to -0.035. We emphasize that the reduction in torsion constant in this intermediate range is statistically significant, outside the rather small standard deviations of these data, even for the 2 month data, for which the reduction is rather modest. The very low value of α (3.4×10^{-12} dyne-cm) observed for the $\sigma = -0.025$ sample at 5 days matches closely that (3.2×10^{-12} dyne-cm) induced by partial relaxation of pBR322 by E. coli single-strand binding protein (Langowski et al., 1985). The latter value was stable for well over a month in a sample stored at 5°C, whereas the former value changed significantly between 5 days and 2 months in a sample stored at 21°C. The two samples (-13 and -20) on the upper curve in Figure 5.2 have abnormal torsional rigidities ($\alpha = 3.4 \times 10^{-12}$dyne-cm for -13 sample and $\alpha = 7.4 \times 10^{-12}$dyne-cm for -20 sample) than other samples which belong to the lower curve in Figure 5.2. Interestingly, the very low value of α at $\sigma = -0.020$ and the very high value of α at $\sigma = -0.038$ are observed for the two samples exposed for the longest time to Topo I (c.f. $\tau = -13$ ant -20 in Figure 5.2). This may indicate that rewinding from a more completely equilibrated secondary structure is not kinetically facile, and unusual metastable intermediates are encountered.

The abruptness and extremely slow kinetics of the transition near $\sigma = -0.018$ argue that it is highly cooperative. The oscillations in D_0 and D_{plat} of the $\sigma = -0.015$ sample from 5 days to 15 days to 2 months suggests that this secondary structure transition may be strongly coupled to a transition in tertiary structure. and that the overall transition proceeds via one or more distinct

intermediates.

5.4.2 Hypotheses Regarding Plasmid Structure

The data in Figures 5.6 and 5.7 point clearly to an abrupt structural transition near $\sigma = -0.018$, and also to a second structural transition near $\sigma = -0.035$. We consider below four hypotheses regarding the nature of these transitions. It should be emphasized at the outset that D_{plat} and α reflect mainly short-range dynamics over distances up to a several hundred base-pairs, and should be rather insensitive to superhelix density, provided it does not affect the twisting and bending rigidities. $[\theta]$ reflects mainly nearest-neighbor electronic interactions, which are perturbed only slightly by small simple twisting and bending strains. The four hypotheses (denoted H1, ... H4) and their comparisons with experimental results are as follows.

(**H1**) Increasing negative superhelix density induces a cooperative allosteric transition near $\sigma = -0.018$ from strained B-helix to an alternate global secondary structure (b) with a lower twisting rigidity, and a subsequent, perhaps broader, allosteric transition near $\sigma = -0.037$ to yet another global secondary structure (a) that exhibits more normal properties by $\sigma = -0.048$ (native superhelix density). This hypothesis provides the simplest interpretation of the most data in Figures 5.4-5.7. Under this hypothesis, the changes in D_0, D_{plat}, $[\theta]$ and α are all expected to occur in the same ranges of superhelix densities, as observed. The proposed global, or extensive, nature of the new secondary structures a and b is consistent with the observed substantial changes in CD, α and D_{plat} and with the uniformity of α exhibited by several of the samples. The more compact tertiary structures observed at intermediate superhelix densities could arise either from a decrease in

bending rigidity, or from a change in type of tertiary structure (e.g. from toroidal to interwound) in response to changes in rigidity. The cooperative nature of the proposed secondary structure transition near $\sigma = -0.018$ is consistent with its observed abruptness and with the extremely slow changes observed in the $\sigma = -0.015$ sample. By itself this hypothesis cannot account for the observed long term changes in $[\theta]$ and α of the $\sigma = -0.025$ sample.

(H2) Increasing negative superhelix density beyond a critical value ($\sigma = -0.018$) induces transitions to radical secondary structures at one or a few sequences of small extent that exhibit major rigidity weaknesses. A similar hypothesis was invoked by Brady et al. (1986) to account for the rapid reduction in writhe of supercoiled COP608 with temperature above 22°C. This hypothesis is not simply consistent with the rather large changes observed here in $[\theta]$ and D_{plat}. It is also difficult to reconcile with the simultaneous decrease in, and uniformity of, α. If the dye is bound sufficiently near a major rigidity weakness to manifest that, its dynamics should also reflect that non-uniformity, which is not observed. Absorption of most of the writhe into twist in small domains of radical secondary structure, as advocated by Brady et al. (1986,1987), should increase the size of the coil envelope, thereby decreasing D_0, should not affect $[\theta]$, should affect the magnitude and uniformity of α together (if at all), and should affect D_{plat} only by shifting it toward the value for the $\sigma = 0$ sample. all contrary to observation. It is particularly difficult to see why the effect of these radical structures on the internal dynamics should vanish with increasing negative superhelix density beyond $\sigma = -0.037$, as it does. For such reasons this hypothesis is discounted.

It is not possible to say precisely what fraction of the DNA in each plasmid

undergoes these transitions in "global" secondary structure, except that it is probably quite substantial.

(H3) Increasing negative superhelix density merely causes a monotonic increase in simple strain of the normal secondary structure (B-helix) without inducing any transitions in the type of secondary or tertiary structure (e.g. from straight interwound to toroidal). In essence this is the standard model of supercoiling. This hypothesis conflicts with the data in several regards. (i) Simple strain should produce no changes in α or D_{plat}, contrary to observation. The observed decrease in the effective torsion constant at intermediate superhelix density is particularly difficult to reconcile with this hypothesis. Any geometrical effect of supercoiling would be expected to cause a tilt of the transition dipole toward the effective helix-axis, which should increase the apparent α. Highly bent and/or compact tertiary structures prevailing in the intermediate range of superhelix densities would be expected to increase the resistance to torsional motion, and thereby also increase the apparent α. (ii) Under this hypothesis, any variation in $[\theta]$ with σ should be monotonic, contrary to observation. (iii) It is highly doubtful whether a progressive change in linking number difference, with no change in rigidity or type of tertiary structure, could account for the observed rapid contraction of the hydrodynamic radius on going from $\Delta\ell = 8$ ($\sigma = -0.015$) to 10 ($\sigma = -0.020$) turns, especially for samples containing several topoisomers. (iv) Under this hypothesis, there is no reason why D_{plat}, α, and $|[\theta]|$ should also decrease at the same critical superhelix densities where D_0 rapidly increases, as they do. (v) Slow changes of any kind are not consistent with this hypothesis, because only incremental changes in linking number difference, rather than transitions in types of secondary or tertiary structure,

are postulated. In summary, the present data only lengthen this list of experimental contradictions of the standard model of supercoiling. Hence, this hypothesis is discounted.

(**H4**) Increasing negative superhelical strain induces abrupt transitions in tertiary structure, though not in secondary structure. In principle, this could occur by discontinuous variation in writhe with linking number difference (LeBret, 1984) or via a change in type of tertiary structure (e.g. from interwound to toroiodial). This hypothesis cannot avoid the contradictions (i) and (iv) under H3. Moreover, no sign of any transitions in tertiary structure is evident in gel electrophoresis. Hence. this hypothesis is discounted.

Of the hypotheses considered, only H1, is respected by most of the data.

5.4.3 The Slow Temporal Changes

Two of the seven samples ($\sigma = -0.025$ and -0.015) showed significant changes in their properties between 5 and 50 days. Although such temporal changes are not central to the main objectives or conclusions of this work, which are substantiated by either the 5 day or 50 day data. they nevertheless merit discussion. In this section we address the possibility that these slow changes are artifacts resulting from chemical changes or degradation of the DNA. The most obvious candidates are depurination and bacterial infection. Reasons why these possibilities are discounted are given below.

(i) The rate of depurination of double-strand DNA at 37°C in 0.15 M NaCl at pH 7.4 is $R = 3 \times 10^{11}$ s^{-1} (Lindahl and Nyberg, 1972). From the reported activation energy $\Delta E = 130$ KJ/mole, we estimate that $R = 1.9 \times 10^{-12}$ s^{-1} at 21°C in 0.15 M NaCl. pH 7.4. It remains to correct for the higher pH (8.0) and lower ionic strength ($I = 0.022$ mM) in our samples. The data

of Lindahl and Nyberg (1972) and Greer and Zamenhof (1962) imply that $R \propto [H^+]$, so raising the pH by 0.6 should decrease the rate by a factor of 3.0-4.0. The effect of decreasing ionic strength is to increase the rate. The data of Greer and Zamenhof (1962) are roughly consistent with $R \propto I^{1/2}$, so decreasing the ionic strength from 0.15 to 0.022 should increase the rate by a factor of 2.6. These two corrections nearly cancel, and are ignored. When the extent of reaction is very small, the probability that any given purine has depurinated in time Δt is $p = R\Delta t$. After 50 days, we estimate $p = 8.2 \times 10^{-6}$. The average number of depurinations per pUC8 dimer is then $p(5434) = 0.045$. Thus, only 1 plasmid in every 22 is expected to contain a depurinated base-pair after 50 days. This is far too little to affect our measurements.

In any case, depurination would be expected to affect all samples equally, not just two of them. In addition, any changes attributable to depurination must be monotonic. thus, depurination cannot account for the temporal oscillations in D_0 and D_{plat} observed for the $\sigma = -0.015$ sample. If depurination significantly affects $[\theta]$, it should induce a change in the same direction in all samples. However, $[\theta]$ increases for the $\sigma = -0.025$ sample but decreases for the $\sigma = -0.015$ sample. DNA degradation of any kind is very difficult to reconcile with increases in α and $[\theta]$, while D_0 and D_{plat} remain constant, as observed for the $\sigma = -0.025$ sample. Instead, such behavior probably reflects a change in base and dye-tilt with no change in torsion constant, as noted above.

In summary, depurination is a most unlikely cause of any temporal changes in our samples.

(ii) Perhaps the strongest argument against degradation due to bacterial infection is that none of our supercoiled DNAs suffered appreciable nicking after two months, even though nicking is the most likely consequence of such infection. Also, the light scattering, which is extremely sensitive to the presence of particles as large as bacteria, showed no hint of such contamination.

The pattern of occurrence of the temporal changes among the different samples also weighs against bacterial infection as the cause. For each superhelix density, the sample is actually stored in three cells, one for DLS, one for CD, and one for FPA. For both the $\sigma = -0.015$ and -0.025 samples, changes are observed in properties measured for two, but not all three, of the cells. If some sort of bacterial infection were responsible for these changes, then a purely random attack would be most unlikely to yield such a pattern. The number of ways in which 4 infections can be placed in 21 cells, only 1 to a cell, is $\eta_{tot} = (21)!/((17)!(4)!) = 5985$. The number of ways in which 4 infections can be placed so that they occur in any two of the seven samples, and then in two of the three cells of each is $\eta_w = [(7)(6)/2!] \cdot [(3)(2)/2!][(3)(2)/2!] = 189$. The probability of the observed distribution then is $p = 189/5985 = 0.032$. Thus, there is only about 1 chance in 32 that random infection would produce the pattern observed. Of course, non-random infection would occur, if the infection were initiated prior to dividing the sample among its cells, for example during the Topoisomerase I treatment. However, that should yield infection in all three samples in each case, not just two out of three. Thus the observed pattern of temporal changes among the cells is rather unlikely to arise from bacterial infection.

Any temporal changes in physical properties of the DNA induced by bacterial infection should be monotonic, and any changes in $[\theta]$ should be in the same direction for all samples, both contrary to observation. Thus, bacterial infection is most unlikely to be the cause of the temporal changes in our samples. Indeed, in many similarly prepared samples under these conditions (10 mM NaCl, 10 mM Tris, 1 mM EDTA pH 8.0) we have never observed bacterial contamination, even after several years storage at 5°C.

Next we consider the connection between the hypothesis H1 and some of the aforementioned contradictions of the standard model. That is, we tentatively accept the notion that the secondary structure undergoes successive allosteric transitions to two alternate global secondary structures with increasing negative superhelix density from $\sigma = 0$ to -0.050, and formulate the following hypothesis.

5.4.4 Hypothesis Regarding the Transition Near $\sigma = -0.018$

It is apparent from our data on the $\sigma = -0.015$ sample that this transition is extremely slow. Our hypothesis is that, upon relaxation of the superhelical stress, some or perhaps even all of the DNA secondary structure becomes kinetically trapped in the intermediate b state with low torsion constant, because its reversion to normal B-helix near $\sigma = -0.018$ is so slow. This provides an explanation for the data in Figure 5.1, expecially if allowance is made for the considerably lower temperature (5°C) at which those samples were stored. An extension of this hypothesis is that intercalating dyes are capable of further kinetically hindering the transition near $\sigma = -0.018$. Thus, relaxation of superhelical stress by intercalating dyes results in even more extended trapping of the intermediate b state with low torsion constant. This provides an explanation

for the observed failure of completely relaxed DNA/dye complexes to exhibit the same local structures, rigidities, and dynamics as linear or nicked circular DNAs, and accounts for the low torsion constants observed. It also accounts for the substantially lower values of the twist energy parameter obtained from dye binding measurements. Not only is the torsion constant of the trapped intermediate state lower, but the free-energy decrease from that state to normal B-helix at $\sigma = 0$ is never completely realized. This hypothesis also accounts for the appearance of metastable secondary structure in relaxed topoisomers resulting from the action of Topoisomerase I on native supercoiled DNAs (Negri et al., 1989).

From this hypothesis follow two predictions.

(1) When supercoiled DNAs are relaxed from an initial superhelix density σ_0 to 0 by intercalating dyes, the structure and properties (e.g. $S^0_{20,w}$) of the completely relaxed product with $\sigma = 0$ should be of one type (corresponding to the kinetically trapped intermediate b state) when $\sigma_0 < -0.018$ (large $|\sigma_0|$), but should correspond to normal B-helix when $-0.018 < \sigma_0$ (small $|\sigma_0|$). More specifically, the translational friction factors, or $S^0_{20,w}$ corrected for differences in buoyant density, should be nearly the same at $\sigma = 0$ for all DNA/ethidium complexes for which $\sigma_0 < -0.018$, whereas for those complexes with $-0.018 < \sigma_0$, the $S^0_{20,w}$ at $\sigma = 0$ should exhibit a significantly different value, which is nearly the same as for $\sigma_0 = 0$ in the absence of dye. This prediction matches quite well the pertinent observations of Upholt et al. (1971) on SV40 DNAs with different σ_0. Those workers report essentially identical $S^0_{20,w}$ values for relaxed DNA/ethidium complexes with $\sigma_0 = -0.078$, -0.136 and -0.170, which indicates that the effect of

intercalated dye to lengthen these DNAs is effectively compensated, perhaps by a decreased (or possibly attractive) excluded volume interaction. They also report 10% higher $S^0_{20,w}$ values for relaxed DNA/ethidium complexes with $\sigma_0 = -0.018$ and for relaxed DNA in the absence of dye. This hypothesis does not explain why $S^0_{20,w}$ of the trapped intermediate state at $\sigma = 0$ is lower (less compact) instead of higher than that of the B-helical state (more compact).

(2) When native supercoiled DNAs are relaxed by Topoisomerase I for various times, different amounts of the intermediate state can occur in a particular topoisomer only when its superhelix density lies in the region $(-0.018 \leq \sigma)$ where that state is metastable, and only if secondary structural equilibration is catalyzed by Topoisomerase I. This prediction matches quite well the pertinent observations of Negri et al. (1989).

One may well ask why the proposed b-state to B-helix transition is so slow. Whenever structural transitions in such systems are highly cooperative, their kinetic rates are expected to be extremely slow. High cooperativity arises from a large free energy and consequent low probability of junctions, or domain walls, between two domains of different secondary structure. Transitions between the presently identified global secondary structures, namely A, B, Z, and denatured DNAs are known to be highly cooperative. A change in extent of the transition "reaction" requires nucleation of new domains of one type of secondary structure in the midst of existing domains of the other. This nucleation process, which involves the formation of two new junctions bounding a small island of new secondary structure, is the kinetically slow step. In addition, metastability is promoted by the fact that the kinetic rate of conversion of the metastable

structure is actually slowest near the midpoint of the transition, so conversion in any given time is more likely to be observed well into the metastable region than near the midpoint. This phenomenon is clearly manifested in the rate of renaturation of DNA, which actually increases with decreasing temperature in the region immediately below T_M (Wetmur and Davidson, 1968). This behavior is attributed to the fact that the size of island required to stabilize a nucleus of the stable structure within a domain of metastable structure becomes very large as relative free-energies of the two structures converge at the midpoint of the transition.

5.4.5 Comparison with Other Transitions and Structures in Supercoiled DNAs

It is interesting to compare the structural transitions observed in this work with those observed in other experiments.

The decrease in D_{plat} and increase in D_0 of pUC8 dimer, as the absolute superhelix density is decreased from native (-0.048) to intermediate (-0.025) values, is quite comparable to the corresponding changes exhibited by supercoiled M13mp7 DNA, when the NaCl concentration is increased from 0.2 to 0.4 M (Wilcoxon, J., and Schurr, J.M., unpublished data). However, this circumstance is not easy to understand, because increasing NaCl concentration should shift σ to slightly more negative, rather than less negative, values (Bauer, 1979). Conceivably, the higher NaCl concentration simply favors the b secondary structure prevailing at intermediate superhelix density ($\sigma = -0.025$) over the a state prevailing at higher negative superhelix density ($\sigma = -0.048$), despite its small opposite effect via the superhelix density itself.

The change in CD of pUC8 dimer, as the superhelix density is decreased

from native (-0.048) to intermediate (-0.025) values, is not identical to that exhibited by M13mp7 DNA, when the buffer is changed from Tris to citrate or cacodylate (Shibata et al., 1984), despite the similar changes in α and D_{plat}. For M13mp7 DNA, a large increase in the CD band at 270 accompanies the decrease in torsion constant and D_{plat}. However, the 270 nm CD band of pUC8 dimer is almost independent of superhelix density, as is apparent from Figure 5.5. If these secondary structures should actually be similar, then their tertiary structures must be rather different to account for the difference in CD.

5.4.6 Additional Puzzles and Base-Tilt

Certain observations are quite baffling, and we consider them separately here, as our interpretations are rather speculative.

The substantial increases in $[\theta]$ and α for the $\sigma = -0.025$ sample between 5 days and two months are quite puzzling. Equally puzzling is the absence of any corresponding changes in D_{plat} and D_0 for that same sample. Conceivably, the actual torsion and bending constants do not change significantly, in which case D_{plat} and D_0 would remain constant. Instead, the tilt of the bases might increase somewhat over time, thereby changing $[\theta]$ and decreasing the polar angle ϵ_0 of the transition dipole of intercalated ethidium with respect to the helix-axis. A modest decrease in ϵ_0 would appreciably increase the apparent torsion constant. (The FPA experiment cannot distinguish an increase in torsion constant from an appropriate decrease in ϵ_0.) This appears to be the only way to rationalize an increase in apparent α without a corresponding change in D_{plat}, barring some measurement artifact.

The apparent torsion constant of the $\sigma = -0.038$ sample is highly non-uniform and abnormally high compared to the $\sigma = -0.048$ sample, although

its D_{plat} is quite normal. This sample was remeasured several times with no change in results. Conceivably, the actual torsion constant of this DNA is the same as that of the $\sigma = -0.048$ sample, but instead the ϵ_0 of its intercalated dye is somewhat lower. In this way, its apparent α could be rather large, even though its D_{plat} is normal. Again, this appears to be the only way to rationalize these puzzling observations. If this were the case, then the pronounced non-uniformity of α for the $\sigma = -0.038$ sample would have to arise from dyes intercalated in two or more kinds of sites or domains with different ϵ_0 values. Indeed, under any interpretation, one would probably have to conclude that the $\sigma = -0.038$ sample is an admixture of two or more domains of different secondary structure, either in the same or different topoisomers.

If these speculations are correct, then one might infer that the equilibrium base-tilt is somewhat greater in the b state prevailing in the intermediate region of superhelix densities than elsewhere. One might also suggest that, with decreasing superhelix density from $\sigma = -0.048$, the base-tilt increases before the actual torsion constant decreases, so the apparent α first rises at $\sigma = -0.038$, then falls at $\sigma = -0.033$, as observed. One might also suggest that, as the negative superhelix density is increased into the intermediate range from $\sigma = -0.015$, the decrease in torsion constant is kinetically more facile than base-tilting.

5.4.7 Potential Significance in Biology

The existence of two (or more) distinct secondary structures that interconvert in a highly cooperative manner would enable long-range communication between distantly bound proteins. (Shibata et al., 1984). High cooperativity implies that the free-energy to form a junction between two domains of different secondary structure is quite large. Hence, such junctions are relatively rare and domains

of either kind of secondary structure are rather extended. A regulatory protein with a significant preference for either structure, or with the ability to reduce the junction free-energy, at its binding site could influence the affinity of the DNA for a second protein (e.g. RNA polymerase) at a binding site some distance away. Both general and specific aspects of possible long-range communication between distantly bound regulatory proteins via allosteric long-range switching of the DNA secondary structure were discussed previously by Shibata et al. (1984).

The extreme slowness of an undriven structural transition does not necessarily disqualify it from a significant role in biology. We note that the relaxation times of polarized states of magnetic storage devices in computer memories, tapes, and disks is extremely long when they are undriven, but still they can be switched in extremely short times ($\sim$1 μs) when the appropriate driving force is applied. Presumably the same is true of the secondary structure states of DNA, whether global or local.

Evidence that (CAP + cAMP) binding may induce a long-range change in secondary structure of superhelical DNAs has been briefly noted (Benight et al., 1987a,b), and will be discussed in detail in a forthcoming communication.

It has been suggested that the superhelix density of bacterial plasmids in vivo lies in the range $-0.025 < \sigma$ (Greaves et al., 1985). If so, then the normal state of the plasmid might well correspond to the one observed here at intermediate superhelix density, which exhibits the low torsion constant. In that case, transitions to alternate states on either side (i.e. at higher twist or lower twist) might be available for purposes of regulation and control via long-range state-switching.

Chapter 6
The Effect of DNA Superhelicity on Structures of pBR322 DNA

6.1 Introduction

The effect of superhelical density on the structure and dynamics of suprecoiled pUC8 dimer DNA was studied in Chapter 4. Evidence for two allosteric transitions in secondary structure was found. Little attention has been paid to the possibility of global secondary structure changes induced by superhelical stress. Most of the previous investigations concern the induction of radical secondary structures at specific sequences. Therefore allosteric transitions in secondary structure induced by superhelical stress need to be examined with other DNAs. Plasmid pBR322 DNA has been widely used in the study of biophysical chemistry of nucleic acids and in molecular biology. It would be interesting to know how the secondary and tertiary structures of pBR322 changes when the superhelix density is varied.

Samples of pBR322 DNA with various linking differences were prepared. DLS. FPA and CD experiments were performed to examine the possibility of allosteric secondary structural transitions in pBR322 DNA.

6.2 Experimental Protocol

6.2.1 Sample Preparation

pBR322 (4363 bp) was prepared according to standard plasmid preparation procedures (see Appendix A). After three phenol extractions and three diethyl ether extractions. the pBR322 DNA solution was dialyzed agaist 2 liters of a buffer(LSTE) consisting 10 mM NaCl. 100 mM Tris. 1 mM EDTA, pH 7.5. for 24 hrs. and then dialyzed against 2 liters of HSTE buffer consisting 0.5 M NaCl, 10 mM Tris. 1 mM EDTA. pH 7.8. for 24 hrs. and finally dialyzed back to

LSTE. UV spectra were taken. The purity of the DNA sample was assumed to be high because the $A_{260}/A_{280} = 1.997$. The total amount of DNA is 14.07 mg. assuming that $A_{260} = 1.0$ corresponds to a 0.05 mg/mL DNA solution. The GEL picture showed that the amount of nicked DNA is about 5% of the total supercoiled DNA. Then. the supercoiled DNA was purified by standard CsCl density gradient in the presence of ethidium bromide. The volume of the DNA solution was measured. exactly 1 gram solid CsCl was added per mL of solution. 0.8 mL of ethidium bromide solution (10mg/mL in H_2O) was added for every 10 mL of CsCl solution. The concentration of ethidium bromide should be approximately 600 μg/mL. Finally the solution was centrifuged at 38K rpm for 44 hrs. at 1°C using a Beckmann Type-50.2 Tl rotor. The lower band which contains supercoiled DNA was collected. The collected DNA-EB solution was extracted repeatedly (15 times) with buffer-washed isopropanol by vigorous shaking and spinning at 4K rpm until ethidium fluorescence could no longer be detected in a 50 mW beam of 351.1 nm light from an Ar-ion laser. The sample was then dialyzed for 24 hrs against 2 liters of LSTE buffer. followed by a second 24 hr dialysis against HSTE buffer. This dialysis cycle of alternating high (0.5 M) and low (10 mM) NaCl concentration every 24 hrs was continued for 7 days. The total amount of ethidium-free suprecoiled DNA was 5.69 mg. The 15x isopropanol extraction causes about 60% loss of DNA. The A_{260}/A_{280} ratio was 1.987. The percent nicked circular DNA was less than about 8%. as judged from relative band intensities in gel electrophoresis. The stock DNA solution was stored at 5°C.

About 1.1 mg DNA sample was treated by Topo I in the presence of various amounts of ethidium. The Topo I reaction mixture was the same as that in chapter 5 (see 5.3.1). Seven pBR322 samples with different median numbers

of superhelical turns were prepared. In producing all the samples, 12 units of Topo I per unit optical density (A_{260}) of DNA were incubated at 37°C for more than one hour. The relaxation of the initial superhelix density is confirmed to be complete by running gels of the reaction mixture. Upon completion of the reaction, each sample was extracted three times with buffered phenol and three times further with diethylether. Each sample was then dialyzed against HSTE buffer for 24 hours, then against LSTE buffer for 24 hrs. This dialysis cycle of alternating high and low salt was continued for 5 days. After such treatment with ethidium and Topoisomerase I, $A_{260}/A_{280} = 1.866 - 1.972$. All of the optical measurements were performed on DNAs in the LSTE buffer at 21°C. The Topo I reaction conditions for seven samples are summerized in Table 6.1. τ_2 is the measured linking number difference or number of superhelical turns. r is the binding ratio of EB per DNA bp. $\tau(EB)$ is the calculated number of superhelical turns removed by EB by employing equation

$$\frac{r}{C} = K\frac{(1-2r)^2}{(1-r)} \tag{6.1}$$

to determine the binding ratio r. and assuming the unwinding angle of EB is 26°C. . The binding constant K is assumed to be 3×10^5 at 21°C. $\Delta\tau(T)$ is the correction of the number of superhelical turns for changing the temperature from the Topo I reaction temperature (37°C) to the gel temperature (21°C) by assuming $\Delta\sigma/\Delta T$ to be 3.1×10^{-4} degree^{-1} (Bauer,1978). Temperature T refers to the Topo I reaction temperature. Time t is the time period of Topo I reaction. τ_1 is the expected number of superhelical turns after temperature correction. $\tau_1 = \tau(EB) + \Delta\tau(T)$.

Table 6.1 Topo I Reaction Conditions of pBR322

τ_2	+3	−2	−4	−14	−16	−24
$\sigma \times 10^2$	0.7	−0.5	−1.0	−3.4	−3.9	−5.8
r	0.000	0.035	0.044	0.080	0.106	0.142
τ(EB)	0.00	−10.88	−13.70	−25.2	−33.5	−44.7
T	37°C	37°C	37°C	37°C	37°C	37°
$\Delta\tau$(T)	−1.94	−1.94	−1.94	−1.94	−1.94	−1.94
t(hrs)	1.0	6.0		4.8	4.3	5.0
τ_1	−1.94	−12.8	−15.6	−27.1	−35.4	-46.6

The −24 sample was made in a somewhat different way. After supercoiled DNA was relaxed by Topo I, ethidium bromide was added to the sample, then Topo I was added again. Because a rather small amount of −24 was made, only FPA and CD experiments were done on that sample. The −10 sample was made out of the +3 sample after DLS experiment was completed for +3 sample. However, the gel showed that the relative amount of nicked DNA is unacceptably high in the −10 sample, so the results for that sample are omitted from consideration. The measured median number of superhelical turns τ_1 vs. the expected median number of superhelical turns of each sample τ_2 is plotted in Figure 6.1. The median numbers of superhelical turns obtained for all the samples vary linearly with the amount of added EB. The median Number of linking number difference determined by band counting method and the number of superhelical turns calculated by using the the binding ratio obtained from equation (6.1) and assuming 26° unwinding angle of bound EB vs. the added

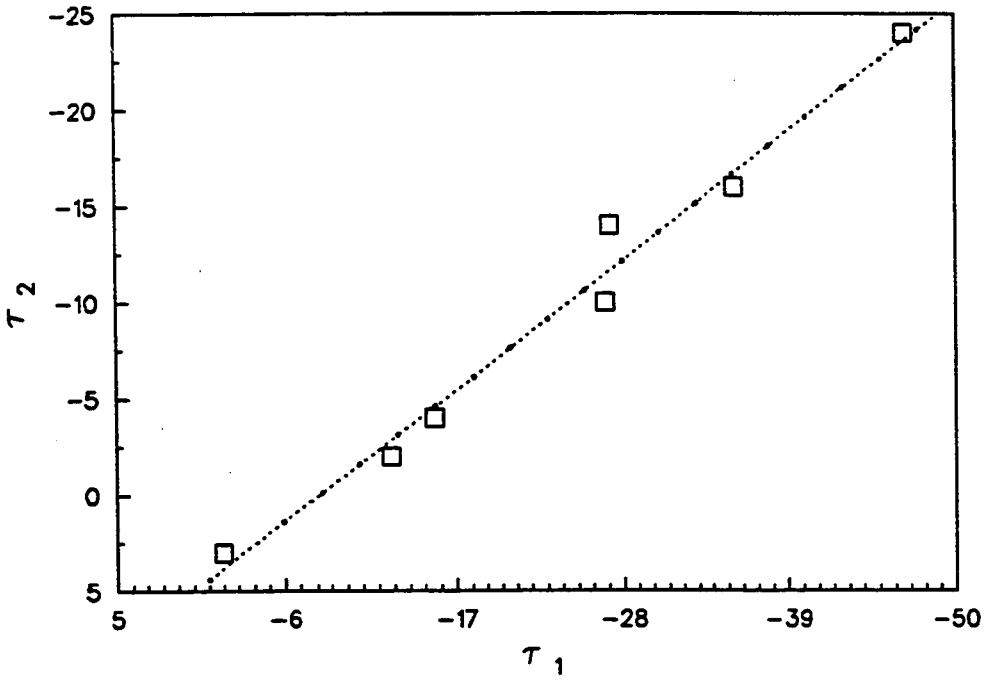

Figure 6.1. The measured median number of superhelical turns τ_2 vs. the expected median number of superhelical turns τ_1 of the topoisomer pBR322 sample preparation.

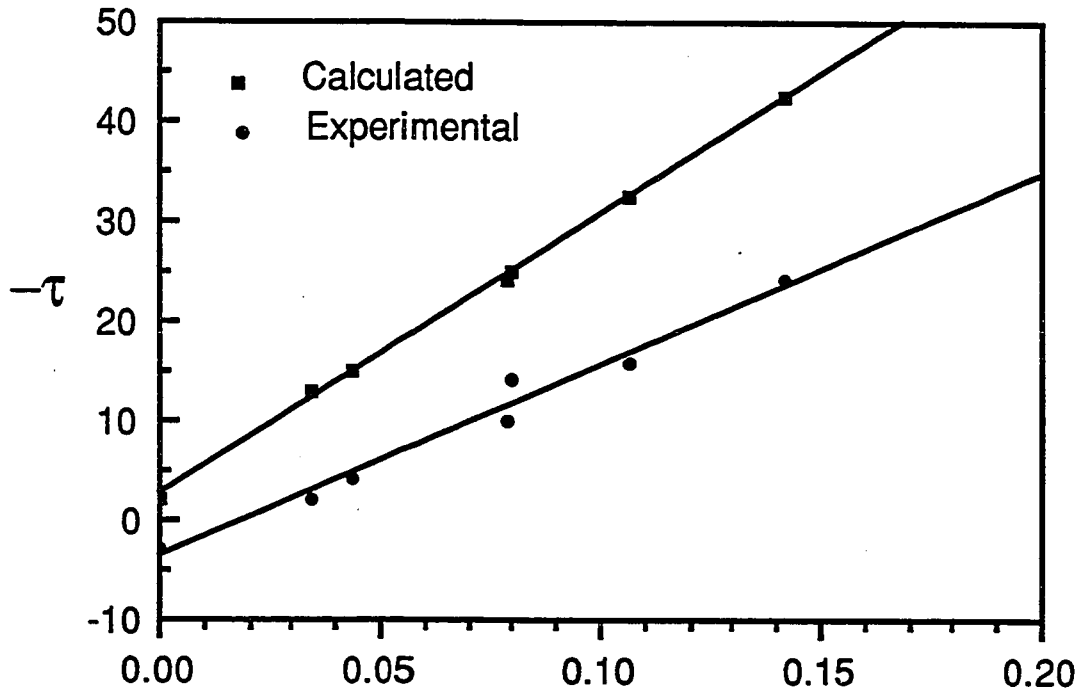

Figure 6.2. Number of median number of superhelical turns obtained from band counting of pBR322 topoisomer preparations and calculted number of superhelical turns assuming the unwinding angle of EB 26°vs. ratio of added EB/bp.

EB/bp ratio are plotted in Figure 6.2. The slope of the curve in figure 6.2 is linearly related to the unwinding angle, because

$$\tau(EB) = \tau N \phi/360 \tag{6.2}$$

where N is the total number of base pair of the supercoiled DNA, and ϕ is the unwinding angle of the dye. The slope of the calculated curve is proportional to 26°. The unwinding angle inferred from the experiment could be obtained by comparing the slopes of the two curves. So, the apparent unwinding of EB in the presence of 10 mM Mg^{2-} is 17.7. It is expected that Mg^{2-} might compete with EB binding sites so that the apparent unwinding angle is much lower than 26°or the unwinding angle of EB under the reaction condition is 17.7°instead of 26°. But the unwinding angle of EB is not temperature dependent. This could be seen in figure 5.2 because the slopes of two curves at different temperatures namely 15°C and 37°C are nearly the same. The apparent unwinding angle of EB obtained from preparation of topoisomers of pUC8 dimer described in Chapter 5 (see 5.3.1) is 15.03°.

6.2.2 Gel Electrophoresis

The electrophoretic analyses were performed in 0.8% (w/v) agarose slab gels in an electrophoresis TBE buffer containing 0.089 M Tris-borate, 0.089 M boric acid and 0.002 M EDTA. PH 8.0, or in a high resolution TBE buffer containing 0.4 to 0.8 μg/mL chloroquine. Current was applied at 2 V/cm for 20 hrs at room temperature. The gels were stained for 1 hr in 0.5 μg/mL ethidium bromide, and photographed with Polaroid type 667 film. Figure 6.2a shows typical results in 0.8 μg/mL chloroquine, and Figure 6.2b shows the results in 0.4 μg/mL chloroquine. For the less twisted samples, the number of superhelical turns of the median

Figure 6.3. Gels of pBR322 samples. The median linking number difference ($\Delta\ell$) is indicated at the top of the pictures. (Gel conditions: 0.8%(w/v) agarose, TBE buffer, pH 8, field strength 2V/cm, 24 hours). Top: with 0.8μg/mL chloroquine. Bottom: with 0.4 μg/mL chloroquine.

0.8 μg/ml Chloroquine

-24 -21 -31 -10 -2 +3

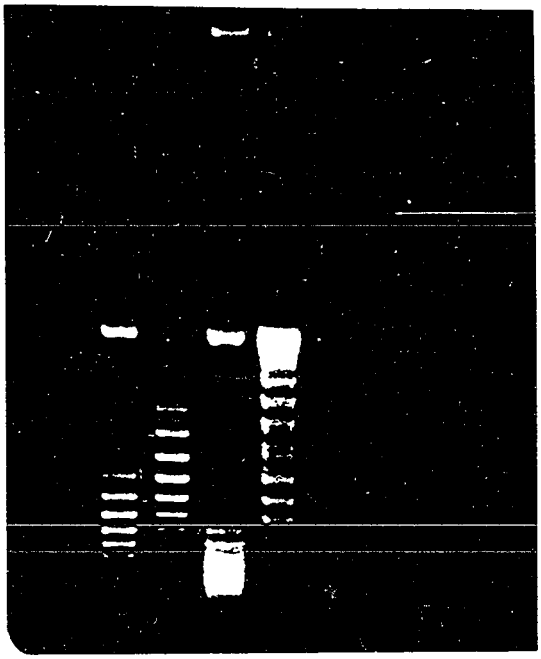

0.4 μg/ml Chloroquine

-24 -21 -16 -14 -14 -10 -4 -2 +3

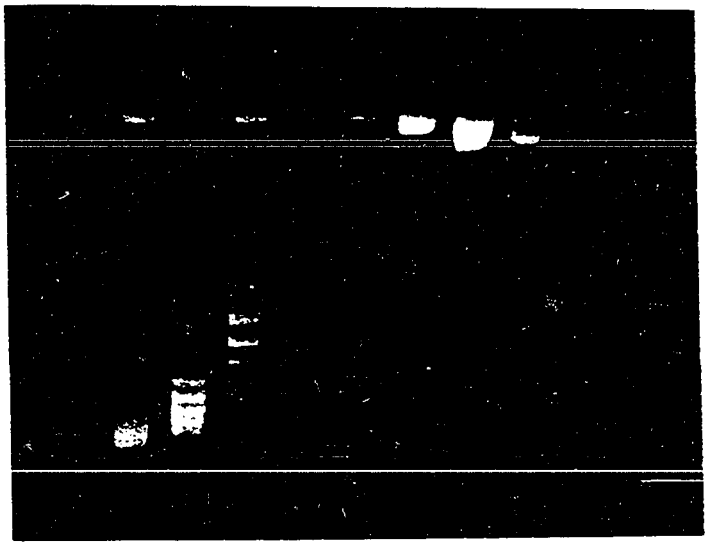

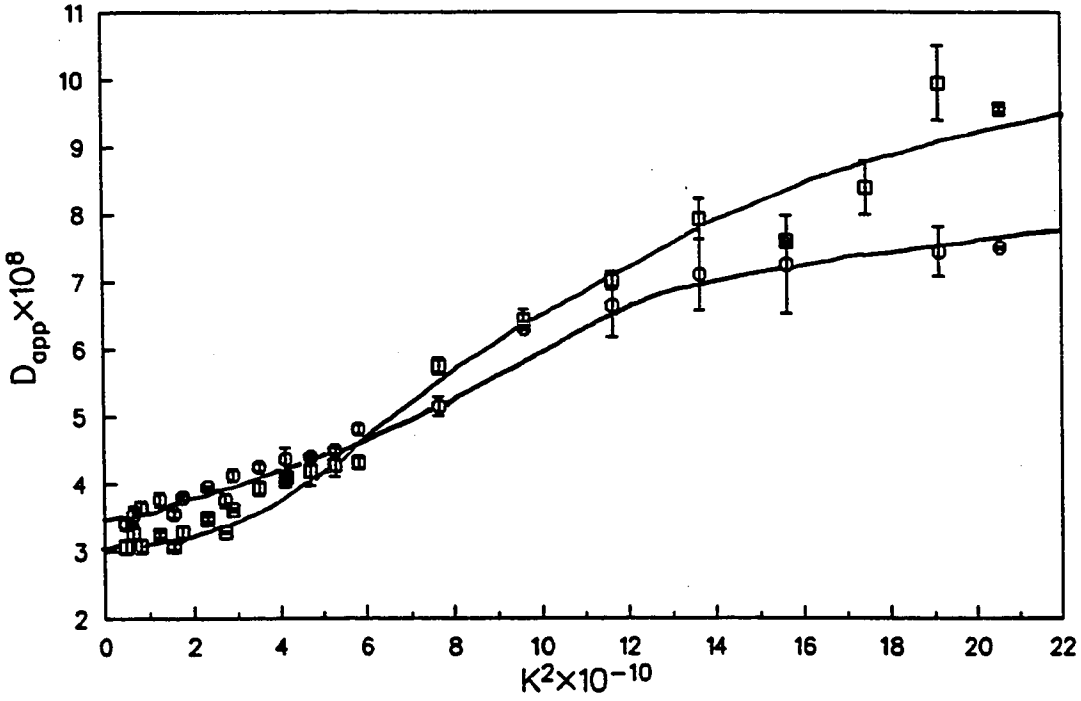

Figure 6.4. $D_{app}(K)$ vs. K^2 for pBR322 dimer DNA samples with different median linking number differences ($\Delta\ell$). □: -2 ($\sigma = -0.005$), ○: -14 ($\sigma = -0.034$), D_c and D_{plat} for each sample are obtained from the small K^2 and large K^2 values of the smooth curves hand-drawn through the data points. DNA is present at 40–50 μg/mL in LSTE buffer, pH 8.0, $T = 21°$.

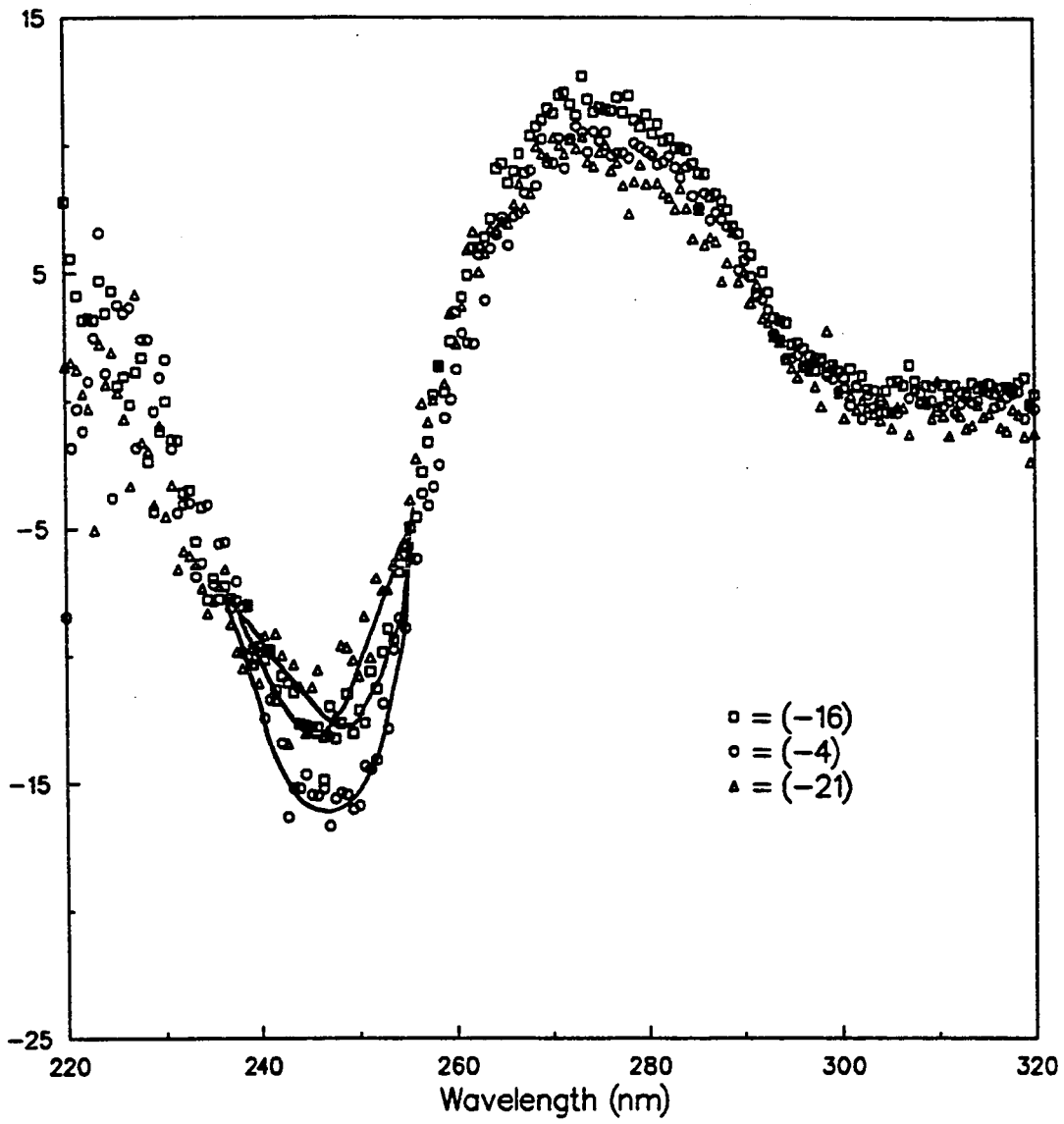

Figure 6.5. CD spectra of pBR322 DNA samples with median linking number differences $\Delta\ell = -4$(circle), -16(square), and -21(triangle). DNA is present at 40–50 μg/mL in LSTE buffer, pH 8.0, $T = 21°$.

(brightest) topoisomers are determined by counting bands from the nicked circle position in gels without chloroquine. This procedure yields +3, −2, and −4, which are regarded as the approximate median linking number differences of those samples. For the more twisted preparations, the difference in number of bands between the median topoisomer of any given sample and that of a known sample is readily determined from gels containing the appropriate amount of chloroquine. This procedure yields −21 (native), −24, −14 and −16 for the linking number differences of the other samples in Figure 6.2a. The median linking number differences $\Delta\ell$(τ_2 in table 6.1) and calculated superhelix densities σ for the different samples are presented in Table 6.1.

6.2.3 DLS, FPA, and CD Experiments

Dynamic light scattering (DLS), time-resolved fluorescence polarization anisotropy (FPA) and circular dichroism(CD) experiments on pBR322 were performed essentially the same as those of pUC8 dimer DNA samples (see Chapter 4). The DLS data for samples with −2, −14, and −16 median linking number diffferences are shown in Figure 6.3, where smooth curves are simply hand-drawn through the data. The translational diffusion coefficient of the center-of-mass (D_0) at $K^2 = 0$ and the quasi-plateau value (D_{plat}) at $K^2 = 20 \times 10^{10}$ cm^{-2} are obtained from the smoothed curves. CD spectra ($\Delta\epsilon$ vs. λ) for the samples were corrected by subtracting that of the buffer in the same cell, and afterwards converted to molar ellipticity units using $[\theta] = 100\Delta\epsilon/c \cdot 1$, where c is the molar concentration of base pairs. CD spectra of three samples (−2, −4 and −25) are shown in Figure 6.4. The the trough at 240 nm of each sample is plotted vs. superhelix density in Figure 6.6.

Figure 6.6. D_o and D_{plat} for pBR322 vs. superhelix density. All samples were prepared from the same stock solution as described in the text. DNA is present at 40–50 μg/mL in LSTE buffer, pH 8.0, $T = 21°$. All samples were measured at 5-7 days after preparation.

Top: D_{plat} *vs.* superhelix density. D_{plat} is the apparent DLS diffusion coefficient at $K^2 = 20 \times 10^{10}\,\mathrm{cm}^{-2}$. The lower values at $\sigma = -0.010$, and -0.034 suggest that in this intermediate range, DNA exhibits a different secondary structure with decreased torsional rigidity.

Bottom: D_o *vs.* superhelix density σ. D_o is the translational diffusion coefficient of the center of mass of pBR322.

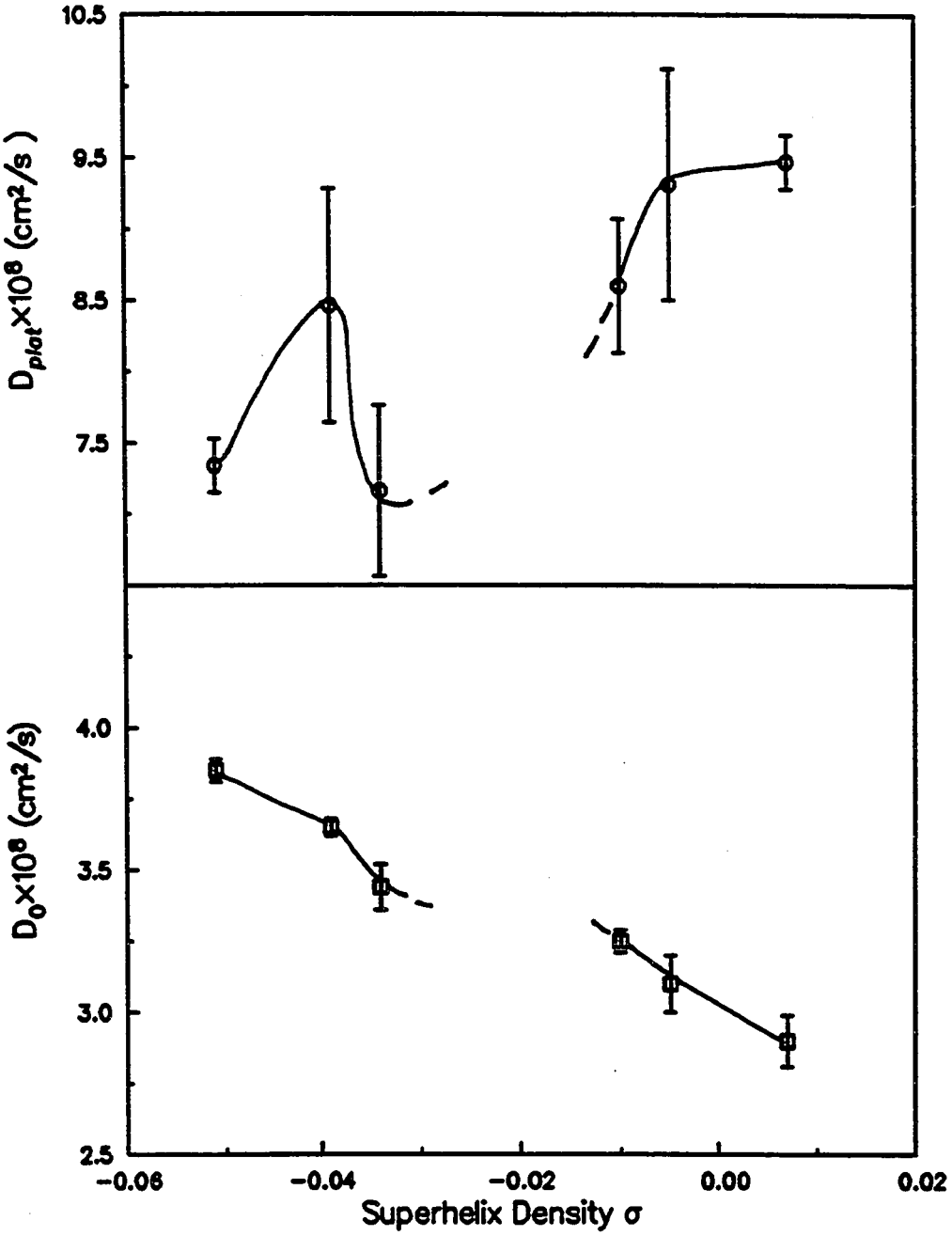
10.5
9.5
8.5
7.5
$D_{plat} \times 10^6$ (cm²/s)
4.0
3.5
3.0
2.5
$D_0 \times 10^6$ (cm²/s)
−0.06
−0.04
−0.02
0.00
0.02
Superhelix Density σ

6.3 RESULTS AND DISCUSSION

6.3.1 Basic Experimental Results

a. Changes of D_{plat} and D_0 with DNA Superhelix Density σ

D_{plat} and D_0 are plotted vs. superhelix density in Figure 6.5. The D_{plat} is the average value of D_{app} for the three highest K^2 values, the standard deviation of these three D_{app} is taken to be the error. All samples are measured at 5-7 days after treatment with Topoisomerase I. With decreasing σ, D_{plat} starts to decrease at $\sigma = -0.005$. It increases at $\sigma = -0.039$, and it decreases again between $\sigma = -0.039$ and $\sigma = -0.051$. The lower value of D_{plat} in the intermediate range of superhelix density could perhaps be considered as evidence for the existence of a different secondary structure.

The steady increase of D_0 as the superhelix density decreases reflects reduction in the radius of gyration of the DNA molecule. The D_0 curve does not show a shape similar to that of pUC8 dimer.

b. Changes of $[\theta]$ and α with Superhelix Density σ

The molar ellipticity $[\theta]$ at the minimum of the CD near 240 nm and the torsion constant α are plotted vs. superhelix density in Figures 6.6a and 6.6b, respectively. $[\theta]$ measurements and α measurements were made at 5-7 days after treatment with Topoisomerase I. The molar ellipticity $[\theta]$ exhibits an interesting feature. As the negative superhelix density $-\sigma$ increases from right to left, $[\theta]$ first increases at $\sigma = -0.005$ and then decreases to a lower value at $\sigma = -0.010$. $[\theta]$ then increases to higher values at $\sigma = -0.039$ and -0.051, then decreases to a lower value at $\sigma = -0.058$. The torsion constant α showed a similar behavior although the changes in α are less significant in the left hand side of the figure.

c. Correlation Coefficients Between D_{plat}, α and $[\theta]$

Figure 6.7. Variation of the molar ellipticity $[\theta]$ (at the minimum near 250 nm) and the torsion constant α of pBR322 with superhelix density. Conditions are the same as in Figure 6.6, with the exception that the torsion constants were measured at 20°C.

Top: $[\theta]$ vs. superhelix density σ.

Bottom: α *vs.* superhelix density. Torsion constants are averages for 70 and 120 ns time spans. For the FPA measurements only, ethidium was added to a concentration of 1 dye per 300 base pairs.

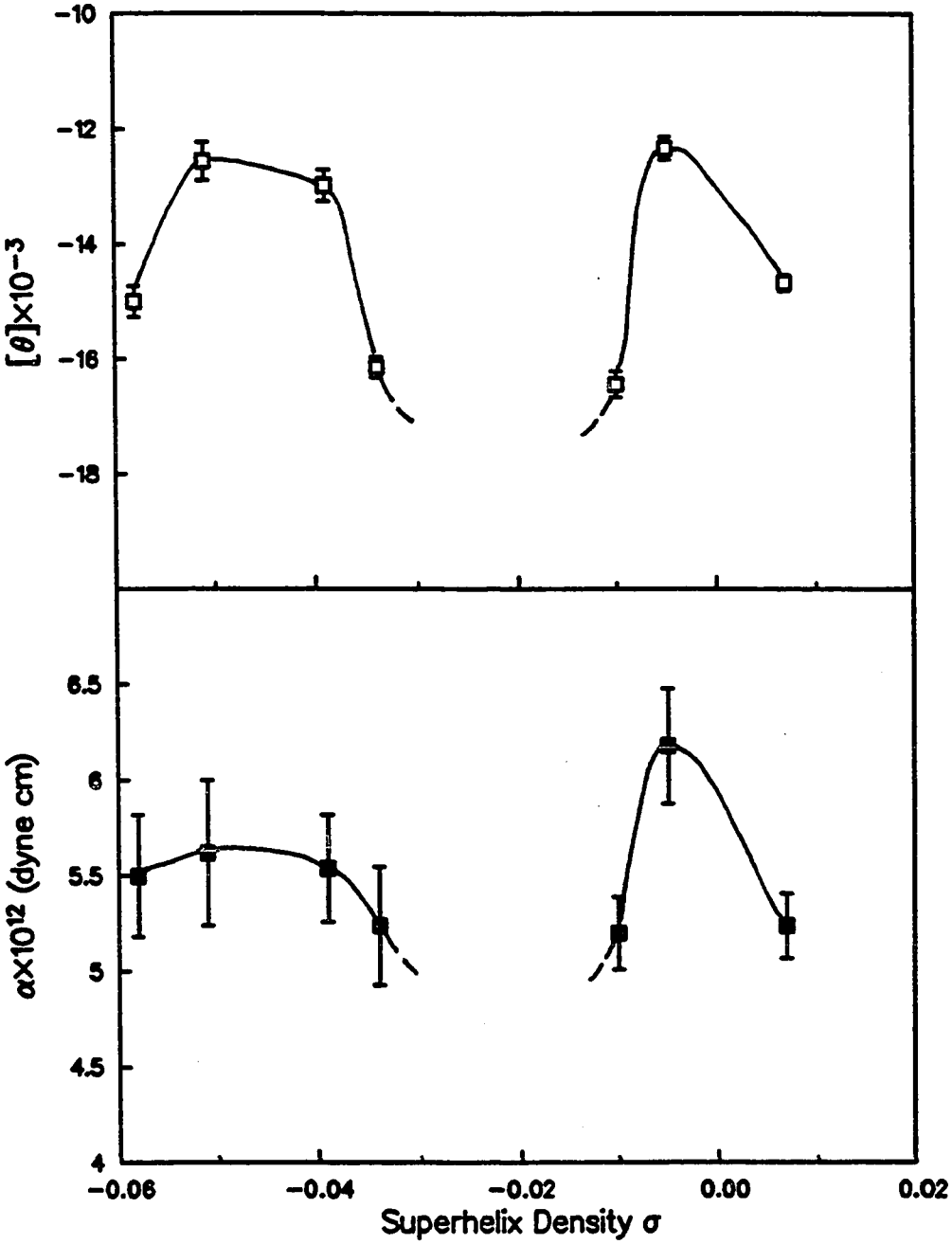
−10
−12
−14
−16
−18
[θ]×10⁻³
6.5
6
5.5
5
4.5
4
α×10¹² (dyne cm)
−0.06
−0.04
−0.02
0.00
0.02
Superhelix Density σ

The changes in D_{plat}, α and $[\theta]$ with changes in σ for pBR322 are relatively small compared with those for pUC8 dimer. However, the changes could not be ascribed to random errors, because the correlation coefficients between the changes of α, $[\theta]$ and D_{plat} are not small numbers. The correlation coefficient of two variables x and y is calculated as following:

$$C_{xy} = \frac{1}{\sigma_x \sigma_y} \frac{1}{N} \sum_{i=1}^{N} (x_i - \bar{x})(y_i - \bar{y})$$

The correlation coefficient of α and $[\theta]$ is 0.7836, of α and D_{plat} is 0.3598, and of $[\theta]$ and D_{plat} is 0.3104. That both α and $[\theta]$ are high in the same σ range and low in the same σ range argues that the changes in α and $[\theta]$ reflect the structural changes in the DNA.

6.3.2 Discussion

An alternate secondary DNA conformation might exist in supercoiled pBR322 DNA when its superhelix density lies the intermediate range. The data in Figures 6.5 and 6.6 probably indicate a structural transition near $\sigma = -0.008$, and also a second structural transition near $\sigma = -0.039$. The changes in D_{plat}, α and $[\theta]$ of pBR322 in Fig. 6.5 and 6.6 are similar but not identical to the changes of pUC8 dimer shown in Fig. 4.6 and 4.7. The first transition from B helix to the alternate secondary structure takes place earlier ($\sigma = -0.008$) than that of pUC8 dimer DNA ($\sigma = -0.018$). The D_0 value also varies monotonically with σ. Of course, this is a different DNA. pBR322 DNA evidently behaves somewhat differently from other DNAs. Linearized pBR322 exhibits an anomalously high torsion constant. pBR322 contains several short inverted repeats (Lilley,1980) as well as sequences capable of the formation of Z-DNA (Nordheim et al., 1982) which could potentially contribute to relieving torsional strain in pBR322 DNA. The supercoiling distributions of pUC9 and pBR322 DNAs isolated from *supX*

mutants differ significantly from each other (Pruss, Gail J.,1985). *Salmonella typhimurium supX* are topoisomerase I mutants which yield plasmid DNAs with ann unusual supercoiling distribution characterized by extreme heterogeneity in linking number and the presence of highly negatively supercoiled topoisomers. When Di Mauro and his coworkers (Negri,at al.,1988) studied the kinetics of relaxation of plasmids by Topoisomerase I, they found that the topoisomers obtained by shorter treatments with DNA topoisomerase I exhibited larger amounts of ethidium-sensitive metastable secondary structure. pBR322 was the only DNA found not to exhibit this phenomenon. In view of these examples, significant differences in the behavior of pBR322 and pUC8 DNAs are perhaps to be expected.

Chapter 7

The Aggregation of Complexes of DNA with EcoRI Endonuclease

7.1 Introduction

Interactions between DNA and proteins plays an important role in living cells. In specific recognition, a protein binds to a particular DNA sequence several orders of magnitude more tightly than in non-specific recognition, where the protien recognizes primarily the general features with little or no specificity for a particular base sequence. The mechanism of how a protein finds a particular sequence in specific recognition is under intense study. The topoisomer distribution pattern of plasmid DNA pRK112-8 which contains 19 EcoRI sites has been obtained by gel eletrophoresis without EcoRI and with EcoRI but no Mg^{2-} at 37°C. The results show that specific recognition appears to induce a conformational change in DNA (interactive recognition) corresponding to duplex unwinding and/or bending that cause negative supercoiling while non-specific binding does not (Kim et al., 1984). The crystal structure of the complex between EcoRI endonuclease and the cognate oligonucleotide TCGCGAATTCGCG was determined, to 3 Å resolution, by the ISIR (iterative single isomorphous replacement) method. The EcoRI endonuclease-DNA recognition complex consists of a distorted double helix and a protein dimer composed of identical subunits related by a twofold axis of rotational symmetry. The distortions of the DNA are induced by the binding of protein (McClarin et al. 1986). Substantial precipitation of the free enzyme at low ionic strength in the absence of DNA was reported when the enzyme was centrifuged. however. the presence of DNA permitted quantitative recovery of the protein in the supernatant (Jen-Jacobson et al., 1983).

It is reported that after linearization. the torsion constants of M13mp7. PBR322. and pUC8 DNAs are sometimes rather low and evolve to a maximum

at 6-8 weeks, before settling to their equilibrium values (see Figure 5.1). In order to test the notion that torsional constant changes as time after linearization, DLS experiments were performed. $D_{app}(K)$ and D_{plat} of linear pUC8 were examined over time. The interaction between linear pUC8 and EcoRI was studied and the results will be presented in section 7.2.2.

The catalytic and sequence recognition functions can be operationally separated by omitting Mg^{2+} (McClarin, et al., 1986). Therefore, the sequence specific recognition interaction between EcoRI and DNA and the catalytic phosphodiester hydrolysis interaction can be studied separately. The hydrodynamic properties of the complex between EcoRI and supercoiled pUC8 dimer both in the absence and in the presence of Mg^{2-} were studied by DLS experiments. The experimental results will be presented in section 7.2.3.

7.2 Experiments and Results

7.2.1 Materials and Methods

pUC8-dimer (5434 bp, two EcoRI sites seperated 2717 base pair apart) was prepared in the same way as in Chapter 4. The DNA was stored in a buffer(LSTE) consisting 10 mM NaCl, 100 mM Tris, 1 mM EDTA, and pH 7.5 at 5°C. Endonuclease EcoRI was purchased from New England Biolab, supplied in 0.3 M NaCl, 5 mM K_3PO_4, 0.1 mM EDTA, 5mM βME, 200 μg/mL BSA, 0.15% Triton X-100, 50% glycecol, the specific activity of EcoRI is 2 million units/mg, and the specific wight is 10 μg/mL.

Dynamic light scattering experiments and gel electrophoresis were performed in the same way as described in Chapter 4.

7.2.2 Linearization of pUC8 dimer, Interaction of Linearized pUC8 and EcoRI

(1) Effects of Time Evolution after Linearization of pUC8 Dimer on the Diffusion Coefficient

Superccoiled pUC8 dimer DNA was first linearized by EcoRI to produce linearized pUC8 monomer. The L-pUC8 monomer was then treated by 0.5 ml of 2 mg/mL Proteinase K at 37°C for one hour, and was extracted three times with Phenol and three times with diethyl ether. The L-pUC8 monomer solution was dialyzed against high salt (0.5 M NaCl, 10 mM TE, pH=7.5) for 24 hours, and against low salt (0.1 M NaCl, 10 mM TE, pH=7.5) for 24 hours. After one more time in high salt, and one more time in low salt, the L-DNA solution was finally changed to low salt by dialysis. 10 mL of L-pUC8 monomer with 0.82 OD (at $\lambda = 260nm$) were prepared in low salt solution and was filtered through double 45 μm Millipore filters into a pre-washed dust-free scattering cell. The DLS experiment of this newly made L-DNA was performed at 5 days after the linearization. The D_0 value obtained is $(3.56\pm0.12)\times10^{-8}cm^2/sec.$ and the D_{plat} value obtained is $(10.31\pm1.44)\times10^{-8}cm^2/sec.$ The $D_{app}(K)$ vs. K^2 of the L-pUC8 is shown in Figure 7.1 (the upper curve). 35 days after the linearization the DLS experiment was again performed on this sample. The D_{app}(K) remains unchanged: D_0 is $(3.62\pm0.16)\times10^{-8}cm^2/sec$ and the D_{plat} is $(10.22\pm1.08)\times10^{-8}cm^2/sec.$

(2) Interaction of L-pUC8 and EcoRI

22.4 μl EcoRI and 0.028 m moles of $MgCl_2$ were added to the L-DNA solution. The solution was filtered through 0.45 μm Millipore filters into a dust-free pre-washed scattering cell. The D_0 is $(3.73\pm0.29)\times10^{-8}cm^2/sec$ and the D_{plat}

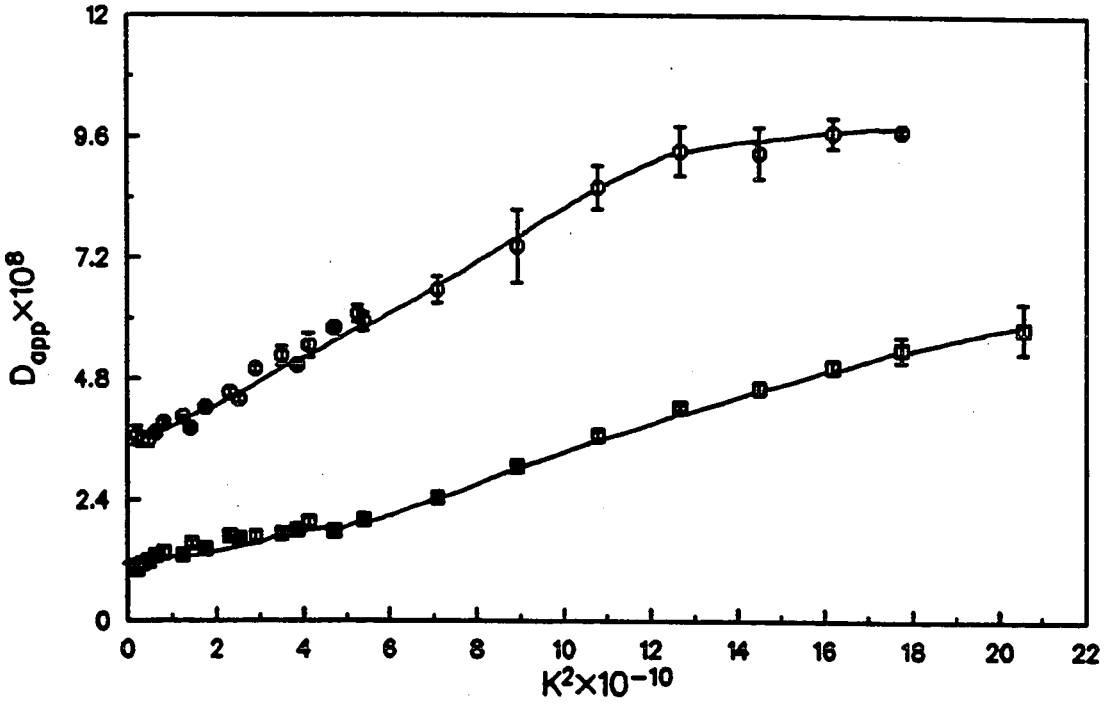

Figyre 7.1. $D_{app}(K)$ vs. K^2 for L-pUC8 monomer/EcoRI complex and clean L-pUC8 samples. Square: L-pUC8 monomer/EcoRI, circle: L-pUC8 monomer. The buffer solution contains 0.1 M NaCl. 10 mM Tris, 10 mM EDTA, pH 7.5. T=21°C.

is $(10.31 \pm 0.57) \times 10^{-8} cm^2/sec$. This L-pUC8/EcoRI sample was then incubated at 37°C for 2 hours. D_0 was still not changed $(3.61 \pm 0.12) \times 10^{-8} cm^2/sec$.

7.2.3 Interaction of Supercoiled pUC8 Dimer and EcoRI

(1) In the presence of Mg^{2-}

28.5 μl of EcoRI was added to 2 mL of pUC8-dimer DNA solution with 5.22 OD, which contains 0.018 mM $MgCl_2$. The reaction mixture was incubated at 37° C for two hours. Then the sample was subjected to gel electrophoresis to check the completion of the linearization reaction. 0.1 mMoles EDTA were added to stop the reaction. The linear DNA with EcoRI sample was filtered by double 0.45 μm millipore filters into a prewashed dust-free scattering cell. The final solution (10 mL) contains 1.0 O.D. DNA, 28.5 μL EcoRI, 0.1 M NaCl, 20 mM Tris, 10 mM EDTA, 2.8 mM $MgCl_2$, pH=7.5.

The DLS curve of $D_{app}(K)$ vs. K^2 was obtained for this sample. The D_0 and D_{plat} for clean and purified linearized pUC8 DNA are $(3.62 \pm 0.16) \times 10^{-8} cm^2/sec$ and $(10.22 \pm 1.08) \times 10^{-8} cm^2/sec$, whereas the D_0 and D_{plat} of the L-DNA/EcoRI cluster is $(1.19 \pm 0.04) \times 10^{-8} cm^2/sec$, $(5.40 \pm 0.25) \times 10^{-8} cm^2/sec$. Both curves of the plain L-DNA and L-DNA/EcoRI are drawn in Figure 7.1. The gel electrophoresis of this L-pUC8/EcoRI sample, supercoiled pUC8 dimer and clean L-pUC8 sample was investigated. Both samples migrated at very close position, characteristic of pUC8 monomer, but the band of L-pUC8/EcoRI appeared slightly slower than that of clean l-pUC8 DNA. There was no retarded band in the L-DNA/EcoRI sample. The diffusion coefficient of the sample was checked after 18, 20, 30, and 40 days. The D_0 and D_{plat} gradually rose up to $(3.09 \pm 0.35) \times 10^{-8} cm^2/sec$ and $(9.23 \pm 0.62) \times 10^{-8} cm^2/sec$, at 40 days after linearization.

Two parallel experiments were done in order to understand the dissociation process. 3.6 mL 5.8 OD pUC8 dimer DNA was dijested by 57 μL EcoRI under the same reaction condition as the above sample. Half of the L-pUC8 and EcoRI solution was filtered through double millipore 0.45 μM filters into dust-free scattering cell. DLS experiment was performed after the filtering. D_0 value is $(2.33\pm0.12)\times10^{-8}cm^2/sec$ and D_{plat} is $(8.48\pm0.48)\times10^{-8}cm^2/sec$. Another half of the sample was extracted three times with phenol and three times with diethylether. Then, this sample was filtered in the same way as the other half of the sample. D_0 is found to be $(3.10\pm0.04)\times10^{-8}cm^2/sec$ and the D_{plat} is $(10.10\pm1.38)\times10^{-8}cm^2/sec$. The gel electrophoresis of clean L-pUC8, L-pUC8/EcoRI (20 days after linearization, with $D_0 = 2.2 \times 10^{-8}cm^2/sec$), and clean pUC8 plus added EcoRI samples ($D_0 = 3.73 \times 10^{-8}cm^2/sec$) show that these three samples run exactly at the same position.

(2) In the absence of Mg^{2-}

28.5 μl of EcoRI were added to 10 mL supercoiled pUC8-dimer with 1 OD, solution which contains 0.1 M NaCl, 10 mM Tris, 1.8 mM EDTA at 22.5°C. After one hour, the solution mixture of DNA and EcoRI was filtered through two 0.45 μm Millipore filters into a prewashed dust-free scattering cell for DLS experiment. The DLS experiment was performed twelve hours later. The $D_{app}(K)$ vs. K^2 of this sample along with that of the clean supercoiled DNA in (0.1 M NaCl, 10 mM Tris, 10 mM EDTA, pH 8.0) are plotted in Figure 7.2. The D_0 and D_{plat} values of the complex of supercoiled pUC8-dimer and EcoRI were $(1.71\pm0.05)\times10^{-8}cm^2/sec$. and $(6.20\pm0.54)\times10^{-8}cm^2/sec$, which are obviously lower than those of plain supercoiled pUC8-dimer ($D_0 = 2.96 \pm 0.03 \cdot 10^{-8}cm^2/sec$. and $D_{plat} = 7.93 \pm 0.68 \times 10^{-8}cm^2/sec$). The gel

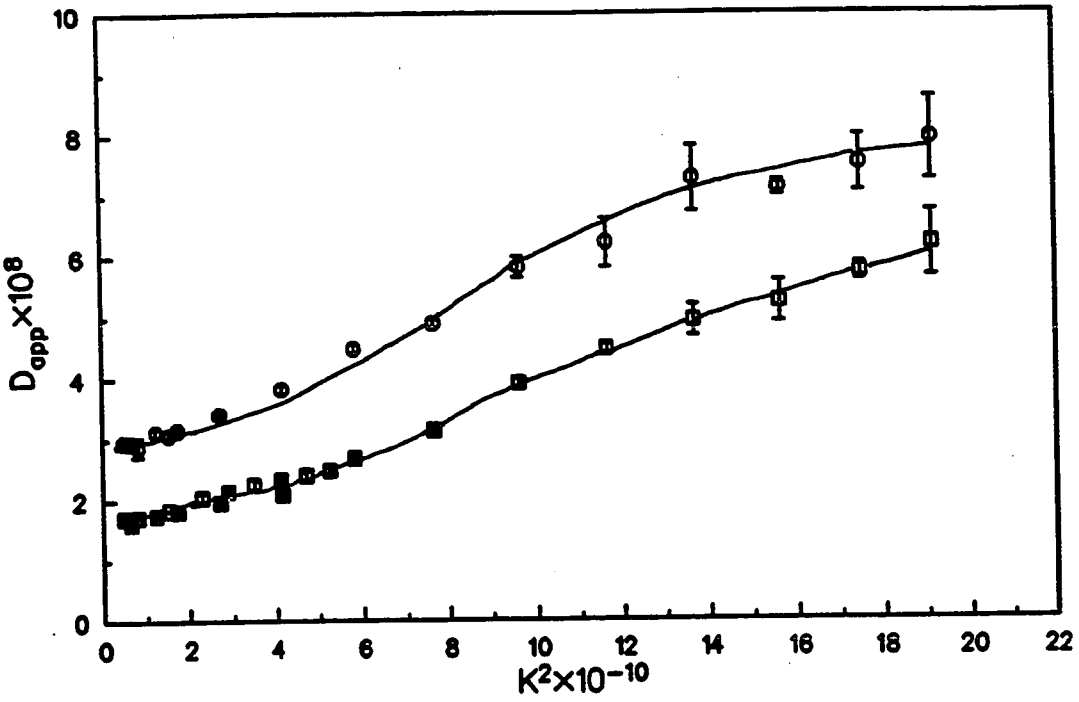

Figure 7.2. $D_{app}(K)$ vs. K^2 for supercoiled pUC8-dimer and pUC8-dimer/EcoRI samples. Square: pUC8-dimer/EcoRI, circle: pUC8-dimer. The buffer solution contains 0.1 M NaCl, 10 mM Tris, 10 mM EDTA, pH 7.5, T=21°C.

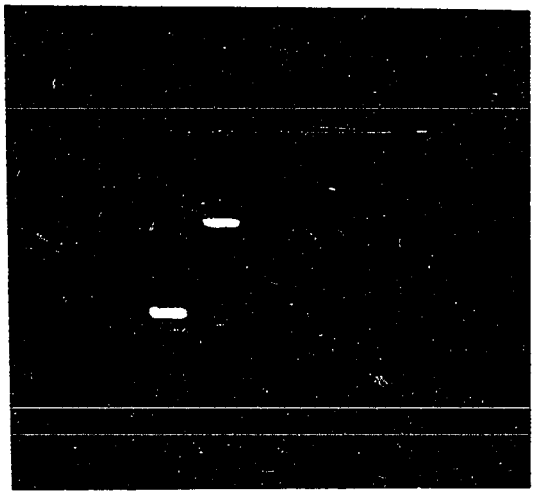

Figure 7.3. Gel of L-pUC8 monomer (on the left) and the complex of supercoiled pUC8 dimer/EcoRI in the absence of Mg^{2-} (on the right) samples. Gel condition: 0.8%(W/V) agarose, TBE buffer, pH 8.0, field strength 2V/cm, 13 hours.

electrophoresis of L-pUC8 monomer and supercoiled pUC8 dimmer/EcoRI (in the absence of Mg^{2+}) complex show that the complex migrates at the supercoiled pUC8 dimer position. and EcoRI alone dose not cut and nick the DNA. The gel picture is shown in Figure 7.3. Then. filtered $MgCl_2$ was added to the mixture of EcoRI and supercoiled pUC8 dimer solution. The concentration of $MgCl_2$ was 5 mM. The solution was kept at 21.5°C for 20 hours. The D_0 decreased to $(1.45 \pm 0.05) \times 10^{-8} cm^2/sec$. The solution was incubated at 37°C for 4 hours and then was cooled down to 21.5°C. The D_0 and D_{plat} were now decreased to $1.20 \times 10^{-8} cm^2/sec$. and $6.23 \times 10^{-8} cm^2/sec$. 14 days later the D_0 did not change very much (from $1.20 \times 10^{-8} cm^2/sec$ to $1.37 \times 10^{-8} cm^2/sec$) but D_{plat} changed from $6.23 \times 10^{-8} cm^2/sec$ to $7.24 \times 10^{-8} cm^2/sec$. Proteinase K was added to the solution to a final concentration of 50 mug/mL 30 days later. The D_0 value is $1.51 \times 10^{-8} cm^2/sec$ and the D_{plat} is $8.19 \times 10^{-8} cm^2/sec$.

7.2.4 The Effect of Glycerol on the Diffusion Coefficient of supercoiled pUC8 dimer

The possibility of the effect of glycerol on the aggregation of the DNA was examined because EcoRI was stored in a solution contains 50% glycerol (200μg/mL). The DNA/EcoRI solution contains glycerol as a result of the addition of EcoRI to DNA. The addition of glycerol up to 1.26% (200 μl of 50% glycerol) has little effect on the apparent diffusion coefficient of supercoiled pUC8 dimer. BSA was added to the solution of the above sample. The diffusion coeffient of the DNA again did not change.

7.3 Discussion

Aggregation of DNA-EcoRI complexes has been found by dynamic light scattering. The D_0 at small K^2 is the diffusion coefficient of the center of mass of the scattering elements. The results presented in Figure 7.1. Figure 7.2 and Figure 7.3 clearly show that:

1. When EcoRI reacts with linearized pUC8. it does not cause the DNA to aggregate. For the D_{app}(K) of linear DNA does not change.
2. The $D_{app}(K)$ of linearized pUC8 studied by the DLS experiment did not change over time from 5 days to 35 days after the restriction reaction.
3. The low diffusion coefficients of the supercoiled pUC8 dimer/EcoRI complexes obviously indicates that aggregation of the complex has occurred both in the absence and in the presence of Mg^{2-}. The aggregation persists for many days even in the linearized pUC8 products.

This study of the interaction between EcoRI and supercoiled pUC8-dimer by DLS reveals that complexes of EcoRI with supercoiled DNA aggregate under standerd conditions. The possibility that the aggregation is the result of partial or complete cutting was excluded by adding EcoRI to the DNA solution without adding Mg^{2-}. Although EcoRI endonuclease requires magnesium as a cofactor for phosphodiester bond cleavage, binding (optimal association constant on the order of $10^{11}M^{-1}$) and recognition specificity are retained in the absence of this ion (Jen-Jacobson et al., 1983). It is obvious that the complex aggregates before linearization of the DNA. This aggregation was not the aggregation of EcoRI itself, but the aggregation of the complex of the supercoiled pUC8 dimer and the EcoRI. If it is the precipitation of EcoRI alone. it would be seen in the case of adding EcoRI to the linearized DNA.

Our conclusion is that when EcoRI binds to supercoiled pUC8 dimer which

has two EcoRI sites, it causes aggregation of DNA. However, it does not cause the aggregation of linearized pUC8 which does not have the specific recognition site, which has been already cleaved. The aggregates dissociate only extremely slowly after the linearization of the supercoiled DNA. One more experiment is suggested in order to conclude that the aggregation occurred during steps involving sequence recognition. Another restriction enzyme such as Hind III should be used to linearize circular DNA first leaving the specific sequence intact. Then the interaction between EcoRI and linearized DNA which has the specific sequence site could be studied. It was suggested by Jen-Jacobson et al. (Jen-Jacobson et al.. 1983) that conformational changes are central features of DNA recognition. This change of DNA conformation might be related to the formation of the aggregation. The long life time of the cleaved complexes is consistent with the possibility that the aggregetion is due in part to the long life time of the metastable state that persists after relieving the superhelical stress.

Chapter 8
Joint Probability Distribution for Three Gaussian Variables

8.1 Introduction

The triple moment $< x(t)x(t+\tau_1)x(t+\tau_1+\tau_2) >$, also known as the bispectrum, of a stochastic process x(t) often provide a better characterization of the process than the lower moments such as $< x(t)x(t+\tau) >$ do. Phillies (Phillies, 1980) has shown that the bispectrum $< I(0)I(t)I(t+\tau) >$ of the intensity I of light scattered quasielastically from a fluid system is a potentially useful tool for studing complex fluids. The all homodyne bispectrum can effectively disdinguish between bidisperse and polydisperse systems. Some other experimental applications of bispectral analysis have been mentioned by Phillies (Phillies, 1980).Oosawa and Masai (Oosawa, et al.. 1982) studied the asymmetric fluctuation of an observed quantity A(t). Their calculations showed that the ordinary two-time correlation function $< A(t)A(t+\tau) >$ provides no information about whether or not the observed quantity comes from a cyclic process in a steady state, whereas the comparision of the third-order time correlation function $< A(t)A(t+\tau_1)A(t+\tau_1+\tau_2) >$ and $< A(t)A(t+\tau) >$ is a simple way to find asymmetry of fluctuation with respect to time reversal in a non-equilibrium steady state. Brillinger has discussed certain mathmatical propertities and applications of polyspectra (Brillinger, 1965).

In this Chapter, the joint distribution function for three Gaussian random variables is derived, and the third order intensity correlation function is calculated directly from that.

8.2 Derivation of the Jiont Probability

Distribution Function

In order to calculate the triple moment of a Gaussian random process, the jiont probability distribution function of three variables has to be derived first.

Suppose x, y, and z are three variables with zero mean which can be expressed as linear combinations of Gaussian random variables $a_1, a_2, \ldots . a_N$:

$$x = \sum_{\ell=1}^{N} \xi_l \, a_l$$

$$y = \sum_{m=1}^{N} \eta_m \, a_m$$

$$z = \sum_{n=1}^{N} \varsigma_n \, a_n \tag{8.1}$$

the variances of x, y. and z are :

$$\begin{aligned} \sigma_x^2 &= < (x - \bar{x})^2 > = < x^2 > - < x >^2 = < x^2 > \\ &= \sum_{\ell=1}^{N} \xi_\ell^2 < a_\ell^2 > \\ \sigma_y^2 &= < y^2 > = \sum_{m=1}^{N} \eta_m^2 < a_m^2 > \\ \sigma_z^2 &= < z^2 > = \sum_{n=1}^{N} \varsigma_n^2 < a_n^2 > \end{aligned} \tag{8.2}$$

the covariances are:

$$\begin{aligned}
\tau_{xy}^2 &=< xy >= \sum_{\ell=1}^{N} \xi_\ell \eta_\ell < \sigma_\ell^2 > \\
\tau_{yz}^2 &=< yz >= \sum_{\ell=1}^{N} \eta_\ell \varsigma_\ell < \sigma_\ell^2 > \\
\tau_{xz}^2 &=< xz >= \sum_{\ell=1}^{N} \xi_\ell \varsigma_\ell < \sigma_\ell^2 >
\end{aligned} \tag{8.3}$$

the normalized correlation coefficients are:

$$\begin{aligned}
\rho_{xy} &= \frac{\tau_{xy}^2}{\sigma_x\, \sigma_y} \\
\rho_{yz} &= \frac{\tau_{yz}^2}{\sigma_y\, \sigma_z} \\
\rho_{xz} &= \frac{\tau_{xz}^2}{\sigma_x\, \sigma_z}
\end{aligned} \tag{8.4}$$

The joint probability distribution $P(x, y, z)$ of x, y, and z is written as

$$\begin{aligned}
P(x,y,z) = \int_{-\infty}^{+\infty} \ldots\ldots \int da_1 da_2 \ldots\ldots da_N \\
\delta(\sum_\ell \xi_\ell a_\ell - x) \cdot \delta(\sum_m \eta_m a_m - y) \cdot \delta(\sum_n \varsigma_n a_n - z) \\
\frac{\mathbf{e}^{-\frac{a_1^2}{2\sigma_1^2}}}{\sqrt{2\pi\sigma_1^2}} \cdot \frac{\mathbf{e}^{-\frac{a_2^2}{2\sigma_2^2}}}{\sqrt{2\pi\sigma_2^2}} \ldots\ldots \cdot \frac{\mathbf{e}^{-\frac{a_N^2}{2\sigma_N^2}}}{\sqrt{2\pi\sigma_N^2}}
\end{aligned} \tag{8.5}$$

The δ- function in Eq. (8.5) can be written in the form

$$\begin{aligned}
\delta(\sum_l \xi_l a_l - x) &= \frac{1}{2\pi} \int_{-\infty}^{+\infty} \mathbf{e}^{it[\sum_l (\xi_l a_l - x)]} dt \\
\delta(\sum_m \eta_m a_m - y) &= \frac{1}{2\pi} \int_{-\infty}^{+\infty} \mathbf{e}^{it'[\sum_m (\eta_m a_m - y)]} dt' \\
\delta(\sum_n \varsigma_n a_n - z) &= \frac{1}{2\pi} \int_{-\infty}^{+\infty} \mathbf{e}^{it''[\sum_n (\varsigma_n a_n - z)]} dt''
\end{aligned} \tag{8.6}$$

substitude δ- functions in Eq. (8.5) with Eq. (8.6),

$$P(x,y,z) = \frac{1}{(2\pi)^3}\int\int\int_{-\infty}^{+\infty} \mathrm{e}^{-itx-it'y-it''z} A(t,t',t'')dtdt'dt'' \tag{8.7}$$

where,

$$A(t,t',t'') = \prod_{i=1}^{N}\int_{-\infty}^{+\infty} da_i \frac{\mathrm{e}^{\left[-\frac{a_i^2}{2\sigma_i^2}+it\xi_i a_i+it'\eta_i a_i+it''\varsigma_i a_i\right]}}{\sqrt{2\pi\sigma_i^2}} \tag{8.8}$$

integrate over a_i and use the definitions in Eq. (8.2) anf Eq. (8.3), $A(t,t',t'')$ becomes

$$\begin{aligned} A(t,t',t'') = exp\{ -\frac{1}{2}[&t^2\sigma_x^2 + t'^2\sigma_y^2 + t''^2\sigma_z^2 \\ &+ 2t't\tau_{xy}^2 + 2tt''\tau_{xz}^2 + 2t't''\tau yz^2]\} \end{aligned} \tag{8.9}$$

replace $A(t,t',t'')$ in Eq. (8.7) with that in Eq. (8.9), and integrate over t'' first, t' second, and t, finally, the $P(x,y,z)$ can be written in the form:

$$\begin{aligned} P(x,y,z) = &\frac{1}{\sqrt{(2\pi)^3\sigma_x^2\sigma_y^2\sigma_z^2R^2}} \cdot exp\left\{-\frac{1}{2R^2}[(1-\rho_{xy}^2)Z^2]\right\} \\ &\cdot exp\left\{-\frac{1}{2R^2}[(1-\rho_{yz}^2)X^2 + (1-\rho_{xz}^2)Y^2]\right\} \\ &\cdot exp\left\{-\frac{1}{2R^2}[-2(\rho_{xz}-\rho_{xy}\rho_{yz})XZ - 2(\rho_{yz}-\rho_{xz}\rho_{xy}YZ]\right\} \\ &\cdot exp\left\{-\frac{1}{2R^2}[-2(\rho_{xy}-\rho_{xz}\rho_{yz}XY]\right\} \end{aligned} \tag{8.10}$$

where the following notations have been used:

$$\begin{aligned} R^2 &= (1-\rho_{xy}{}^2 - \rho_{xz}{}^2 - \rho_{yz}{}^2 + 2\rho_{xy}\rho_{yz}\rho_{xz}) \\ X &= \frac{x}{\sigma_x} \\ Y &= \frac{y}{\sigma_y} \\ Z &= \frac{z}{\sigma_z} \end{aligned} \tag{8.11}$$

If we make the following transformation:

$$\begin{aligned} S &= X + \frac{\rho_{yz}\rho_{xz} - \rho_{xy}}{1-\rho_{yz}^2}Y + \frac{\rho_{yz}\rho_{xy} - \rho_{xz}}{1-\rho_{yz}^2}Z \\ T &= T + \rho_{yz}Z \\ Z &= Z \end{aligned} \tag{8.12}$$

the cross terms in Eq. (8.10) are avoid, $P(x,y,z)dxdydz$ becomes the product of three probability distribution

$$\begin{aligned} P(x,y,z)dxdydz &= P(S,T,Z)dSdTdZ \\ &= \frac{1}{\sqrt{2\pi}}e^{-\frac{Z^2}{2}} \cdot \frac{1}{\sqrt{2\pi(1-\rho_{yz}^2)}}e^{-\frac{T^2}{2(1-\rho_{yz}^2)}} \\ &\cdot \frac{1}{\sqrt{2\pi\left(\frac{R^2}{1-\rho_{yz}^2}\right)}}e^{-\frac{S^2}{2(R^2/(1-\rho_{yz}^2))}} dSdTdZ \\ &= P(Z)dZ \cdot P(T)dT \cdot P(S)dS \end{aligned} \tag{8.13}$$

as can be seen, the probability distribution function for each variable has the normalized Gaussian form. The transformation gives the following conveniences:

(1) S, T and Z are not correlated to each other:

$$< STZ > = < S >< T >< Z > \tag{8.14}$$

(2) For any Gaussian variable r

$$\begin{aligned} < r^n > &= \int_{-\infty}^{+\infty} r^n \frac{1}{\sqrt{2\pi\sigma^2}}e^{-\frac{r^2}{2\sigma^2}}dr \\ &= (n-1)(n-3).....1 \cdot \sigma^n \end{aligned} \tag{8.15}$$

for even n, we have:

$$
\begin{aligned}
&< S^2 > = \frac{R^2}{1-\rho_{yz}^2} \\
&< Z^2 > = 1 \\
&< T^2 > = (1-\rho_{yz}^2) \\
&< Z^4 > = 3 \\
&< T^4 > = 3(1-\rho_{yz}^2)^2 \\
&< Z^6 > = 5 \times 3 = 15
\end{aligned}
\tag{8.16}
$$

8.3 Calculation of $< I(0)I(t)I(\tau) >$

To calculate $< x^2y^2z^2 >$, wa need to make the transformation from x, y and z to T, S, Z first:

$$
\begin{aligned}
x &= \sigma_x S + \frac{\sigma x(\rho_{xy} - \rho_{xz}\rho_{yz})}{1-\rho_{yz}^2} T + \sigma_x \rho_{xz} Z \\
y &= \sigma_y T + \sigma_y \rho_{yz} Z \\
z &= \sigma_z Z
\end{aligned}
\tag{8.17}
$$

it can be shown that

$$
\begin{aligned}
< x^2y^2z^2 > = & \Big\langle \Big[\sigma_x S + \frac{\sigma x(\rho_{xy} - \rho_{xz}\rho_{yz})}{1-\rho_{yz}^2} T + \sigma_x \rho_{xz} Z\Big]^2 \cdot \\
& \Big[\sigma_y T + \sigma_y \rho_{yz} Z\Big]^2 \cdot \Big[\sigma_z Z\Big]^2 \Big\rangle \\
= & \sigma_x^2\sigma_y^2\sigma_z^2 \Big[< S^2 >< T^2 >< Z^2 > + \rho_{yz}^2 < S^2 >< Z^4 > \\
& + \frac{(\rho_{xy} - \rho_{xz}\rho_{yz})^2 \rho_{yz}^2}{(1-\rho_{yz}^2)^2} < T^2 >< Z^4 > \\
& + \rho_{xz}^2 < T^2 >< Z^4 > + \rho_{xz}^2\rho_{yz}^2 < Z^6 > \\
& + 4\frac{(\rho_{xy} - \rho_{xz}\rho_{yz})\rho_{yz}\rho_{xz}}{1-\rho_{yz}^2} < T^2 >< Z^4 > \Big]
\end{aligned}
\tag{8.18}
$$

by using the rsults in Eq. (8.16)

$$
< x^2y^2z^2 > = \sigma_x^2\sigma_y^2\sigma_z^2 \Big[1 + 2\rho_{yz}^2 + 2\rho_{xy}^2 + 2\rho_{xz}^2 + 8\rho_{xy}\rho_{yz}\rho_{xz}\Big] \tag{8.19}
$$

In the calculation of the bispectrum of the scattered light $< I(0)I(t)I(\tau) >$, the result in Eq. (8.19) is needed assuming $x = E(0)$, $y = E(t)$ and $z = E(\tau)$. Expressing power I in E(t): $I = AE(t)^2$, Generalized Siegert for power I is:

$$
\begin{aligned}
< I(0)I(t)I(\tau) > &= A^3 < E(0)^2E(t)^2E(\tau)^2 > \\
&= A^3 < E(0)^2 >^3 \Big\{1 + 2\rho(t)^2 + 2\rho(\tau)^2 \\
&\quad + 2\rho(\tau - t)^2 + 8\rho(t)\rho(\tau - t)\rho(\tau)\Big\}
\end{aligned}
\tag{8.20}
$$

and generalized Siegert for light scattering is:

$$
\begin{aligned}
< I(0)I(t)I(\tau) > &= \frac{A^3}{8} < (E_r(0)^2 + E_i(0)^2) \cdot (E_r(t)^2 + E_i(t)^2) \\
&\cdot (E_r(\tau)^2 + E_i(\tau)^2) > \\
&= \frac{A^3}{8} < E_r(0)^2 E_r(t)^2 E_r(\tau)^2 > \\
&+ < E_i(0)^2 E_i(t)^2 E_i(\tau)^2 > \\
&+ < E_r(0)^2 E_r(t)^2 >< E_i(\tau)^2 > \\
&+ < E_r(0)^2 E_r(\tau)^2 >< E_i(t)^2 > \\
&+ < E_i(0)^2 >< E_r(t)^2 E_r(\tau)^2 > \\
&+ < E_i(0)^2 E_i(t)^2 >< E_r(\tau)^2 > \\
&+ < E_i(0)^2 E_i(\tau)^2 >< E_r(t)^2 > \\
&+ < E_r(0)^2 >< E_i(t)^2 E_i(\tau)^2 > \\
&= \frac{A^3}{4} < E_r(0)^2 >^3 \left\{ \left[1 + 2\rho(t)^2 + 2\rho(\tau)^2 \right.\right. \\
&+ \left.\left. 2\rho(\tau - t)^2 + 8\rho(t)\rho(\tau - t)\rho(\tau) \right] \right. \\
&+ \left. \left[1 + 2\rho(t)^2 + 1 + 2\rho(\tau)^2 + 1 + 2\rho(\tau - t)^2 \right] \right. \\
&=< I >^3 \left\{ 1 + \rho(t)^2 + \rho(\tau - t)^2 + \rho(\tau)^2 \right. \\
&+ \left. 2\rho(t)\rho(\tau - t)\rho(\tau) \right\}
\end{aligned}
\tag{8.21}
$$

when τ is much larger than t. $E(t)^2$ and $E(\tau)^2$ are no longer correlated, $\rho(\tau) = 0$, and $\rho(\tau - t) = 0$ are valid, the three point correlation function should be reduced to two point correlation function. Eq. (8.21) can be reduced to

$$
< I(0)I(t)I(\tau) >=< I >^3 \left\{ 1 + \rho(t)^2 \right\} \tag{8.22}
$$

which is the correlation function of two point. Eq.(8.21) can be reduced to

$$
< I(0)I(t)I(\tau) >=< I >^3 \left\{ 1 + \rho(t)^2 \right\} \tag{8.23}
$$

which is the correlation function of two point in the expression of light scattering.

I have shown the derivation of the joint probability distribution of three Gaussian variables. The third order correlation function has been calculated directly by using this distribution function. The third order time correlation function of the scattered light gives the same infromation as the ordinary correlation function does. This might be served as the additional requirement for Gaussian light.

Chapter 9
Interactions between DNA with Dye Molecules Studied by Dynamic Light Scattering

9.1 Introduction

Interactions between DNA and dye molecules are important in the understanding of physical properties of nucliec acids. Because of the photochemistry of the complexes of DNA with dye molecules, it has been very hard to study the DNA:dye interactions by dynamic light scattering. It was reported that long-time irradiation at high fluence (62 J m^{-2} s^{-1}) of the proflavin-oXRFI DNA complexes clearly caused an important conversion of the closed RFI molecules into the relaxed RFII molecules, and it was believed that H_2O_2, e^-, $O_2 - \cdot$ and $OH\cdot$, respectively, are involved in the cleavage process. It was also reported that adding radical scavengers such as sodium benzoate, and t-butanol could totally supress the nicking reaction of DNA-proflavine complexes when exposed to visible light (Piette, et. al., 1981). Efforts have been made to reduce the the extent of photochemistry by adding sodium benzoate to DNA/dye solution, by degassing the DNA solution. Dynamic Light Scattering experiments of DNA/dye samples were performed. Results of these experiments are presented in this chapter.

9.2 Experiments and Results

9.2.1 Materials and Methods

pUC8-dimer (5434 bp, two EcoRI sites) was prepared in the same way as in Chapter 4. The DNA was stored in a buffer(LSTE) consisting 10 mM NaCl, 10 mM Tris, 1 mM EDTA, and pH 7.5 at 5°C. pBR322 DNA was prepared in a similar way, and was stored in buffer containing 0.1 M NaCl, 10 mM Tris, 10 mM EDTA, pH=8.5.

Linearized pBR322 and pUC8 were prepared by cutting supercoiled DNAs

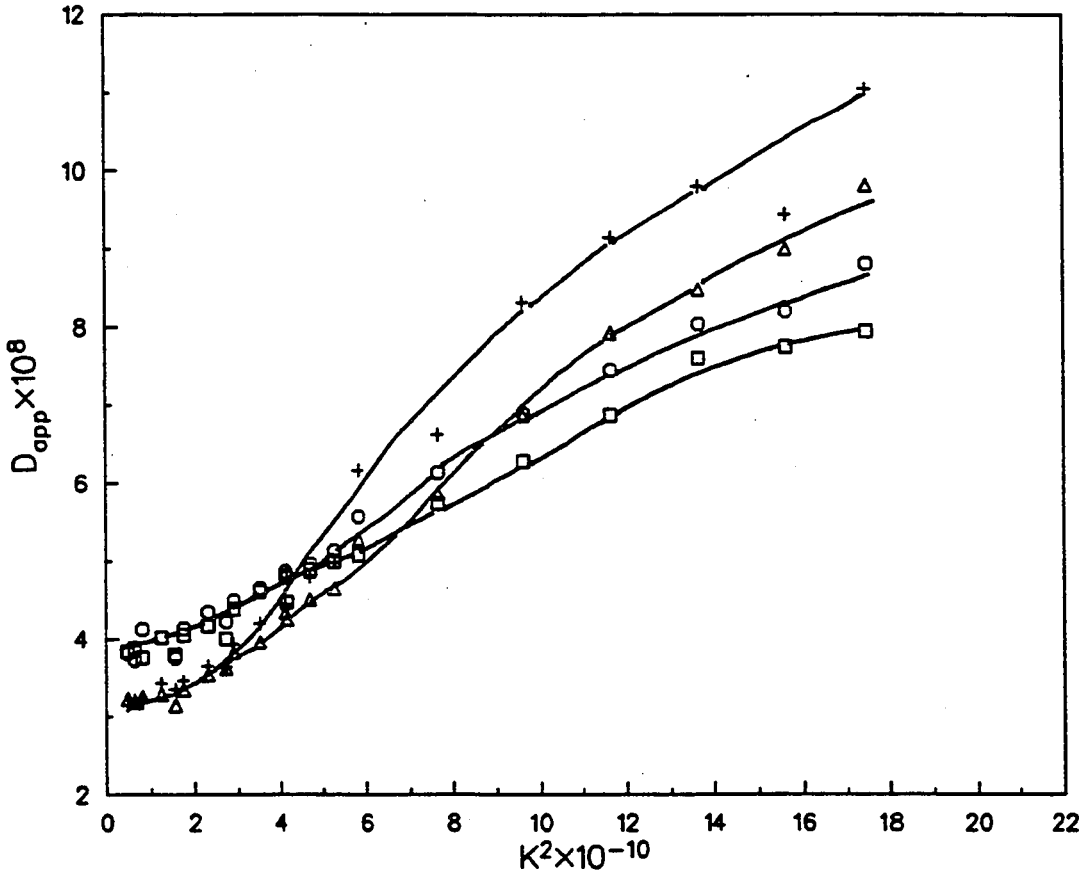

Figure 9.1. $D_{app}(K)$ vs. K^2 for supercoiled pBR322 DNA with chloroquine samples. Square: plain pBR322. circle: EB/bp=0.01. triangle: EB/bp=0.05, plus: EB/bp=0.1. The buffer solution contains 0.1 M NaCl. 10 mM Tris, 10 mM EDTA, pH=7.5, T=21°C.

with EcoRI, and were purified by Proteinase K treatment, and phenol(3x) and ether(3x) extractions. The buffer solutions with three changes of dialyzate of L-DNA were changed to those indicated in the text by dialysis three times.

Nicked pBR322 DNA and pUC8 dimer DNA were obtained by taking the upper band of the two bands seen in CsCl gradient tubes. Then samples were dialyzed along with supercoiled DNAs. Nicked pBR322 was stored in buffer containing 0.1 M NaCl, 10 mM Tris, 10 mM EDTA, pH=8.5. Nicked pUC8 dimer were stored in a buffer containing 10 mM NaCl, 10 mM Tris, 1 mM EDTA, pH=7.5.

Dynamic light scattering experiments and gel electrophoresis were essentially performed in the same way as described in Chapter 4, except that samples were degassed by bubbling N_2 or Ar to remove O_2.

9.2.2 Interactions Between Supercoiled pBR322 DNA with Dye Molecules

(1) Interaction of Supercoiled pBR322 DNA with Chloroquine (chl)

DLS experiments on 0.964 OD of supercoiled (sc) pBR322 DNA containing 0.1 M NaCl, 10 mM EDTA, 10 mM Tris, and pH=8.5 was performed. The D_0 is $(3.84 \pm 0.08) \times 10^{-8} cm^2/s$, and the $D_{plat}(K)$ is $(7.95 \pm 0.19) \times 10^{-8} cm^2/s$. Then filtered chloroquine (0.085 M) was added to the DNA solution so that the ratio of chloroquine molecules per base pair was 0.01, 0.05, or 0.1, when the DLS experiment was performed. The $D_{app}(K) vs. K^2$ for supercoiled pBR322 DNAs with added chl/bp 0.0, 0.01, 0.05, and 0.1 are shown in Figure 9.1. As the added dye/DNA ratio increases, D_0 decreases from $3.84 \times 10^{-8} cm^2/s$ to $3.11 \times 10^{-8} cm^2/s$ between chl/bp= 0.01 and 0.05, whereas D_{plat} continuously increases from $(7.95 \pm 0.19) \times 10^{-8} cm^2/s$ to $(11.21 \pm 1.21) \times 10^{-8} cm^2/s$. Gel

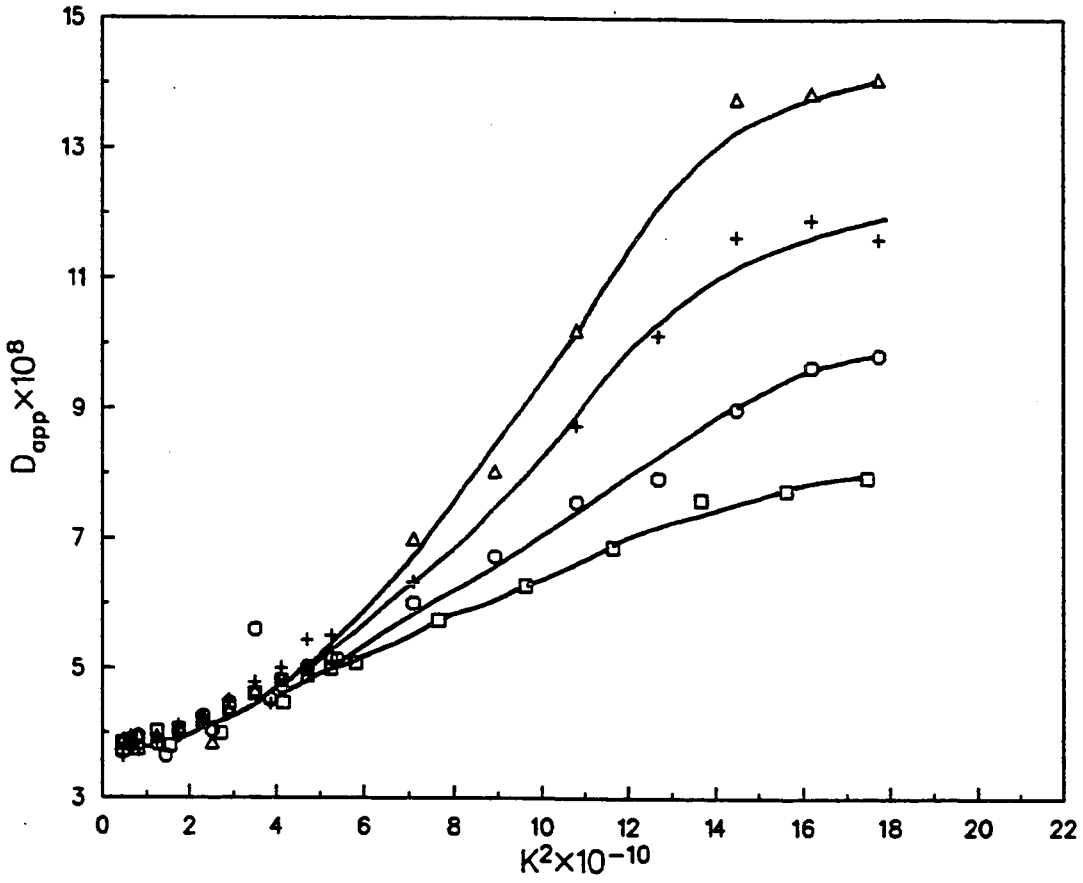

Figure 9.2. $D_{app}(K)$ vs. K^2 for supercoiled pBR322 DNA with ethidium bromide samples. Square: plain pBR322, circle: pBR322 with 15 mM sodium benzoate, triangle: pBR322 DNA with EB/bp=0.03 in the presence of 15 mM sodium benzoate, plus: after removing EB and sodium benzoate from the above sample. The buffer solution contains 0.1 M NaCl, 10 mM Tris, 10 mM EDTA. pH=7.5, T=21°C.

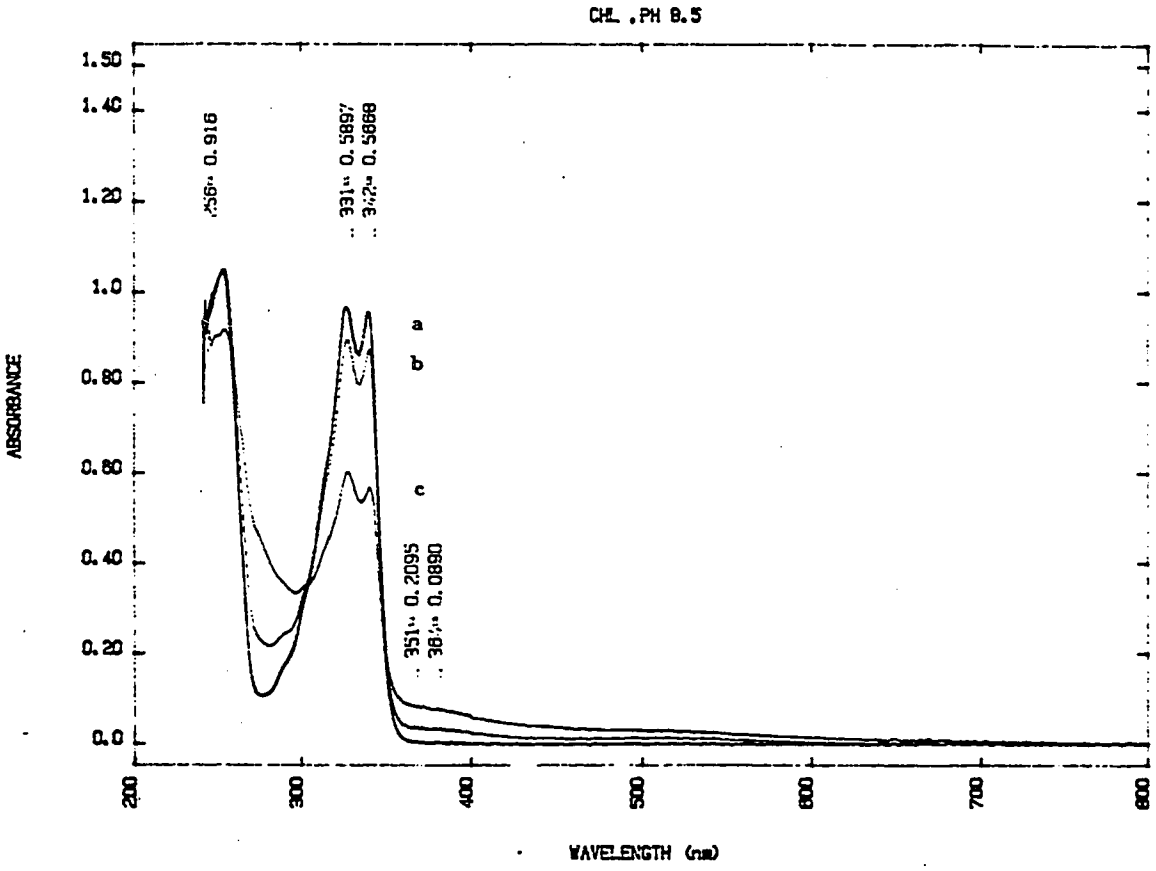

Figure 9.3. UV-visible spectra of chloroquine (a), chloroquine irradiated with 636.8 nm (100 mW total output power of two lines: 363.8 nm and 351.1 nm) for 4 hours (b), chloroquine irradiated for another 4 hours with 200 mW output power (c).

electrophoresis of the sample with chl/bp ratio 0.1 after the DLS experiment shows that about 40% of the DNA are linearized, 60% are nicked, and also a very weak smear appearing in front of the linear band.

The D_0 of nicked pBR322 with DNA concentration of 0.28 OD was measured to be $(2.32 \pm 0.11) \times 10^{-8} cm^2/s$ at 21°C. The gel picture show that in this sample, 70% are nicked, 5% are supercoiled, 25% are in a band which migrate slower but close to the nicked band.

The amount of DNA chain breakage induced photochemically was examined by the following irradiation test. 1 mL of supercoiled pBR322 DNA solution with chl/bp ratio= 0.2 contained in a quartz cell was degassed by bubbling N_2 for 1.5 hours. The cell was sealed. and was put in a 364 nm laser beam with an output power of 200 mW and irradiated for 4 hours. Gel electrophoresis of this irradiated circular DNA sample shows that about 2-3% are linearized DNA, 50% are nicked , and 47% remained in supercoiled form. The same sample was degassed again for one hour by bubbling N_2 through the sample, and irradiated for 4 hours in the $\lambda = 364nm$ laser beam with an output power 100 mW. Gel picture shows that 10% are supercoiled, 10% are linear, 80% are nicked. The sample was degassed again for 1 hour and irradiated for 2 hours in the same laser beam with 100 mW output. Gel picture shows that about 90% are nicked, 10% are linear, no supercoiled band could be seen for a originally supercoiled pBR322 DNA (8.46×10^{-8} molar base pair) after 1400 mW · hour irradiation in $\lambda = 364$ nm laser beam.

The irradiation test of photochemistry of chloroquine was performed by analyzing UV-visible absorption spectra. The spectrum of chloroquine solution at pH 8.5 exhibits an trough around 280 nm. and two group of peaks around

260 nm and 330 nm. The peaks around 260 nm are higher than those around 330 nm. After 4 hours of irradiation in the 364 nm beam with 100 mW output power, the two peaks around 330 nm (329 nm and 343 nm) were decreased by 10%, the trough was increased from 0.1 to 0.24 OD (about 140% increase), the peak around 260 did not change significantly. The spectra did not show any detectable position shift. After another 4 hours irradiation in a beam with an 200 mW output power, the peaks around 330 nm decreased from 0.95 to 0.60 (about 58% decrease), and the trough increased from 0.1 to 0.34 (about 240% increase). UV-visible absorption spectra of chloroquine, chloroquine irradiated for 4 hours with 363.8 nm laser beam with 100 mW output power, and chloroquine irradiated for another 4 hours with 363.8 nm laser beam with 200 mW power laser beam are shown in Figure 9.3. At pH 5.5, the peaks around 330 nm are higher than those around 260 nm. After 4 hours of irradiation with 200 mW output power, the peaks around 330 nm decreased by 10%.

(2) Interactions of Supercoiled pBR322 DNA with EtBr

In order to prevent strand-breaking of the DNA-EtBr complex when it is exposed to near-UV (λ = 363.8 nm)laser light, following irradiation tests were performaed. 1 mL of 0.5 OD sc pBR322 with EB/bp= 0.05 solution containing 2 mM NaN_3 was made, and irradiated in 363.8 nm laser beam with 100 mW output power for 8.5 hours. The gel results show that 20% are supercoiled, 15% are linearized, and 65% are nicked. The same DNA solution containing 4 mM CsCl instead of 2 mM NaN_3 was prepared. Half of the sample was then degassed by bubbling Ar through the solution for 3 hours and irradiated for 2 hours by a 363.8 nm with 200 mW output power. The gel of irradiated and non-irradiated sample was performed, the results show that about 50% are nicked, and a weak

linearized band can be seen in the irradiated sample. The supercoiled band of the non-irradiated sample migrates slightly slower than the irradiated one and there is neither nicked nor linearized bands due to irradiation can be detected. Sodium benzoate was added to the non-irradiated sample to make a concentration of 15 mM. It was degassed by bubbling Ar for 3 hours, and irradiated for 2 hours by 363.8 nm laser beam with 200 mW output power. The gel show that about 30% are nicked. UV spectra of sodium benzoate exhibits a peak at 223 nm, it has little effect on the absorption peak of EB at 478 nm before and after irradiation. The irradiated sample was treated with T4 DNA Ligase (from Sigma) in the present of 1 mM ATP at 37°C for 4 hours. The gel show that the photochemically nicked and linearized DNA can not be ligased.

pBR322 solution containing 0.1 M NaCl, 10 mM Tris, 10 mM EDTA, and 15 mM sodium benzoate pH 8.0 was prepared. The $D_{app}(K) vs. K$ curve was obtained from DLS experiments. The D_{plat} of this pBR322 DNA sample exhibits low value compared with (?) . The addition of sodium benzoate makes the D_{plat} to change from $(7.95 \pm 0.19) \times 10^{-8} cm^2/s$ to $(9.83 \pm 0.09) \times 10^{-8} cm^2/s$. It has been noticed that two kinds of pBR322 DNA might be obtained from preparation. One kind has lower D_{plat}. The D_{plat} of this kind of pBR322 DNA could be increased by changing DNA solution from 10 mM Tris buffer to 10 mM calcodylate buffer (Unpublished data of Benight and Langousky). Similarly, sodium benzoate could switch the D_{plat} of this sample from low value to high value. EtBr was added to a ratio of EB/bp= 0.03, stayed overnight for equalibration. The sample was degassed by bubbling Ar through for 2.5 hours. The $D_{plat}(K)$ increased to $(14.08 \pm 0.56) \times 10^{-8} cm^2/s$, but D_0 didn't change very much. The gel electrophoresis of the sample after DLS experiments show that about 10% of the supercoiled DNA was nicked. Then, an attempt was made to

remove EtBr, sodium benzoate and any small photochemical products from the sample by dialyzing against high salt and low salt buffer each time for 20 hours, but EB fluorescence could still be discerned in the UV beam. The $D_{app}(K)$ of this sample was also obtained. Results of these experiments on a single pBR322 sample by itself, in the presence of 15 mM sodium benzoate, in the presence of 15 mM sodium benzoate and ethidium, and after dialysis to remove ethidium, sodium benzoate and photochemical products are shown in Figure 9.2. Another pBR322 sample with EB/bp=0.06 containing 0.1 M NaCl, 10 mM Tris, 10 mM EDTA, and 15 mM sodium benzoat was prepared.the sample was degassed by filtered Ar. The D_{plat} change to $(12.66 \pm 0.80) \times 10^{-8} cm^2/s$, and D_0 change to $(2.94 = 0.11) \times 10^{-8} cm^2/s$. Then, EB was added to the solution so that EB/bp=0.09, the D_{plat} decreases to $(9.22 \pm 0.31) \times 10^{-8} cm^2/s$, and D_0 decreases to $(2.2 \pm 0.33) \times 10^{-8} cm^2/s$. The gel electrophoresis analysis of this sample with EB/bp= 0.09 after DLS experiment showed that only 10% are supercoiled DNA, and 10% are linear, 80% are nicked, no retarded band has been seen.

9.2.3 Interactions Between pUC8 Dimer DNA with Ethidium Bromide

(1) Interactions of Linearized pUC8 monomer DNA with EB

DLS experiments on L-pUC8 DNA (0.8 OD) in buffer solution containing 0.1 M NaCl, 10 mMTris. 1 mM EDTA, 15 mM sodium benzoate pH=8.0 was performed. The D_0 value is $(4.04 \pm 0.07) \times 10^{-8} cm^2/s$, and the D_{plat} value is $(11.22 = 0.13) \times 10^{-8} cm^2/s$. EB was added to the DNA solution with EB/bp=0.02. the D_0 value is $(3.91 = 0.05) \times 10^{-8} cm^2/s$ almost the same as that of plain DNA. and the D_{plat} values decreased to $(10.64 \pm 0.26) \times 10^{-8} cm^2/s$. The gel electrophoresis of this sample dose not show any smear in front of this

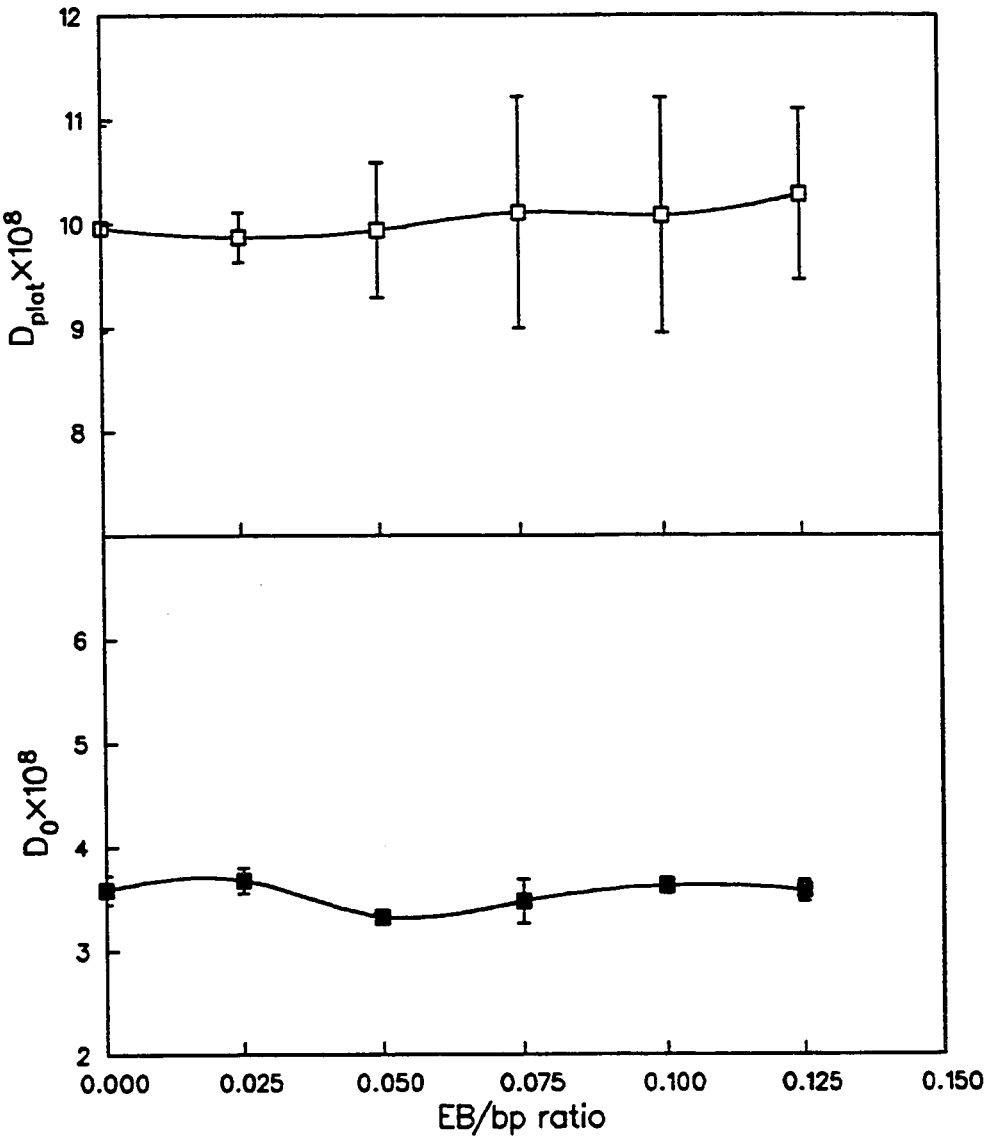

Figure 9.4. D_{plat} and D_0 for samples of L-pUC8/EB complexes vs. EB/bp ratio. Top: D_{plat}. Bottom: D_0.

sample.

DLS experiments on L-pUC8 (0.82 OD) in the same buffer without sodium benzoate, pH 7.5 was performed. The effect of EB on the twisting and bending rigidities are examined by adding EB up to EB/bp=0.025, 0.050, 0.075, 0.10, and 0.125. Both D_0 and D_{plat} remained unchanged. The D_0 vs. added EB/bp and D_{plat} vs. EB/bp curves are plotted in Figure 9.4. The gels after DLS for samples with EB/bp 0.075, 0.10, 0.125 were run, they migrate at the same position as L-pUC8 sample. A slight smear can be seen for sample with EB/bp 0.125 after DLS experiment.

(2) Interactions of Supercoiled pUC8 Dimer DNA with Ethidium Bromide

Experiments were performed on 13 mL supercoiled pUC8 dimer at a concentration of 1.54 OD. The solution contains 0.1 M NaCl, 10 mM Tris, 10 mM EDTA, PH=8.0. DLS experiments on the plain DNA solution and DNA with 15 mM sodium benzoate solution were performed. For this supercoiled DNA, $D_{app}(K)$ is affected very little by sodium benzoate (from 8.02 to $7.86 \times 10^{-8} cm^2/s$). After adding Ethidium up to EB/bp = 0.025, the D_{plat} increased from $(7.86 \pm 0.26) \times 10^{-8} cm^2/s$ to $(8.99 \pm 0.35) \times 10^{-8} cm^2/s$. The amount of UV irradiation is 296.6 mW· hour. More EB was added up to EB/bp ratio of 0.051. The sample was degassed by bubbling Ar for 2 hours. The UV laser experiment was performed prior to the red laser. D_{plat} and D_0 decreased to very low values namely $D_0 = (0.8 \pm 0.01) \times 10^{-8} cm^2/s$, and $D_{plat} = (4.07 \pm 0.82) \times 10^{-8} cm^2/s$. Upon irradiation with near-UV laser beam, the $D_{app}(K)$ exhibits very low value indicating that the DNA molecules start to associate to each other. The gel electrophoresis of this sample showed that 65% are nicked, 5% are linear, and 30%

are supercoiled. As more EB was added to the sample up to EB/bp 0.076, D_{plat} values becomes $(7.03 \pm 0.51) \times 10^{-8} cm^2/s$, D_0 becomes $(1.63 \pm 0.05) \times 10^{-8} cm^2/s$. 20% are supercoiled, 10% are linearized, and 70% are nicked by roughly analyzing the intensity of each band from gel. When EB/bp was changed to 0.102, D_{plat} value is $(7.78 \pm 0.47) \times 10^{-8} cm^2/s$, and D_0 value is $1.50 \times 10^{-8} cm^2/s$. When EB/bp was changed to 0.127, D_0 value is $(0.97 \pm 0.33) \times 10^{-8} cm^2/s$, and D_{plat} value is $(5.59 \pm 0.17) \times 10^{-8} cm^2/s$. The gel showed that 90% are nicked, and 10% are linearized.

8 mL of 1.2 OD sc pUC8 dimer DNA solution containing 0.1 M NaCl, 0.01 M Tris, 0.01 M EDTA, 15 mM sodium benzoate, pH8.0 was prepared. The D_0 value of this plain DNA is $(3.23 \pm 0.01) \times 10^{-8} cm^2/s$. D_{plat} value is $(8.15 \pm 0.18) \times 10^{-8} cm^2/s$, EB was added so the EB/bp ratio was 0.0255. Ar was used to bubble the solution for 2 hours to remove O_2 dissolved in solution. D_0 value of this sample is $(3.42 \pm 0.04) \times 10^{-8} cm^2/s$, D_{plat} is $(9.87 \pm 0.10) \times 10^{-8} cm^2/s$. After UV experiment, D_0 value was remeasured and only decreased to $(3.28 \pm 0.19) \times 10^{-8} cm^2/s$. More EB was added to the sample up to EB/bp = 0.051, D_0 value changed to $(2.77 \pm 0.21) \times 10^{-8} cm^2/s$ before UV experiment, and D_{plat} changed to $(6.34 \pm 0.65) \times 10^{-8} cm^2/s$. After UV, D_0 value decrease to $(2.38 \pm 0.04) \times 10^{-8} cm^2/s$. the gel of this sample showed that 20% of the supercoiled DNA has been nicked.

In order to study the change of D_{plat} with the changing of added EB for DNA sample with EB/bp ratio of 0.051, 9.2 mL of 1.522 OD sc pUC8 dimer DNA solution containing 0.1 M NaCl, 10 mM Tris, 10 mM EDTA, and 15 mM sodium benzoate, pH 8.0 was prepared. The D_0 value is $(3.32 \pm 0.06) \times 10^{-8} cm^2/s$, the D_{plat} value is $(8.05 \pm 0.21) \times 10^{-8} cm^2/s$. EB was added to the DNA solution

up to EB/bp ratio of 0.051. The solution was degassed by bubbling Ar through for 3 hours. The D_0 value is $(3.02 \pm 0.09) \times 10^{-8} cm^2/s$, the D_{plat} value in the first 42 minutes in the 363.8 nm beam is $(8.78 \pm 0.37) \times 10^{-8} cm^2/s$, then, the value starts to drop, after 84 minutes of irradiation, D_{plat} becomes $3.79 \times 10^{-8} cm^2/s$, D_0 becomes $(0.94 \pm 0.01) \times 10^{-8} cm^2/s$, the gel of this sample show that 20% supercoiled DNA have been nicked.

A fresh DNA solution with EB/bp ratio of 0.051 was prepared. D_{plat} value of this sample is $(9.31 \pm 0.13) \times 10^{-8} cm^2/s$. After UV, D_0 value changed from $(2.77 \pm 0.21) \times 10^{-8} cm^2/s$ to $(2.32 \pm 0.11) \times 10^{-8} cm^2/s$. When D_{plat} was remeasured again , the value changes to $(5.22 \pm 0.15) \times 10^{-8} cm^2/s$, and later, changes to $(4.39 \pm 0.42) \times 10^{-8} cm^2/s$. The gel showed that 20% of the supercoiled has been nicked.

A fresh supercoiled pUC8 dimer DNA with EB/bp ratio= 0.10 in the same solution as the above samples was prepared. The D_{plat} value was measured on the 363.8 nm laser system. D_{plat} was $(7.97 \pm 0.50) \times 10^{-8} cm^2/s$ at the very begining of the measurement, after 47 minuts staying in the laser beaser beam, D_{plat} value droped to $(4.69 \pm 0.13) \times 10^{-8} cm^2/s$, and D_0 value is $(1.99 \pm 0.06) \times 10^{-8} cm^2/s$. After 12 days staying at 5°C, D_0 did not change, D_{plat} increased to $(5.27 \pm 0.44) \times 10^{-8} cm^2/s$ at the begaining of the measurement on the 363.8 nm laser system, and droped to $(2.90 \pm 0.02) \times 10^{-8} cm^2/s$ after 61 minutes of exposure to UV beam. D_0 value then changes to $(1.29 \pm 0.09) \times 10^{-8} cm^2/s$. Gel of this sample before and after UV exposure, and of nicked pUC8 dimer DNA with and without ethidium of 0.05 EB/bp were performed. About 20% sc DNA, 5% linearized, and 75% nicked DNA can be seen in the corresponding bands of the EB/bp 0.10 sample. The relative intensities of these three bands

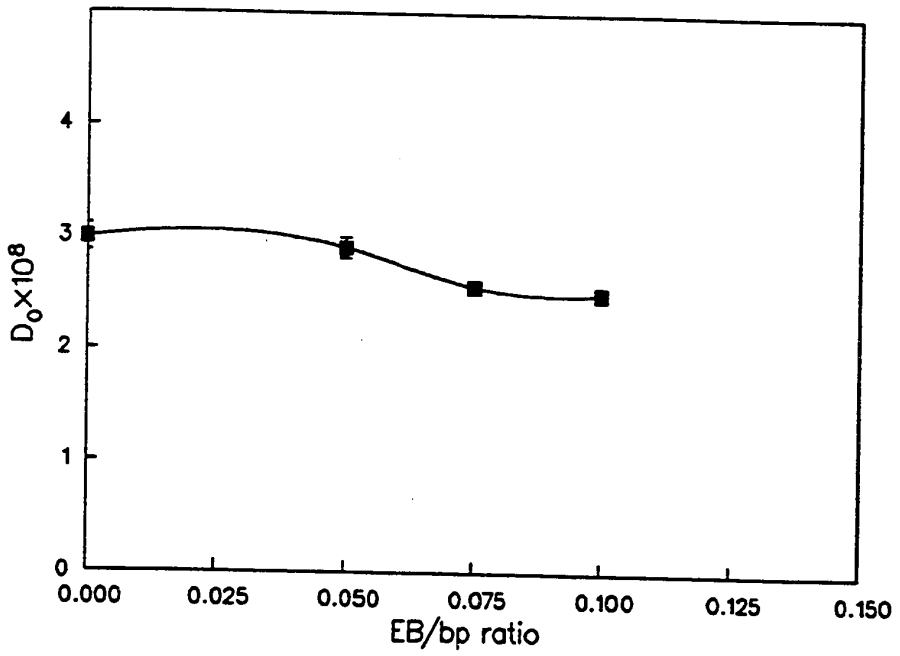

Figure 9.5 D_0 for Supercoiled pUC8 dimer DNA and Ethidium Bromide vs. EB/bp ratio.

are quite close to those of nicked DNA. In order to get rid of EB, the sample was dialized against high salt (0.5 M)–low salt (0.01 M)–high salt–low salt–low salt respectively. It took one day for each dialysis to be completed in the salt solution specified above. Then, D_0 value raised to 2.62, and the D_{plat} value raised to 7.93, D_0 value was then remeasured after UV, it remained 2.60. The gel of the DNA/EB aggregates and DNA after dialysis showed that they contain similar amounts of linearized, supercoiled, and nicked DNA.

(3) Effect of Ethidium Bromide on D_0 of Supercoiled pUC8 Dimer DNA

Because the UV irradiation causes strand breaking of the DNA/dye complexes, experiment was done to obtain the D_0 of DNA/dye complexes with various amount of dye on the red laser (wavelength 632.8 nm) in order to avoid photochemistry. Solution of 1.2 OD Supercoiled pUC8 dimer DNA containing 15 mM sodium benzoate, 0.1 M NaCl, 10 mM Tris, 10 mM EDTA, pH 8.0 was prepaired. $D_{app}(K)$ was measured from $K^2 = 0.47 \times 10^{10} cm^{-2}$ to $K^2 = 5.26 \times 10^{10} cm^{-2}$ on the 632.8 nm laser light scattering apparatus. EB was added up to EB/bp 0.05, 0.075, and 0.1, the D_0 of each sample was obtained. The results are plotted in Figure 9.5. D_0 decreases by 12% as EB/bp increased from 0.05 to 0.075. This decrease in D_0 could be due to the titration of the unwinding of the superhelical turns by ethidium bromide.

(4) Interactions of Nicked pUC8 Dimer DNA with Ethidium Bromide

When ethidium bromide binds to supercoiled DNA, it unwinds supercoiled DNA to relaxed DNA. Does relaxed DNA with EB behave the same as nicked DNA with EB? The effect of changing EB on the $D_{app}(K)$ of nicked pUC8 dimer DNA was examined. 10 mL of 1.2 OD nicked pUC8 dimer solution containing

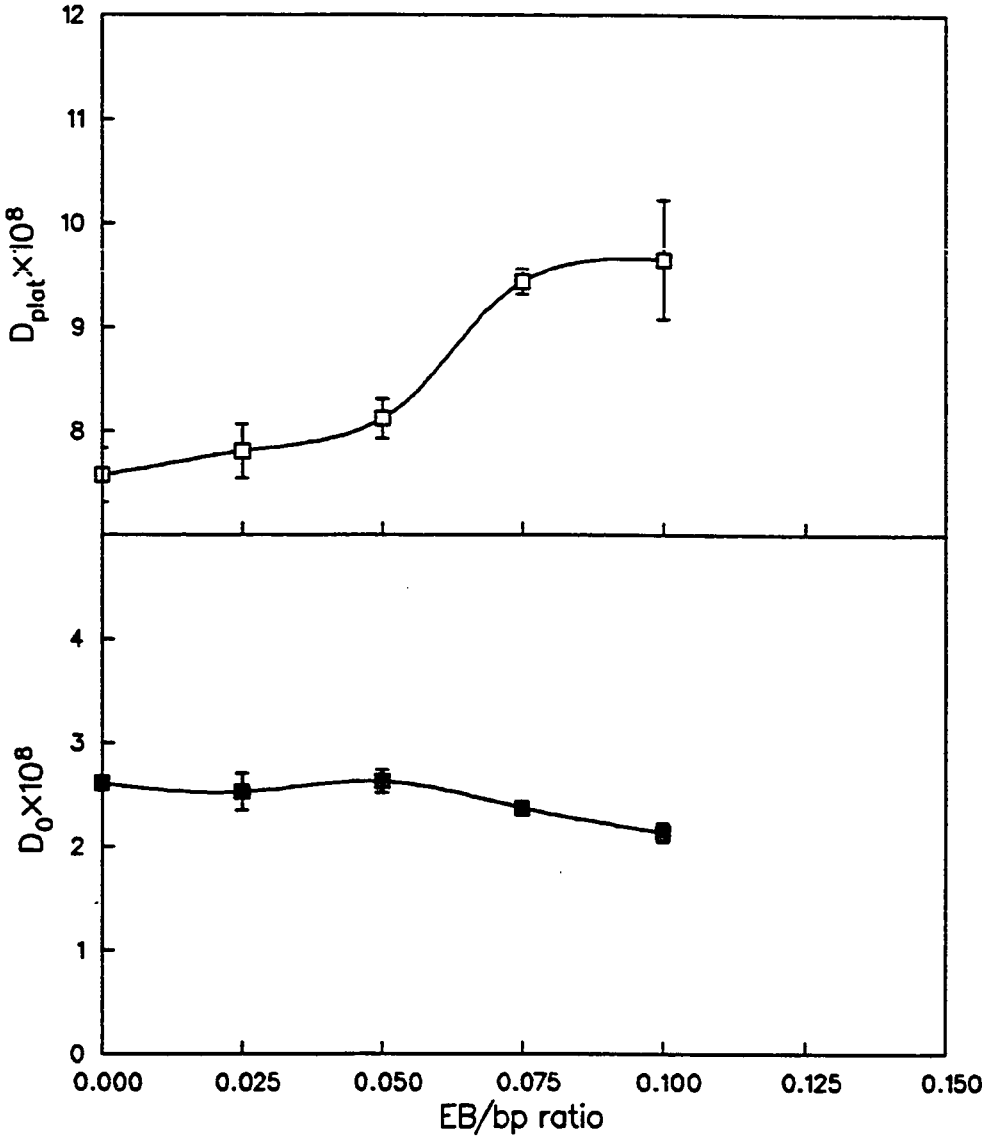

Figure 9.6. D_{plat} and D_0 for relaxed pUC8 dimer vs. EB/bp ratio. Upper: D_{plat}. Lower: D_0.

0.1 M NaCl, 10 mM Tris, 10 mM EDTA was prepared. D_0 value of pure nicked pUC8 dimer is $(2.61 \pm 0.04) \times 10^{-8} cm^2/s$, D_{plat} value is $(7.58 \pm 0.26) \times 10^{-8} cm^2/s$. Filtered EB was added up to a ratio of EB/bp 0.025, 0.05, 0.075, and 0.10. D_{plat} value of the sample with EB/bp 0.075 increased to a higher value of $(9.31 \pm 0.47) \times 10^{-8} cm^2/s$, and D_{plat} value of the sample with EB/bp 0.10 is $(10.05 \pm 0.97) \times 10^{-8} cm^2/s$. The gel picture shows that plain nicked pUC8 dimer DNA sample contains 10% supercoiled, 5% linearized; sample with EB/bp 0.075 contains less than 5% supercoiled; sample with EB/bp 0.10 contains no supercoiled DNA at all. The $D_{plat} vs.$ added EB/bp and $D_0 vs.$ added EB/bp curves are plotted in Figure 9.6. D_0 decreases slightly, and D_{plat} increases as EB/bp is increased.

9.3 Discussion

The irradiation of DNA/dye complexes by near-UV light induces strand-breaking. The results of the irradiation test of my work show that degassing and adding scavenger molecule such as sodium benzoate could inhibit the nicking by 20% if 0.5 mL of DNA/dye solution was exposed to 363.8 nm laser beam with total output power 200 mW for 2 hours.

Adding Ethidium to linear pUC8 monomer up to EB/bp ratio of 0.125 has little effect on the D_0 and D_{plat}. This indicates that the twisting and bending rigidities of linear DNA could hardly change upon EB intercalation. If the effect of EB binding to linear DNA is mainly to lengthen DNA chain, that would not alter the secondary structure of linear DNA. On contrast, upon EB binding, the D_0 of nicked pUC8 dimer decrease slightly, and a transition in D_{plat} could be seen from a value which is close to supercoiled DNA's to a value which is close to linear DNA's between EB/bp ratio 0.05 and 0.075. This is the first time

the comparision in D_0 and D_{plat} of supercoiled, linear and nicked DNAs could be made. D_{plat} of nicked pUC8 dimer is close to that of supercoiled instead of linear DNA, and D_{plat} of nicked pUC8 dimer/EB complexes when the EB/bp ratio higher than 0.05 is close to that of linear DNA. It is also clear that the effect of EB binding to circular DNA could switch the twisting rigidity to the value exhibited by that of linear DNA/dye complex.

The effect of dye (EB,chl) binding to both supercoiled pBR322 and pUC8 dimer DNAs on the D_{plat}s of these DNA is to increase D_{plat} value. Increasing the dye/bp ratio, the D_{plat} of supercoiled pBR322 DNA always increases. Accompanying the nicking of the strand by near-UV irradiation, supercoiled pUC8 dimer DNA/EB complexes exhibit very low D_{app} indicating the association of the complex which is not seen in linear pUC8. In some fresh made dye/DNA sample, the D_{plat} would always exhibit increasing value before the associations occur. The aggregates could be dissociated when the bound EB is removed from the associated sample by dialysis. This might be another indication of the existence of a metastable state in secondary structure of pUC8 dimer DNA which could be switched upon EB binding and in which the association could be facilitated when the photochemistry takes place. The differnet behavior between pBR322 and pUC8 DNAs upon dye binding, upon changing superhelix densities, upon photochemistry of DNA/dye complexes have been noticed (see Chapter 5 and chapter 6).

The relaxation of supercoiled DNA by dye titration could be observed by the reduction of D_0 measured on the red laser in the absence of nicking.

Bibliography

Allison, S.A., (1986) *Macromolecules* **19**, 118-124.

Allison, S.A., Austin, R.H., and Hogan, M.E. (1989) *J. Chem. Phys.* 90, 3845-3854.

Allison, S.A., and McCammon, J.A., (1984) *Biopolymers* **23**, 363-375.

Allison, S.A., and Schurr, J.M. (1979) *Chem. Phys.* 41, 35-59.

Aragon, S.R., and Pecora, R. (1985) *Macromolecules* **18**, 1868-1875.

Baase, W., Staskus, P.W., and Allison, S.A. (1984) *Biopolymers* **23**, 2835-2851.

Barkley, M.D., and Zimm, B.H. (1979) *J. Chem. Phys.* 70, 2991-3007.

Bauer, W., and Vinograd, J. (1970) J. Mol. Biol. 47, 419-435.

Bauer, W. (1979) Ann. Rev. Biophys. Bioeng. 7, 287-313.

Benight, A.S., Langowski, J., Wu, P.-G., Wilcoxon, J., Shibata, J.H., Fujimoto, B.S., Ribeiro, N.S., and Schurr, J.M. (1987a) in Laser Scattering Spectroscopy of Biological Objects, Eds. J. Stepanek, P. Anzenbacher, and B. Sedlacek, Elsevier, Amsterdam, pp. 407-422.

Benight, A.S., Ribeiro, N.S., Song, L., Fujimoto, B.S., Wu, P.-G., Clendenning, J.B., and Schurr, J.M. (1987b) Biophys. J. 51, 422a.

Berg, O.G. (1979) *Biopolymers* **18**, 2861-2874.

Berne, J., and Pecora, R. (1976) Dynamic Light Scattering, John Wiley and Sons, New York.

Bloomfield, V.A. Crothers, D.M., and Tinoco, I., Jr. (1974) Physical Chemistry

of Nucleic Acids, Harper and Row, New York, p. 161.

Borochov, N., Kam, Z., and Eisenberg, H. (1981) *Biopolymers* **20**, 231-235.

Borochov, N., and Eisenberg, H. (1984) *Biopolymers* **23**, 1757-1769.

Brady, G.W., Satkowski, M., Foos, D., and Benham, C.J. (1986) Biomolecular Stereodynamics, Eds. R.H. Sarma and M.H. Sarma, Adenine Press, Guilderland, NY, p. 63-74.

Brady, G.W., Satkowski, M., Foos, D., and Benham. C.J. (1987) J. Mol. Biol. 195, 185-191.

Brandes. R., Vold, R. R., Kearns, D. R.. and Rupprecht, A. (1988) *J. Mol. Biol.* **202**, 321-322. Cairney, K.L., and Harrington, R.E. (1982) *Biopolymers* **21**, 923-934.

Brillinger, D. R., (1965) *Ann. Math. Stat.* **36**, 1351-1374. Diekmann. S., Hillen, W., Morgenmeyer, B., Wells, R.D., and Pörschke, D., (1982) *Biophys. Chem.* **15**. 263-270.

Campbell, A.M. (1978) Biochem. J. (London) 171, 281-283.

Chen, Y. (1981) J. Chem. Phys. 75, 2447-2453.

Courey, A.J., and Wang, J.C. (1983) Cell 33, 817-829.

Depew, R.E., and Wang, J.C. (1975) Proc. Natl. Acad. Sci. USA 72, 4275-4279.

Diekmann, S., Hillen, W., Morgenmeyer, B., Wells, R.D., and Pörschke, D.. (1982) *Biophys. Chem.* **15**, 263-270.

Diekmann, S., and Wang. J. C. (1985) *J. Mol. Biol.* **186**. 1-11.

Edmonds, A. R.. (1974) Angular Momentum in Quantum Mechanics, Princeton University Press, Princeton. N.J. Elias. J.G., and Eden, D., (1981) *Macromolecules* **14**. 410-419.

Förster, D. (1975) Hydrodynamic Fluctuations, Broken Symmetry, and Correlation Functions, Benjamin, New York.

Fujime, S., and Maeda, T. (1984) *Macromolecules* **17**, 2381-2391.

Fujime, S., and Maeda, T. (1985) *Macromolecules* **18**, 191-195.

Fujimoto, B.S., Shibata, J.H., Schurr, R.L. and Schurr, J.M. (1985) Biopolymers 24, 1009-1022.

Fujimoto, B.S., Kim, U.S., Schurr, J.M., and Wu, P.G. (1989) Biophys. J. 55, 364a.

Fuller, F.B. (1971) Proc. Natl. Acad. Sci. USA 68, 815-819.

Gellert, M., Mizuuchi, K., O'Dea, M.H., Ohmori, H., and Tomizawa, J. (1979) Cold Spring Harbor Symp. Quant. Biol. 43, 53-60.

Gellert, M., O'Dea, M.H., and Mizuuchi, K., (1983) Proc. Natl. Acad. Sci. USA 80, 5545-5549.

Giaever, G.N., Snyder, L., and Wang, J.C. (1988) Biophysical Chemistry 29, 7-15.

Greaves, D.R., Patient, R.K., and Lilley, D.M.J. (1985) J. Mol. Biol. 185, 461-478.

Greer, S., and Zamenhof, S. (1962) J. Mol. Biol. 4, 123-141.

Griffith, J. D., (1988) *Biophys J.* **53**, 621a.

Haniford, D.B., and Pulleyblank, D.E. (1983) Nature (London) 302, 632-634.

Haniford, D.B., and Pulleyblank, D.E., (1985) Nucleic Acids Research 13, 4343-4363.

Harris, R.A., and Hearst, J.E. (1966) *J. Chem. Phys.* **44**, 2595-2602.

Hagerman, P.J., (1981) *Biopolymers* **20**, 1503-1535 .

Hagerman, P. J. (1985) *Biochemistry* **24**, 7033-7037.

Haniford, D.B., and Pulleyblank, D.E. (1983) Nature (London) 302, 632-634.

Haniford, D.B., and Pulleyblank, D.E., (1985) Nucleic Acids Research 13, 4343-4363.

Hinton, D.M., and Bode, V.C. (1975) J. Biol. Chem. 250, 1061-1079.

Hogan, M.E., Dattagupta, N., and Crothers, D.M. (1979) Biochemistry 18, 280-288.

Hogan, M., Wang, J., Austin, R.M., Monitto, C., and Hershkowitz, S. (1982) Proc. Natl. Acad. Sci. USA 79, 3518-3522 .

Horowitz, D., and Wang, J.C. (1984) J. Mol. Biol. 173, 75-91.

Hsieh, T.S., and Wang, J.C. (1975) Biochemistry 14, 527-535.

Jen-Jacobson, L., Kurpiewski, M., Lesser, D., Grable, J., Boyer, H. W., Rosenberg, J. M., and Greene, P. J. (1983) J. Biol. Chem. 258, 14638-14646.

Jones, R.L., Lanier, A.C., Keel, R.A., and Wilson, W.D. (1980) Nucleic Acids Res. 8, 1613-1624.

Kam, Z., Borochov, N., and Eisenberg, H. (1981) *Biopolymers* **20**, 2671-2690.

Keller, W. (1975) Proc. Natl. Acad. Sci. USA 72, 4276-4880.

Kim, R., Modrich, P., Kim, S.-H. (1984) Nucleic Acids Research 12, 7285-7292.

Kim, U.S., Fujimoto, B.S., and Schurr, J.M. (1989) Biophys. J. 55, 364a.

Kowalski, D., Natale, D.A., and Eddy, M.J. (1988) Proc. Natl. Acad. Sci. USA 85, 9464-9469.

Klysik, J., Stirdivant, S.M., Larson, J.E., Hart, P.A., and Wells, R.D. (1981) Nature (London) 290, 672-677.

Kovacic, R.T., and Van Holde, K.E. (1976) *Biochemistry*, **16**, 1490-1498.

Kowalski, D., Natale, D.A., and Eddy, M.J. (1988) Proc. Natl. Acad. Sci. USA 85, 9464-9469.

Langowski, J. (1987) Biophys. Chem. 27, 263-271.

Langowski, J., Benight, A.S., Fujimoto, B.S., Schurr, J.M., and Schomburg, U. (1985) Biochemistry 24, 4022-4028.

Langowski, J., Fujimoto, B.S., Wemmer, D.E., Benight, A.S., Drobny, G., Shibata, J.H., and Schurr, J.M. (1985) Biopolymers 24, 1023-1056.

Langowski, J., Giesen, U., and Lehmann, Chr. (1986) Biophys. Chem. 25, 191-200.

LeBret, M. (1979) Biopolymers 18, 1709-1725.

LeBret, M. (1980) Biopolymers 19, 619-637.

LeBret, M. (1984) Biopolymers 23, 1835-1867.

Lee, G., Arscott, P. G., Bloomfield, V. A., and Evans, D. F. (1989) *Science*, in press.

Levene, S.D., and Crothers, D.M. (1986) J. Mol. Biol. 189, 73-83.

Lewis, R.J., Huang, J.H., and Pecora, R. (1985) Macromolecules 18, 944-948.

Lilley, D.M.J. (1980) Proc. Natl. Acad. Sci. USA 77, 6468-6472.

Lilley, D.M.J., and Hallam, L.R. (1984) J. Mol. Biol. 180, 179-200.

Lilley, D. (1986) Nature 320, 14-15.

Lin, S.C., and Schurr, J.M., (1978) *Biopolymers* **17**, 425-461.

Lin, S.-C., Thomas, J.C., Allison, S.A., and Schurr, J.M. (1981) Biopolymers 20, 209-230.

Lindahl, T., and Nyberg, B. (1972) Biochemistry 19, 3610-3618.

Lyamichev, V.I., Panyutin, I.G., and Kamenetskii, F. (1983) FEBS Letts. 153, 298.

Mandel, M., and Schouten, J. (1980) *Macromolecules* **13**, 1247-1251.

Maret, G., and Weill, G. (1983) *Biopolymers* **22**, 2727-2744.

Marini, J., Levene, S., Crothers, D. M., and Englund, P. T. (1982) Proc. Natl. Acad. Sci. USA 79, 7664-7668.

McClarin, J. A., Frederick, C. A., Wang, B. C., Greene, P., Boyer, H. W., Grable, J., Rosenberg, J. M. (1986) Science 234, 1526-1541.

McClellan, J.A., and Lilley, D.M.J. (1987) J. Mol. Biol. 197, 707-721.

Millar, D.P., Robbins, R.J., and Zewail, A.H. (1982) J. Chem. Phys. 76, 2080-2094.

Mizuuchi, K., Mizuuchi, M., and Gellert, M. (1982) J. Mol. Biol. 156, 229-243.

Murchie, A.I.H., and Lilley, D.M.J. (1987) Nucleic Acids Res. 15, 9641-9653.

Negri, R., Della Seta, F., di Mauro, E., and Camilloni, G., (1989) "Topological Evidence for Allosteric Transitions in DNA Secondary Structure," preprint submitted to Biophys. J.

Nelson, N. C. M., Finch, J. T., Liusi, B. F., and Klug, A. (1987) *Nature* **330**, 221-226.

Nordheim, A., and Rich, A. (1983a) Nature (London) 303, 674-679.

Nordheim, A., and Rich, A. (1983b) Proc. Natl. Acad. Sci. USA 80, 1821-1825.

Odijk, T. (1979) *Biopolymers* **18**, 3111-3113.

Oosawa, fumio, and Masai, Junji (1982) *Biophys. Chem.* **16**, 33-40.

Panayotatos, N., and Wells, R.D. (1981) Nature (London) 289, 466-470.

Panyutin, I., Klishko, V., and Lyamichev, V. (1984) J. Biomolec. Struc. and Dyn. 1, 1311-1324.

Peck, L.J., Nordheim. A., Rich, A., and Wang, J. (1982) Proc. Natl. Acad. Sci. USA 79, 4560-4564.

Phillies, George D. J., (1980) *J. Chem. Phys.*, **72**, 6123-6133.

Piette, J., Lopez, M.,Calberg-Bacq, C.M. and Van De Vorst, A. (1981) Int. Radiat. Biol. 40, 427-433.

Pörschke, D., Zacharias, W., and Wells, R.D. (1987) Biopolymers 26, 1971-1974.

Pulleyblank, D.E., Shure, M., Tang, D., Vinograd, J., and Vosberg, H.P. (1975) Proc. Natl. Acad. Sci. USA 72, 4280-4284.

Pulleyblank, D.E., Haniford, D.B., and Morgan. A.R. (1985) Cell 42, 271-280.

Pruss, Gail J. (1985) J. Mol. Biol. 185, 51-63.

Rizzo, V., and Schellman. J. (1981) *Biopolymers* **20**, 2143-2163.

Rotne, J., and Prager, S. (1969) *J. Chem. Phys.* **50**, 4831-4837.

Schurr, J.M. (1976) *Biopolymers* **16**, 461-464.

Schurr, J.M. (1983) Biopolymers 22, 2207-2217.

Schurr, J.M., (1984) *Chemical Physics* **84**, 71-96.

Schurr, J.M., and Fujimoto, B.S. (1988) Biopolymers, in press.

Schurr, J.M., Fujimoto. B.S., Wu, P.-G., and Song, L. (1989) "Fluorescence Studies of Nucleic Acids. Dynamics, Rigidities, and Structures," to appear in Fluorescence Spectroscopy, Ed. by J.R. Lakowicz, Plenum Publ. Corp., New York.

Schurr. J.M., and Schmitz, K.S. (1986) *Annu. Rev. Phys. Chem.* **37**, 271-305.

Schutle, C.J.H. (1984) *Appl. Spectr. Rev.* **20**, 347-371

Sharp, P., and Bloomfield, V. (1968) *Biopolymers* 6), 1201-1211.

Shibata, J.H., Fujimoto, B.S., and Schurr, J.M. (1985) Biopolymers 24, 1909-1930.

Shibata, J.H., Wilcoxon, J., and Schurr, J.M. (1984) *Biochemistry* **23**, 1188-1194.

Shimada, J., and Yamakawa, H. (1984) *Macromolecules* **17**, 689-698.

Shimada, J., and Yamakawa, H. (1984b) Biopolymers 23, 853-857.

Shimada, J., and Yamakawa, H. (1985) *J. Mol. Biol.* **184**, 319-329.

Shore, D., and Baldwin, R.L. (1983) J. Mol. Biol. 170, 957-1007.

Singleton, C.K., Klysik, J., Stirdivant, S.M., and Wells, R.D. (1982) Nature (London) 299, 312-316.

Smith, S. B., Aldridge, P. A., and Callis, J. B. (1989) *Science* **243**, 203-206.

Soda, K., (1985) *Macromolecules* **17**, 2365-2375.

Soda, K., (1973) *J. Phys. Soc. Japan* **35**, 866-870.

Song, L., Allison, S.A., and Schurr, J.M. (1989) "Normal Mode Theory for the Brownian Dynamics of a Weakly Bending Rod. Comparison with Brownian Dynamics Simulations," companion paper.

Stellwagen, N. C. (1988) *Biophys. J.* **53**, 484a.

Sullivan, K.M., and Lilley, D.M.J. (1986) Cell 47, 817-827.

Swenberg, C.E., Carberry, S.E., and Geacintov, N.E. (1968) Biophys. J. 53, 44a.

Théveny, B., Coulaud, D., LeBret, M., and Révet, B., in Structure and Expression, Vol.3: DNA Bending and Curvature, Eds. W.K. Olson, M.H. Sarma, and M. Sundaralingam, Adenine Press, pp. 39-55 (1988).

Thomae, R., Beck, S., and Pohl, F.M. (1983) Proc. Natl. Acad. Sci. USA 80, 5500-5553.

Thomas, J.C. Allison, S.A., Appellof, C.J., and Schurr, J.M. (1980) Biophys. Chem. 12, 177-188.

Thomas. J.C., Allison, S.A., Schurr, J.M., and Holder, R.D. (1980) Biopolymers 19, 1451-1474.

Thomas. J.C., and Schurr, J.M. (1983) Biochemistry 22, 6194-6198.

Thomas. T.J., and Bloomfield, V.A., (1983) *Nucleic Acids Res.* **11**, 1919-1929.

Tirado, M.M., and Garcia de la Torre, J., (1979) *J. Chem. Phys.* 71, 2581-2587.

Tirado, M.M., and Garcia de la Torre, J., (1980) *J. Chem. Phys.* 73, 1986-1993.

Uhlenbeck, G.E., and Ornstein, L.S. (1930) *Phys. Rev.* **36**, 823-841.

Upholt, W.B., Gray, H.B., Jr., and Vinograd, J. (1971) J. Mol. Biol. 62, 21-38.

Vologodskii, A.V., Anshelvich, V.V., Lukashin, A.V., and Frank- Kamenetskii, M.D. (1979) Nature (London) 280, 294-298.

Wang, J.C. (1974) J. Mol. Biol. 87, 794-816.

Wang, J.C. (1982) Scientific American 247, 94-109.

Wang, W.C., and Uhlenbeck, G.E. (1945) *Rev. Mod. Phys.* **17**, 323-342.

Wells, R.D. (1988) J. Biol. Chem. 263, 1095-1098

Wetmur, J.G., and Davidson, N. (1968) J. Mol. Biol. 31 349-370.

Wilcoxon, J., and Schurr, J.M. (1983) Biopolymers 22, 2273-2321.

Wilcoxon, J. (1983b) Ph.D Thesis, Univ. of Washington.

Wilcoxon, J., Shibata, J.H., Thomas, J.C., and Schurr, J.M., in Biomedical Applications of Laser Light Scattering, Eds. W.I. Lee, D.B. Sattelle, and B.R. Ware, Elsevier Biomedical Press, Amsterdam (1982) pp. 27-36.

Wohlraub. F., McLean, M.J., and Wells, R.D. (1987) J. Biol. Chem. 262, 6407-6416.

Wu, P.-G., Fujimoto, B.S., and Schurr, J.M. (1987) Biopolymers 26, 1463-1488.

Wu, P.-G., and Schurr, J.M. (1989a) "Effect of Chloroquine on the Torsional Dynamics and Rigidities of Linear and Supercoiled DNAs at Low Ionic Strength." Biopolymers, in press.

Wu, P.-G., Song, L., Fujimoto, B.S., Clendenning, J.B., and Schurr, J.M. (1989b) "Allosteric Transitions in Secondary Structure Induced by Superhelical Stress." in Laser Scattering Spectroscopy of Biological Objects, Vol, II, Elsevier, Amsterdam.

Wu, P.-G., Fujimoto, B.S., and Schurr, J.M., (1987) *Biopolymers* **26**, 1463-1468.

Wu, P.-G., Fujimoto, B.S., and Schurr, J.M. (1989c) Biopolymers, in press.

Wu, P.-G., Song, L., Clendenning, J.B., Fujimoto, B.S., Benight, A.S., and Schurr, J.M., Biochemistry, in press.

Wu, H.-M., and Crothers, D. M. (1984) *Nature* **308**, 509-513.

Yamakawa, H., (1984) *Annu. Rev. Phys. Chem.* **35**, 23-47.

Yamakawa, H., and Fujii, M., (1974) *Macromolecules* **7**, 128-135.

Yamakawa, H., and Fujii, M., (1974) *Macromolecules* **7**, 649-654.

Yamakawa, H., and Fujii, M., (1973) *Macromolecules* **6**, 407-415.

Yamakawa, H., (1970) *J. Chem. Phys.* **53**, 436-443 .

Yanagida, M., Hiraoka, Y., and Katsura, I. (1983) *Cold Spring Harbor Symp. Quant. Biol.* **47**, 177-187.

Zimm, B.H. (1956) *J. Chem. Phys.* **24**, 269-278.

Appendix A
Procedures of Large-scale Isolation of Plasmid DNA

I. Growth of Bacteria and Amplification of the Plasmid

1. Inoculate 10 mL of LB metium containing 50 μg/mL Ampicillin with a single E.ColiHB101 colony. Incubat at 37°C overnight with vigorous shaking.
2. Inoculate 10 mL of the overnight culture into a 2-liter flask containing 1000 mL of M9 medium and 50 μg/mL Ampicillin. Incubate at 37°C with vigorous shaking until the culture reaches an OD_{600} of 0.9-1.0.
3. Inoculate 1 liter of the 0.9 OD_{600} culture into a 20-liter fermentor containing 10 liters of M9 medium and 50 μg/mL Ampicillin. Incubate at 37°C with air flow rate 12, agitation 350 r.p.m. until the culture reaches an OD_{600} of 1.0-1.5.
4. Add 10 mL of a solution of Chloramphenicol (1.0 g/10 mL in ethanol). Continue incubation for a further 12-16 hrs.
5. Harvest the bacterial cells by centrifugation at 4.2K r.p.m. for 20 min. at 0°C. Discard the supernatent.
6. Redisolve cell pellets in 15% sucrose. 50 mM Tris. 50 mM EDTA(pH 8.2). Spin 7 K for 20 min at 0°C. Pour out the supernatant. Measure the weight of cells.

II. Lysis of Bacteria and Purification of Closed Circular DNA

For 50 gm cells:

1. Resuspend the bacterial pellets in 50 mL of an ice-cold solution of 15% sucrose. 50 mM Tris, 50 mM EDTA (pH 8.2).
2. Add 10 mL of a freshly made solution of lysozyme (100 mg/mL in 0.25 M Tris, 0.1 M EDTA, pH 8.0). Mix by gently inverting. Place on ice for 1/2 hr.
3. Add 20 mL of 5 M KAc(pH 5.2), gently invert. Add 10 mL of 10% SDS, gently invert. Place on ice for 1 hr.
4. Spin at 12 K for 70 min at 4°C.
5. Pour off and save the supernatent. Discard the pellet.
6. Make RNase solution 20 mg/mL in 0.1 M NaAc, pH 5.2. Boil for 10 min, let it cool slowly at room temperature. Add RNase to obtain final concentration 0.2 mg/mL, leave at 37°C for 30 min.
7. Add 1 mL 12 mg/mL proteinase K, incubate at 37°C for 30 min.
8. Measure the volume of DNA solution. Add half of that volume of 30% PEG, 1.5 M NaCl, let it stand ad −20°C overnight.
9. Centrafuge at 9 K r.p.m. for 40 min at 4°C. Discard the supernatent. Disolve pellet in 50 mL of 50 mM Tris, 50 mM EDTA, pH 8.5
10. Wash phenol with solution containing 0.2 M NaCl, 0.1 M Tris for three times until pH=8.0, add 8-hydroxyquine to make 0.1% concentration
11. Add equal volume phenol, mix vigorously with DNA solution, spin at 7 K for 5 min. repeat the same extraction procedure for three times. Then, extract DNA solution three times with ether.

Appendix B

Program LSFEX.FOR

```
C       PROGRAM LSFEX.FOR

c       this program is used to deal with experimental data trsferred
c       from the autocorrelator.the autocorrelation function from the
c       autocorrlator is exponantial decay.in this program a formular
c       F(T)=A*EXP(-T/TAU)+B  is used to fit the experimental curve.
c       there are 256 channels in the autocorrelator.first 240
c       channels are for the autocorrlation function.
c
c       subroutine GETDATA does the job of getting data from the
c       autocorrelator. Whenever it is called it makes the interface
c       get data from the autocorrelator if the autocorrelator is
c       halted.
c
c       subroutine FUNCTION returns value of panel switch setting
c       specified by code as follows:
c       code    value returned
c        1       time between normal channels in nanoseconds
c        2       number of shifts per transfer
c        3       amount by which delayed channel counts are prescaled
c                (diviser)
c        4       amount by which delayed channel counts are multiplied
```

```
c        5       dust limit estting
c        6       time between extra-delayed channels in nanoseconds
c        7       crosscorel=0,autocorel=1
c        8       dust limit enabled=1,disabled=0
c
c       to link the program,you type:
c       LINK LSFEX+GETDATA+FUNCTION+IPORT+WPORT+$I4AND
c       [LIB.] \FORTRAN+GUTIL
c
c       to compile ,link the program ,you could type:
c       COLIGO LSFEX
c
c       variable name   meaning
c         F(I)          the calculated value at the Ith point
c         Y(I)          the experimental value at the Ith point
c
```

```
        IMPLICIT INTEGER (I-N)
        IMPLICIT REAL    (A-H,O-Z)
$INCLUDE: 'XYCMN.FOR'
        DIMENSION  F(250),Y(250),Z(20),T(3),W(3,3),B(2,2),G(2),
     *             DA(3),A(3),H(240),DF(240),RR(240)
        REAL*4  SRNS,SBNT,SCAN
```

```
      INTEGER IDATA(256), SWITCH
      CHARACTER*12 XT,YT
      CHARACTER*79 EMSG,FNAME,DATAFILE
1000  OPEN (2,FILE='LSF.OUT',STATUS='NEW')

      WRITE(*,111)
111   FORMAT(5X,'READ DATA FROM THE AUTOCORRELATOR(1) OR A FILE(2)?',$)
      READ (*,*) DSET
      IF(DSET .EQ. 1)THEN

C        Read data from the correlator
         CALL GETDATA (IDATA)
      ELSE
         WRITE(*,112)
112      FORMAT(5X,'ENTER NAME OF THE FILE: ',$)
         READ(*,113)DATAFILE
113      FORMAT(A)
         OPEN(3,FILE=DATAFILE,STATUS='OLD')
         READ(3,*)IDATA
      ENDIF
C
C     Determine the shift period
      DT= SWITCH(IDATA, 1) * 1E-9
C
C Now build the real data arrays
      DO 8 I=1, 240
```

```
        RR(I)=FLOAT(I)
        H(I)= I*DT*1E+6
        Y(I)= IDATA(I)*32.
8       CONTINUE
C
C draw real data from the autocorrelator or a data file
290     IMODE=16
        N=240
        XT='CHANNEL'
        YT='A(T)'
        CALL GINIT(IMODE,IERR,EMSG)
        LSTYL=0
        LCOL=COLSEL(2)
        CALL XYPLOT(RR,XT,Y,YT,N,IERR)
        CALL INKEY2(I,J)
        CALL CLSCR(0)
        CALL VMODE(3)

c       determine prescale
        PRESCA=SWITCH(IDATA,3)
        WRITE(*,602)PRESCA
602     FORMAT(5X,'PRESCALE=',E14.7)

c       determine counts/photon
        COPH=SWITCH(IDATA,4)
        WRITE(*,603)COPH
```

```
603     FORMAT(5X,'COUNTS/PHOTON=',E14.7)

c       determine dust limit
        DULI=SWITCH(IDATA,5)
        WRITE(*,604)DULI
604     FORMAT(5X,'DUST LIMIT=',E14.7)

c       determine delay time
        DETI=SWITCH(IDATA,1)*1.E-9
        WRITE(*,605)DETI
605     FORMAT(5X,'DELAY TIME(sec)=',E14.7)

c       determine shifts/transfer
        SHTR=SWITCH(IDATA,2)
        WRITE(*,606)SHTR
606     FORMAT(5X,'SHIFTS/TRANSFER=',E14.7)

c       determine experiment length
        RNSHIFT=(FLOAT(2**27)*FLOAT(IDATA(250))+FLOAT(IDATA(249)))
        EXLE=DT*RNSHIFT
        WRITE(*,607) EXLE
607     FORMAT(5X,'EXP LENGTH(SEC)=',E14.7)

c       determine total counts
        COUNTS=FLOAT(IDATA(251))*32.
```

```
c       determine count rate(dust limit setting or
c     &  (total counts/experiment length)
        CORATE=FLOAT(IDATA(251))*32./EXLE
        WRITE(*,608)CORATE
608     FORMAT(5X,'COUNT RATE(COUNTS/SEC)=',E14.7)

9       WRITE   (*,50)
10      FORMAT  (5X,'NSTART(1-NTOTAL)=',$)
        READ    (*,*) NT
20      FORMAT  ( I4)
        WRITE   (*,10)
30      FORMAT  (5X,'NFINAL(NS-NTOTAL)=',$)
        READ    (*,*) NS
        WRITE   (*,30)
50      FORMAT  (/,5X,'NTOTAL(1-248)=',$)
        READ    (*,*) NL
        WRITE(*,51)
51      FORMAT(5X,'AFTERPULSING CORRECTION(0-1.0)=',$)
        READ (*,*)AFPU

        PI=3.141592654
        S=0
        DO 70 I=231,240
        S = S + Y(I)
70      CONTINUE
        A(3) = S / 10.
```

```
      A(1) = Y(NS) - A(3)


      Q = .368 * A(1)
      P = A(3) + Q
      I = NS
80    IF ( Y(I) - P ) 82,82,81
81    I=I+1
      IF ( I - 240 ) 80,80,16
82    RI = FLOAT(I)
      ALAM = 1 / RI
      XM1 = EXP (ALAM )
      X = 1 / XM1
      IF ( X .EQ. 1 ) GO TO 26
      IF ( X .EQ. 0 ) GO TO 26
      Y(1)=Y(1)*(1-AFPU)
      N = NT
      DO 83 I=1,N
      Y(I) = Y ( NS - 1 + I )
83    CONTINUE


      NTRY=0
85    NTRY=NTRY+1
      IF (NTRY .EQ. 100) GO TO 16
      X2 = X * X
      XN = 1
      DO 90 I=1,N
```

```
      XN = XN * X
90    CONTINUE
      X2N = XN * XN
      D1 = 1 - X2
      D2 = D1 * D1
      D3 = D1 * D2
      D = 1 - X
      W(1,1) = (X2 * (1 - X2N)) / D1
      W(1,2) = A(1) * X * ((1 - X2N)/D2 - N * X2N / D1 )
      W(1,3) = X * (1 - XN) / D
      W(2,1) = W(1,2)
      Z1 = 1 - X2N - N * X2N * (1+X2)
      Z2 = 2 * X * X * (1 - X2N)

      Z3 = N * (N+1) * X2N

      W(2,2) = A(1)*A(1) * (Z1/D2 + Z2/D3 - Z3/D1)
      W(2,3) = A(1) * ((1-XN)/(D**2)  - N*XN/D )
      W(3,1) = W(1,3)
      W(3,2) = W(2,3)
      W(3,3) = N
      T(1) = 0
      T(2) = 0
      T(3) = 0
      DO 100 I=1,N
      F(I) = A(1) * (X**I) + A(3)
```

```
      DF(I)= Y(I) -F(I)
      T(1) = T(1) + (X**I)* DF(I)
      T(2) = T(2) + I*A(1)*(X**(I-1))*DF(I)
      T(3) = T(3) + DF(I)
      DF(I)= DF(I)+ 0.5*A(1) + A(3)
100   CONTINUE
      CALL SIMEQ ( W,T,DA,B,G,C )

      S1=DA(1)/A(1)
      S2=DA(2)/X
      S3=DA(3)/A(3)
      SBNT=SQRT(A(3)*RNSHIFT*PRESCA)
      RELER=ABS(SBNT-COUNTS)/COUNTS
106   FORMAT (5X,'ERROR=',E14.7)

      IF ( S1 - 1.E-6 ) 120,120,150
120   IF ( S2 - 1.E-6 ) 130,130,150
130   IF ( S3 - 1.E-6 ) 140,140,150
140   GO TO 160
150   A(1) = A(1) + DA(1)
      X = X + DA(2)
      A(3) = A(3) + DA(3)

      GO TO 85

160   SUM = 0.
```

```
      DO 170 I=1,N
      SUM = (Y(I) - F(I))**2 + SUM
170   CONTINUE
      XM1 = 1/X
      RLAM = ALOG(XM1)
      RI = 1/RLAM
      TAU = RI * DT
      GO TO 180
16    WRITE  (*,7)
7     FORMAT (/,'BAD INITIAL GUESS.TRY AGAIGIN')
26    WRITE(*,27)X
27    FORMAT(/,'X=',E10.4)
      GO TO 400

180   WRITE (*,200) A(1)
200   FORMAT (/,5X,'AMPLITUDE=',E14.7)
C     WRITE (*,210) TAU
210   FORMAT (5X,'TAU(SECONDS)=',E14.7)
      WRITE (*,215) RI
215   FORMAT (5X,'TAU( CHANELL)=',E14.7)
      WRITE (*,220) A(3)
220   FORMAT (5X,'BASE LINE=',E14.7)
      WRITE(*,225)
225   FORMAT(5X,'WAVELENGTH(ANGSTROMS)=',$)
      READ(*,*)WALE
      WRITE(*,230)
```

```
230     FORMAT(5X,'SCATTERING ANGLE(DEG)=',$)
        READ(*,*)SCAN
        WRITE(*,235)
235     FORMAT(5X,'INDEX OF REFRACTION=',$)
        READ(*,*)REIN
        WRITE(*,240)
240     FORMAT(5X,'TEMPERATURE(DEG C)=',$)
        READ(*,*)TEMP

        SCAN=SCAN*PI/180.
        SINAN=SIN(SCAN)
        CRSIAN=CORATE*SINAN
        WRITE(*,245)CRSIAN
245     FORMAT(/,5X,'(COUNT RATE)*(SIN AN)='E14.7)

        SRNS=A(3)*RNSHIFT*PRESCA
        SBNT=SQRT(SRNS)
        WRITE(*,250)SBNT
250     FORMAT(5X,'SQRT(B*NSHIFT)=',E14.7)

        COUNTS=FLOAT(IDATA(251))*32.
        WRITE(*,255)COUNTS
255     FORMAT(5X,'TOTAL COUNTS #=',E14.7)

        ANHA=SCAN/2.
        SHA=SIN(ANHA)
```

```
      RK=(4.* REIN * PI * SHA)/(WALE*1.E-8)
      RK2=(RK)**2
      WRITE(*,260)RK2
260   FORMAT(5X,'K**2(CM**-2)='E14.7)

      WRITE(*,210)TAU
      WRITE(*,106)S2

      DAPP=1./(2.*TAU*RK2)
      WRITE(*,265)DAPP
265   FORMAT(5X,'DAPP(CM**2/SEC)=',E14.7)


c     to plot the originol data and exponantial fitting
c     data on the screen
      WRITE (*,600)
600   FORMAT(/,5X,'PLOT DATA ON SCREEN? STRIKE ANY KEY')
C     WAIT FOR KEYBOARD RESPONSE
      CALL INKEY2(I,J)
      XT='TIME'
      YT='A(T)'
      IMODE=16
C     INITIALIZE GRAPHICS
      CALL GINIT(IMODE,IERR,EMSG)
C     SET LINE STYLE FOR LINE
      LSTYL=1
```

```
C       DRAW LINE IN COLOR 3
        LCOL=COLSEL(3)
C       DRAW X-Y PLOT OF EXPERIMENTAL DATA Y(I)-I(CHANNEL)
        CALL XYPLOT(H,XT,Y,YT,N,IERR)
C       WAIT FOR KEYBOARD RESPONSE
        CALL INKEY2(I,J)
C       DRAW LINE IN COLOR 2
        LCOL=COLSEL(2)
C       DRAW X-Y PLOT OF FITTING DATA F(I)-I (CHANNEL)
        CALL XYDRAW(H,F,N,IERR,EMSG)
C       WAIT FOR KEYBORD RESPONSE
        CALL INKEY2(I,J)
C       DRAW LINE IN COLOR 5
        LCOL=COLSEL(5)
C       DRAW X-Y PLOT OF DF(I)=Y(I)-F(I) VS. I
        CALL XYDRAW(H,DF,N,IERR,EMSG)
C       WAIT FOR KEYBOARD RESPONSE
        CALL INKEY2(I,J)
C       CLEAR SCREEN
        CALL CLSCR(0)
C       EXIT IN TEXT MODE
        CALL VMODE(3)

400     WRITE (*,500)
500     FORMAT(5X,'TRY AGAIN (1/2)?',$)
        READ (*,*)TRY
```

```
      IF(TRY .EQ. 1)THEN
         GO TO 290
      ELSE
         WRITE (*,510)
510      FORMAT (5X,'SAVE DATA (1/2)?',$)
      ENDIF
      READ (*,*) SAVE
      IF (SAVE .EQ. 2)GO TO 530
c        to write raw data file IDATA on a data file
         WRITE(*,333)
333      FORMAT(5X,'ENTER NAME OF OUTPUT FILE:',$)
         READ(*,444)FNAME
444      FORMAT (A)
         OPEN(1,FILE=FNAME,STATUS='NEW')
         WRITE(1,*)IDATA,TEMP
         WRITE(2,520) (H(I),Y(I),I=1,N)
520      FORMAT (2(E10.4))
530      WRITE(*,521)
521      FORMAT (5X,'QUIT (1/2)?',$)
         READ(*,*)QUIT
         IF (QUIT .EQ. 1) GO TO 2000
         GO TO 1000

C     CLOSE(1,STATUS='CLOSE')
C     CLOSE(2,STATUS='CLOSE')
```

```
2000    STOP
        END



        SUBROUTINE SIMEQ (W,T,DA,B,G,C)
        REAL   W(3,3),T(3),DA(3),B(2,2),G(2),C

        B(1,1) = W(1,2) - W(3,2)*W(1,1)/W(3,1)
        B(1,2) = W(1,3) - W(3,3)*W(1,1)/W(3,1)
        B(2,1) = W(2,2) - W(3,2)*W(2,1)/W(3,1)
        B(2,2) = W(2,3) - W(3,3)*W(2,1)/W(3,1)
        G(1) = T(2) - W(3,2)*T(1)/W(3,1)
        G(2) = T(3) - W(3,3)*T(1)/W(3,1)
        C = B(1,2) - B(2,2)*B(1,1)/B(2,1)
        DA(1)=(G(2)-B(2,2)*G(1)/B(2,1))/ C
        DA(2)=G(1)/B(2,1)-B(1,1)*DA(1)/B(2,1)
        DA(3)=(T(1)/W(3,1))-(W(1,1)*DA(1)/W(3,1))-(W(2,1)*DA(2)/W(3,1))
        RETURN
        END



C Subroutine to read autocorrelator memory
```

```
C Returns the values of the 256 correlator memory
C locations in I*4 array IDATA

      SUBROUTINE GETDATA(IDATA)
      INTEGER IDATA(256)
      INTEGER*2 IPORT, BITS0T7, BITS8T11, BITS12T19, BITS20T23,
     1          BITS23T26, CSR
      DATA CSR/#300/
C
C Set CSR bit 6 to put correlator in I/O mode
      CALL WPORT(CSR, 2#01000000)
C
C Check CSR bit 7 to determine if correlator is now in I/O mode.
C Correlator will only enter I/O mode if it is halted.
      IF (IPORT(CSR) .LT. 128) THEN
          WRITE(*,*) 'Waiting for correlator to be halted...'
100       IF (IPORT(CSR) .LT. 128) GOTO 100
      ENDIF
C
C Set scale factor to zero, clear the memory pointer,
C and leave it in I/O mode
      CALL WPORT(CSR, 2#01010000)
C
C Now enter the loop that reads the 256 memory values
      DO 200 I=1, 256
C
```

```
C Read bits 0 thru 11 of the correlator memory word
      BITS0TO7= IPORT(CSR+1)
      BITS8T11= IPORT(CSR+2)
C
C Read bits 12 thru 23 of the correlator memory word
C First change the scale factor to 12
      CALL WPORT(CSR, 2#01001100)
      BITS12T19= IPORT(CSR+1)
      BITS20T23= IPORT(CSR+2)
C
C Read bits 15 thru 26 of the correlator memory word
      CALL WPORT(CSR, 2#01001111)
      BITS23T26= IPORT(CSR+2)
C
C Now assemble the 27 bit integer from the five pieces
      IDATA(I)= BITS0T7           + BITS8T11*(2**8)    +
     1        BITS12T19*(2**12) + BITS20T23*(2**20)  +
     2        (BITS23T26/2)*(2**24)
C
C Now increment the memory pointer, set the scale
C factor back to 0, and the loop
      CALL WPORT(CSR, 2#01100000)
C
200   CONTINUE
C
C Now release the correlator from I/O mode
```

```
      CALL WPORT(CSR, 0)
C
C and were all done
      RETURN
      END

    INTEGER FUNCTION SWITCH(DATA, CODE)
      IMPLICIT INTEGER (A-Z)
      DIMENSION DATA(256)
C
C FUNCTION RETURNS VALUE OF PANEL SWITCH SETTING
C SPECIFIED BY CODE AS FOLLOWS:
C     CODE  VALUE RETURNED
C      1    TIME BETWEEN NORMAL CHANNELS IN NANOSECONDS
C      2    NUMBER OF SHIFTS PER TRANSFER
C      3    AMOUNT BY WHICH DELAYED CHANNEL COUNTS ARE
c           PRESCALED (DIVISOR)
C      4    AMOUNT BY WHICH DELAYED CHANNEL COUNTS ARE MULIPLIED
C      5    DUST LIMIT SETTING
C      6    TIME BETWEEN EXTRA-DELAYED CHANNELS IN NANOSECONDS
C      7    CROSSCOREL=0, AUTOCOREL=1
C      8    DUST LIMIT ENABLED=1, DISABLED=0
C
      GOTO (100,200,300,400,500,600,700,800)  CODE
      WRITE (*,*) 'ILLEGAL CODE FOR PANEL FUNCTION= ', CODE
      STOP
```

```
C
100   EXP= IBITS(DATA(254), 4, 4)
      MNTSA= IBITS(DATA(254), 0, 4)
      SWITCH= MNTSA*(10**(9-EXP))
      RETURN
C
200   SWITCH= IBITS(DATA(254),8,4) + IBITS(DATA(254),12,4)*10 +
     1 IBITS(DATA(254),16,4)*100 + IBITS(DATA(254),20,4)*1000
      RETURN
C
300   SWITCH= 2**IBITS(DATA(255), 0, 4)
      RETURN
C
400   SWITCH= IBITS(DATA(255), 4, 4)
      RETURN
C
500   SWITCH= IBITS(DATA(255),8,4) + IBITS(DATA(255),12,4)*10 +
     1 IBITS(DATA(255),16,4)*100
      RETURN
C
600   EXP= IBITS(DATA(254), 4, 4)
      MNTSA= IBITS(DATA(254), 0, 4)
      SHIFT= MNTSA*(10**(9-EXP))
      IF (SHIFT .LT. 200) THEN
            SWITCH= SHIFT
      ELSE
```

```
            SWITCH= SHIFT * 2**IBITS(DATA(255),20,4)
      ENDIF
      RETURN
C
700   SWITCH= IBITS(DATA(254), 24, 1)
      RETURN
C
800   SWITCH= IBITS(DATA(255), 24, 1)
      RETURN
      END
```

```
        INTEGER FUNCTION IBITS(SOURCE, OFFSET, SIZE)
C
C Support function for PC.  Extracts SIZE bits starting at bit number
C OFFSET from SOURCE.
C
        IMPLICIT INTEGER (A-Z)
C
C First right shift it the number of bits specified by OFFSET
        TEMP= SOURCE/(2**OFFSET)
C
C Now build a mask
        MASK= 2**SIZE - 1
```

```
C
C Now perform an AND
        IBITS= I4AND(TEMP, MASK)
        RETURN
        END
```

Appendix C
Program QQ9.FOR

```
c       SUBROUTINE DQ4(AA,RH,RL,P,T,Q,DPER,DPLL,DR)
c       Program to solve the eigen value and eigen
c       vector problem for weakly bending rod.
c       To transpose Y vector in Langivin equation.
c       A(N,N) is thr force matrix, B(N) is the eigenvalue
c       of A(N,N). C(N,N) is the eigenvector matrix,
c       H(N,N) is the hydrodynamic interaction matrix in
c       Y direction, HT(N,N) in Z. The eigen values of HA
c       matris is stored in D(N), eigenvector in Q(N,N)

        PARAMETER(N=30,n10=3,nd=10)
        implicit double precision(A-h,o-z)
        common/worksp/rwksp
c       N---matrix dimention,N=n10*nd,
c       nd---dimention of the output,n10=N/nd
c       real*8 LAMH(N,N),H21INV(N,N),U(N,N),QA(N,N),
c       real*8 QAINV(N,N),YQ(N,N),blf(n),HAH(N,N),LAM(N)
C       REAL*8 xc(n,n),yc(n,n),XE(N,N),YE(N,N),XQ(N,N)
c       REAL*8 ATA(N),DH(N,N),DHN(N,N),SDH(N),H21(N,N)
C       REAL*8 SQ(N),QP(N,N),QPINV(N,N),SQP(N),QINV(N,N)
C       REAL*8 qt(n,n),qbb(n),qx1(n),CTP(N),DXMP(N)
```

```
      REAL*8 A(N,N),B(N),C(N,N),SC(N),CN(N,N),HT(N,N)
      real*8 h(n,n),A21(n,n),AHA(n,n),r(n,n)
      REAL*8 D(N),E(N,N),EN(N,N),SE(N),HA(N,N)
      REAL*8 QH(N,N),QC(N,N),QB(N,N),bsqt(n),qa(n,n)
      real*8 Q(N,N),T(N),CT(N),DXM(N),hinv(n,n)
      real rwksp(13016),HTINV(N,N),RhLM(N,N)
      INTEGER NM1,NM2,NM3
      OPEN(UNIT=8,FILE='QQ9DXM.DAT',STATUS='NEW',
     *     FORM='FORMATTED')
      OPEN(UNIT=1,FILE='QQ9.OUT',STATUS='NEW',
     *     FORM='FORMATTED')
      OPEN(UNIT=3,FILE='QQ9T.DAT',STATUS='NEW',
     *     FORM='FORMATTED')
      call iwkin(13016)
C     WRITE(*,1)
1     FORMAT(2X,'NUMBER OF BEADS IN THE ROD N1=',$)
C     READ(*,*)N
      rn=real(n)

      write(*,11)
11    format(2x,'bead radius aa=',$)
      read(*,*)aa
      AA=AA*1.D-8
      write(*,92)
92    format(2x,'bead seperation rh=',$)
      read(*,*)rh
```

```
      RH=RH*1.D-8
      WRITE(*,952)
952   FORMAT(2X,'PERSISTENCE LENGTH P=,CONTOUR LENGTH L=',$)
      READ(*,*)P,RL
      P=P*1.D-8
      RL=RL*1.D-8
      F1=1.38E-16*293./(6.*3.14159*0.01*AA)

c     RG2 IS THE MEAN SQUARE RADIUS OF GYRATION OF
C     WORM LIKE CHAIN
c     RG2=2.*RL*P*(1./6.-P/(2.*RL)+P*P/(RL*RL)-
     *     (P/RL)**3*(1.-DEXP(-RL/P)))
C     CALCULATE RH CORRESPONDS TO RG2
c     RH1=RH
c2200 RH=RH1
c     RH2=RG2/(RN*RN/12.+2.*RN1*RH)
c     RH1=DSQRT(RH2)
c     IF(ABS(RH1-RH) .LE. 1.E-12) GO TO 2201
c     GO TO 2200
c2201 RH=RH1
c     AL2 IS THE MEAN SQUARE END-TO-END DISTANCE
c     OF WLC,P160,BLOOMFIELD
C     RhLM(I,J) is the corrected averaged distance
c     between bead l and m
      DO 100 I=1,N
      DO 100 J=I,N
```

```
      IF (I .EQ. J) GO TO 100
      R(I,J)=ABS(real(I-J))
      AL2=2.*P*(R(I,J)*RH-P+P*DEXP(-R(I,J)*RH/P))
      RH2=AL2/( R(I,J) * R(I,J) )
      RhLM(I,J)=DSQRT(RH2)*r(i,j)

      A(I,J)=0.
100   CONTINUE
      WRITE(*,2202)RLM
2202  FORMAT(2X,'CALCULATED averaged distance
     *       between beads RH=',E12.5)

      A(1,1)=1.
      A(1,2)=-2.
      A(1,3)=1.
      A(2,1)=-2.
      A(2,2)=5.
      A(2,3)=-4.
      A(2,4)=1.
      NM1=N-1
      NM2=N-2
      NM3=N-3
      A(N,NM2)=1.
      A(N,NM1)=-2.
      A(N,N)=1.
      A(NM1,NM3)=1.
```

```
      A(NM1,NM2)=-4.
      A(NM1,NM1)=5.
      A(NM1,N)=-2.
      DO 200 I=3,NM2
      J=I-2
      A(I,J)=1.
      A(I,J+1)=-4.
      A(I,J+2)=6.
      A(I,J+3)=-4.
      A(I,J+4)=1.
200   CONTINUE
8     format(2x,10F12.5)

      CALL DEVCSF(N,A,N,B,C,N)
C     A--D matrix,B(J)--eigenvalue,J=1,n,
c     C(I,J)--eigenvector,I=1,n,J=1,n
C     to normalize eigenvectors and
c     WRITE(*,*)B,C
      DO 250 J=1,N
      SC(J)=0.
      DO 240 I=1,N
      SC(J)=SC(J)+C(I,J)**2
240   CONTINUE
      DO 230 L=1,N
      CN(L,J)=C(L,J)/DSQRT(SC(J))
C     CN(L,1)=1./DSQRT(RN)
```

```
C       cn(L,2)=real(2*L-(n+1))/(2.*Dsqrt
     *             (Rn*(Rn+1)*(Rn-1)/12.))
230     CONTINUE
        if (abs(b(j)) .le. 1.e-12) b(j)=abs(b(j))
        bsqt(j)=dsqrt(b(j))
250     CONTINUE

C       do 232 j=1,n
C       do 233 i=1,n
C       Xc(i,J)=0.
C       do 231 k=1,n
C       Xc(i,J)=Xc(i,J)+A(i,k)*Cn(k,J)
C231    CONTINUE
C       Yc(I,J)=B(J)*Cn(I,J)
C       WRITE(*,*)Xc(i,J),Yc(i,J)
C233    continue
C232    continue

c       WRITE(1,13)
13      FORMAT(2X,'EIGENVALUE AND NORMALIZED
     *        EIGENVECTOR OF D MATRIX')

c       do 20 l=1,n10
c       WRITE(1,6)
c       k=(l-1)*nd+1
c       kn=l*nd
```

```
c       WRITE (1,10)(B(I),I=k,kn)
c       WRITE(1,6)
c       WRITE(1,10)((CN(I,J),J=k,kN),I=1,N)
c20     continue
c       WRITE(1,6)
C       TO CHECK IF CN IS UNITARY,OR CN*CN+=LAMDA
C       WRITE(1,5)(B(I),I=6,N)
c       WRITE(1,6)
C       WRITE(1,10)((CINV(I,J),J=1,N),I=1,N)
5       FORMAT(2X,10(1X,E12.4),/)
6       FORMAT(2X,'*')
C       to generate H matrix,bead radius aa ,
c       bead seperation rh from the main
C       program
        WRITE(*,9005)F1
9005    format(2x,'f1=',e12.5)
        do 400 i=1,n
        do 350 j=I,n
        if (i .eq. j)go to 351
        h(i,j)=3.*aa/(4.*rhLM(i,j))
     *        +(aa/(rhLM(i,j)))**3/2.
        H(J,I)=H(I,J)
        ht(i,j)=3.*aa/(2.*rhLM(i,j))*(1.-
     *         2.*aa**2/(3.*(rhLM(i,j))**2))
        HT(J,I)=HT(I,J)
C       if (ht(i,j) .gt. 0.)go to 351
```

```
C       WRITE(*,*)ht(i,j),AA,RH,i,j,R(I,J)
351     h(i,i)=1.
        HT(I,I)=1.
350     continue
400     continue
C       to construct A1/2 matrix,called A21(i,j)
C       (A1/2)mn=sump.sumq[CN(m,p)*B(p)
     *          1/2*delt(pq)*CN(n,q)
        do 500 i=1,n
        do 450 j=I,n
        A21(i,j)=0.
        do 420 l=1,n
c       if (abs(b(l)) .le. 1.e-12) b(l)=ABS(B(L))
        A21(i,j)=A21(i,j)+cn(i,l)*cn(j,l)*bsqt(l)
420     continue
        A21(J,I)=A21(I,J)
450     continue
500     continue
C       to construct A1/2 H A1/2 matrix,called AHA
        do 600 i=1,n
        do 600 j=i,n
        AHA(i,j)=0.
        do 601 l=1,n
        do 601 m=1,n
        AHA(i,j)=AHA(i,j)+A21(i,l)*H(l,m)*A21(m,j)
601     continue
```

```
      AHA(J,I)=AHA(I,J)
c     write (*,*)aha(i,j)
600   continue
C     write(1,6)
10    format(2x,10(1X,E12.4))

C     TO FIND THE EIGENVALUE(D)
c     AND EIGENVECTOR(E) OF AHA,
      CALL DEVCSF(N,AHA,N,D,E,N)
      write(*,*)d
C     TO NORMALIZE THE EIGENVECTORS OF
c     AHA,AND TO CHECK EIGENVALUES
      DO 700 J=1,N
      SE(J)=0.
      DO 680 I=1,N
      SE(J)=SE(J)+E(I,J)**2
680   CONTINUE
c     XE(I,J)=0.
      DO 650 L=1,N
      EN(L,J)=E(L,J)/DSQRT(SE(J))
c     XE(I,J)=XE(I,J)+AHA(I,L)*E(L,J)
650   CONTINUE
c     YE(I,J)=D(J)*E(I,J)
c     WRITE(*,*)XE(I,J),YE(I,J)
C     write(*,*)D(j)
700   CONTINUE
```

```
      WRITE(1,6)
      WRITE(1,12)
12    FORMAT(2X,'EIGENVALUE AND NORMALIZED
     *       EIGENVECTOR OF AHA')
      do 23 l=1,n10
      k=(l-1)*nd+1
      kn=l*nd
      WRITE(1,6)
      WRITE(1,10)(D(I),I=k,kN)
      WRITE(1,6)
      WRITE(1,10)((EN(I,J),J=k,kN),I=1,N)
      WRITE(1,6)
23    continue
      write(1,31)
      do 33 l=1,n10
      k=(l-1)*nd+1
      kn=l*nd
      write(1,5)(B(j),j=k,kn)
33    continue
      write(1,32)
      do 30 l=1,n10
      k=(l-1)*nd+1
      kn=l*nd
      write(1,5)(D(j),j=k,kn)
30    continue
```

```
31      format(2x,'eigenvalue of D matrix')
32      format(2x,'eigenvalue of AHA matrix')

c       WRITE(*,15)
15      FORMAT(2X,'EN INVERSE')
C       WRITE(1,10)((ENINV(I,J),J=1,N),I=1,N)

        DO 800 I=1,N
         DO 800,J=1,N
          HA(I,J)=0.
          DO 800 L=1,N
           HA(I,J)=HA(I,J)+H(I,L)*A(L,J)
800     CONTINUE
c       WRITE(*,801)
801     FORMAT(2X,'HA IS FINISHED')
C       TO CALCULATE THE EIGENVECTORS FOR HA MATRIX
C       TO FIND Q(n,1) OF THE TRANSFORMATION Y=Q P ,
c       P IS THE NORMAL MODE,Q-1*HA*Q=LAMDA

        DO 892 M=1,N
        DO 892 I=1,N
           X=0.
           DO 891 K=3,N
           X=X+CN(M,K)*CN(I,K)/BSQT(K)
891     CONTINUE
        QC(M,I)=X
```

```
892     CONTINUE


        DO 880 L=3,N
        DO 880 M=1,N
           QB(M,L)=0.0
           DO 880 I=1,N
C       write(*,914)i
C914    format(2x,'i',i2)
           QB(M,L)=QB(M,L)+QC(M,I)*EN(I,L)
880     CONTINUE


        q1nf=DSQRT((rn))
        q2nf=DSQRT((Rn-1)*(Rn+1)*Rn/12.)


        DO 910 J=1,N
c       WRITE(*,911)J
911     FORMAT(2X,'Q(I,J),J=',I3)
        q(j,1)=1./q1nf
        q(j,2)=(real(j)-(rn+1)/2.)/q2nf
         DO 900 L=3,N
C       write(*,912)l
C912    format(2x,'l',i2)
          QH(J,L)=0.0
          DO 890 M=1,N
C       write(*,913)m
C913    format(2x,'m',i2)
```

```
      QH(J,L)=QH(J,L)+HA(J,M)*QB(M,L)
890   CONTINUE
      Q(J,L)=QH(J,L)/D(L)
c     write(*,*)q(j,l)
900   CONTINUE
910   CONTINUE
c     write(3,9)
9     format(2x,'Q MATRIX')
c     do 22 l=1,n10
c     k=nd*(l-1)+1
c     kn=l*nd
c     write(3,10)((Q(i,j),J=k,kn),I=1,n)
c22   continue

C     WRITE(1,35)
35    FORMAT(2X,'EIGEN VALUE AND VECTOR OF HA')
C     WRITE(1,6)
C     DO 920 L=1,N10
C     K=(L-1)*ND+1
C     KN=L*ND
C     WRITE(1,10)(D(J),J=K,KN)
C     WRITE(1,6)
c     WRITE(1,10)((Q(I,J),J=K,KN),I=1,N)
C     WRITE(1,6)
C920  CONTINUE
c     to check if (Q transpose D Q)(l,k)=1,
```

```
c       if l=k;=0,if l .ne. k
        write(*,9292)
9292    format(2x,'QDQ')
        do 9293 l=1,n
        do 9294 k=1,n
        qdq=0.
        do 9296 j=1,n
        qa(l,j)=0
        do 9295 i=1,n
        qa(l,j)=qa(l,j)+q(i,l)*a(i,j)
9295    continue
        qdq=qdq+qa(l,j)*q(j,k)
9296    continue
c       write(*,*)l,k,qdq
9294    continue
9293    continue
        WRITE(*,*)P,RL,AA,RH
C       TO CALCULATE RELAXATION TIME
c       CORRESPONDING TO EACH EIGENVALUE OF HA
C       write(*,1119)
1119    format(2x,'relaxation time for each eigenvalue of HA')
        DO 1050 J=1,N
        T(J)=RH*RH*RH/(F1*P*D(J))*1.E+9
        WRITE(*,*)T(J)
1050    CONTINUE
C       WRITE(1,951)
```

```
C951    FORMAT(1X,'RELAXATION TIME OF EACH MODE
C     %  TAU(L)=6*PI*ITA*AA*H**3/kTP*D(L)  NS')
C       WRITE(1,5)(T(J),J=1,N)

C       TO CALCULATE THE MEAN SQUARE ANGULAR
c       DISPLACEMENT OF THE MIDDLE BEAD ABOUT X
c       AXIS:  DXM,IN ORDER TO COMPARE WITH
c       STUART'S ln<P2(U(0)*U(t))> vs. t
C       NEED TO CALCULATE DPERP FIRST
c       IN ORDER TO CALCULATE DXM

C ****************************************

C       NEED TO CALCULATE Q INVERSE FIRST
c       IN ORDER TO CALCULATE Dperp
c       to fIND Q INVERSE QINV(i,j),i,j=1,n

c       to find the eigenvalue and eigenvector
c       of H,ata(n),dh(n,n)
c       call devcsf(n,H,n,ata,dh,n)

C       to normalize eigenvectors
c       do 1060 J=1,n
c       sdh(j)=0.
c       do 1061 I=1,n
c       sdh(j)=sdh(j)+dh(i,j)**2
```

```
c1061   continue
c       do 1062 l=1,n
c       dhn(l,j)=dh(l,j)/DSQRT(sdh(j))
c1062   continue
c1060   continue
c       to consttruct h1/2 matrix,h1/2=dh*ata1/2*dh-1
c       do 1063 i=1,n
c       do 1064 j=1,n
c       h21(i,j)=0.
c       do 1065 l=1,n
c       if (abs(ata(l)) .le. 1.e-10) ata(l)=abs(ata(l))
c       h21(i,j)=h21(i,j)+dhn(i,l)*dhn(j,l)*DSQRT(ata(l))
c1065   continue
c1064   continue
c1063   continue
c       to construct H1/2 A H1/2,HAH
c       DO 1066 I=1,N
c       DO 1066 J=1,N
c       HAH(I,J)=0.0
c       DO 1066 L=1,N
c       DO 1066 M=1,N
c       HAH(I,J)=HAH(I,J)+H21(I,L)*A(L,M)*H21(M,J)
c1066   CONTINUE
C       TO FIND THE EIGEN VALUE LAM(N),
c       EIGENVECTOR LAMH(N,N) OF HAH
c       CALL DEVCSF(N,HAH,N,LAM,LAMH,N)
```

```
C       write(*,1116)
1116    format(2x,'EIGENVECTOR OF HAH matrix')
C       WRITE(*,*)LAMH
C       write(*,1117)
1117    format(2x,'eigenvalue of HAH')
C       do 1006 i=1,n
C       WRITE (*,*)LAM(i)
C1006   continue

C        to check the eigenvalue
c       HAH*LAMH(J)=LAM(J)*LAMH(J),x(i)=y(i)

C       write(1,1118)
1118    format(2x,'LAM(EIGENVALUE),QP(eigenvector)
     *        of HA made of h21*lamh')
C       DO 1218 L=1,N10
C       K=(L-1)*ND+1
C       KN=L*ND
C       WRITE(1,6)
C       WRITE(1,10)(LAM(I),I=K,KN)
C       WRITE(1,6)
C       WRITE(1,5)((QP(I,J),J=K,KN),I=1,N)
C       WRITE(1,6)
C1218   CONTINUE

C       TO FIND THE INVERSE OF H21
```

```
c       CALL DLINRG(N,H21,N,H21INV,N)
C       to check h21 inverse
C       TO FIND THE QINV TRANNSPOSE CALLED U
c       DO 1067 I=1,N
c       DO 1035 J=1,N
c       U(I,J)=0.
c       DO 1068 L=1,N
c       U(I,J)=U(I,J)+H21INV(I,L)*LAMH(L,J)
c1068   CONTINUE
c1035   CONTINUE
c1067   CONTINUE

C       TO CHECK U,TO MAKE QA
c       DO 550 L=1,N
c       DO 551 M=1,N
c       QA(I,J)=0.0
c       DO 552 K=1,N
c       QA(L,M)=QA(L,M)+U(K,L)*Q(K,M)
c552    CONTINUE
C       WRITE(*,*)L,M,QA(L,M)
c551    CONTINUE
c550    CONTINUE
C       TO FIND QA INVERSE
c       CALL DLINRG(N,QA,N,QAINV,N)
c       DO 543 I=1,N
c       DO 543 J=1,N
```

```
c       QINV(I,J)=0.
c       DO 543 L=1,N
c       QINV(I,J)=QINV(I,J)+QAINV(I,L)*U(J,L)
c543    CONTINUE
C       WRITE(*,*)QAINV
C       TO CHECK U TRANSPOSE IS THE LEFT VECTOR OF HA
C       DO 1000 J=1,N
C        DO 980 I=1,N
C          XE(I,J)=0.
C          DO 950 L=1,N
C       XE(I,J)=XE(I,J)+QINV(I,L)*HA(L,J)
C            XE(I,J)=XE(I,J)+U(L,I)*HA(L,J)
C950    CONTINUE
C       YE(I,J)=LAM(I)*QINV(I,J)
C       YE(I,J)=LAM(I)*U(J,I)
C       WRITE(*,*)XE(I,J),YE(I,J)
C980    CONTINUE
C1000   CONTINUE

C       WRITE(1,14)
14      FORMAT(2X,'QP INVERSE')
c       write(1,6)
c       write(1,7)
7       format(2x,'QINV MATRIX')

c       do 21 l=1,n10
```

```
c       k=nd*(l-1)+1
c       kn=l*nd
c       write(1,8)((QINV(i,j),J=k,kn),I=1,n)
c       write(1,6)
c21     continue
C ****************************************

C       TO CALCULATE D PERP TRANSLATIONAL
c       DTPP=0.
c       DO 1214 K=1,N
c       DO 1214 L=1,N
c       DTPP=DTPP+QINV(1,L)*H(L,K)*QINV(1,K)
c1214   CONTINUE
c       DTPP=DTPP*1.38E-16*293./(6.*3.14159*0.01*AA*1.E-8*RN)
c       WRITE(*,1217)DTPP
1217    FORMAT(2X,'DTPP=',E12.5)
C       TO CALCULATE perpendicular rotational DRPP

C       TO FIND HT INVERSE
        CALL DLINRG(N,HT,N,HTINV,N)

c       to find h inverse
        call dlinrg(n,h,n,hinv,n)

c       to calculate Dpll(fz),Dtpp(dp)
c       to calculate DR(rz),according
```

```
c       to p6 of equation of motion
        dp=0.
        FZ=0.
        rz=0.
        DO 3100 M=1,N
        DO 3100 L=1,N
        dp=dp+hinv(m,l)
        FZ=FZ+HTINV(M,L)
        rz=rz+hinv(m,l)*(m-(rn+1)/2.)*(l-(rn+1.)/2.)
3100    CONTINUE
C       WRITE(*,*)FZ
        DPLL=F1/FZ
        dper=f1/dp
        DR=f1/(rh**2*rz)
        DZO=(DPLL+2.*DPER)/3.
        WRITE(*,3102)dper,DPLL,dr,DZO
3102    FORMAT(2X,'dper=',e12.5,/,2x,'DPLL=',E12.5,
     %         /,2x,'DR',e12.5,/,2X,'DO=',E12.5)

c       DRPP=0.
c       DO 1213 K=1,N
c       DO 1213 L=1,N
c       DRPP=DRPP+QINV(2,L)*H(L,K)*QINV(2,K)
c1213   CONTINUE
c       DRPP=DRPP*1.38E+8*293*12./(6*3.14159*
c     *         0.01*AA*RH**2*RN*(RN-1)*(RN+1))
```

```
c       WRITE(*,1218)DRPP,dpp
1218    FORMAT(2X,'DRPP=',E12.5,'dpp=',e12.5)

C       WRITE(*,1200)
1200    FORMAT(2X,'Drpp=',$)
C       READ(*,*)DRPP

c to calculte DXM

        WRITE(8,*)30
        WRITE(3,*)N
        M=INT(N/2)
        M1=M+1
        write(*,1313)m
1313    format(2x,'DXM calculation,m=',I3)
C       CTO IS C(t) AT TIME 0
        CTO=0.
        DO 1302 L=3,N
        CTO=CTO+(Q(M1,L)-Q(M,L))**2
1302    CONTINUE
        RI=0
        DO 1300 I=1,30
        RI=RI+FLOAT(I)*0.44
C       RI=FLOAT(I)
        CT(I)=0.
        DO 1301 L=3,N
```

```
C       WRITE(*,*)Q(M1,L),Q(M,L)
        CT(I)=CT(I)+EXP(-RI/T(L))*(Q(M1,L)-Q(M,L))**2
1301    CONTINUE
C       WRITE(*,*)CT(I)
        CT(I)=CT(I)/CTO
        DXM(I)=3.*(2.*DR*RI*1.E-9+2.*CTO*RH/P*(1-CT(I)))
        WRITE(8,*)RI,DXM(I)
        write(*,*)RI,dxm(I)
1300    CONTINUE
        WRITE(3,*)T

C       WRITE(*,546)
546     FORMAT(2X,'CHECK HTINV')
C       TO CHECK HTINV
C       DO 544 L=1,N
C       DO 544 M=1,N
C       SCQ=0.0
C       DO 545 K=1,N
C       SCQ=SCQ+HTinv(L,K)*HT(K,M)
C545    CONTINUE
C       WRITE(*,*)L,M,SCQ
544     CONTINUE

        STOP
        END
```

Appendix D
Program CORLAT.FOR

```
C       PROGRAM CORLAT.FOR
C       S(K,T)/S(K,O) IS CALCULATED AT DIFFERENT TIME,THE CORRELATION
C       FUNTION IS FITTED BY LSF OF SINGLE EXPONENTIAL DECAY.

C       THIS PROGRAM CALCULATES THE STATIC STRUCTURE FACTOR FOR WEAKLY
C       BENDING ROD. DYNAMIC STRUCRURE FACTOR IS CALCULATED BY USING THE
C       NUMERICAL COMPUTATION OF THE EIGENVALUE AND EIGENVECTOR OF HA
C       MATRIX.SUBROUTINE EIGQV.FOR GIVES EIGENVALUE AND EIGENVECTOR OF
C       HA MATRIX. DIFFUSION COEFFICIENT AT INCREASING VARIED K**2 IS
C       OBTAINED BY G(K,T)/G(K,O). THE MAXIMUM NUMMBER FO NORMAL MODE
C       NEEDS TO BE DECIDED THE STATIC STRUCTURE FACTOR CAN ALSO BE
C       CALCULATED FROM PROGRAM NSSF.FOR OR SSF.FOR. SUMMATION IS
C       CARRIED OUT FIRST,INTEGRATION IS CARRIED OUT THEREAFTER.

C       sum the ALL internal modes only
C       PERPENDICULAR DIFFUSION COEFFICIENT IS CALCULATED BY USING
C       MODE SELECTION RULE
```

```
C
C       DIFFERENT L,DIFFERENT # OF SEGMENT.DATA STORED IN SSF.INP

C       FILE DAPP.DAT HAS THE RESULT OF DAPP AND K**2

        PARAMETER(N=96,nn1=97)
        IMPLICIT DOUBLE PRECISION(A-H,O-Z)

        real rwksp(13016)
        REAL*8 X3,RN,RN1,RK21,G2,G2K2,TSKL,RKL,X1,X2,TSKO,CFUMU(nN1)
        REAL*8 VTSKO,VTSKL,X(nN1,nN1),DU,DELTA,RL,SKL,RG,TLP(nN1),XTT(NN1)
        REAL*8 MU(nN1),FU(nN1),SP(nN1),DTAU(nN1),AAA(NN1),QQ(NN1,NN1)
        REAL*8 CANVE,ANVE,Q(nn1,nn1),QY(nN1,nN1),D(NN1),TAUQ(nN1),TAUU(NN1)
        REAL*8 TAUJ(NN1),DAPJ(NN1),XT1(NN1),QX(NN1,NN1),TP(nN1),TAUO(nN1)
        COMMON N1,RN1,DR,DPER,DPL,TW,RK,RK2,RH,P,BR,YT1(NN1,NN1)
        common R(nN1,nN1),THETA(nN1,nN1),Y1(nN1,nN1),ATV(nN1)
        common/worksp/rwksp

        OPEN (UNIT=1,FILE='COR.DAT',STATUS='NEW',FORM='FORMATTED')
        OPEN (UNIT=6,FILE='COR.OUT',STATUS='NEW',FORM='FORMATTED')
c       OPEN
        OPEN (UNIT=5,FILE='TQQq.DAT',STATUS='OLD',FORM='FORMATTED')
        OPEN (UNIT=2,FILE='Tddd.DAT',STATUS='OLD',FORM='FORMATTED')
c       OPEN (UNIT=3,FILE='5VTSKL.DAT',STATUS='NEW',FORM='FORMATTED')
c       OPEN (UNIT=7,FILE='DAPP5.DAT',STATUS='NEW',FORM='FORMATTED')
C       OPEN (UNIT=8,FILE='TAUQ.DAT',STATUS='old',FORM='FORMATTED')
```

```
      READ(5,5656)Q
C     WRITE(*,*)Q
      read(2,5656)D
C     WRITE(*,*)D
5656  FORMAT(3(E24.16))

C     call iwkin(13016)
1000  WRITE (*,1)
1     FORMAT (1X,'CONTOUR LENGTH (L LE. P)L(anstrum)=',$)
      READ (*,*) RL
      RL=RL*1.E-8
      RL2=RL*RL
      WRITE(*,666)
666   FORMAT(1X,'BEAD RADIUS BR=',$)
      READ(*,*)BR
      BR=BR*1.E-8
      write(*,233)
233   format(2x,'rh=',$)
      read(*,*)rh
      rh=rh*1.e-8

C     WRITE (*,3)
3     FORMAT (1X,'TOTAL NUMBER OF SUBUNITS OF THE ROD N=',$)
C     READ(*,*)RN
c     RN=RL/(2*BR)
```

```
C       N=INT(RN)
        RN=DFLOAT(N)
        RN1=RN+1.
        N1=N+1

        WRITE(*,23)
23      FORMAT(1X,'PERSISTENCE LENGTH (P .GE. L)P=',$)
        READ(*,*)P
        P=P*1.E-8


C       f1 IS A CONSTANT f1=Kb*T/GAMM=Kb*T/(6*PI*AITA*BR)

        f1=293.*1.38E-16/(6.*3.1315926*0.01*BR)
C       WRITE(*,888)f1
888     FORMAT(2X,'f1=',E13.5)

C       WRITE (2,*)22
C       WRITE (3,*)22
c       WRITE(1,*)20
C       WRITE(7,*)20

C SKL IS THE STATIC STRUCTURE FACTOR FOR RIGID ROD
C SKO IS THE STATIC STRUCTURE FACTOR FOR WEAKLY BENDING ROD
C XLM IS CALCULATED HERE SO THAT THEY CAN BE USED LATER W/O THE
C CALCULATION EVERY TIME THE K**2 IS CHANGED
```

```
C       TPD=0.
C TPD is the sum term in D perpendicular
         DO 100 L=2,N1
          N2=L-1
          DO 90 M=1,N2
c          X1=DFLOAT(L-M)
c          X2=(DFLOAT(L))**2-(DFLOAT(M))**2
c          X3=(DFLOAT(L))**3-(DFLOAT(M))**3
           j=l-m
           K=ABS(j)
           R(L,M)=REAL(k)

c********
c          X(l,m)=((RN*RN+3.*RN+2.)/(3.*RN))*X1*X1-(RN+2)*X1*X2/(2*RN)
c     %         +X1*X3/(3.*RN)
c*********

c          WRITE(*,*)l,m,r(l,m),X(l,m)


C          TPD=TPD+3.*BR/(4.*R(L,M)*RH)
C     %         +BR*BR*BR/(RH*RH*RH*R(L,M)*R(L,M)*R(L,M))
           SP(J)=RN1*RH*DSIN(R(L,M)*3.14159/RN1)/3.14159
           TP(J)=3.*BR/(4.*SP(J))+BR*BR*BR/(2.*SP(J)*SP(J)*SP(J))
           TLP(J)=3.*BR/(4.*R(L,M)*RH)
```

```
     %          +BR*BR*BR/(2.*R(L,M)*R(L,M)*R(L,M)*RH*RH*RH)
c       SP(n) corrected length for weakly bending rod
c       tp(n) corrected hydrodynamic interactions for corrected length
c       tlp(n) hydrodynamic interaction for rigid rod
90        CONTINUE
100      CONTINUE

C          WRITE(*,889)TPD
889        FORMAT(2X,'TPD=',E13.5)
C       if (P .GT. 6.E-5)GO TO 5555
c       call subroutine DQR to calculate dper,dpl,dr,Q
C------>>>COMONT FOR THE MOMENT,WHEN THE Q,D CAN BE READ FROM DATA FILE
C       CALL DQR(BR,RH,RL,P,D,Q,DPER,DPL,DR)

C5555   DO 5556 K=3,N1
        DO 5556 K=3,N1
C       d(k)=rh*rh*rh/(f1*p*tauu(k))
        TAUQ(K)=RH*RH*RH/(F1*P*D(K))
5556    CONTINUE

C       write(5,*)q
        WRITE(*,*)N1
C       write(2,*)d
C       WRITE(*,*)Q
c       WRITE(*,*)TAUQ
C       WRITE(*,*)D
```

```
C RG2 IS THE MEAN SQUARE RADIUS OF THE CHAIN OF CONTOUR LENGTH L OF
C       WORM-LIKE CHAIN GIVEN BY EQUATION (5-21)IN V.BLOOMFIELD

        RG2=2.*RL*P*(1./6.-P/(2.*RL)+P*P/(RL*RL)-(P/RL)**3*(1.-DEXP(-RL/P)))

c       to calculate corresponding to RG2
        RH2=RG2/(RN*RN/12.+2.*RN1*0.01)
        RH1=DSQRT(RH2)
200     RH=RH1
        RH2=RG2/(RN*RN/12.+2.*RN1*RH)
        RH1=DSQRT(RH2)
        IF(ABS(RH1-RH) .LE. 1.E-12) GO TO 201
        GO TO 200
201     RH=RH1
C       IF (P/(RH*RH) .GE. 3.28E9)GO TO 3020
        WRITE(*,202)RH
C       RH=94.E-8
        CL=RN*RH
        WRITE(*,203)CL
203     FORMAT(1X,'CALCULATED LENGTH CL=',E13.5)
202     FORMAT(1X,'BEAD SEPERATION H=',E13.5)

C G2 IS THE RADIUS OF GYRATION OF A RIGID ROD WITH A LENGTH RL,G**2=RL**2/12
        G2=RL*RL/12.
```

```
C       DPER=f1/(RN1*RN1)*(RN1+2.*TPD)
C DPER is the d perpendicular
C       write(*,444)DPER
444     FORMAT(1X,'DPER=',E13.5)
C       DPL=1.5*DPER

        DPER=0.1986E-07
        DPL=0.3205E-07
        DR=0.2166E+02


C       WRITE(*,22)DPL
22      FORMAT(1X,'D PARALLEL DPL=',E13.5)
C       READ(*,*)DPL
        DZO=DPL/3.+2.*DPER/3.
        WRITE(*,413)DR,DPER,DPL,DZO
413     FORMAT('DR=',E12.4,1x,'DPER=',E12.4,1x,'DPL=',E12.4,1x,'DO=',E12.4)
C       READ(*,*)DR
C       DR=DPER/RG2
C       WRITE(7,433)
433     FORMAT(7X,'RK2',20X,'DAPP',//)
        WRITE (6,4) RL,P,n1,BR,RH,CL
4       FORMAT(//,2X,'CONTOUR LENGTH L=',E11.5,5X,'PERSISTENCE LENGTH P=',
     %  E11.5,5x,'number of beads N+1=',I3,
     %  //,2X,'BEAD RADIUS BR=',E11.5,5X,'BEAD SEPERATION H=',
     %  E11.5,5X,'CALCULATED LENGTH CL=N*RH=',E11.5,//)
```

```
      WRITE(6,411)G2,RG2
411   FORMAT(2X,'RADIUS OF GYRATION OF A RIGID ROD WITH A CONTOUR
     % LENGTH RL <G**2>=L**2/12=',
     % E13.5,//,2X,'RADIUS OF GYRATION OF WORM-LIKE CHAIN <RG**2>=
     % 2PL[1/6-P/2L+P*P/L*L-(P/L)**3*(1-DEXP(-L/P)=',E13.5,//)

      WRITE(6,400)DZ0,DPL,DPER,DR
400   FORMAT(2X,'D0=DPL/3+DPER*2/3=',E13.5,2X,'DPL=',E13.5,2X,
     % 'DPER=',E13.5,2X,'DR=',E13.5,//,120('*'))

      WRITE (6,15)
15    FORMAT(//,7X,'K**2',55X,'WEAKLY BENDING',
     % 3X,'RIGID ROD',3X,5X,'DAPP',12X,'DPERH',/,6X,'(CM**-2)',
     % 11X,'RKL=K*L',5X,'<RG2>K2',9X,'G2K2',
     % 11X,'S(K,0)',10X,'S(K,T)',10X,'S(K,T)/S(K,0)',/)
C     QQ(M,L)=SUM(3-N+1) OF dq**2/tau(q)*Q(m,q)*Q(l,q)
C     WRITE(*,3033)
3033  FORMAT(2X,'L,QQ(L,L)[Slm in Mickey note]')
         do 3000 l=2,n1
         n2=L-1
         do 3010 m=1,n2
C     QY(L,M) IS TO SUBSTITUDE X(L,M) IN ANALYTICAL CALCULATION IN STATIC
C     PART,SO IT IS SUMEED OVER THE WHOLE SET OF NORMAL MODES
         QY(L,M)=0.
         DO 3301 J=3,N1
```

```
            QY(L,M)=QY(L,M)+(Q(L,J)-Q(M,J))**2
3301        CONTINUE
c       X(L,M)=QY(L,M)
C       write(5,*)l,m,x(l,m),qy(l,m),QQ(L,M)
3010    continue
3000        continue

C       look up table of channel delay TAUO(J)
c       at each K**2 FROM 1 TO 20,INCREMENT 1
C*****************************************************
        TAUO(1)=65E-6
        TAUO(2)=35E-6
        TAUO(3)=20E-6
        TAUO(4)=10E-6
        TAUO(5)=8E-6
        TAUO(6)=6E-6
        TAUO(7)=5E-6
        TAUO(8)=4E-6
        TAUO(9)=3.5E-6
        TAUO(10)=3E-6
        TAUO(11)=2.5E-6
        TAUO(12)=2E-6
        TAUO(13)=2E-6
        TAUO(14)=2E-6
        TAUO(15)=2E-6
        TAUO(16)=1.5E-6
```

```
      TAU0(17)=1.5E-6
      TAU0(18)=1E-6
      TAU0(19)=1E-6
      TAU0(20)=1E-6
      TAU0(21)=1E-6
      TAU0(22)=1E-6
C*****************************************************

C*****************************************************
C     LOOK UP TABLE OF DAPP(K) OF M13,FROM JESS'S DATA
      DAPJ(1)=2.50
      DAPJ(2)=3.00
      DAPJ(3)=3.30
      DAPJ(4)=3.56
      DAPJ(5)=3.80
      DAPJ(6)=3.99
      DAPJ(7)=4.15
      DAPJ(8)=4.29
      DAPJ(9)=4.41
      DAPJ(10)=4.52
      DAPJ(11)=4.61
      DAPJ(12)=4.68
      DAPJ(13)=4.76
      DAPJ(14)=4.82
      DAPJ(15)=4.88
      DAPJ(16)=4.92
```

```
      DAPJ(17)=4.97
      DAPJ(18)=5.00
      DAPJ(19)=5.03
      DAPJ(20)=5.08
      DAPJ(21)=5.08
C*****************************************************


3012  WRITE(*,17)
17    FORMAT(1X,'INCREMENT OF K**2 DK=',$)
      READ(*,*)DK
      WRITE(*,88)
88    FORMAT(1X,'MAXIMUM K**2=',$)
      READ(*,*)FK2
      FK=DSQRT(FK2)
      NK=int(FK2/DK)+1
C     IF (DK*20 .GT. 20)GO TO 3010
C     WRITE(*,*)NK
      DK=DK*1.E+10
      FK2=FK2*1.E+10

      DO 2000 J=NK,nk

       NJ=J-1
       RK2=0.005e+10+DK*DFLOAT(NJ)
       RK=DSQRT(RK2)
```

```
      RKL=RK*RL
      RG2K2=RG2*RK2
      G2K2=G2*RK2
C     IF(NJ .EQ. 0)GO TO 3005

      TAUJ(J)=1/(2.*DAPJ(J)*1.E-8*RK2)
      WRITE(*,3006)TAUJ(J)
3006  FORMAT(2X,'TAUJ(KK)=',E11.5)
      dtw=tauj(j)/8.
c     TW=TAUJ(J)/4./2.
      DO 2120 JT=1,50
c     TW=TW*2
      tw=jt*dtw

C     TO DETERMINE NQ,CRETERIA FOR NQ IS EXPERIMENTAL TAUJ=1/(2*DAPJ*K*K)
C     TAUQ .GE. TAUJ
      DO 3009 K=3,N1
      IF(TAUQ(K) .LT. TAUJ(J))GO TO 3008
3009  CONTINUE
3008  NQ=K-1
      WRITE(*,3007)NQ
3007  FORMAT(2X,'NQ=',I3)
      nq=N1

c     write(*,*)rk2
3005   TPDH=0.
```

```
          SKL=0.
          SUM2=0.
          SUM3=0.
          tqq=0.
          TTQQ=0.
c         write(*,3414)
3414      format(2x,'tauq(i),xtt(i)')
C to calculate xt1(k) first,outside 1,m do loop
          do 3004 i=3,n1
c         write(*,*)tauq(i),xtt(i)
          xt1(i)=dexp(-TW/tauq(i))
3004      continue
C         write(*,3404)
3404      format(2x,'xt1=exp(-tauj(j)/(30.*tauq(k)))')
C         write(*,*)xt1
C         write(*,*)tauq
           DO 50 L=2,N1
            N2=L-1
            DO 40 M=1,N2
             I=L-M
             FENM=RK*RL/RN*R(L,M)
             SITH=DSIN(FENM)
             COTH=DCOS(FENM)
             SKL=SKL+DSIN(FENM)/FENM
             SUM2=SUM2+(SITH/(FENM*FENM*FENM)-COTH/(FENM*FENM))
             SUM3=SUM3
```

```
     %      +DFLOAT(L)*DFLOAT(M)*(SITH/(FENM*FENM*FENM)-COTH/(FENM*FENM))
C           TPDH=TPDH+F(I)
            THETA(L,M)=RK*RH*R(L,M)
            Y1(l,m)=-RK2*RH*RH*RH*QY(l,m)/(2.*P)
c       IF(NJ .EQ. 0)GO TO 40
c       IF(NQ .LT. 3)GO TO 40

C       TO SUM dq**2/tauq(k)*q(l,k)*q(m,k)  terms of k=3,nq
            QQ(l,m)=0.
            QX(L,M)=0.
            do 3001 k=3,nq
            QX(L,M)=QX(L,M)+Q(L,K)*Q(L,K)+Q(M,K)*Q(M,K)
     %             -2.*Q(L,K)*Q(M,K)*XT1(K)
            QQ(l,m)=QQ(l,m)+XT1(K)*q(l,k)*q(m,k)/TAUQ(K)
3001    continue
            QQ(L,M)=QQ(L,M)*(RH*RH*RH/P)
            YT1(L,M)=DPER*TW+RH*RH*RH*QX(L,M)/(2.*p)
     %      +(L-(N+2)/2)*(M-(N+2)/2)*DR*TW*RH*RH
40        CONTINUE
C       DO 3013 I=3,NQ


C3013   CONTINUE


        qq(1,1)=0.
```

```
      AAA(L)=0.
      do 3011 i=3,nq
      qq(1,1)=qq(1,1)+RH*RH*RH/P*XT1(I)*q(1,i)*q(1,i)/tauq(i)
      AAA(L)=AAA(L)+Q(L,I)*Q(L,I)*(1-XT1(I))
3011  continue
      ATV(L)=DPER*TW+RH*RH*(L-(N+2)/2)*(L-(N+2)/2)*DR*TW
     %       +AAA(L)*RH*RH*RH/P
C     AAA(L)=AAA(L)*RK2
C     ATV(L)=2./3.-8.*AAA(L)/15.+24.*AAA(L)*AAA(L)/105.
C     WRITE(*,*)AAA(L),ATV(L)
         tqq=tqq+qq(1,1)
         TTQQ=TTQQ+QQ(L,L)*ATV(L)
50     CONTINUE

C     write(*,3030) ttqq
3030  format(2x,'ttqq=',e12.4)

C      DPERH=f1*TPDH/(RN1*RN1)
C      DPLH=1.5*DPERH
C     WRITE(*,737)DPERH
737   FORMAT(2X,'DPERH=',E13.5)
      TSUM1=RN1+2.*SKL
      TSUM2=RN1/3.+2*SUM2
      TSUM3=1./18.*RN1*(RN1+1)*(2*RN1+1)+2*SUM3
      FKL=TSUM2/TSUM1
      GKL=(TSUM3/TSUM1)/(RN1*RN1)
```

```
      RDAPP=DO+2*(DPL-DPER)*(1./3.-FKL)+2.*RL2*DR*GKL


        A=0.0DO

        B=1.0DO

        DELTA=1.0D-8

        CALL INTEG(J,A,B,DELTA,NSTEP,ERROR,SUMS,SUMA,SUMT)

C       SUMS is the integration of sum of
c       cos(theta(l,m)*u)*exp(y1(l,m)*(1-u**2))  in S(K,0)
c       SUMA is the integration of sum of
c       u**2*cos(theta(l,m)*u)*exp(y1(l,m)*(1-u**2))=A  in T11 OF ATA(K)
c       SUMT is the integration of sum of F(J)*A
c
        WRITE(*,738)SUMS,SUMA,SUMT
738     FORMAT(2X,'SUMS,SUMA,SUMT=',3E12.5)
        TSKO=(1+2*SUMS/RN1)
        TSKL=(1+2*SKL/RN1)/RN1
C       TSKO AND TSKL ARE NORMALIZED BY A FACTOR OF N+1
C       VTSKO=1./TSKO
C       VTSKL=1./TSKL
C       VTSKO,VTSKL ARE THE INVERSE OF TSKO AND TSKL
101     FORMAT(1X,'RG2K2=',E12.6,5X,'VTSKO=',E12.6,5X,'VTSKL=',E12.6)
C       WRITE(*,101)RG2K2,VTSKO,VTSKL


C       TP11=DPL/RN1*(RN1/3.+2.*SUMA)
```

```
C        TMM=2.*DPER/3.+RH*RH*DR*RN*(RN+2)/18.+2.*ttqq/(RN1)
C       REPLACE TQQ/3 BY TTQQ
C        TLM=(2./rn1)*SUMT
C       WRITE(*,739)TPLL,TMM,TLM
739     FORMAT(2X,'TPLL,TMM,TLM=',3E12.5)

C        ATA=TPLL+TMM+TLM
C        DAPP=ATA/TSK0

        TSKT=(2*SUMT+SUMA)/RN1
        G1=TSKT/TSK0

         WRITE  (6,111) RK2,RKL,RG2K2,G2K2,TSK0,TSKT,G1
111      FORMAT (2X,7(E15.4),/)
C        WRITE (2,*) RG2K2,VTSK0
C        WRITE (3,*) G2K2,VTSKL
C        WRITE (4,*) RK2,TSK0
C        WRITE (5,*) RK2,TSK

         WRITE(*,*)RK2,TW,G1
         RK2b=RK2*1.E-10
         DAPP=DAPP*1.E+6
         RDAPP=RDAPP*1.E+6
C        WRITE(7,*)RK2b,DAPP
         WRITE(1,*)TW,G1
```

```
C DPL IS D PARALLEL
C2002    WRITE(*,*)NQC
2120     CONTINUE
2000     CONTINUE
         WRITE (*,120)
120      FORMAT (1X,'CONTINUE?(1 OR 2)')
         READ (*,*) DU
         IF ( DU .EQ. 1 ) GO TO 1000


         CLOSE(UNIT=1)
         CLOSE(UNIT=2)
         CLOSE(UNIT=3)
         CLOSE(UNIT=4)
         CLOSE(UNIT=5)
         CLOSE(UNIT=6)

C        GO TO 9000
C        STOP
C        END

C NEGLECTED PART


c
```

```
c**************************************************************************
c       DO 330 I=1,N
c        MU(I)=4.*(COS(2.*3.14159*FLOAT(I)/RN1)-1)**2
c        NM=INT(RN/2.)
c        FU(I)=1
c        FUO=1.
c        DO 320 J=1,NM
c         FU(I)=FU(I)+2.*COS(2.*3.14159*FLOAT(I)*FLOAT(J)/RN1)*TP(J)
c         FUO=FUO+2.*TP(J)
c FUO is FU(I) at I=0
c320     CONTINUE
c       TAUQ(I)=RH**3/(f1*P*FU(I)*MU(I))
c       WRITE(8,*)I,TAUQ(I)
c330    CONTINUE
c       WRITE(*,*)I

C PC is critical P in the CANVE calculation,P must be bigger than PC
c       PC=0.09*RH**3/(64.*BR*BR*f1)
c       IF ( P .LE. PC ) GO TO 3020

c criteria for overdamped mode,on page 2 of maximum eigenvalue
c 4g<r**2/m,g=(Kh/h**2)*C,C=4*Co,Co=(cosK-1)**2,final  derivation is
c Co< 6.5332E+9/(P*BR/H**3),take  Co=0.5*6.5332E+9/(P*BR/H**3)


c       CO=0.5*6.5332E+9/(P*BR/RH**3)
```

```
c3022   IF(CO .LE. 4) GO TO 3021
c       CO=0.5*CO
c       GO TO 3022
c       following is to calculate the maximum
c       number of mode which is still overdamped
C3021   CANVE=1-DSQRT(CO)
C       WRITE(*,*)CANVE
C       ANVE=ACOS(CANVE)
C       FOPMODE=ANVE*RN/(2*3.14159)
C       WRITE(*,383)FOPMODE
C383    FORMAT(2X,'MODE WHICH IS STILL OVERDAMPED=',E14.5)

C       MMD=INT(FOPMODE)

C        (OR J=1,22*N IF SSFINP IS USED FOR DATA INPUT)
C        RK2=FK2*1.E10-DK*(FLOAT(J)-1)
C        RK2=RK2-(DK-1)
C       WRITE(*,345)RK2
C345    FORMAT(2X,'RK2=',E13.5,'CHANNEL  DELAY TAU0=')
C       READ(*,*)TAU0(1)
C        JQ=20-J+1
C        CQ=TAUQ(MMD)/TAU0(20)
C       WRITE(*,358)CQ
358     FORMAT(2X,'CQ=',E13.5)
C        CFUMU(J)=RH**3/(CQ*TAU0(J)*f1*P)
C        STAU=ABS(CQ*TAU0(JQ)-TAUQ(1))
```

```
C        DO 350 I=1,NM
C         DTAU(I)=ABS(CQ*TAUO(JQ)-TAUQ(I))
C       WRITE(*,346)STAU,DTAU(I)
346     FORMAT(2X,'STAU=',E13.5,'DTAU(I)=',E13.5)
C         I
C         STAU=DTAU(I)
c         NQC=I
C349     NQC=NQC
C350     CONTINUE
c       WRITE(*,353)TAUO(J),TAUQ(J),STAU,NQC
353     format(2x,'TAUO(J)=',E13.5,'TAUQ(j)=',E13.5,'STAU=',E13.5'NQC=',I3)

C       write(*,354)nqc
354     format(2x,'nqc=',I3)
C        DO 373 I=1,N
C        F(I)=TLP(I)-TP(I)+FUO/RN1
C        DO 370 K=1,NQC
C         F(I)=F(I)+2.*FU(K)*COS(2.*3.14159*R(L,M)*FLOAT(K)/RN1)/RN1
C370     CONTINUE
C373    CONTINUE
C       WRITE(*,369)I,F(I)
C369       FORMAT(2X,'F(',I3,')=',E13.5)

C constraint:K*H less or equale to 0.2,maximum K2 is 20E+10,K=4.47E+5
C       IF(FK*1.E+5*RH .GT. 0.2) GO TO 3000
C       IF (NQC .EQ. NQC) GO TO 2002
```

```
C58
C        WRITE (6,16)RK2
C16      FORMAT(1X,E15.5)

C        WRITE(*,773)RK2,RDAPP,FKL,GKL
773      FORMAT(1X,'RK2=',E13.5,'RDAPP=',E13.5,'FKL',E13.5,'GKL',E13.5)


C3000    WRITE(*,3001)RH*4.47E+5
C3001    FORMAT(1X,'!!! RH*RKmax GREATER THAN 0.2,RH*4.47E+5=',E13.5)
C        RN=5.*RL*4.47E+5
C        GO TO 1000
C3010    WRITE(*,3011)20*DK
C3011    FORMAT(1X,'!!! K**2 EXCEED 20,RESET DK')
C        GO TO 3012
C3020    PP=P/PC
C        WRITE(*,3025)PP
3025     FORMAT(1X,'!!! P IS LESS THAN PC,P/PC = ',E13.5,' REENTER A BIGGER P
     %   VALUE')
C        GO TO 1000
C*******************************************************************************

         STOP
         END
```

```
C       FOLLOWING IS THE FUNCTION TO BE INTEGRATED IN SUMS IN S(K,O)
        FUNCTION FUN1(X)
        IMPLICIT DOUBLE PRECISION(A-H,O-Z)
        parameter(nn1=97)
        COMMON N1,RN1,DR,DPER,DPL,TW,RK,RK2,RH,P,BR,YT1(NN1,NN1)
        common R(nn1,nn1),THETA(nn1,nn1),Y1(nn1,nn1),ATV(nn1)
        common/worksp/rwksp
        SKO=0
        DO 510 L=2,N1
         N2=L-1
         DO 500 M=1,N2
C        I=L-M
         SKO=SKO+DCOS(THETA(L,M)*X)*DEXP(Y1(l,m)*(1.-X*X))
500      CONTINUE
510     CONTINUE
        FUN1=SKO
        RETURN
        END

c       following is the integrand in T OF ata(K) calculation
C       IN Tlm(WHEN L .NE. M,T),ATA(K)=T+T11
        FUNCTION FUN2(X)
        IMPLICIT DOUBLE PRECISION(A-H,O-Z)
        parameter(nn1=97)
        COMMON N1,RN1,DR,DPER,DPL,TW,RK,RK2,RH,P,BR,YT1(NN1,NN1)
        common/worksp/rwksp
```

```
      common R(nn1,nn1),THETA(nn1,nn1),Y1(nn1,nn1),ATV(nn1)
C TINP IS SUMMATON OVER L AND M IN T TERMS IN ATA(K) ,IN SUMT
C IN T1m
      TINP=0
      DO 610 L=2,N1
       N2=L-1
       DO 600 M=1,N2
C        I=L-M
      TINP=TINP+DCOS(THETA(L,M)*X)
     %       *DEXP(-RK2*(X*X*DPL*TW+YT1(l,m)*(1.DO-X*X)))
C     WRITE(*,599)I,F(I)
599   FORMAT(2X,'F(',I3,')=',E13.5)
600    CONTINUE
610   CONTINUE
      FUN2=TINP
      RETURN
      END

C function in tHE INTEGRATION IN S(K,T) WHEN L=M,in SUMA
C TPP IS SUMMATION OVER L AND M TERMS IN T-11 in ATA(K) CALCULATION
      FUNCTION FUN3(X)
      IMPLICIT DOUBLE PRECISION(A-H,O-Z)
      parameter(nn1=97)
      COMMON N1,RN1,DR,DPER,DPL,TW,RK,RK2,RH,P,BR,YT1(NN1,NN1)
      common/worksp/rwksp
      common R(nn1,nn1),THETA(nn1,nn1),Y1(nn1,nn1),ATV(nn1)
```

```
      TPP=0.D0
      DO 590 L=1,N1
       TPP=TPP+DEXP(-RK2*(X*X*DPL*TW+ATV(1)*(1.D0-X*X)))
580    CONTINUE
590   CONTINUE
      FUN3=TPP
      RETURN
      END

      SUBROUTINE INTEG(J,A,B,DELTA,NSTEP,ERROR,SUMS,SUMA,SUMT)
C     A PROGRAM TO DO INTEGRAL USE SIMPSON FORMULAR FOR S(K,0),ATA(K)
      IMPLICIT DOUBLE PRECISION(A-H,O-Z)
      parameter(nn1=97)
      COMMON N1,RN1,DR,DPER,DPL,TW,RK,RK2,RH,P,BR,YT1(NN1,NN1)
      common R(nn1,nn1),THETA(nn1,nn1),Y1(nn1,nn1),ATV(nn1)
      common/worksp/rwksp
      N=100
      H=(B-A)/DFLOAT(N)
      SUM2S=0.D0
      SUM4S=0.D0
      SUM2A=0.D0
      SUM4A=0.D0
      SUM2T=0.D0
      SUM4T=0.D0
      DO 140 I=2,N-2,2
      SUM2S=SUM2S+FUN1(A+DFLOAT(I)*H)
```

```
      SUM2A=SUM2A+FUN3(A+DFLOAT(I)*H)
      SUM2T=SUM2T+FUN2(A+DFLOAT(I)*H)
140   CONTINUE
150   H=(B-A)/DFLOAT(N)
      SUM1S=0.D0
      SUM1A=0.D0
      SUM1T=0.D0
      DO 160 I=1,N-1,2
      SUM1S=SUM1S+FUN1(A+DFLOAT(I)*H)
      SUM1A=SUM1A+FUN3(A+DFLOAT(I)*H)
      SUM1T=SUM1T+FUN2(A+DFLOAT(I)*H)
160   CONTINUE
      SUM3S=H/3.D0*(FUN1(A)+FUN1(B)+4.D0*SUM1S+2.D0*SUM2S)
      SUM3A=H/3.D0*(FUN3(A)+FUN3(B)+4.D0*SUM1A+2.D0*SUM2A)
      SUM3T=H/3.D0*(FUN2(A)+FUN2(B)+4.D0*SUM1T+2.D0*SUM2T)
      STS=DABS(SUM3S-SUM4S)/DABS(SUM3S+SUM4S)*2.D0
      IF( STS .GT. DELTA) GO TO 162
c     WRITE(*,7777)DELTA,STS
7777  FORMAT(2X,'DELTA=',E12.5,'STS=',E12.5)
      STA=DABS(SUM3A-SUM4A)/DABS(SUM3A+SUM4A)*2.D0
c     WRITE(*,7778)STA
7778  FORMAT(2X,'STA=',E12.5)
      IF( STA .GT. DELTA) GO TO 162
      STT=DABS(SUM3T-SUM4T)/DABS(SUM3T+SUM4T)*2.D0
c     WRITE(*,7779)STT
7779  FORMAT(2X,'STT=',E12.5)
```

```
      IF( STT .LT. DELTA) GO TO 170
162   SUM4S=SUM3S
      SUM2S=SUM2S+SUM1S
      SUM4A=SUM3A
      SUM2A=SUM2A+SUM1A
      SUM4T=SUM3T
      SUM2T=SUM2T+SUM1T
      N=N*2
      GO TO 150
170   NSTEP=N
      SUMS=(SUM3S+SUM4S)/2.DO
      SUMA=(SUM3A+SUM4A)/2.DO
      SUMT=(SUM3T+SUM4T)/2.DO
      ERROR=DABS(SUM3S-SUM4S)
      RETURN
      END
```

Vita

Lu Song was born to Yong-wu Song and Gui-zheng Wang in Huhhot, China Febrary 1, 1958. She graduated from the Ninth High School in Baotou, China in 1975. She took the national entrance examination for college in 1977 and entered the University of Science and Technology in China. She received her bachelor's degree in chemistry from the University of Science and Technology in China in 1982. She took the CGP (Chemistry Graduate Program between China and U.S.A.) examination and entered the University of Washington in Fall 1983. She joined Professor J.M. Schurr's research group in 1984. She received her Ph.D. in Biophysical Chemistry in Summer 1989.